

Wilfrid Laurier University

Scholars Commons @ Laurier

---

Theses and Dissertations (Comprehensive)

---

2004

**Circulation mapping of the North Atlantic Ocean during the 1990's and from 1974 to 1984 as determined from the World Ocean Circulation Experiment (WOCE) Eulerian current meter moorings**

Roger Palmi  
*Wilfrid Laurier University*

Follow this and additional works at: <https://scholars.wlu.ca/etd>



Part of the [Geographic Information Sciences Commons](#), and the [Physical and Environmental Geography Commons](#)

---

**Recommended Citation**

Palmi, Roger, "Circulation mapping of the North Atlantic Ocean during the 1990's and from 1974 to 1984 as determined from the World Ocean Circulation Experiment (WOCE) Eulerian current meter moorings" (2004). *Theses and Dissertations (Comprehensive)*. 460.  
<https://scholars.wlu.ca/etd/460>

This Thesis is brought to you for free and open access by Scholars Commons @ Laurier. It has been accepted for inclusion in Theses and Dissertations (Comprehensive) by an authorized administrator of Scholars Commons @ Laurier. For more information, please contact [scholarscommons@wlu.ca](mailto:scholarscommons@wlu.ca).

## INFORMATION TO USERS

This manuscript has been reproduced from the microfilm master. UMI films the text directly from the original or copy submitted. Thus, some thesis and dissertation copies are in typewriter face, while others may be from any type of computer printer.

**The quality of this reproduction is dependent upon the quality of the copy submitted.** Broken or indistinct print, colored or poor quality illustrations and photographs, print bleedthrough, substandard margins, and improper alignment can adversely affect reproduction.

In the unlikely event that the author did not send UMI a complete manuscript and there are missing pages, these will be noted. Also, if unauthorized copyright material had to be removed, a note will indicate the deletion.

Oversize materials (e.g., maps, drawings, charts) are reproduced by sectioning the original, beginning at the upper left-hand corner and continuing from left to right in equal sections with small overlaps.

ProQuest Information and Learning  
300 North Zeeb Road, Ann Arbor, MI 48106-1346 USA  
800-521-0600

**UMI**<sup>®</sup>



## **NOTE TO USERS**

**This reproduction is the best copy available.**

UMI<sup>®</sup>



**CIRCULATION MAPPING OF THE NORTH ATLANTIC OCEAN  
DURING THE 1990S AND FROM 1974 TO 1984 AS DETERMINED  
FROM THE WORLD OCEAN CIRCULATION EXPERIMENT  
(WOCE) EULERIAN CURRENT METER MOORINGS**

by

**Roger Palmi**

(Honours Bachelor of Arts, Wilfrid Laurier University, 1999)

THESIS

Submitted to the Department of Geography and Environmental Studies  
in partial fulfillment of the requirements for the  
degree of Master of Environmental Studies

Wilfrid Laurier University  
Waterloo, Ontario, Canada  
2004

© Roger Palmi, 2004

**In compliance with the  
Canadian Privacy Legislation  
some supporting forms  
may have been removed from  
this dissertation.**

**While these forms may be included  
in the document page count,  
their removal does not represent  
any loss of content from the dissertation.**

## ABSTRACT

The Study of the ocean presents many challenges due to its vast size and the difficulty in representing such a system with the availability of few data measurements. The World Ocean Circulation Experiment (WOCE) is the largest oceanographic experiment ever conducted. Data collection has been completed and we are now in the analysis, interpretation, modeling and synthesis phases (AIMS).

An analysis and interpretation of the North Atlantic Ocean was conducted using a subset of the WOCE data. In the pre-WOCE period between Apr-11-74 and Sep-03-84 a total of 272 records were obtained having a spatial range of 23.2° - 60.2°N and 9.2° - 71.8°W. The WOCE dataset consisted of 653 records obtained between Mar-09-90 and Aug-19-99 and having a spatial range of 0.1° - 65.3°N and 9.5° - 76.8°W. Data rich areas included the eastern shore of North America, especially the Gulf Stream and its extension, and the west coast of Europe and the United Kingdom. Data poor areas were found predominately north of the equator between 5° and 15°N.

Shallow and intermediate depth water currents showed similar pathways between the two datasets, whereas deep water current meters did not. Near bottom flows showed the effect of bathymetry on deep water flows with acceleration of flow down the continental slope evident, this is due to a combination of slope and water density. Annual mean circulation was examined for the period 1991 – 1993 and revealed a steady sub-tropical gyre. Eastward movement of a large warm water core was evident in 1992, with a smaller warm water core moving northward in 1993.

By combining vector plots, depth profiles, and flow statistics a more complete coverage of the ocean was established. A good representation of current flows at various depths was observed. Variability in the circulation revealed the formation of eddies, movement of deep water masses and a highly dynamic state of the ocean.



## ACKNOWLEDGEMENTS

Though the majority of time spent on thinking, planning, organizing, researching, analyzing, writing, procrastinating, discussing, rewriting, and various troubleshooting of a thesis is spent in solitary confinement with endless hours in the lab or in front of a computer there are many people who have contributed and helped in getting this achievement accomplished.

My time at WLU has been plagued by separation, death, responsibilities both here and at home, duties, demands, wrong turns and deadlines. I believe I have seen the down side of life from almost every possible angle. But at the same time I have met many wonderful people and made many new friends who have allowed the good times in life to balance the more melancholy.

First of all I would like to thank my supervisor Dr. Houston Saunderson who has stayed with me through it all. He has shown me patience, kindness and confidence, and has allowed me to stumble, fall, and pick myself up again in order to find my way through this process on my own merit.

With regards to data acquisition I would like to thank Joseph Bottero of the Oregon State University Buoy Group for the WOCE dataset; Bertrand Chapman of CERSAT, the French Processing and Archiving Facility for the wind data; P. Dickson and K. Medler, of the WOCE World Climate Research Program for the flow statistics; and B. M. Fekete of the Oak Ridge National Laboratory Distributed Archive Center for the global river discharge data.

I would also like to thank Dr. Mike English, Dr. Brent Wolfe, Dr. Sean Doherty and Dr. Barry Boots for giving me the opportunity to join their research projects and gain

valuable experience and insight into academic life above and beyond the thesis. not to mention a paycheck when I really needed one. They are also friends whom I can talk to and discuss things with, rather than superiors who I must report to – a phenomenon. I have been told, that is missing in many universities throughout the world.

Around the department I would like to thank Dr. Bob Sharpe, Dr. Mary Lou Byrne and Joanne Horton for their help in things academic, Pam Schauss for her help in all things cartographical, Grant Simpson for maintaining and troubleshooting the computer which has contained the last few years of my life, Doreen Dassen for her friendship, expertise, kindness, and counseling, and Merrin Macrae for her insight into conducting research, organizing ideas and most importantly for her friendship (congratulations to you and Rich on your new baby). I would also like to thank and remember the late Dr. Jerry Hall for truly instilling a love of geography in me, for our discussions and differing points of view, and for showing me how this field can be used to develop a caring relationship with the environment.

Around the university I need to thank the staff at the library for finding the publications I needed, the people in grad studies, especially Helen Paret and Dianne Duffy, who kept me abreast of deadlines, and at the end pushed the envelope for me and treated me as a human being, and the folks at Tim Horton's who always had coffee when I really needed it (especially Agnes who allowed me to finish off any muffins remaining at days end).

The last few years of my life at WLU have been the spatial analysis lab. From a place to work, to surf the net, to endless all-nighters, and most importantly for all the people who have been a part of my life and become friends through this all. The lab

became a place to call home and to enjoy coming to each day, and so I thank (in no particular order – ok how about alphabetically, so no one takes anything personally) Susanna Barreras, Flavia Bianchi, Rob Brown, Alastair Dempster, Shauna Flanagan, Niem Hyun, Suresh Kandaswamy, Mark Lefebvre, Jessica Mueller, Sean Mueller, Trisalyn Nelson, Cheryl Robertson, Claudia Saheb, Vera Spektor, Chris Storie, Kim Tran and Kevin Tupman. WLU and its significant people will always be dear to me. As Bilbo Baggins so eloquently penned it, “The road always goes there and back again”

I would like to thank my mom who never understood what I was doing, but supported me anyway, and my late father, who went back to school late in life to become an electrician and taught me that it’s never too late for anything.


Finally I want to thank the most important person in my life, though we have separated, she is the reason why I struggled, doubted, cried, despaired, fell defeated, but ultimately triumphed. This thesis is not for me, it’s for the person that I still love and cherish, my wife Joanne – as Brian Adams so well put it “Everything I do, I do it for you.”

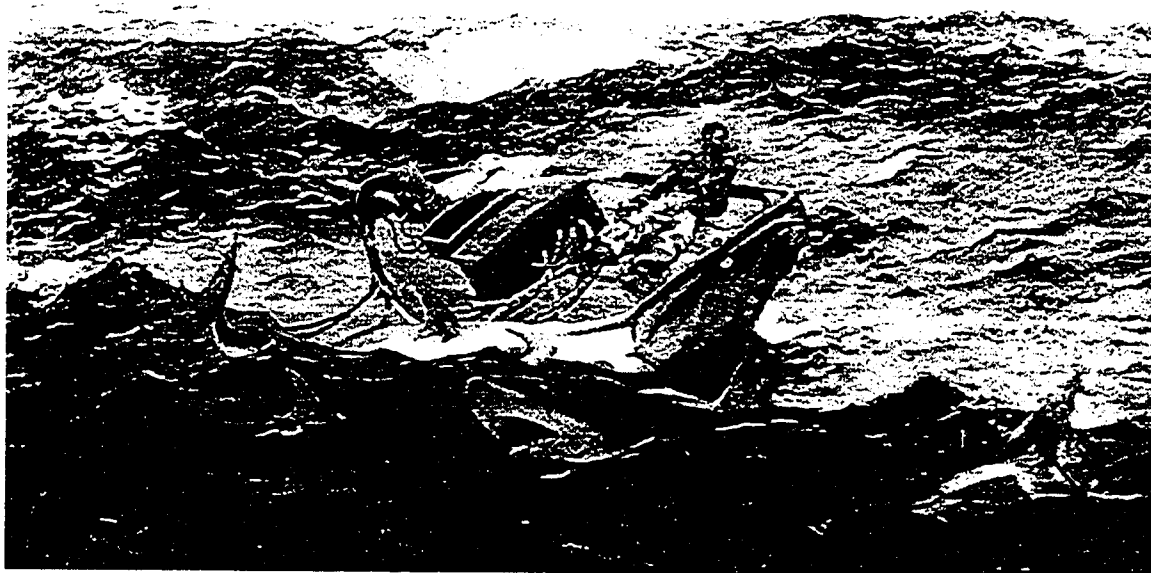
**“It is ever so with the things that a man begins: there is a frost in spring, or a blight in summer, and he fails of his promise. Yet seldom does he fail of his seed, and that will lie in the dust and rot to spring up again in times and places unlooked for.”**

**J.R.R. Tolkien**

Roll on thou deep and dark blue ocean – roll!  
Man marks the earth with his ruin –  
his control stops with the shore

Lord Byron

 OceanWorld



*The Gulf Stream, Winslow Homer (1899)*

# TABLE OF CONTENTS

ABSTRACT.....	i
ACKNOWLEDGEMENTS .....	ii
TABLE OF CONTENTS .....	vi
LIST OF FIGURES .....	ix
LIST OF TABLES .....	xiii
ACRONYMS, ABBREVIATIONS AND TERMS.....	xiv
<b>1. INTRODUCTION.....</b>	<b>1</b>
<i>1.1 Background.....</i>	<i>2</i>
<i>1.2 The World Ocean Circulation Experiment (WOCE) .....</i>	<i>4</i>
<i>1.3 Why Look at Ocean Circulation? .....</i>	<i>5</i>
<i>1.4 Goal and Objectives.....</i>	<i>7</i>
<b>2. Review of Literature on North Atlantic Circulation .....</b>	<b>10</b>
<i>2.1 The North Atlantic Ocean .....</i>	<i>10</i>
2.1.1 Bathymetry.....	10
2.1.2 Fresh Water Inflows and Outflows to the North Atlantic Ocean.....	12
2.1.3 Wind Patterns.....	13
2.1.4 Sea Surface Temperature and Salinity.....	17
2.1.5 The Subtropical and Subpolar Gyres .....	18
2.1.6 Surface Currents.....	20
2.1.6.1 Atmospheric Circulation and the Coriolis Force .....	20
2.1.6.2 Continental Effects.....	22
2.1.7 Equatorial, Western Boundary and Eastern Boundary Currents .....	24
2.1.8 The Deep Ocean Circulation.....	29
2.1.9 The Overall Thermohaline Circulation System in the Atlantic Ocean .....	32
2.1.10 Thermocline and Surface Layer Water Masses .....	33
<i>2.2 What Do We Know?.....</i>	<i>34</i>
<i>2.3 Graphic Display Methods for Ocean Currents.....</i>	<i>35</i>
2.3.1 Vector Representations of Current Flow .....	37
2.3.1.1 The Streamfunction - Definition.....	37
2.3.1.2 The Streamfunction - Streamlines in Time Dependent Flow .....	37
2.3.1.3 Progressive Vector Diagrams in Steady State Flow .....	38
2.3.1.4 Progressive Vector Diagrams in Horizontally Uniform, Time-Variable Flow .....	39
2.3.2 Other Display Methods for Ocean Currents .....	39
2.3.2.1 Current Component Plots.....	40

2.3.2.2	Speed and Direction Plots.....	41
2.3.2.3	Stick Diagrams.....	43
2.3.2.4	Hodographs and Scatter Diagrams.....	44
2.3.2.5	Current Roses.....	45
2.4	Summary.....	47
<b>3.</b>	<b>Attributes of WOCE Data and Surfer7 Methods .....</b>	<b>48</b>
3.1	<i>WOCE Current Meter Dataset for the Atlantic Ocean</i> .....	48
3.1.1	Overview of the WOCE Dataset.....	49
3.1.1.1	WOCE Data Set.....	50
3.1.1.2	Pre-WOCE Data Set.....	54
3.1.1.3	Data Processing at WOCE.....	55
3.1.2	Stranger Format.....	56
3.1.3	Spatial Coverage of Current Meters in the North Atlantic Ocean.....	57
3.2	<i>Surfer7 Gridding Procedures</i> .....	60
3.2.1	Duplicate Data Points.....	60
3.2.2	Appropriate Gridding Methods.....	62
3.2.3	The Use of Exact and Smoothing Interpolators.....	63
3.3	<i>Generation of Maps in Surfer7</i> .....	64
3.3.1	Generation of Vector Plots.....	64
3.3.2	Generation of Contour Maps.....	65
3.3.3	Generation of Wire-Frame Maps.....	65
3.4	<i>North Atlantic Bathymetry</i> .....	66
3.5	<i>Location of WOCE and pre-WOCE Data</i> .....	66
3.6	<i>Preliminary Analysis of Surfer 7.0 Vector Plots</i> .....	69
3.6.1	The Relevance of Anisotropy.....	72
3.6.2	Are We Really Going to Get it Right?.....	73
3.7	<i>A Note on Interpreting Current Flows</i> .....	74
<b>4.</b>	<b>Analytical Results and Visualization of pre-WOCE and WOCE Data .....</b>	<b>75</b>
4.1	<i>Introduction</i> .....	75
4.2	<i>Pre-WOCE Dataset</i> .....	76
4.2.1	Variation in Range of Variables for the pre-WOCE Dataset.....	78
4.2.2	Dynamics of the pre-WOCE Data.....	80
4.2.3	Pre-WOCE Depth Profiles.....	89
4.3	<i>Pre-WOCE Individual Components</i> .....	95
4.3.1	Gulf Stream Extension.....	95
4.3.1.1	Variation in Range of Variables.....	97
4.3.1.2	Dynamics of the Gulf Stream Extension.....	97
4.3.1.3	Gulf Stream Extension Depth Profiles.....	100
4.3.2	Pre-WOCE Low Level Waste Ocean Disposal Program (LLWODP).....	103
4.3.2.1	Variation in Range of Variables.....	105

4.3.2.2 Dynamics of LLWODP .....	107
4.3.2.3 LLWODP Depth Profiles.....	107
4.4 <i>1990's WOCE Data and Patterns in the General Circulation</i> .....	111
4.4.1 Variation in Range of Variables .....	112
4.4.2 WOCE Data Dynamics.....	112
4.4.3 WOCE Depth Profiles.....	125
4.5 <i>Comparison of pre-WOCE and WOCE General Circulation</i> .....	130
4.6 <i>Does River Discharge Affect Current Flow along the Continental Margins?</i> .....	138
4.7 <i>WOCE Data Revisited – A Look at the Annual Mean Circulation in the 1990s</i> ..	142
4.7.1 Mean Current Flows (1990 – 1997).....	142
4.7.2 Shallow Mean Current Flows and the Mean Wind Field (1992 – 1995).....	150
4.8 <i>Eddy Kinetic Energy Flow Data in the North Atlantic Ocean</i> .....	153
4.8.1 Introduction.....	153
4.8.2 Eddy Kinetic Energy Plots.....	158
<b>5. Discussion.....</b>	<b>165</b>
5.1 <i>Regional Patterns</i> .....	165
5.2 <i>The General Circulation</i> .....	168
5.3 <i>Average Temperature Depth Profile and Relation to El Nino</i> .....	170
<b>6. Conclusion .....</b>	<b>172</b>
6.1 <i>Limitations of Research</i> .....	172
6.1.1 Physical Limitations.....	172
6.1.2 Computational Limitations .....	173
6.2 <i>Research Conclusions</i> .....	173
6.3 <i>Future Research</i> .....	174
<b>7. References.....</b>	<b>176</b>
<b>8. Appendices.....</b>	<b>185</b>
8.1 <i>WOCE in the Atlantic Ocean</i> .....	185
8.2 <i>A Note about Rotor Type Current Meters</i> .....	219
8.2.1 The RCM series of current meters.....	219
8.2.2 The vector averaging current meter (VACM) .....	219
8.2.3 Vector measuring current meter (VMCM) .....	220

## LIST OF FIGURES

Figure 1.1 The Geoid (Image obtained from European Remote Sensing satellite, ERS-1 from 780 km (source: <a href="http://www.geoinnovations.com.au/posacc/paspace.htm">www.geoinnovations.com.au/posacc/paspace.htm</a> ) .....	3
Figure 2.1 North Atlantic Ocean Study Region.....	11
Figure 2.2 Oceanic Surface Winds (a) in February, (b) in August (adapted from Gross 1993, p. 107) .....	15
Figure 2.3 Major Ocean Currents of the North Atlantic Ocean (Sources: Fratantoni 2001, Reid 1994, Tomczak and Godfrey 1994, Gross 1993). .....	16
Figure 2.4 Sea-surface temperatures in February (left) and August (right). Note that isotherms are generally parallel to the equator (Source: Gross 1993, pp. 126-127). 18	18
Figure 2.5 A model of an Ekman spiral through a wind-driven current in deep water in the North Atlantic Ocean. Current speeds decrease with increased depth, and water movements in each subsequent layer is shifted over to the right (Source: Gross 1993, p. 161). .....	21
Figure 2.6 – Relationship between wind, surface current and Ekman transport for the North Atlantic Ocean (Source: Gross 1993, p. 161).....	21
Figure 2.7 Continental Effects on Currents .....	23
Figure 2.8 Classic model of the thermohaline circulation due to heating near the equator and cooling towards polar latitudes (Garrison 1996, p. 218).....	30
Figure 2.9 Deep-water masses in the Atlantic Ocean (Source: Kershaw 2000).....	30
Figure 2.10 Atlantic Ocean - Water Masses (Source: adapted from Garrison 1996).....	33
Figure 2.11 Coordinate System used in oceanography.....	36
Figure 2.12 (a) Streamfunction Diagram, (b) Lagrangian Flow (Source: Tomczak and Godfrey, 1994).....	37
Figure 2.13 Diagram to show predicted vs. actual movement (Source: Tomczak and Godfrey, 1994).....	39
Figure 2.14 Different methods of plotting current components (Source: Tomczak and Godfrey, 1994).....	40
Figure 2.15 v- and u-current component plots for Abyssal Circulation, mooring 296 (41.203°N, 63.023°W at 500 meters depth).....	41
Figure 2.16 Speed and Direction plots for Abyssal Circulation, mooring 296 (41.203°N, 63.023°W at 500 meters depth) .....	42
Figure 2.17 Stick Diagram for Abyssal Circulation, mooring 296 (41.203°N, 63.023°W at 500 meters depth). A time-series of sticks laid down incrementally with respect to magnitude and direction.....	43
Figure 2.18 Hodograph plotting three successive current vectors (from Tomczak and Godfrey 1994).....	44
Figure 2.19 Scatter diagram for Abyssal Circulation, mooring 296 (41.203°N, 63.023°W at 500 meters depth).....	45
Figure 2.20 Current Roses for Abyssal Circulation, mooring 296 (41.203°N, 63.023°W at 500 meters depth). (a) Plot of current direction generated in Oriana for Windows. v. 1.06. (b) Plot of current speed vs. current direction generated in SigmaPlot 2000. . 46	46
Figure 3.1 WOCE Current Meter Moorings in the North Atlantic Ocean Categorized by Depth of Current Meter.....	58



Figure 3.2 Three-dimensional representation of North Atlantic Ocean Current Meters located between 30°N and 65°N latitude and 35°W and 75°W longitude (a) Latitudinal View, (b) Longitudinal View .....	59
Figure 3.3 WOCE North Atlantic Ocean Experiments, Sep-89 to Aug-99. Note that the current meter moorings are denoted by elongated tacks, the tops of which indicate latitude/longitude position and the bottom which points to the depth at which the current meter is situated.....	67
Figure 3.4 Current Meter Moorings of Pre-WOCE North Atlantic Ocean Experiments Decadal Averages from April 1974 to August 1984. Note, current meter moorings are denoted by elongated tacks – tops of which indicate latitude/longitude position and bottoms which point to depth at which current meter is situated.....	68
Figure 3.5 Variation in Interpolation of Vector Plots between Polar (angle, length) co-ordinates and Cartesian (x, y) co-ordinates.....	70
Figure 3.6 Variation in Interpolation of Vector Plots by using an Anisotropy Ratio .....	73
Figure 4.1 Variable Plots of Min, Mean, and Max Values for Current Meter Speed ( $\text{cm s}^{-1}$ ) vs. Latitude, Longitude and Depth and for Mean Temperature ( $^{\circ}\text{C}$ ) vs. Depth....	80
Figure 4.2 Pre-WOCE North Atlantic Ocean Components Shallow Water Current Vector Plots recorded from Apr-11-1974 to Aug-12-1984 for depths $\leq 530$ meters.....	82
Figure 4.3 Pre-WOCE North Atlantic Ocean Components Intermediate Depth Water Current Vector Plots recorded from Apr-11-1974 to Aug-09-1984 for depths of 550 to 1,030 meters.....	83
Figure 4.4 Pre-WOCE North Atlantic Ocean Components Deep Water Current Vector Plots recorded from Apr-11-1974 to Sep-03-1984 for depths of 1,200 to 5,430 meters.....	84
Figure 4.5 Pre-WOCE North Atlantic Ocean Components Near-Bottom Water Current Vector Plots recorded from Apr-11-1974 to Sep-03-1984 for depths within 10% of the Seafloor .....	85
Figure 4.6 Interpolated Mean Current Vectors with Location of Current Meter Buoys and ETOPO-5 Bathymetry of the North Atlantic Ocean during the pre-WOCE Study Period of Apr-11-1974 to Sep-03-1984 for Near Bottom Depths .....	86
Figure 4.7 Three-Dimensional pre-WOCE North Atlantic Ocean Components Mean Current Speed Vector Plots for Shallow, Intermediate and Deep Depth Regimes of Figures 4.2 to 4.4 .....	87
Figure 4.8 Three-Dimensional pre-WOCE North Atlantic Ocean Components Mean Current Speed Vector Plots superimposed on Mean Temperature Contour Map for Shallow, Intermediate and Deep Depth Regimes .....	88
Figure 4.9 Pre-WOCE North Atlantic Mean Temperature Depth Profiles vs. Longitude for Moorings sampled between April 11, 1974 and August 28, 1984.....	91
Figure 4.10 Pre-WOCE North Atlantic Mean Temperature Profiles vs. Latitude for Moorings sampled between April 11, 1974 and August 28, 1984.....	92
Figure 4.11 Pre-WOCE North Atlantic Ocean Mean Current Velocity Depth Profiles for Current Meter Moorings sampled between April 11, 1974 and August 28, 1984 (Red square denotes homogeneous water mass – see discussion on page 90) .....	93
Figure 4.12 Site Map for the pre-WOCE Gulf Stream Extension in the North Atlantic Ocean (30°N to 65°N latitude, 30°W to 65°W longitude) showing Bathymetry and Landmasses .....	96

Figure 4.13 Location of Gulf Stream, North Atlantic Current and Gulf Stream Extension (Source: adapted from <a href="http://oceancurrents.rsmas.miami.edu/atlantic/img_topo2/gulf-stream2.jpg">http://oceancurrents.rsmas.miami.edu/atlantic/img_topo2/gulf-stream2.jpg</a> ) .....	96
Figure 4.14 Variable Plots of Min, Mean, and Max Values versus Current Meter Depth for Current Speed ( $\text{cm s}^{-1}$ ) and Temperature ( $^{\circ}\text{C}$ ) .....	97
Figure 4.15 Pre-WOCE Gulf Stream Extension Experiment – Three-Dimensional View of Shallow, Intermediate and Deep Water (10/24/79 – 11/24/80).....	98
Figure 4.16 Pre-WOCE Gulf Stream Extension Component in the North Atlantic Ocean .....	101
Figure 4.17 Pre-WOCE Gulf Stream Extension Component in the North Atlantic Ocean .....	103
Figure 4.18 Pre-WOCE Low Level Waste Ocean Disposal Program (LLWODP) Component in the North Atlantic Ocean – Current Meters Deployed Sep-16-1980 to Sep-03-1984.....	104
Figure 4.19 Variable Plots of Min, Mean, and Max Values for Current Meter Speed ( $\text{cm s}^{-1}$ ) vs. Latitude, Longitude and Depth and for Mean Temperature ( $^{\circ}\text{C}$ ) vs. Depth .....	106
Figure 4.20 Pre-WOCE LLWODP East Experiment Near-bottom Current Vector Plots .....	108
Figure 4.21 Pre-WOCE LLWODP East Experiment Near-bottom Current Vector Plots with Deployment at 2,370 to 5,430 meters depth (09/16/80 – 09/03/84) showing Local Bathymetry.....	109
Figure 4.22 Pre-WOCE LLWODP East Experiment Depth Profiles .....	110
Figure 4.23 Variable Plots of Min, Mean, and Max Values for Current Meter Speed ( $\text{cm s}^{-1}$ ) vs. Latitude, Longitude and Depth and for Mean Temperature ( $^{\circ}\text{C}$ ) vs. Depth	115
Figure 4.24 WOCE North Atlantic Ocean Surface Water Current Vector Plots.....	116
Figure 4.25 WOCE North Atlantic Ocean Shallow Water Current Vector Plots.....	117
Figure 4.26 WOCE North Atlantic Ocean Intermediate Depth Current Vector Plots...	118
Figure 4.27 WOCE North Atlantic Ocean Deep Water Current Vector Plots.....	119
Figure 4.28 WOCE North Atlantic Ocean Near-Bottom Water Current Vector Plots..	120
Figure 4.29 Interpolated Mean Current Vectors with Location of Current Meter Buoys .....	121
Figure 4.30 Three-Dimensional WOCE North Atlantic Ocean Mean Current Speed Vector Plots for Surface, Shallow, Intermediate and Deep Water Depths of Figures 4.24 to 4.27 .....	122
Figure 4.31 Three-Dimensional WOCE North Atlantic Ocean Mean Current Speed Vector Plots superimposed on Mean Temperature Contour Map for Surface, Shallow, Intermediate and Deep Water Depths.....	123
Figure 4.32 WOCE North Atlantic Ocean Depth Profiles of (a) Mean Temperature vs. Longitude and (b) Mean Temperature vs. Latitude for Period Mar-1990 to Aug-1999 .....	128
Figure 4.33 WOCE North Atlantic Ocean Depth Profiles of Mean Current Velocities for (a) Latitude vs. Depth and (b) Longitude vs. Depth for Period Mar-1990 to Aug- 1999 (Note: Longitude vs. Depth plotted using an anisotropy ratio of 3.0 to smooth out the contours) .....	129

Figure 4.34 Comparison of pre-WOCE and WOCE North Atlantic Ocean Current Vector Plots.....	132
Figure 4.35 Comparison of pre-WOCE and WOCE North Atlantic Ocean Current Vector Plots.....	133
Figure 4.36 Comparison of pre-WOCE and WOCE North Atlantic Ocean Current Vector Plots for Deep Water Currents (pre-WOCE depths: 1200 to 5430 meters, WOCE depths: 1108 to 5483 meters).....	134
Figure 4.37 Comparison of pre-WOCE and WOCE North Atlantic Ocean Current Vector Plots for Near-Bottom Water Depth Water Currents.....	135
Figure 4.38 Interpolated Mean Current Vectors with Location of Current Meters and ETOPO-5 Bathymetry of the North Atlantic Ocean during the pre-WOCE and WOCE Study Periods for Near-Bottom Depths .....	136
Figure 4.39 Mean Annual River Discharge into North Atlantic Ocean (based on yearly means calculated over period Jan-1966 to Dec-1984).....	139
Figure 4.40 WOCE North Atlantic Ocean Mean Current Velocity Vectors for Shallow Water showing Relative Magnitude of Mean Fresh Water Discharge from Major Rivers .....	140
Figure 4.41 Temporal and Spatial Distribution of Current Meter Moorings for the WOCE Period of 1990 to 1999 (n = number of current meter moorings).....	144
Figure 4.42 Annual Mean Eulerian Current Speeds in the North Atlantic Ocean (Figure continues over the next three pages, i.e. 145-148 inclusive) .....	145
Figure 4.43 Annual Mean Eulerian Current Speeds for the Western North Atlantic Ocean with Annual Mean Wind Speeds superimposed for Comparison Purposes .....	151
Figure 4.44 Plots of Eddy Kinetic Energy (KE), Energy per Unit Mass of the Mean Flow (KM), and Mean Eddy Momentum Flux (UV) against Depth for the North Atlantic Ocean for pre-WOCE (left) and WOCE (right) Period Datasets.....	155
Figure 4.45 (a) – (c) Pre-WOCE Flow Statistics to January 1989 and WOCE Period Flow Statistics to May 1998 for Shallow, Intermediate and Deep Waters in the North Atlantic Ocean (Shallow = 0 to 500 meters, Intermediate = 500 to 2000 meters, Deep = >2000 meters).....	159
Figure 4.46 Surface Water Flow Statistics of KE, KM, and UV for the pre- and WOCE Periods of Study for Waters that are 0 to 60 meters below mean sea level.....	163

## LIST OF TABLES

Table 1.1 Basic Characteristics of the Atlantic Ocean (Source: Burkov, 1993).....	3
Table 2.1 Contrast between Eastern and Western Boundary Currents (Sources: Garrison 1996, Brown et al. 1989a).....	23
Table 2.2 Things everyone “knew” .....	35
Table 2.3 Things many (some?) people “know” now.....	35
Table 2.4 Data for explanation of progressive vector diagram (Source: Tomczak and Godfrey, 1994).....	38
Table 3.1 Spatial & Temporal Details of WOCE Components.....	50
Table 3.2 Spatial & Temporal Details of pre-WOCE Components.....	55
Table 3.3 Data Summary for WOCE ACM25 Southeast Mooring.....	62
Table 3.4 Synthesized Sample Data.....	69
Table 4.1 pre-WOCE Flow Statistics for Shallow (< 500 meters depth), Intermediate (500 – 2000 meters depth), and Deep (>2000 meters depth) Water.....	153
Table 4.2 WOCE Period Flow Statistics for Shallow (<500 meters depth), Intermediate (500 – 2000 meters depth), and Deep (>2000 meters depth) Water.....	154

## ACRONYMS, ABBREVIATIONS AND TERMS

AABW – Antarctic Bottom Water

AADW – Antarctic Deep Water

AAIW – Antarctic Intermediate Water

ABCIRC – Abyssal Circulation Experiment (northwest Atlantic)

ABW – Arctic Bottom Water

ACCP – Atlantic Climate Change Program (1, 2, 3)

ACM – Atlantic Moorings (1, 6, 7, 8, 10, 11, 27/28, 29)

ACW – Atlantic Central Water

ADCPs - upward-looking current profilers

AIMS - Analysis Interpretation Modeling and Synthesis

AIW – Arctic Intermediate Water

BIO – Bedford Institute of Oceanography moorings

CMDAC - Current Meter Data Assembly Center

Conslx - experiment of the Institute of Oceanographic Sciences

CPW – Circumpolar Water

CTD – conductivity-temperature-depth

DEM – digital elevation model

ETOPO5 - Earth Topography - 5 Minute digital average land and sea floor elevations, assembled from several uniformly gridded data bases into a worldwide gridded data set with a grid spacing of 5 minutes of latitude by 5 minutes of longitude

ITCZ – Intertropical Convergence Zone

LLWODP – Low Level Waste Ocean Disposal Program

LocalDyn – Local Dynamics experiment

Lotus – northwest Atlantic Ocean experiment

MIW – Mediterranean Intermediate Water

NACW – North Atlantic Central Water

NADW – North Atlantic Deep Water

Nares – Subseabed disposal project

Neads – British experiment in North Atlantic

NOAA – National Oceanic and Atmospheric Administration

OSU – Oregon State University

SACW – South Atlantic Central Water

SST – Sea surface temperature

STACS – Subtropical Atlantic Climate Studies

WATTS – Western Atlantic Thermohaline Transport Study

WOCE – World Ocean Circulation Experiment

## 1. INTRODUCTION

Water is the lifeblood of virtually all physical, chemical and biological systems and processes. Estimates show the Earth to be made up of 70 to 75% water, roughly the same proportion as is found in the human body (Wilson 2000). The cyclic flow of water, including the nutrients that are transported with it, is perhaps the most important transportation pathway within living organisms and throughout the physical world.

Mammalian physiology relies on the transport of blood through kilometers of arteries and veins, in order to replenish oxygen supplies and dispose of waste products (Wilson 2000). Similarly, plant physiology is dependent on the pathways provided by xylem and phloem in order to transport water, sugars, and other essential nutrients through the plant. In the physical world, rivers and groundwater are the transportation network of the Earth's water circulation system. Within the oceans, currents are the rivers that circulate water, heat, and nutrients (Garrison 1996). These have been documented since the fourth century B.C., when Pytheas of Massalia recorded a southward flow of water in the Atlantic Ocean just west of the Strait of Gibraltar. He described the flow as part of a large river that was too wide to sail across (Garrison, 1996). This river is now called the Canary Current and is one of many such rivers flowing through the world ocean, which are now known to be currents.

## **1.1 Background**

The World Ocean covers roughly 71% of Earth's surface - 361,060,000 square kilometers, with a mean depth of 3,795 meters. The Atlantic Ocean covers an area of 106,460,000 square kilometers - 30% of the World Ocean and 21% of Earth's surface. has a mean depth of 3,332 meters and a volume of 354,680,000 cubic kilometers - 26% of the World Ocean (Leier 2000, Brown et al. 1989b).

Total volume of the ocean below sea level is much greater than the volume of land above sea level. The mean level of Earth's crust is 2,240 meters below mean sea level (\* see below) with the mean level of the ocean floor being 3,795 meters below mean sea level and the mean level of land being 245 meters above mean sea level. The maximum elevation on the surface of the earth is 8,882 meters above mean sea level, and the lowest elevation on the seafloor is 10,863 meters below mean sea level (Leier 2000, Brown et al. 1989b).

The ocean surface has roughly the same shape as the geoid (Figure 1.1), which is the shape that a stationary, homogeneous water envelope would have if the only forces acting upon it were rotation and gravity (Burkov, 1993). In reality the surface of the ocean deviates from the geoid due to various factors, including the driving effect of wind systems over the ocean surface; atmospheric pressure being unevenly distributed over the ocean surface; and differences between evaporation and precipitation and the mean, depth integrated density of water (Burkov, 1993).

\* Mean sea level is the average height of the sea referenced to a suitable reference surface. With respect to the measurements contained in this thesis we are referring to the level of the sea with all motions, such as wind waves, averaged over a period of time such that changes in sea level also get averaged out. In addition, the changes in sea level at various points in the ocean are so minute relative to the depths of the ocean that a value difference of a few meters is considered not significant.



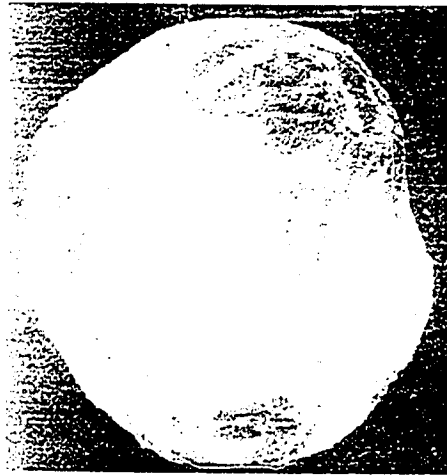


Figure 1.1 The Geoid (Image obtained from European Remote Sensing satellite, ERS-1 from 780 km (source: [www.geoinnovations.com.au/posacc/paspace.htm](http://www.geoinnovations.com.au/posacc/paspace.htm))

Some basic characteristics of the Atlantic Ocean are shown in Table 1.1. The normal range of salinity in the ocean is between 33.00 and 37.00‰, and the total mass of salt is  $4.8 \times 10^{16}$  tons. Temperatures range from  $-2^{\circ}\text{C}$  to  $35^{\circ}\text{C}$ , density falls in the range of 1.02 to 1.06  $\text{g}/\text{cm}^3$  and pressure reaches 1,000 bars or  $10^9$  dynes/cm<sup>2</sup> – approximately 1,000 standard atmospheres (Burkov 1993).

Table 1.1 Basic Characteristics of the Atlantic Ocean (Source: Burkov, 1993)

<b><i>Water Properties</i></b>	<b><i>Mean Values</i></b>
Temperature ( $^{\circ}\text{C}$ )	4.0
Potential temperature ( $^{\circ}\text{C}$ )	3.73
Salinity (‰)	34.90
Anomalies of potential specific volume (cl/ton)	45
Dissolved oxygen (ml/l)	5.26

The Atlantic Ocean is the most heterogeneous of the oceans, however large-scale features in the distribution of temperature, salinity, density and other oceanographic characteristics tend to have a high degree of stability (Tomczak and Godfrey 1994). Burkov 1993 made the assumption that the oceans are generally stationary in the temporal sense, since during the past fifty years there have been no significant changes in the thermal or saline states of the ocean. The reason for this is the continuous circulation of the oceanic water masses that provides the mixing that creates stability.

## ***1.2 The World Ocean Circulation Experiment (WOCE)***

The World Ocean Circulation Experiment (WOCE) is the largest oceanographic experiment ever conducted. One of the primary reasons for undertaking this experiment is to better understand the ocean's role in climate and climatic changes. WOCE is an initiative that brings together scientists from over 30 countries (Chapman 1998). WOCE data was available for proprietary use for the first two years and became available to the general public thereafter. At present there is a large body of data that is in the public domain, as most of the WOCE experiments have gone to completion.

Some of the initial findings of WOCE have revealed large-scale patterns of decadal change rather than the initial assumption of a steady-state ocean. Also evident have been large horizontal and vertical variations in small-scale mixing as opposed to the uniform pattern which has been an underlying assumption in earlier climate models (Grassl, 2001).

The current phase of the WOCE experiment is termed Analysis Interpretation Modeling and Synthesis (AIMS). Due to the large extent of the ocean, and the difficulty in collecting data, the primary challenge is in generating a realistic representation of ocean structure and ocean circulation with the use of a few data measurements, over varying temporal and spatial extents (Lindstrom and Legler 2001).

As opposed to the collection of meteorological data, oceanographic data collection is in its infancy. Therefore the analyses that are a result of this data collection initiative should give a better picture of ocean dynamics.

### ***1.3 Why Look at Ocean Circulation?***

In reading the extensive literature on the general circulation of the ocean, Wunsch 2001 came to the conclusion that the field suffers from a multiple personality disorder, whereby the different personalities don't recognize the existence of the other individuals. Below are some of the personalities he describes.

The descriptive oceanographer's classical ocean describes ocean circulation as large scale, steady and laminar and is derived from ship-based observations between the mid-nineteenth and late-twentieth centuries. A consequence of this view is the idea of a unique general circulation, given in terms of mass instability, with all other changes, such as temperature, calculated as the product of the mean flows and the local, supposed smoothly varying, property distributions (Wunsch, 2001).

The analytical theorist's ocean can be traced to Sverdrup and Stommel, in the 1940s, in which the ocean is viewed as almost-steady, and in which certain features such as the Gulf Stream have nearly set paths. Time variability, as in the view above, is referred to as noise, and indeed there are many similarities between these two views. The field of 'geophysical fluid dynamics', in which geophysical systems are reduced to sufficiently simple terms in order to understand the various dynamical processes, is a representation of the analytical theorist's ocean (Wunsch, 2001). The inherent problem with this view is that the original simplifications are forgotten when analyzing results and the reduced models become confused with the actual system under study.

The observers' highly variable ocean focuses on the components of ocean circulation that are time variable and display strong spatial structures over very short distances of 30 kilometers or less. The emphasis has been on regionally varying elements

and has emerged following studies undertaken in the early 1970s. This view espouses multiple, local general circulations where mean mass fluctuations are thought to be complex spatially varying fields (Wunsch, 2001). Due to the regional focus of this view, the differing general circulations are not woven into a global picture.

Finally, the high-resolution numerical modelers' ocean, which began about 1990, is a basin-to-global scale model containing variability that is similar to the oceanic mesoscale eddy field (Wunsch, 2001). When averaged these results are qualitatively similar to some properties of the above three views, but differ quantitatively from all of them. The changes in the general circulation differ much like the observers' highly variable ocean view.

The main realization of the above four points of view are that little communication exists between these multiple personalities and the literature does not connect these other points of view (Wunsch, 2001).

As a geographer, with no initial biased view on interpreting the general oceanic circulation pattern, this thesis focuses on observing short-term, spatially diverse data gathered from the North Atlantic Ocean, in order to see what these data are telling us. The available data span a time-period of twenty years, with two decadal snapshots of ocean circulation (1974-1984 and 1990-1999), as well as annual means for the period 1990 to 1999. Therefore this analysis is in the short-term time scale of studies, and a bias may very well be that long-term, large-scale, steady patterns cannot be observed or extrapolated from the available data.

As studies progressed in the 1970s it was clear that the actual oceanic flow field differed greatly from the steady, large-scale simple flow field and in fact was dominated

by ‘mesoscale eddies’. A major hypothesis behind much of the World Ocean Circulation Experiment design was that the ocean changes on all space scales from the local to the entire global circulation and on all time scales out to the oceanic lifetime (Wunsch, 2001).

### **1.4 Goal and Objectives**

The goal of this thesis is to plot the available data in order to determine current flow patterns in the North Atlantic Ocean at various depths. Some of the objectives to be pursued are to compare the results of this current mapping to the generalized flows that have been analyzed in the North Atlantic by means of other methods, such as hydrographic profiles, various direct velocity measurements, and satellite-tracked Lagrangian drifters. A comparison of the pre-WOCE dataset collected between 1974 and 1984 with the WOCE -period dataset collected in the 1990s is undertaken to perceive if there are any observable circulation changes.

In looking at variability of ocean currents, the need is to address the temporal and spatial scales of interest. The majority of are hourly, collected from moored current buoys, which has been averaged to provide decadal averages of the general circulation for the two time periods. With respect to the WOCE data of the 1990s, the data was divided into annual mean flows of the circulation to observe any changes over this smaller time scale. It is thought that within these spatial and temporal limits to the study various oceanic meanders and eddies can be discerned, since they are long-term phenomena which ebb and flow, leaving a footprint of their paths within the decadal and yearly mean flows.

The effect of fresh water discharges, primarily from the Amazon River into the North Atlantic Ocean, is briefly touched upon to give some insight of what climate change may have in store for the ocean circulation in the future. In order to add some ancillary data that was collected during the two time periods of study, eddy kinetic energy plots were composed to observe the differences in this parameter between the two decadal averages.

Chapter 2 is a review of the literature pertinent to the North Atlantic Circulation and includes a general overview of the North Atlantic Ocean with respect to bathymetry, freshwater flows, wind patterns, and sea surface temperature and salinity. An introduction to the subtropical and subpolar gyres is presented, as well as a summary of surface currents – including equatorial, western boundary and eastern boundary currents, and finally an overview of deep ocean circulation is presented. A brief chronology on what is “known” about ocean circulation is presented, followed by a review of various graphic display methods that are used for ocean currents.

A preview of the WOCE data for the North Atlantic Ocean is given in Chapter 3, including a breakdown of the pre-WOCE (1974 – 1984) dataset and the WOCE (1990-1999) dataset. Some of the data processing carried out by the Current Meter Data Assembly Center at Oregon State University is described, as are the data preparation and processing that was necessary to be carried out in this study before any analysis was possible. An introduction and analysis of the suitability of Surfer7 as the mapping tool for this thesis is carried out, followed by a discussion of how the various output maps were produced.

Analytical results and visualizations of the pre-WOCE and WOCE data are presented in Chapter 4. Current vector plots and depth profiles are created for each of the pre-

WOCE and WOCE decadal averaged data, as well as for two sub-sample study sites – one along the Gulf Stream Extension and the other in the Hatteras Abyssal Plain with regards to the Low Level Waste Ocean Disposal Program (LLWODP). A comparison of the pre-WOCE and WOCE decadal averages is undertaken, followed by a discussion on the effects of river discharges on the current flow. The WOCE data are revisited with a look at the mean annual circulation throughout the 1990s, including mean current flows from 1990 to 1997, and surface mean current flows combined with the mean wind field from 1992 to 1995. The results conclude by mapping the flow statistics, such as eddy kinetic energy, for both the pre-WOCE and WOCE datasets.

Chapter 5 is the discussion focusing on regional patterns, the general circulation and the average temperature depth profile and its relationship to El Nino. The conclusions follow in Chapter 6 with a description of the limitations of this research, thesis conclusions, and areas for future research. A list of references comprise Chapter 7, and the appendices follow in Chapter 8 with a detailed breakdown of the pre-WOCE and WOCE datasets and a brief note about rotor type current meters.

## **2. Review of Literature on North Atlantic Circulation**

This chapter begins by taking a detailed look at the regional geography and hydrology of the North Atlantic Ocean, and the various currents lying in the study area. Particular attention is paid to bathymetry, wind patterns, surface currents, deep ocean water masses, sea surface temperature and salinity. An overview of what we know, or perhaps what we think we know follows. Finally some of the graphical display methods that are used in ocean current analysis are introduced.

### ***2.1 The North Atlantic Ocean***

#### **2.1.1 Bathymetry**

The Atlantic Ocean extends from the Bering Strait in the Arctic through the Southern Ocean to the Antarctic continent, a distance of over 21,000 kilometers. Its largest zonal distance spans from the Gulf of Mexico to the coast of northwest Africa, a distance of approximately 8,300 kilometers (Leier 2000). The Atlantic Ocean contains a number of neighbouring seas, including the Mediterranean, Caribbean, North and Baltic Seas, the Gulf of Mexico, and the seas comprising the Arctic region. It is also divided into a number of eastern and western basins by the Mid-Atlantic Ridge, which has a strong influence on deep-water circulation (Figure 2.1)



# North Atlantic Ocean Study Region

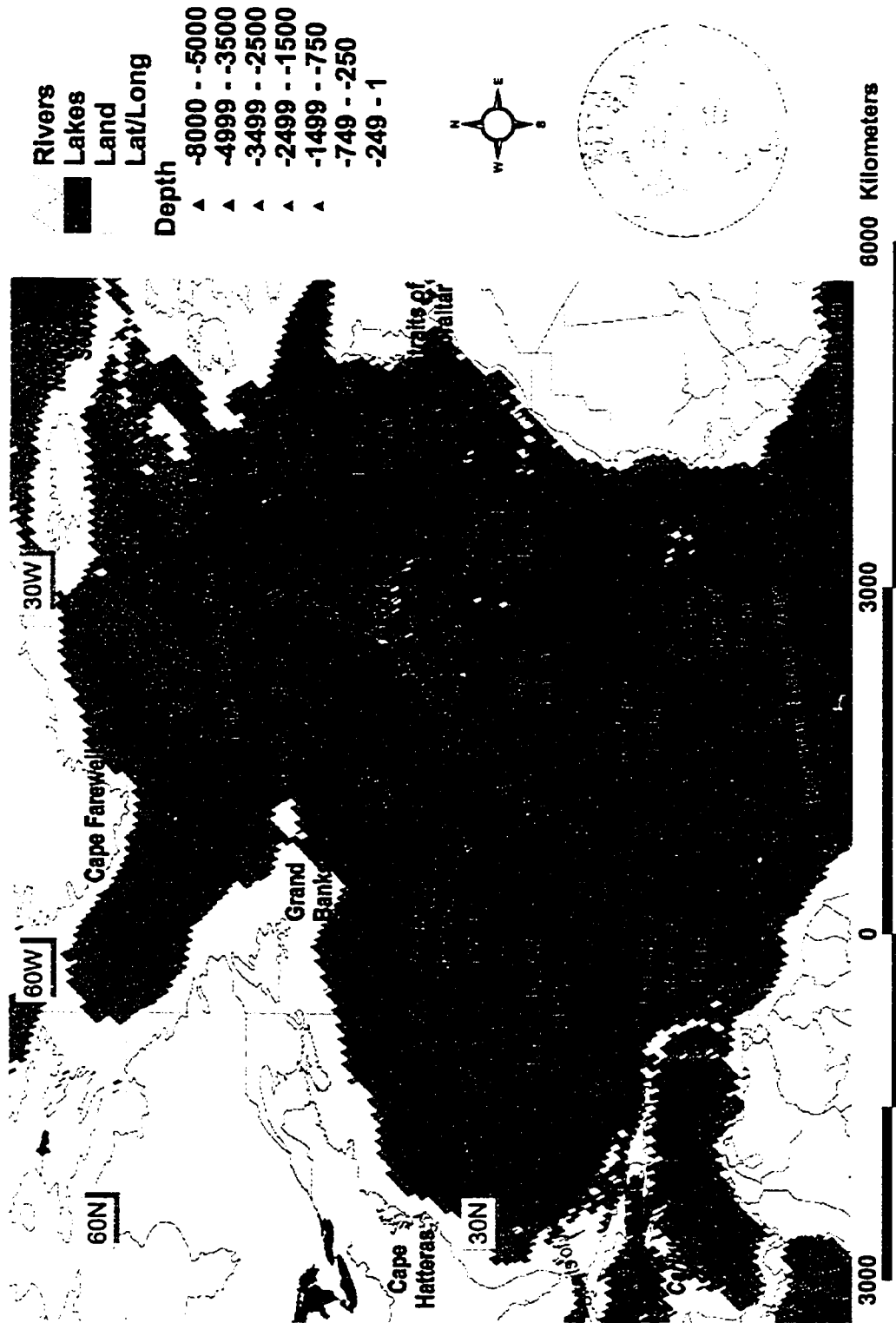


Figure 2.1 North Atlantic Ocean Study Region  
 (Sources: Digital bathymetry is ETOPO5 topographical data for NOAA, place names obtained from Fratantoni 2001, and Leier 2000)

Including its neighbouring seas, the Atlantic Ocean encompasses an area greater than 106 million square kilometers. The Atlantic Ocean's abyssal basins extend beyond 5,000 meters below mean sea level with most being deeper than 6,000 meters in their deepest areas (Figure 2.1). However, the Atlantic Ocean has a mean depth of only 3,300 meters, due to its neighbouring seas and continental shelf zones making up over 13% of its surface area.

Some topographic features of note that pertain to oceanic circulation are the presence of the Romanche Fracture Zone (Figure 2.1), located about 20 kilometers north of the equator, which allows water to pass between the western and eastern deep basins at around 4500 meters depth. This is the first chance for southern flowing water to circumvent the Mid-Atlantic Ridge barrier (Garrison 1996, Tomczak and Godfrey 1994). Another feature is the Gibbs Fracture Zone (Figure 2.1) situated around 53°N which allows the passage of Arctic Bottom Water at 3,000 meters. In the South Atlantic Ocean there is a large difference in depth near 30°S, east and west of the Mid-Atlantic Ridge. West of the Mid-Atlantic Ridge, the Rio Grande Ridge rises to 650 meters, while west of this the Rio Grande Gap, running adjacent to the 40°W meridian, permits the flow of deep water near 4,400 meters. East of the Mid-Atlantic Ridge, the Walvis Ridge blocks flow at 4,000 meters (Garrison 1996, Tomczak and Godfrey 1994).

### **2.1.2 Fresh Water Inflows and Outflows to the North Atlantic Ocean**

Precipitation shows wide variability over the Atlantic Ocean with a minimum of roughly 10 centimeters per year in the subtropics near St. Helena and the Cape Verde Islands and a maximum upwards of 200 centimeters per year in the tropics along the ITCZ along 5°N (Tomczak and Godfrey 1994). There is a secondary stretch of high

precipitation that follows the path of the Westerly storm systems from Florida to Ireland, Scotland, and Norway. This totals 100 to 150 centimeters per year with the majority occurring during the summer near Florida, and during the winter near Europe (Tomczak and Godfrey 1994).

There is still much to learn about the mechanism of the water cycle over the ocean, however one known fact is that evaporation is far less variable than precipitation (Schmitt 1996). The ITCZ is a region of positive precipitation-evaporation (P-E) values, as is the strip of high rainfall mentioned above (Xie and Arkin 1996, Trenberth and Guillemot 1995, Tomczak and Godfrey 1994). The effect on sea surface salinity is lessened by the large drainage area of the Atlantic Ocean, where many of the world's largest rivers empty either directly into the Atlantic Ocean – the Amazon, Orinoco, Rhine, Niger and Congo Rivers, or into its adjacent seas – the Mississippi, St. Lawrence, Nile, Ob, Jenisej, Lena and Kolyma Rivers (Vorosmarty et al. 1998). The overall contribution of freshwater flux from the rivers to the Atlantic Ocean is not enough to balance the low level of rainfall over the sea surface (Tomczak and Godfrey 1994).

### **2.1.3 Wind Patterns**

There is great seasonal variation in winds in the northern hemisphere due to the presence of the Siberian and North American landmasses and their impact on air pressure distribution (Figure 2.2). During the northern hemisphere winter there are strong westerly winds due to the presence of the subtropical high pressure belt running from Bermuda across the Canary Islands, Azores, and Madeira and continuing across the Sahara and the Mediterranean Sea into central Siberia (Garrison 1996, Summerhayes and Thorpe 1996, Briggs et al. 1993, Gross 1993, Bishop 1984). The winds are a result of the flow from this

high towards the low pressure area lying between Iceland and Greenland, the Icelandic Low (Garrison 1996, Gross 1993). In the northern hemisphere summer the high pressure cell migrates northward and is centered near the Azores, the Azores high, and has more moderate winds. When this cell migrates westward it is termed the Bermuda High (Garrison, 1996, Gross 1993).

In the Atlantic Ocean, the position of the Intertropical Convergence Zone (ITCZ) varies (Figure 2.2) from a location along the equator during the northern hemisphere winter to about 7°N near Sierra Leone during the northern hemisphere summer (Garrison 1996, Gross 1993, Bishop 1984). One of the results of this migration of the ITCZ is that the Northeast Trade Winds are stronger during the winter months (Garrison 1996, Tomczak and Godfrey 1994, Gross 1993).

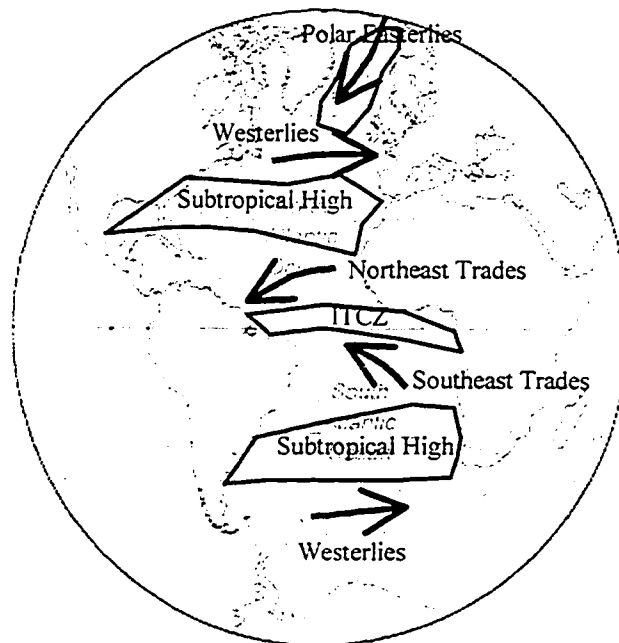
The wind stress distribution in the North Atlantic Ocean (Figure 2.2) consists of the following major wind systems (Garrison 1996, Gross 1993):

1. The aforementioned Northeast Trade Winds sandwiched between the ITCZ and the North Atlantic Subtropical High;
2. The Westerlies to the north of the Subtropical High, carrying cold, dry air over the Gulf Stream and veering to a north-easterly direction in the eastern North Atlantic Ocean;
3. The Polar Easterlies which originate over the Arctic and move in a south-westerly direction.

Additional phenomena of the North Atlantic Ocean are the presence of two areas that are under the influence of seasonal wind reversals. One is located along the African coastline from Senegal to the Ivory Coast and another off Bermuda. The east coast of

North America experiences seasonal change in wind direction with offshore winds during the bulk of the year and warm alongshore winds during the summer (Garrison 1996, Summerhayes and Thorpe 1996).

(a)



(b)

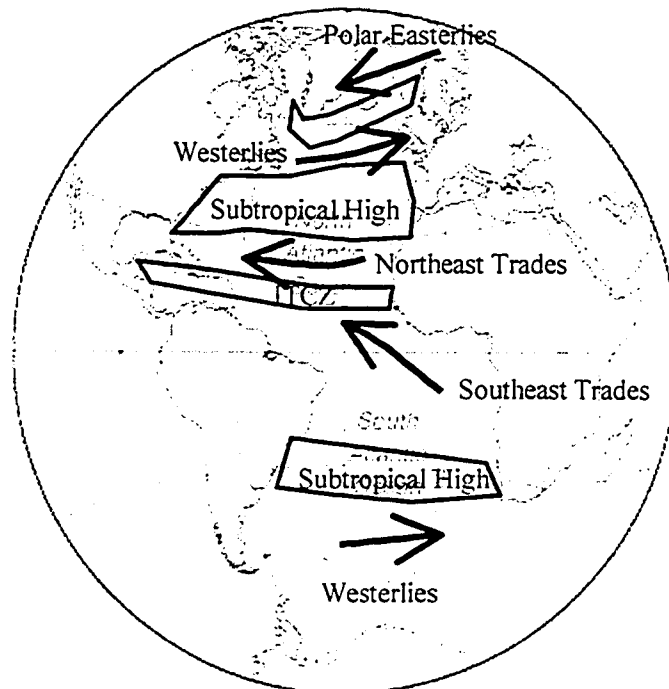


Figure 2.2 Oceanic Surface Winds (a) in February, (b) in August (adapted from Gross 1993, p. 107)

# Major Ocean Currents of the North Atlantic Ocean

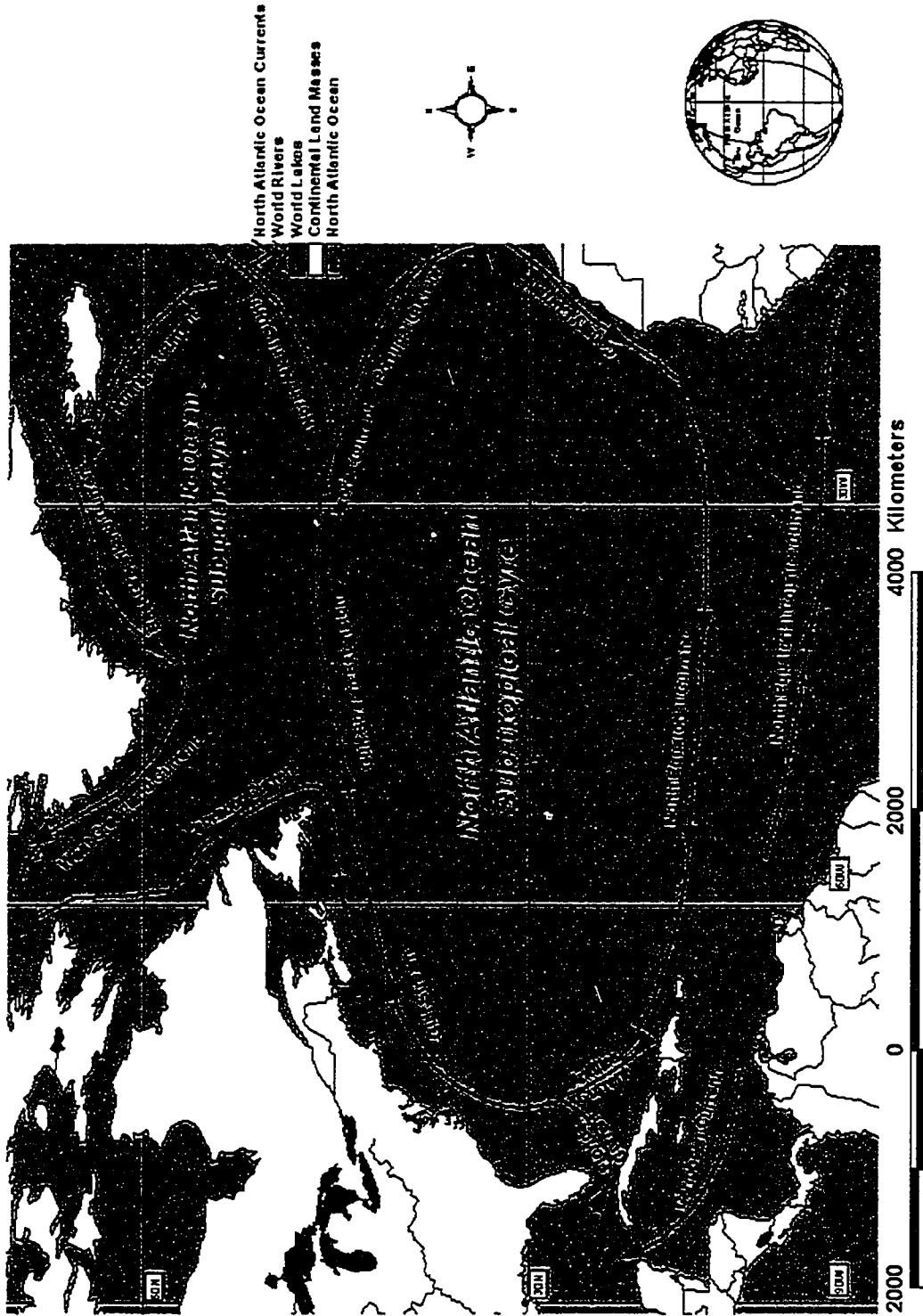


Figure 2.3 Major Ocean Currents of the North Atlantic Ocean (Sources: Fratantoni 2001, Reid 1994, Tomczak and Godfrey 1994, Gross 1993).

#### 2.1.4 Sea Surface Temperature and Salinity

North of the Westerlies, sea surface salinity decreases due to an influx of freshwater from glaciers and icebergs, the low salinity area is centred in the western North Atlantic (Tomczak and Godfrey 1994, Briggs et al. 1993, Bowden 1983). This salinity decrease is concurrent with advection by the East and West Greenland Currents and the Labrador Current (Rudels et al. 1999). Along the Polar Front, at the boundary between the Labrador Current and the Gulf Stream, a sharp salinity increase is found (Rudels et al. 1999).

In the subtropics, highly saline water is carried west with the North Equatorial Current (Figure 2.3) and the salinity increases due to constant evaporation along the track of the current (Schmitz and McCartney 1993). Due to mixing with less saline water from the North Brazil, Guyana, and Antilles Currents, high surface salinity water does not reach the American coastal shelf (Tomczak and Godfrey 1994, Borstad 1982). This is the water that is redirected towards the Gulf Stream and therefore is unavailable for mixing with waters that lie to the east. The result is that some of the highest salinity water, not including any of the adjacent seas, is found in the area of the Canary and North Equatorial Currents (Tomczak and Godfrey 1994, Mittelstaedt 1991)

With regard to sea surface temperature (SST), the thermal equator is located at roughly 5°N, coinciding with the ITCZ extending northwards in the western Atlantic into the Gulf of Mexico (Kershaw and Cundy 2000, Gross 1993). The narrow strip of the ITCZ is a region of weak and variable winds with annual mean sea surface temperatures over 27.0°C over most of the region (Kershaw and Cundy 2000, Gross 1993).

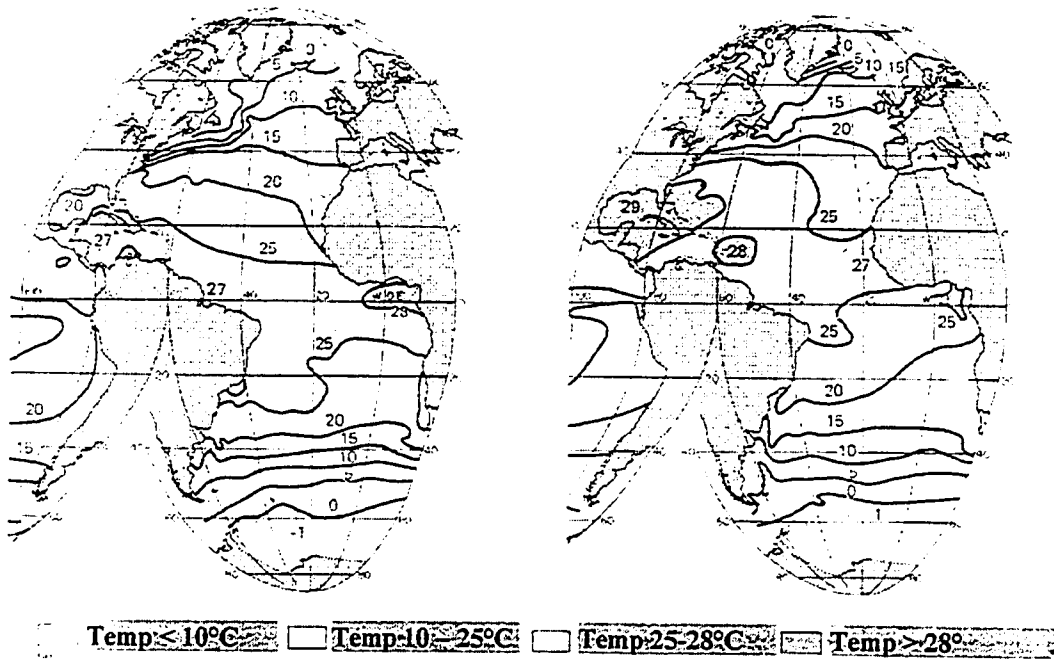


**Figure 2.4** Sea-surface temperatures in February (left) and August (right). Note that isotherms are generally parallel to the equator (Source: Gross 1993, pp. 126-127)

A major characteristic of the sea surface temperature distribution (Figure 2.4) is the departure from a zonal distribution and the subsequent crowding of isotherms along the Polar Front in the North Atlantic Ocean (Garrison 1996, Gross 1993). Temperature variation between the shelves off Newfoundland and France is about 8°C (Tomczak and Godfrey 1994). In the North Atlantic Ocean there is a large deviation from an east-west isotherm track which is supplemented by Arctic water exchange (Cuny et al. 2002, Tomczak and Godfrey 1994). The 5°C isotherm and the 35‰ isohaline are oriented across the North Atlantic from roughly 45°N near Newfoundland to about 72°N off of Spitsbergen (Tomczak and Godfrey 1994).

### 2.1.5 The Subtropical and Subpolar Gyres

The Atlantic Ocean shows the largest variations between fields of flow as determined from both wind stress and conductivity-temperature-depth (CTD) data (Huthnance et al.



2002, Bigg and Wadley 2001, Clarke et al. 2001, Chapman and Maslin 1999, Doscher et al. 1994, Foreman 1990).

Previous work has shown the presence of a strong subtropical gyre, and a weaker subpolar gyre in the North Atlantic Ocean (Cunningham 2000, Reid 1994, Schmitz and McCartney 1993, Greatbatch et al. 1991). The subtropical gyre flows clockwise and is composed of the North Equatorial Current centered around 15°N, the Antilles Current, and Caribbean Current, the Florida Current, the Gulf Stream, the Azores Current, and finally the Portugal and Canary Currents (Figure 2.3). The subpolar gyre does not resemble a typical gyre due to the presence and effect of the Arctic circulation upon it (Garrison 1996, Reid 1994, Tomczak and Godfrey 1994, Schmitz and McCartney 1993). This effect forces a circulation that flows around southern Greenland and along the Labrador coast and is therefore less completely defined. The gyre itself rotates counter-clockwise and is made up of the North Atlantic Current, the Irminger Current, the East and West Greenland Currents, and the Labrador Current (Figure 2.3). There is a large amount of water exchange with the Arctic Seas through the North Atlantic Current and the East Greenland Current (Figure 2.3).

Near the equator there is an equatorial counter current lying between the North and South Equatorial Currents flowing parallel to the ITCZ (Figure 2.3). This current is wide and of moderate intensity owing to the small zonal width of the Atlantic Ocean as compared to the Pacific Ocean, and that the ITCZ is not zonal per se, but flows obliquely from Sierra Leone to Brazil.

## 2.1.6 Surface Currents

Forces responsible for driving surface currents include (i) prevailing winds, or more specifically the wind stress (a frictional force), which causes the formation of waves and wind drift currents – typically at 3% of the wind speed; (ii) the Coriolis Force, which causes currents in the northern hemisphere to deflect clockwise, and develop Ekman spirals; (iii) the pressure gradient, both the hydrostatic pressure gradient which at any depth is equal to the weight of the water acting on a unit of area, and the horizontal pressure gradient, which is balanced by the Coriolis force and results in the formation of geostrophic currents; (iv) density variations, particularly barotropic and baroclinic conditions, and (v) continental margins, which deflect and redirect currents (Kershaw 2000, Brown et al, 1989a).

### *2.1.6.1 Atmospheric Circulation and the Coriolis Force*

Prevailing winds cause waves that form surface ocean currents in a particular direction. This produces strong equatorial currents due to the prevailing trade winds and mid-latitude easterly currents because of the prevailing westerly winds. Ocean currents in the northern hemisphere are deflected to the right of their path of motion by the Coriolis force and form Ekman spirals, Figures 2.5 and 2.6 (Knauss 1997, Garrison 1996). This causes ocean currents to spiral toward the right with increasing water depth while the current velocities decrease. At greater depths, surface ocean currents eventually subside as they lose momentum. Due to large-scale Coriolis effects, the Trade winds push surface water to the west and north while the mid-latitude westerlies push water east and south (Garrison 1996, Stommel and Moore 1989). The result is a wide column of water near 30° latitude between the two wind belts. As this column builds, a pressure gradient is

formed which causes water to be deflected by the Coriolis force, and to flow in the same direction as the prevailing winds on either side of the column (Garrison 1996).

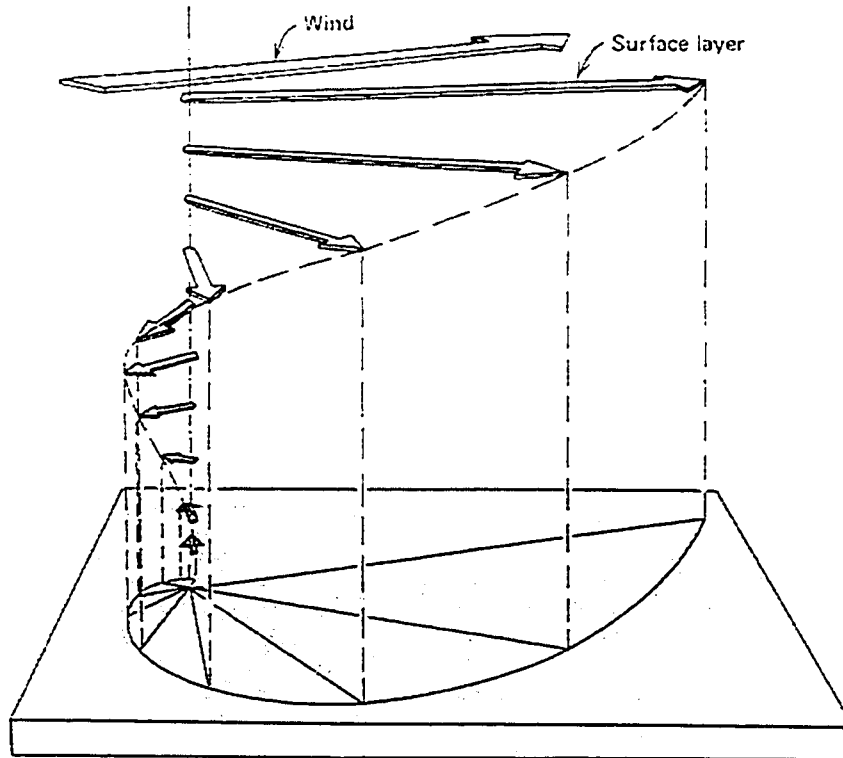


**Figure 2.5** A model of an Ekman spiral through a wind-driven current in deep water in the North Atlantic Ocean. Current speeds decrease with increased depth, and water movements in each subsequent layer is shifted over to the right (Source: Gross 1993, p. 161).

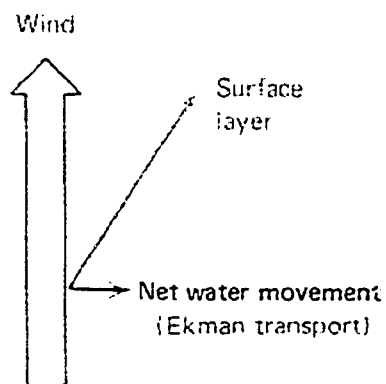


**Figure 2.6** – Relationship between wind, surface current and Ekman transport for the North Atlantic Ocean (Source: Gross 1993, p. 161)

### *2.1.6.2 Continental Effects*

Westward flowing currents eventually collide with continental barriers and are predominately deflected northward in the northern hemisphere by the Coriolis effect (Garrison 1996, Brown et al. 1989a). The result is the formation of Western Boundary Currents (Figure 2.4), of which the Gulf Stream is a prime example. The Gulf Stream is a warm, saline meandering current approximately one hundred kilometers wide and one kilometer in depth (Summerhayes and Thorpe 1996, Brown et al. 1989a). Water speeds within the current are typically in the range of 5 kilometers per hour (Fratantoni 2001). The Gulf Stream carries warm water to the North Atlantic and has high salinity, which aids in the formation of North Atlantic Deep Water (NADW). Some water is also deflected southward towards the equator where it meets similar northward flowing water from the southern hemisphere (Fratantoni 2001, Garrison 1996). These currents merge and form Equatorial Counter-Currents, which slowly flow eastward in the Doldrums (Figure 2.7).

In the mid-latitudes, eastward flowing currents under the influence of prevailing westerlies also collide with continental barriers and are deflected primarily toward the south in the northern hemisphere. These groups of currents are labeled the Eastern Boundary Currents (Figure 2.7).

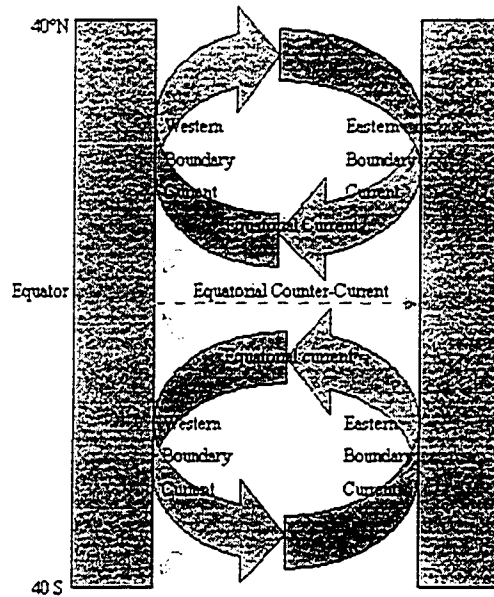


Figure 2.7 Continental Effects on Currents

Table 2.1 contrasts the differences between Eastern and Western Boundary Currents. In general, Eastern Boundary Currents are much wider, shallower, slower and transport smaller volumes of water as opposed to Western Boundary Currents (Garrison 1996, Gross 1993).

Table 2.1 Contrast between Eastern and Western Boundary Currents (Sources: Garrison 1996, Brown et al. 1989a).

	<i>EASTERN BOUNDARY CURRENT</i>	<i>WESTERN BOUNDARY CURRENT</i>
<b>Width</b>	Broad ~ 1000 km.	Narrow < 100 km.
<b>Depth</b>	Shallow < 500 meters	Deep ~ 2 km.
<b>Transport</b>	Slow - 10's of km per day	Fast - 100's of km per day
<b>Volume</b>	Small - 10-15 million m <sup>3</sup> /s	Large ~50 million m <sup>3</sup> /s

### 2.1.7 Equatorial, Western Boundary and Eastern Boundary Currents

The equatorial current system shows a banded pattern with the Equatorial Undercurrent being the strongest, transporting upwards of 15 Sverdrups (Sv), where one Sv =  $10^6 \text{ m}^3 \text{ s}^{-1}$ , with speeds greater than  $1.2 \text{ m s}^{-1}$  at about 100 meters depth (Fratantoni 2001, Cunningham 2000, Reid 1994). This current is stronger in the west and weakens due to frictional losses to its surroundings. Its flow oscillates once every two to three weeks around 90 kilometers either side of the equator, its speed ranges from  $0.6 \text{ m s}^{-1}$  to  $1.2 \text{ m s}^{-1}$ , and its transport capacity extends from 4 to 15 Sv (Schmidt et al. 2001, Cunningham 2000). The Equatorial Undercurrent is revealed by conductivity, temperature, and pressure (CTD) profiles through the vertical spreading of isotherms in the thermocline (Schmidt et al. 2001, Cunningham 2000).

The North Equatorial Current, North Equatorial Counter Current, and South Equatorial Current dominate the surface flow near the equator. The North Equatorial Current is found north of  $10^\circ\text{N}$ ; it has a broad and uniform westward flow with speeds ranging from  $0.1$  to  $0.3 \text{ m s}^{-1}$  (Stramma and Schott 1999). The North Equatorial Counter Current flows eastward from about  $3^\circ\text{N}$  to about  $15^\circ\text{S}$ , has speeds similar to the North Equatorial Current, and mixed together with eastward flow at the surface and below the thermocline (Stramma and Schott 1999). The North Equatorial Under Current is a narrow, fast current with speeds reaching  $0.4 \text{ m s}^{-1}$  near 200 meters depth (Schmidt et al. 2001).

An important characteristic of the equatorial circulation is the powerful cross-equatorial transport in the North Brazil Current along the coast of South America. Twelve Sv of the 16 Sv carried by the South Equatorial Current across  $30^\circ\text{W}$  cross the equator

(Schott et al. 1998, Stramma et al. 1995), this is comparable to the 15 Sv which are required to supply the NADW source in the North Atlantic Ocean. Little hemispheric exchange takes place in the eastern equatorial zone of the Atlantic Ocean (Fratantoni 2001, Reid 1994).

Geographically, the North Equatorial Counter Current is blocked from flowing north by the east to west orientation of the African coast (Figure 2.3). Its flow increases to a speed of  $0.4 \text{ m s}^{-1}$  near the Ivory Coast and its energy is dispersed in the Gulf of Guinea (Zhang et al. 2003). A small portion of its flow manages to reach northward and combines with the North Equatorial Under Current to power a small cyclonic gyre centered at  $10^{\circ}\text{N}$ ,  $22^{\circ}\text{W}$  (Schmidt et al. 2001).

The most powerful of the western boundary currents is the Gulf Stream, which was originally thought to flow out of the Gulf of Mexico (Fuglister 1951, Iselin 1936). The Gulf Stream is a system which incorporates the Florida Current, the Gulf Stream itself, the Gulf Stream Extension, the North Atlantic Current and the Azores Current.

The Florida Current is primarily supplied by the North Equatorial Current passing through the Yucatan Strait, and partly by the North Brazil Current. Through the Florida Strait the current transports 30 Sv with a maximum speed of  $1.8 \text{ m s}^{-1}$  (Wilson and Johns 1997). The current breaks away from the coastal shelf some 1,200 kilometers downstream near Cape Hatteras, where it attains a transport of 70 to 100 Sv (Reid 1994, Hogg 1992). The Gulf Stream itself flows across the North Atlantic Ocean as a free inertial jet for the next 2,500 kilometers reaching a maximum transport of 90 to 150 Sv near  $65^{\circ}\text{W}$  (Fratantoni 2001, Reid 1994). From here water is steadily lost to the Sargasso Sea recirculation with transport being reduced to 50 to 90 Sv near the Grand Banks at

about 50°W (Reid 1994, Hall and Fofonoff 1993). Throughout the length of the Gulf Stream, current speed is predominately swift at the surface and decreases fairly quickly with depth, with flow often extending to the ocean floor (Fratantoni 2001, Reid 1994).

East of 50°W the Gulf Stream Extension diverges into three distinct flows: The North Atlantic Current continuing northeast towards Scotland transports about 30 Sv from the subtropical gyre to fuel the Norwegian Current, and ultimately replenishes Arctic Bottom Water (Rossby 1996, Reid 1994); The Azores Current, which is part of the subtropical gyre, carrying about 15 Sv between 35° to 40°N where it feeds the Canary Current (Cromwell et al. 1996); The remaining water is returned to the Florida Current and Gulf Stream by way of the Sargasso Sea recirculation system (New et al. 2001, Schmitz and McCartney 1993, Halliwell et al. 1991).

When free inertial jets, such as the Gulf Stream, make their way into the open ocean they become unstable forming meanders that separate as eddies. Two types of eddies are associated with the Gulf Stream – north of the Gulf Stream anticyclonic, warm-core eddies are formed, while south of the Gulf Stream cyclonic, cold-core eddies are formed (Garrison 1996, Gross 1993, Brown 1989a). Most of these rings are formed in the Gulf Stream Extension and flow back against the main current. Rings to the south of the Gulf Stream dominate the Sargasso Sea recirculation and are responsible for the region having a high level of eddy kinetic energy (Tomczak and Godfrey 1994).

The pressure gradient associated with the Gulf Stream is due to a 0.5 meter drop in sea level across the current towards the coast and temperature differences corresponding to a thermocline rise of approximately 500 meters (Garrison 1996, Tomczak and Godfrey 1994). The Gulf Stream is an important heat sink for the ocean,



with net annual mean heat loss exceeding  $200 \text{ W m}^2$  (Frankignoul et al. 2001). This is primarily due to advection of cold dry continental air originating from the west. Alternatively, the Gulf Stream undergoes a period of net heat gain from late May to August due to the advection of warm saturated southerly air (Frankignoul et al. 2001, ).

The western boundary current of the subpolar gyre is the Labrador Current, which receives a large amount of Arctic water from the East Greenland Current (Rudels et al. 2002). Speeds for the combined flow of the East Greenland and Irminger Currents south of Cape Farewell approach  $0.3 \text{ m s}^{-1}$  on the shelf and at depths of 2,000 to 3,000 meters, while slowing down to roughly  $0.15 \text{ m s}^{-1}$  at the surface (Cuny et al. 2002, Fratantoni 2001, Reid 1994). These currents, like all western boundary currents, extend to the ocean floor. The Labrador Current shows its greatest transport capabilities in February by carrying roughly 6 Sv more water than it does in the month of August (Reynaud et al. 1995, Lazier and Wright 1993). Current variability is much greater in the winter months with a standard deviation of 9 Sv as opposed to only 1 Sv in the summer.

The North Brazil Current and Guyana Current form another western boundary current system along the east coast of South America and play an important role in global heat transport. Studies have shown that the North Brazil Current is a jet-like boundary current with speeds of  $0.8 \text{ m s}^{-1}$  (Johns et al. 2002, Fratantoni 2001). Recent studies have raised doubts as to whether the Guyana Current and the Antilles Current exist as permanent currents . However, flow from the North Equatorial Current is connected to the Florida Current by some northwest movement of water. Therefore the Guyana and Antilles Currents must somehow play a role in this transport (Johns et al. 2002, Fratantoni 2001).

Circulation in the eastern margin of the North Atlantic Ocean is a result of the Canary Current, a broad, moderately flowing current in which the temperate waters of the Azores Current are transformed into the subtropical water supplying the North Equatorial Current (New et al. 2001, Stramma and Muller, 1989). Water temperatures in the eastern North Atlantic have comparatively lower temperatures than their counterparts in the western North Atlantic (Garrison 1996, Tomczak and Godfrey 1994). From the Cape of Good Hope at the southern tip of Africa to near the equator, and from Spain to 10°N, winds along the eastern shores are responsible for coastal upwelling which brings cooler waters to the surface (Tomczak and Godfrey 1994). Geostrophic eddies are commonplace in the eastern North Atlantic and are responsible for producing current reversals (Tomczak and Godfrey 1994).

The Canary Current upwelling system is characterized by strong seasonal variability and a large disparity between northern and southern waters (Mittelstaedt 1991, Bishop 1984). In absolute terms, the width of the upwelling region is fairly narrow, however in comparative terms, it is wider than the adjoining continental shelf (Tomczak and Godfrey 1994). Previous studies have indicated offshore flow to a depth of about 30 meters, intermediate flow towards the equator, and a deeper layer of onshore flow, all occurring in a region with a mean depth of 60 to 80 meters (Zhou et al. 2000, Mittelstaedt 1991).

In winter, when the Trade Winds are at their strongest, upwelling in the Canary Current reaches its furthest southern extent (Verstraete 1992). The Canary Current eventually turns westward and intersects a cyclonic circulation of water around the Guinea Dome (Figure 2.3). This is the boundary between North Atlantic and South Atlantic Central Water (Figure 2.9), constituents of the thermocline (Schmidt et al. 2001,

Tomczak and Godfrey 1994). South Atlantic Central Water has comparatively low salinity compared to its neighbouring water masses, and is transported poleward along with the surface current located along coastal Mauritania (Schmidt et al. 2001).

### **2.1.8 The Deep Ocean Circulation**

The thermohaline circulation is the mechanism whereby deep, cold, saline waters are moved around the global oceans (Figure 2.8). Changes in both water temperature and salinity alter water mass density, causing a vertical movement until water masses of comparable densities meet (Kershaw and Cundy 2000, Garrison 1996, Gross 1993, Brown et al. 1989a). Due to cooling and/or increased salinity, water masses at the ocean's surface become denser. In the process of maintaining stable density stratification, these dense masses sink. Thermohaline circulation affects water in the deep oceans below the zone of surface ocean circulation, producing nutrient-rich waters that rise to the surface during upwelling (Kershaw and Cundy 2000, Garrison 1996, Gross 1993, Brown et al. 1989a).

The Atlantic Ocean has the most heterogeneous composition of all the world's oceans, primarily due to mixing with its adjacent seas, especially those in the Arctic and the Mediterranean Sea (Leier 2000, Brown et al. 1989b). Antarctic Bottom Water (AABW) comprises Atlantic Ocean water at depths below 4,000 meters (Figure 2.6). Originating from the Circumpolar Current, AABW moves northward both east and west of the Mid-Atlantic Ridge (Garrison 1996, Tomczak and Godfrey 1994). On the eastern flank it is blocked by the Walvis Ridge, however on the western edge of the ridge it flows into the western hemisphere past 50°N (Tomczak and Godfrey 1994). Temperatures increase northward from the Southern Ocean to the Labrador Basin due to the effect of

thermal diffusion produced by mixing with warmer overlying waters in the tropics and subtropics.

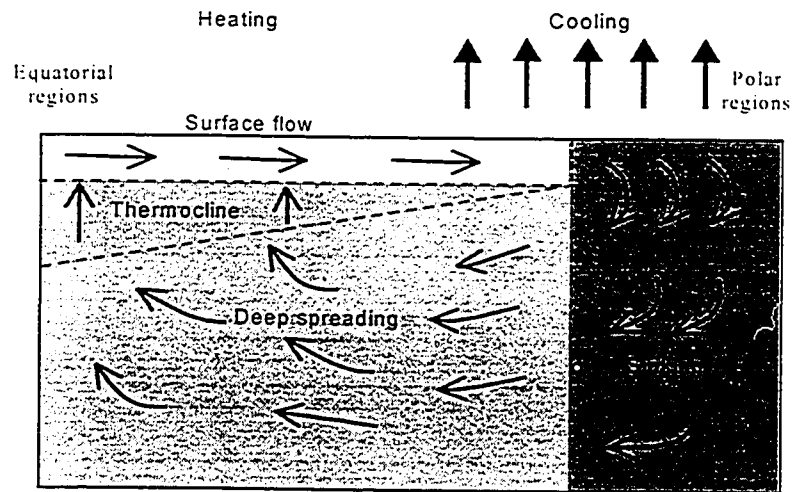


Figure 2.8 Classic model of the thermohaline circulation due to heating near the equator and cooling towards polar latitudes (Garrison 1996, p. 218).

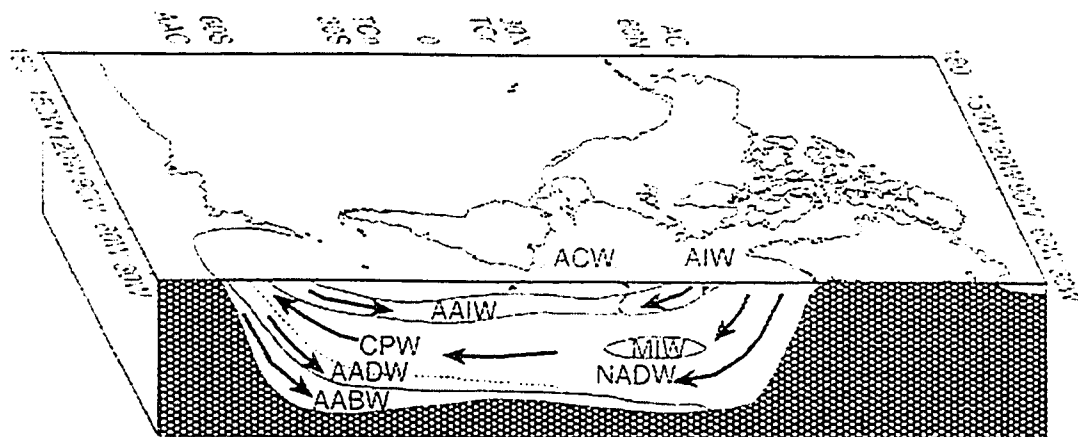


Figure 2.9 Deep-water masses in the Atlantic Ocean (Source: Kershaw 2000).

Notes: (1) Antarctic Deep Water (AADW) and Circumpolar Water (CPW) are terms used by Kershaw and are not referred to in this thesis.

(2) Atlantic Central Water is subdivided into North and South Atlantic Central Water (NACW and SACW respectively) in this thesis.

Arctic Bottom Water (ABW) is found adjacent to the Greenland-Iceland-Scotland Ridge, and chiefly contributes to the formation of North Atlantic Deep Water (NADW)

which is found between 1000 and 4000 meters depth (Garrison 1996, Tomczak and Godfrey 1994). NADW is a layer of comparatively high salinity which spans from the Labrador Sea to the Antarctic Divergence (Tomczak and Godfrey 1994, Brown et al. 1989b). NADW consists of two varieties - eastern or lower NADW originates in the Greenland-Iceland-Scotland overflow area and is abundant in the eastern basins; western or middle NADW is a product of ABW mixing with water from the Labrador Sea and is less dense than eastern NADW. As these water masses flow southward they remain vertically layered (Reid 1994, Tomczak and Godfrey 1994, Pickart 1992). Atmospheric and oceanic variability can affect the long-term stability of NADW when it first forms (Pickart 1992). Thermohaline convection in the Labrador Sea during the winter produces a volume of vertically homogenous water, however this phenomenon does not occur every year (Cuny et al. 2002, Reid 1994).

A third type of NADW is often cited in the literature as upper NADW. This is described as being western NADW mixed with Mediterranean Intermediate Water (MIW), which leaves the Strait of Gibraltar (Tomczak and Godfrey 1994). This form of NADW has higher temperatures and salinity than other water masses having the same density. MIW follows the Portuguese shelf northward due to the Coriolis force and enters the subtropical gyre circulation where it spreads both south and west (Tomczak and Godfrey 1994). At the 2000 meter level there is an MIW signature throughout most of the North Atlantic Ocean (Tomczak and Godfrey 1994). The mechanism which allows MIW to penetrate so deeply into the ocean is high eddy activity in the eastern North Atlantic, which prevents initial mixing and allows the MIW to gradually mix with neighbouring water masses (Ivey and Nokes 1989).

Antarctic Intermediate Water (AAIW) is formed in the South Pacific, enters the Atlantic Ocean through Drake Passage, and spreads isopycnally into the North Atlantic Ocean (Tomczak and Godfrey 1994). Its northward flow along the western boundary can be determined by the northward extension of the isohalines with the Guyana and Antilles Currents (Tomczak and Godfrey 1994, Flagg et al. 1986).

Arctic Intermediate Water (AIW) consists of two varieties: western AIW formed in the Labrador Sea is subducted along the Polar Front between the Gulf Stream and Labrador Current and extends southward to 40°N; and eastern AIW formed in the Iceland Sea with subduction occurring between the North Atlantic and East Iceland Currents, and reaching only to 60°N (Cuny et al. 2002, Bersch 1995, Aagard et al. 1985).

### **2.1.9 The Overall Thermohaline Circulation System in the Atlantic Ocean**

NADW forms in the high North Atlantic Ocean and flows southward beneath surface water masses and intermediate water masses until it is diverted to the surface in the Antarctic (Figure 2.10). AABW forms in coastal Antarctica, sinks to the bottom, and flows northward beneath all other water masses. Upon reaching the mid-latitude North Atlantic Ocean its water is entrained with NADW and swings back southward (Figure 2.10). The AABW is so dense that it underlies NADW and deflects NADW to the surface near Antarctica (Garrison 1996, Tomczak and Godfrey 1994). The MIW flows westward above the NADW and AABW and reaches the western North Atlantic Ocean. The AAIW flows northward above NADW and AABW but beneath surface water masses (Figure 2.10). The surface water is thickest in the central ocean gyres, like the Sargasso Sea. The central gyres are warm, saline, low-nutrient waters with low biological productivity (Garrison 1996, Tomczak and Godfrey 1994).

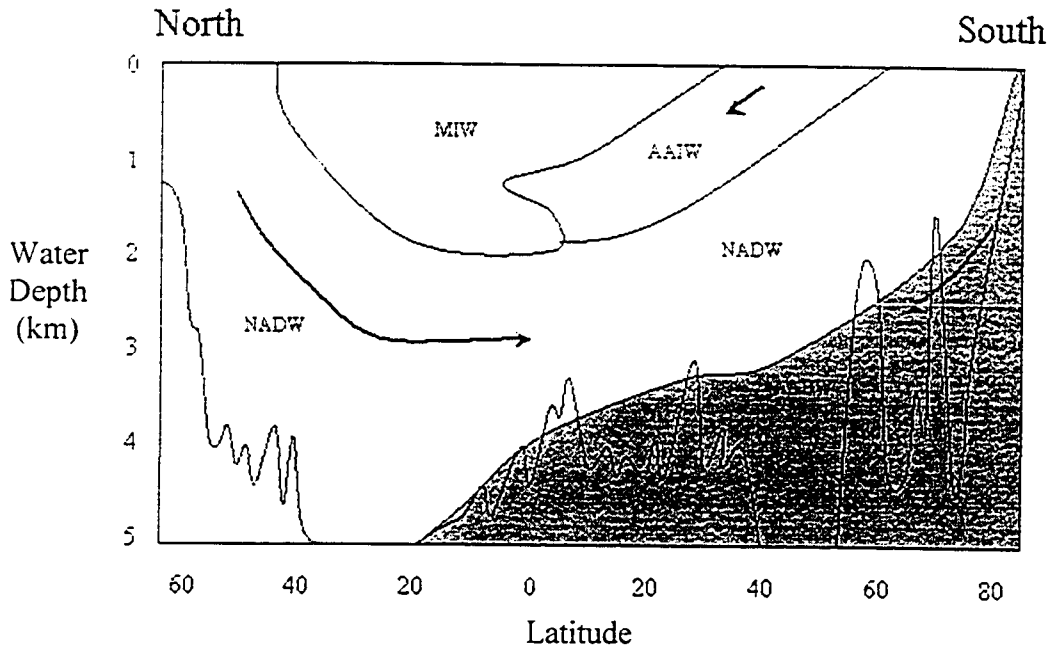


Figure 2.10 Atlantic Ocean - Water Masses (Source: adapted from Garrison 1996).

### 2.1.10 Thermocline and Surface Layer Water Masses

There are two distinct water masses that make up the thermocline in the Atlantic Ocean (Figure 2.9), South Atlantic Central Water (SACW) and North Atlantic Central Water (NACW). These water masses are delineated at 15°N with SACW infiltrating northward underneath the NACW resulting in a downward south to north slope (Tomczak and Godfrey 1994, Tomczak 1981). One of the main consequences of the convergence of these water masses is a south to north salinity increase between the North Equatorial Counter Current and North Equatorial Current at around 10°N (Tomczak and Godfrey 1994, Bayev and Polonskiy 1991).

There is a large volume of water between the North American continental shelf and the Gulf Stream that is cut off by the western boundary current from any direct contact with ocean water masses of the same depths. This water is influenced by

interactions between shelf water, Labrador Current water, and Gulf Stream water (Reynaud et al. 1995, Bowden 1983). Due to freshwater influx from the St. Lawrence River, shelf water has very low salinity, as does the Labrador Current. The mixture of these waters results in a water mass referred to as Slope Water, existing in the upper 1000 meters north of Cape Hatteras (35°N) along the North American continental rise (Tomczak and Godfrey 1994, Bowden 1983). This less dense, low salinity water is often trapped in cyclonic Gulf Stream rings and carried across the Gulf Stream into the Sargasso Sea (Tomczak and Godfrey 1984, Brown et al. 1989a).

## ***2.2 What Do We Know?***

With the data collection of the WOCE having been completed and the analysis of data having begun, a quick look at some of the initial conclusions show the time dependence of oceanic circulation and the turbulent nature of the flow. Some tracer results indicate that transport to the abyssal seafloor operates on a time scale of decades rather than on the centennial or millennial scales suggested by the ‘historical’ view (Wunsch, 2001). In addition, coarse-resolution models using WOCE data as inputs have shown that ocean circulation may undergo dramatic shifts on much shorter time scales than the historical view promoted (Talley et al. 2001, Willebrand and Haidvogel 2001, Han 2000).

One of the main climatic roles of the ocean lies in its three dimensional transport of the scalar fields of heat, fresh water, carbon, etc. It needs to be determined whether their variability through space and time are the result of either a simple time-dependent version of a laminar conveyor belt, a complex integration over fully turbulent elements or some complex combination of both (Wunsch, 2001).



One common theme that has changed from year to year is what researchers “know” about oceanic circulation. Tables 2-2 and 2-3 list what oceanic researchers knew and what is claimed to be known now.

**Table 2.2 Things everyone “knew”**

<b>Things everyone “knew”</b>	<b>Year hypothesis started being tested</b>
No interesting currents at depth on the equator	1950
The deep interior ocean moves at climatological speeds	1958
Vertical temperature and salinity profiles are smooth	1965
No interesting abyssal flow structures in the Pacific Ocean	1965
Ocean heat transport is negligible compared to the atmosphere	1970
Ocean mixing is geographically uniform	1970

Source: Wunsch, 2001 (p. 52)

**Table 2.3 Things many (some?) people “know” now**

<b>Things many (some?) people “know” now</b>
There is a global conveyor belt whose strength controls the climate state through thousands of years.
Only the upper ocean is relevant to ‘climate’.
Coarse resolution ocean models can be run for 1000+ years with climate forecast skill.
The strength of the oceanic heat transport is controlled by the surface density gradient alone.
Only the upper tropical ocean influences the El Nino-Southern Oscillation phenomenon (ENSO).
All changes in the circulation have deterministic causes.
The ocean is in equilibrium with the atmosphere.

Source: Wunsch, 2001 (p. 54)

### **2.3 Graphic Display Methods for Ocean Currents**

Currents, unlike temperature or salinity, require two quantities to be fully described – these quantities could be speed and direction, or the resolved east and north components of the former. Ocean currents are therefore a vector quantity requiring a direction and a magnitude.

A coordinate system is required to display vector data. At distances up to approximately 1000 kilometers a Cartesian coordinate system is suitable. Beyond that scale a spherical coordinate system is necessary due to the curvature of the earth (Demers 1997).

In oceanography,  $x$ ,  $y$  and  $z$  data denote direction and distance in space, positive in the east, north and depth directions (Figure 2.11). Another data triple,  $u$ ,  $v$  and  $w$  denotes the current components in the aforementioned directions (Thiebaux 1994, Tomczak and Godfrey 1994). In oceanography, a “left-handed” coordinate system is used in which the vertical coordinate  $z$  is positive for the downward direction.

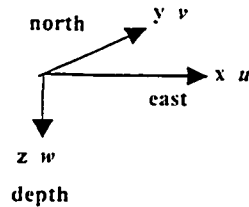


**Figure 2.11 Coordinate System used in oceanography**

Two ways of measuring velocity and displaying vectors are the Eulerian approach, first developed by Leonhard Euler in the mid-1700s, and the Lagrangian approach, developed by Joseph Louis Lagrange in the late-1700s (Knauss 1997, Thiebaux 1994, Tomczak and Godfrey 1994). The description of ocean currents by Eulerian methods is based on observations at a fixed point, as for example, from a moored current meter. Water flows past a measuring instrument and the current is recorded as a function of time (Knauss 1997, Thiebaux 1994, Tomczak and Godfrey 1994). The Lagrangian method of current description is based on following the movement of a water particle, by using either a drifting buoy or float. The position of the buoy is recorded as a function of time (Knauss 1997, Thiebaux 1994, Tomczak and Godfrey 1994). Both of the above methods describe the movement of water, however they represent this movement in very different ways.

## 2.3.1 Vector Representations of Current Flow

### 2.3.1.1 The Streamfunction - Definition

If we were to consider a rectangular basin of uniform depth (width =  $W$ , length =  $L$ ), filled with water, and assume both no vertical motion and a clockwise steady flow, then the movement of water can be broken down into its zonal component  $u$  and its meridional component  $v$  (Tomczak and Godfrey 1994). This is a Lagrangian approach to looking at current flow with streamline paths under the condition of steady flow (Figure 2.12 (a), (b)).

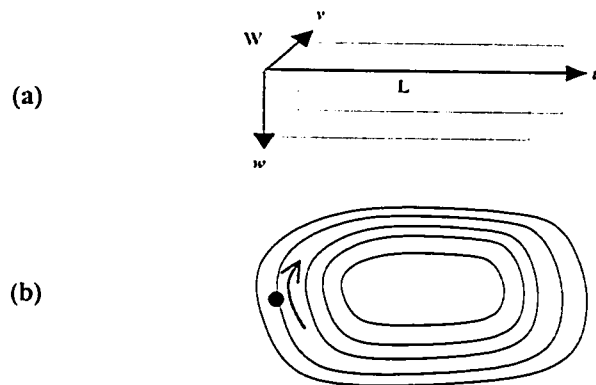


Figure 2.12 (a) Streamfunction Diagram, (b) Lagrangian Flow (Source: Tomczak and Godfrey, 1994)

### 2.3.1.2 The Streamfunction - Streamlines in Time Dependent Flow

The above rectangular basin can be viewed as a model of an ocean basin in the subtropics of the northern hemisphere, without taking into account Coriolis force, with the streamlines representing the path of water moving in the subtropical gyre in steady motion (Dyke 1996, Tomczak and Godfrey 1994). If we assume that the gyre is not in steady state, but that its velocity fluctuates due to seasonal variations in wind magnitude, the current and streamfunction become functions of time (Dyke 1996, Tomczak and Godfrey 1994). Therefore, there can be a periodic increase and decrease about a mean

value, which represents the acceleration and deceleration of the gyre at various times of the year (Dyke 1996, Tomczak and Godfrey 1994). A Lagrangian description of oceanic currents is not a vector plot since positions are given by a pair of  $x$  and  $y$  co-ordinates and not by a magnitude and a direction (Tomczak and Godfrey 1994). However, speed and direction can be deduced from the coordinates of position.

### 2.3.1.3 Progressive Vector Diagrams in Steady State Flow

Intuitively, the Lagrangian method of following the movement of water parcels is more graphic than observing data of current speed and direction. The progressive vector diagram was developed to simulate a Lagrangian display from Eulerian measurements (Tomczak and Godfrey 1994). Suppose that a current meter averages the current over one hour, recording the hourly averages and giving us Table 2.4.

**Table 2.4 Data for explanation of progressive vector diagram (Source: Tomczak and Godfrey, 1994).**

<i>Record number</i>	<i>Time (UTC)</i>	<i>East component u (m/s)</i>	<i>North component v (m/s)</i>
1	08:25	0.2	0.1
2	09:25	0.1	0.2
3	10:25	-0.2	0.1
4	11:25	0.0	-0.2

A progressive vector diagram is constructed by placing the tail of each successive vector on the head of the preceding vector. The  $x$ - and  $y$ - axes are in velocity units (m/s) and are converted into space units (m), knowing that a water parcel traveling at 1 m/s for 1 hour will cover a distance of  $1 \text{ m/s} * 3600 \text{ s} = 3.6$  kilometers (Thiebaux 1994, Tomczak and Godfrey 1994).

The problem inherent with the above is that if a current meter is located at the position shown in Figure 2.13, the current meter will always show northward flow at that

location, while the actual water parcel will follow the streamline (Tomczak and Godfrey 1994). After some time, the progressive vector diagram won't indicate the parcel's actual movement, instead it will indicate a flow beyond the edge of the basin (Figure 2.10).

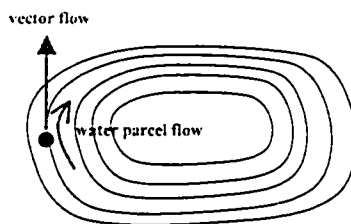


**Figure 2.13** Diagram to show predicted vs. actual movement (Source: Tomczak and Godfrey, 1994).

The progressive vector diagram is a hybrid between a Lagrangian and Eulerian method, using Eulerian measurements to simulate a Lagrangian display. As seen above, this method can lead to errors in interpretation if the nature of progressive vector diagrams isn't accounted for.

#### ***2.3.1.4 Progressive Vector Diagrams in Horizontally Uniform, Time-Variable Flow***

How useful are these diagrams for time-variable flow due to the problems discussed above? When a current varies with time, but direction and speed of water movement are the same everywhere at every moment in time, the current measured at the current meter is the same as the current at all other locations. Therefore, a progressive vector diagram constructed from its data represents the true movement of a water parcel (Tomczak and Godfrey 1994).

#### **2.3.2 Other Display Methods for Ocean Currents**

The development of satellite-tracked drifters and satellite altimetry has opened up new avenues for observing ocean currents (Fu 2001, Gowda et al. 1993). However, the use of moored current meters is essential for understanding oceanic circulation. The

Eulerian methods of data display including current component plots, speed and direction plots, stick diagrams, hodographs, scatter diagrams, and current roses will now be presented.

### 2.3.2.1 Current Component Plots

A component plot consists of a graph of the two current components against time (Figure 2.14). The components are aligned east-west ( $u$ -component – zonal, positive eastward) and north-south ( $v$ -component – meridional, positive northward). If a current meter is located close to a coastline, it may be more useful to display the current component parallel to the coast along with the current component normal to the coast (Emery and Thomson 1997, Tomczak and Godfrey 1994). The components for the plot would be  $u'$  and  $v'$  rather than  $u$  and  $v$  (Figure 2.14).

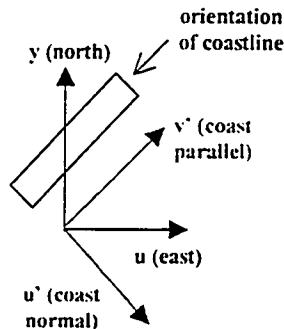


Figure 2.14 Different methods of plotting current components (Source: Tomczak and Godfrey, 1994).

Current component plots are useful and can display data which contain a wide range of processes, such as tidal currents, wind-driven currents and ocean scale variability (Emery and Thomson 1997). The plots in Figure 2.15 show the data for the Abyssal Circulation mooring number 296, part of the Abyssal Circulation experiment (see Appendix 8.1), which is located at 41.203°N, 63.023°W at 500 meters below mean sea level.

### 2.3.2.2 Speed and Direction Plots

This type of plot consists of a graph of speed and direction against time (Figure 2.16). There are many times where the strength or force of a current, which is related to current speed, is of interest and a plot of current speed is therefore useful (Emery and Thomson 1996).

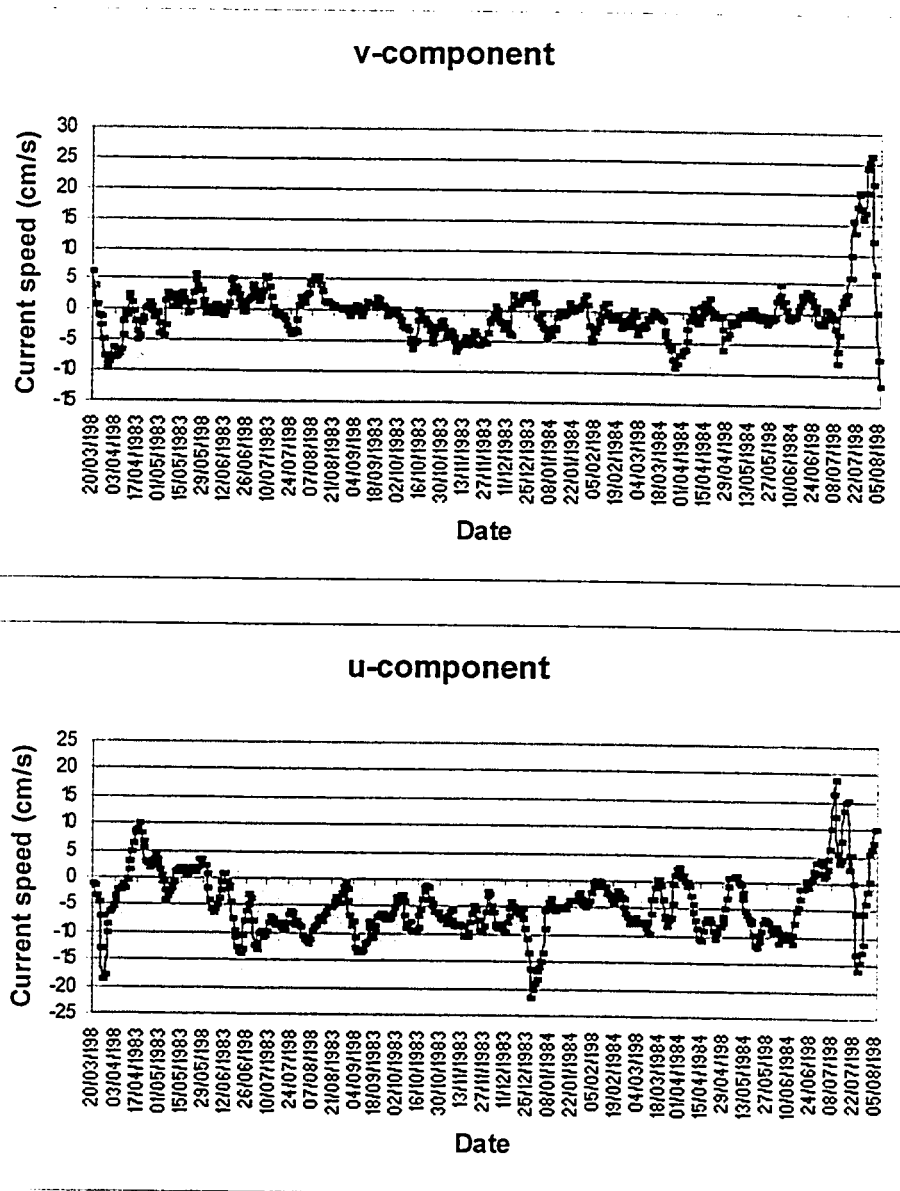


Figure 2.15 v- and u-current component plots for Abyssal Circulation, mooring 296 (41.203°N, 63.023°W at 500 meters depth)

Compared to current component plots, a speed and direction plot has some distinctive drawbacks. Current direction is expressed in degrees, clockwise from north, going from 0° to 360°. A plot of current direction shows a dramatic change of direction every time the current swings from one side of north to the other, as in going from 20° to 355° (Emery and Thomson 1996, Kovach 1994). Figure 2.16 shows the data from Figure 2.15 plotted as speed and direction plots.

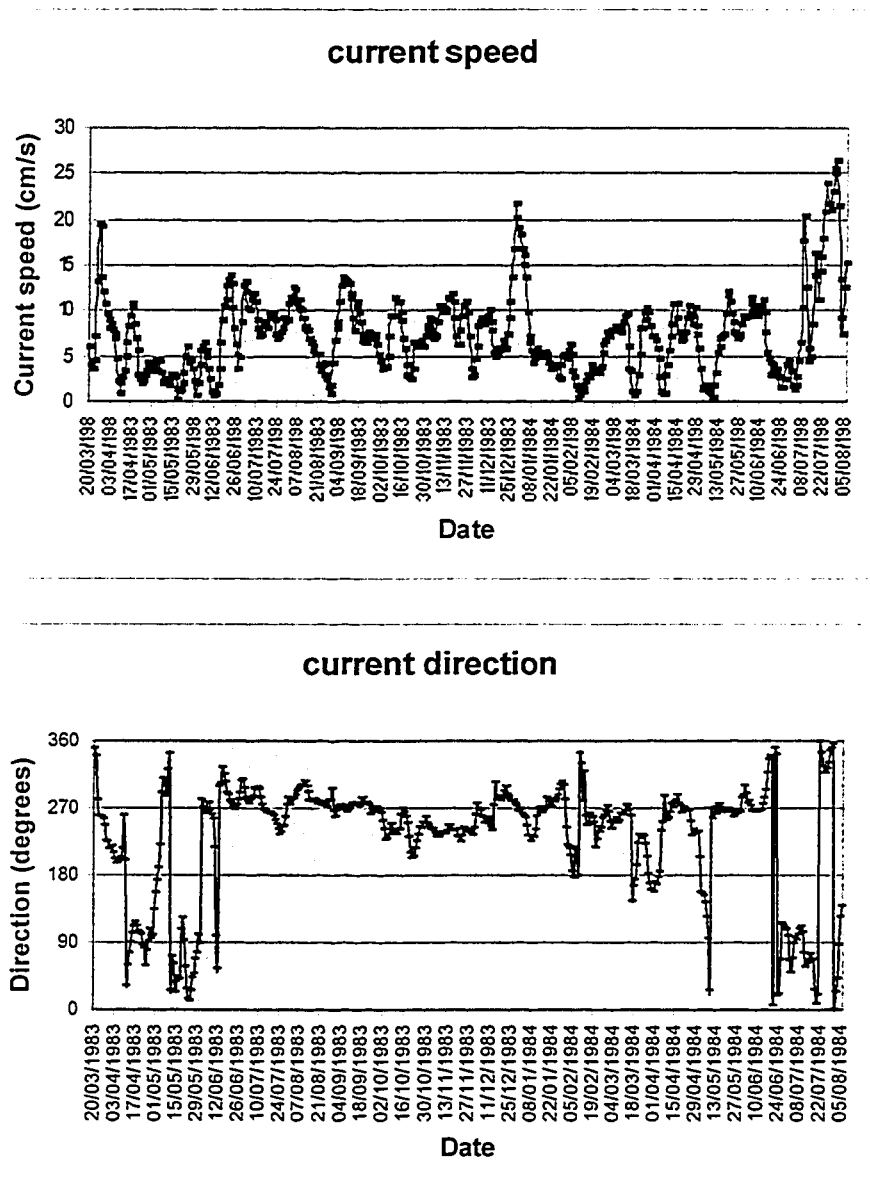


Figure 2.16 Speed and Direction plots for Abyssal Circulation, mooring 296 (41.203°N, 63.023°W at 500 meters depth)



### 2.3.2.3 Stick Diagrams

This is a graph that displays current as vectors against time, and is constructed by drawing time along the x-axis. For each current record, the corresponding current vector is positioned with its tail on the time axis at the time of observation. The x-axis gives time, the y-axis shows north, and a unit vector shows the length of a vector of 1 m/s (Emery and Thomson 1997, Godfrey and Tomczak 1994). When the vectors are plotted, their length corresponds to current speed and the direction in which they point gives the direction of the current.

Stick diagrams are useful for displaying the general position of currents and are very good at displaying slowly varying currents which contain only changes on time scales of days, months or seasons (Tomczak and Godfrey 1994). Figure 2.17 shows the stick diagram for the data used in Figures 2.15 and 2.16.

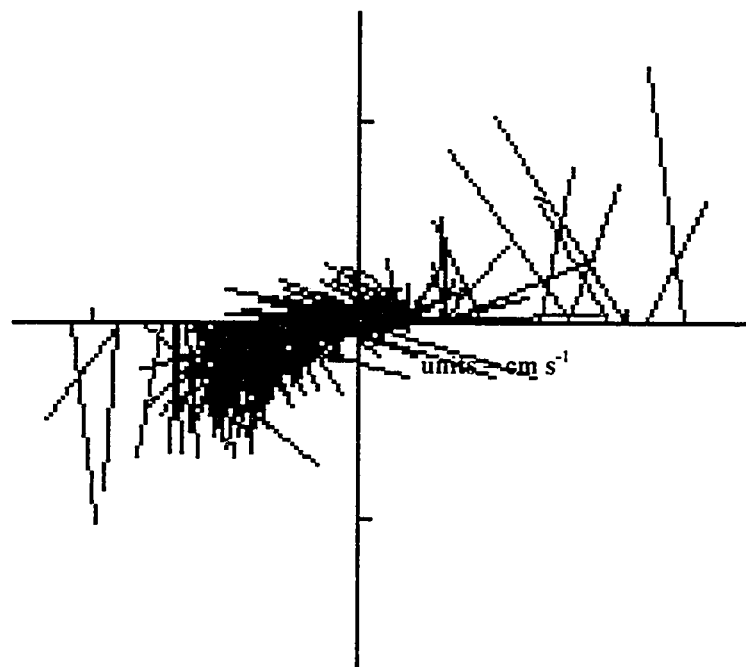


**Figure 2.17** Stick Diagram for Abyssal Circulation, mooring 296 (41.203°N, 63.023°W at 500 meters depth). A time-series of sticks laid down incrementally with respect to magnitude and direction.

### 2.3.2.4 Hodographs and Scatter Diagrams

A hodograph (Figure 2.18) connects the endpoints of the current vectors in a component co-ordinate system as a function of time (Emery and Thomson 1997). It's closely related to a scatter diagram, which shows the endpoints of the current vectors unconnected. The primary use of a hodograph is for displaying tidal currents, since the continuous change of current direction produces a well defined line pattern thereby giving a good representation of tidal current strength and variability (Tomczak and Godfrey 1994).

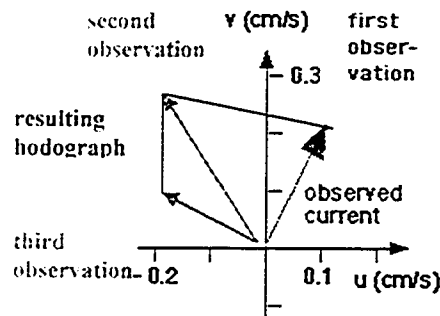


Figure 2.18 Hodograph plotting three successive current vectors (from Tomczak and Godfrey 1994).

A scatter diagram (Figure 2.19) shows the endpoints of the current vectors in a component co-ordinate system as a function of time. If the current is mainly tidal, the scatter diagram will give the same information as a hodograph but can result in a less confusing display for long time series. If the current record spans a period of months or years, a scatter diagram can display the prevailing current speed and direction for different seasons or other events (Emery and Thomson 1997, West 1996, Tomczak and Godfrey 1994). In the scatter diagram of Figure 2.19 the center gives an estimate of the mean current, while its width and breadth give an estimate of the variability.

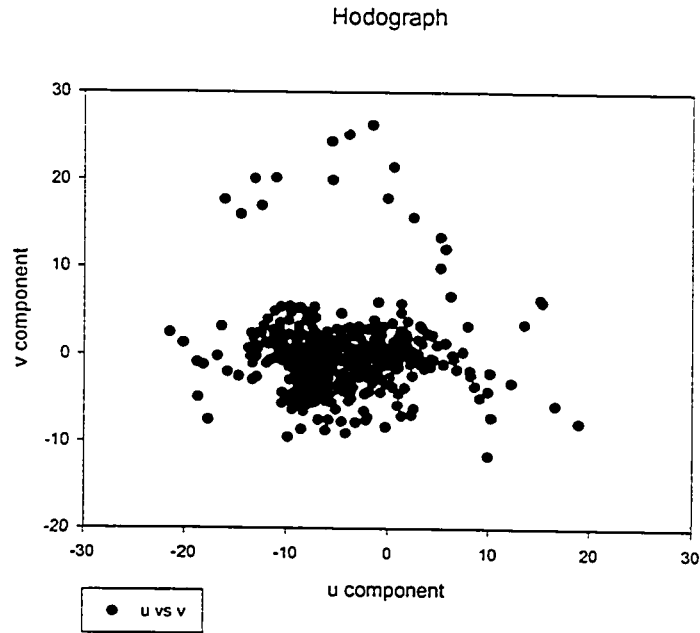


Figure 2.19 Scatter diagram for Abyssal Circulation, mooring 296 (41.203°N, 63.023°W at 500 meters depth)

### 2.3.2.5 Current Roses

An alternative method of representing current flow is the current rose, identical to the wind rose (with the exception that the direction indicated is pointing towards the current flow as opposed to from the direction the wind is blowing from). In a current rose the group of data are displayed in a sector of the circle, with the radius of each sector being proportional to the square root of the relative frequency of the group (Kovach 1994, Fisher 1993). Therefore the area of the sector is proportional to the group frequency. Figure 2.20 shows two different types of current roses for the Abyssal Circulation data presented above. Figure 2.20 (a) is a plot of the current direction while (b) is a plot of current speed vs. current direction. The former was produced in Oriana for Windows, a software package which is made specifically for circular data. The latter was produced in SigmaPlot 2000 which has a function for plotting circular data.

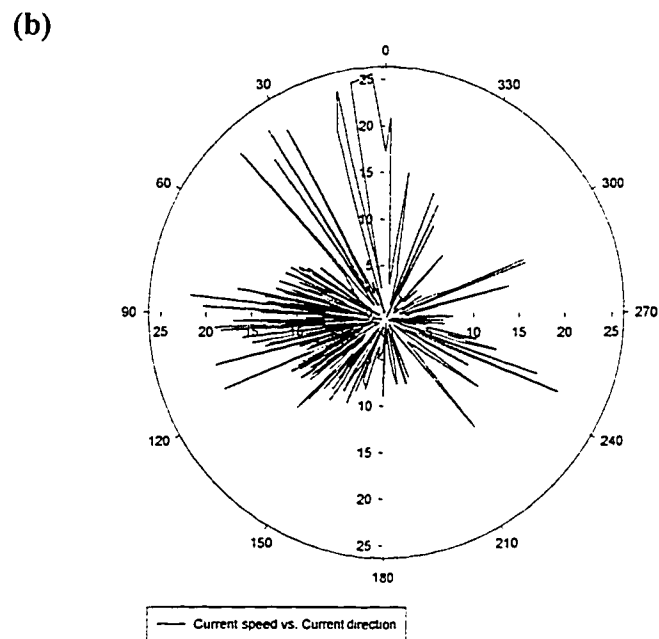
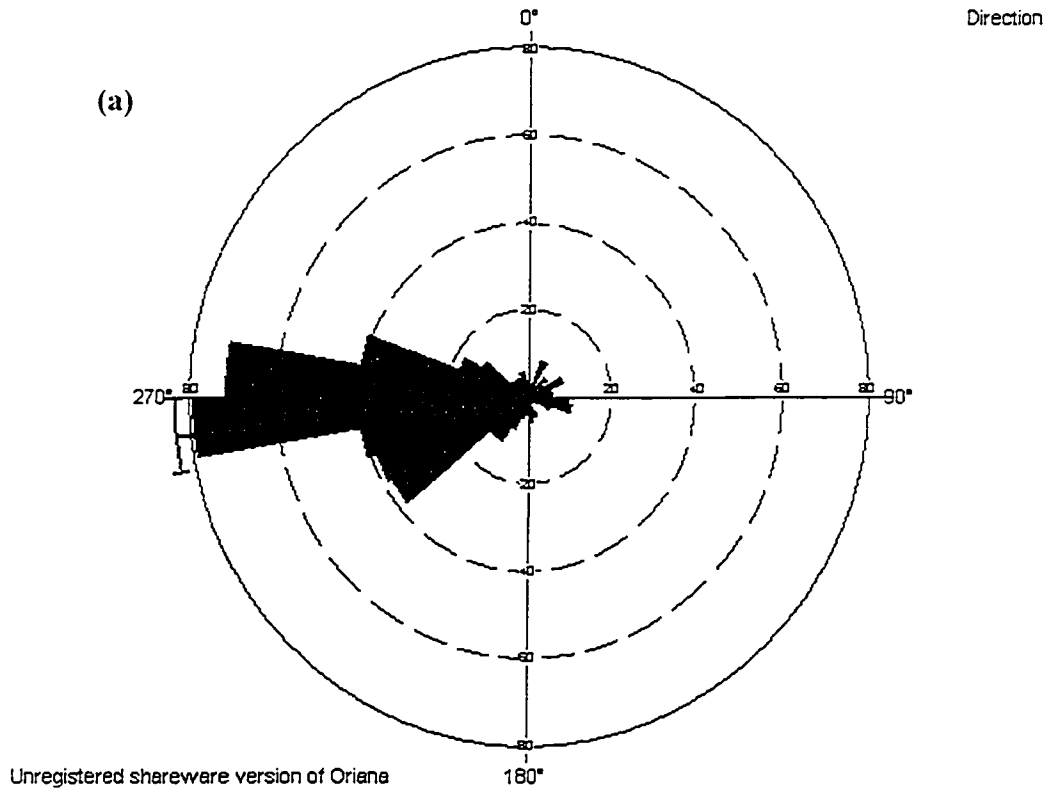


Figure 2.20 Current Roses for Abyssal Circulation, mooring 296 (41.203°N, 63.023°W at 500 meters depth). (a) Plot of current direction generated in Oriana for Windows, v. 1.06. (b) Plot of current speed vs. current direction generated in SigmaPlot 2000.

## **2.4 Summary**

This chapter has provided a background of literature pertaining to the physical properties of the North Atlantic Ocean, including its bathymetry, fresh water flows, wind patterns, sea surface temperature, salinity, surface circulation and thermohaline circulation. The constantly changing view of what we know about the oceans was presented with an eye toward the impact of decadal changes rather than the centennial or millennial scales once suggested.

Some of the graphical display methods that are used in ocean current analysis were introduced. All of these methods were applied to the WOCE dataset, however the remainder of this thesis focuses on the use of vector representations of the current flow. Current vector plots are used throughout to describe the circulation of the North Atlantic at various depths and at varying time scales.

### **3. Attributes of WOCE Data and Surfer7 Methods**

#### **3.1 WOCE Current Meter Dataset for the Atlantic Ocean**

The data used in this research were obtained from the Oregon State University (OSU) Buoy Group. The records contained in their archived database include roughly 4000 records from current meters and other instruments that were deployed on current meter moorings.

The OSU Buoy Group ensures that data available to researchers undergo thorough quality control procedures before being placed on their database. Current meters do not always give a truthful representation of water properties, especially if they are poorly maintained. The OSU Buoy Group has over 35 years of experience with these instruments and is familiar with the problems inherent in obtaining good-quality data.

Some of the problems that are addressed include (i) sticking compasses, that result in a very narrow range of directions; (ii) sticking encoder pins, especially in the Aanderaa RCM 4 and 5 units, that produce spikes in all the measured parameters; (iii) rotorcounter failure, which results in a sudden drop in speed to zero for several measurement cycles; (iv) failure of the speed sensor or its bearings, that result in a gradual reduction in speed readings; (v) tape glitches that result in erroneous readings; and (vi) sensor drift in which the response of the sensor varies (WOCE 2002, Woodward

Most of the errors in data measurement concern speed, and are a result of the sensor being mechanical and therefore prone to moving parts failing, and the nature of the medium that is being measured – with the inherent corrosive properties of salt water (WOCE 2002, Woodward et al. 1990). The stresses on surface and subsurface meters are

variable despite the medium being identical to both. Surface meters are subjected to a highly energized environment of wind stresses, waves, and also shipping activities and fishing. Subsurface meters have their buoyancy distributed vertically along a mooring line and are not as prone to the environmental extremes of the surface (Woodward et al. 1990).

In cases where there are obvious errors in the data, interpolation is used to replace the erroneous data. Single-point errors are replaced by linear interpolation, while longer segments are replaced by either linear interpolation or predictive interpolation (WOCE 2002). This latter method is used if a bad segment is a few hours to a few days in length since it uses an algorithm based on the maximum entropy method of analysis (WOCE 2002). This method extracts as much information from a measurement as is justified by the data's signal-to-noise ratio and has been adopted for use in many fields, such as spectral analysis and image restoration (Wu, 1997). Therefore no contamination is introduced into the spectral makeup of the time series, which can be a problem if using linear interpolation. When the error in the data exceeds a few days then interpolation is not employed, rather the bad segment is removed and a gap in the time series is inserted (WOCE 2002).

In summary, the OSU Buoy Group endeavors to provide researchers with current records that can be used with confidence and that are "less likely" to lead to false conclusions about ocean dynamics.

### **3.1.1 Overview of the WOCE Dataset**

Two dataset groups were selected for this research, one was collected during the WOCE study and another, which augmented this dataset, was collected previous to the

commencement of the WOCE study and is referred to here as the pre-WOCE dataset. The complete dataset including maps for the WOCE data is given in Appendix 8.1.

### 3.1.1.1 WOCE Data Set

The WOCE North Atlantic Ocean dataset is a compilation of a number of datasets made available by the OSU Buoy Group at Oregon State University. It includes current speed and temperature data from the following WOCE components:

Table 3.1 Spatial & Temporal Details of WOCE Components

<i>Experiment Name</i>	<i>Latitude Range</i>	<i>Longitude Range</i>	<i>Dates</i>	<i>Number of Records</i>
ACM1	26.4 – 26.5N	71.2 – 76.8W	06/19/90–06/15/97	148
ACM6	41.9 – 43.1N	44.6 – 49.0W	08/01/93–07/02/95	42
ACM7	0.1 – 1.6N	44.0 – 44.4W	10/13/90–03/04/94	65
ACM8	52.3 – 65.3N	15.4 – 41.2W	03/09/90–08/19/99	111
ACM10/11	0.5 – 0.8N	14.8 – 35.9W	09/29/92–11/01/94	24
ACM25/26	18.0 – 33.0N	22.0 – 34.0W	06/18/92–06/19/93	216
ACM27/28	41.0 – 42.2N	9.5 – 10.9W	05/29/93–06/01/95	22
ACM29	55.1 – 56.8N	52.4 – 54.1W	05/29/94–06/30/98	22
STACS11	3.9 – 3.9N	48.7 – 48.7W	09/25/90–09/14/91	3
<b>TOTAL</b>	0.1 – 65.3N	9.5 – 76.8W	03/09/90–08/19/99	653

The ACM1, ACM7 and STACS11 data have time increments of 12 hours and all of the time series have been filtered, with diurnal tides and all higher frequencies removed. There were no metadata available for the remainder of the datasets. The data consists of 653 records located between 0.087°N and 65.298°N latitude and 9.475°W and 76.850°W longitude, with depths ranging from 1 to 5483 meters below sea level. The study area is therefore approximately 38,425,000 square kilometers in area. Calculations are based on means for the period March 9, 1990 to August 19, 1999. Following is a brief description of the WOCE current meter data with regards to their initial purpose for deployment.



### **ACMI (STACS-10)**

These data were a result of the third of five consecutive current meter arrays deployed off Abaco Island in the subtropical western Atlantic Ocean. In all, the five current meter arrays spanned a 7-year period from 1986 to 1993 and were designed to provide data that could be used to analyze any climate-relevant flow that was transient in the western boundary current (WOCE 2002)

### **ACMI (WATTS)**

The goal of this study was to quantify the meridional volume and heat transport in the western boundary currents and in the recirculating gyres east of Abaco Island. Ongoing work is making simultaneous measurements of both the upper and lower layer parts of the inter-hemisphere thermohaline circulation. The current meter deployment also preserves the continuity of western boundary time series begun by the STACS program in 1986 (WOCE 2002).

### **ACMI (ACCP-1, ACCP-2, ACCP-3)**

The goal of this study was to measure volume and heat transports of the thermohaline circulation in the western subtropical Atlantic Ocean, and to maintain the continuity of the western boundary current transport time series begun by STACS in 1986 (WOCE 2002).

### **ACM6**

This involved a boundary current array deployed to measure the volume transport and heat flux of the North Atlantic Current – the western boundary current of the North Atlantic subtropical gyre. The moorings formed a linear array from the Grand Banks of

Newfoundland southeast into deep water, with depths of 400, 800, 1500, 2500, 3500, 4000 meters and 100 meters from seafloor being used (WOCE 2002).

#### **ACM7**

The purpose of these current meter arrays was to measure the northwestward flow of warm water in the upper layers, and the southeastward counterflow of North Atlantic Deep Water, along the Brazilian slope at the equator. Some of the moorings were upward-looking current profilers (ADCPs) at 300 meters, which allowed for the calculation of upper layer transports. Moorings K359 K360 and K361 contain vertical velocity, as well as horizontal velocity data (Schott et al. 1993).

#### **ACM8 (Denmark Strait Overflow)**

This experiment was set-up to measure the flow of cold, dense water southwestward across the Denmark Strait and into the Irminger Basin, where it becomes part of the North Atlantic Deep Water. This water is drawn from intermediate depths in the Norwegian Sea, crosses a sill of some 600 meters depth in the Denmark Strait and continues southwestward, following the topography, along the Greenland Slope. The current meter arrays were set normal to the Greenland Slope in order to measure the downstream changes in speed, transport, and entrainment associated with this current (Dickson and Brown, 1994; Dickson and Gmitrowicz, 1990).

#### **ACM8 (Iceland-Faroe Overflow)**

An experiment set-up to measure intermittent flow of cold, dense bottom water southwestward from the Norwegian Sea, across the Iceland-Faroe Ridge into the North Atlantic, where it becomes part of the North Atlantic Deep Water (Saunders, 1996).

### **ACM8 (German Component)**

This portion of ACM8 was set-up in order to measure the transports of mass, heat, and salt associated with the dominant meridional circulation in the North Atlantic Ocean. This circulation carries near-surface waters of tropical and subtropical origin northward, and carries deep arctic and subarctic water southward. These data are important in order to model the ocean's role in climate (WOCE 2002).

### **ACM10 (Deep Basin)**

The objective of ACM10 was to measure the northward flow of Antarctic Bottom Water (AABW) coming out of the Brazil Basin in the South Atlantic and flowing into the Guiana Basin in the North Atlantic. The current meters were placed across the opening at the equator between the Brazil Basin and the Guiana Basin west of the Mid-Atlantic Ridge. The current meters evenly filled the passage between the Brazil and Guiana Basins from north to south and were located in the east-west center of the zonal gap that steers the AABW (WOCE 2002).

### **ACM11 (Deep Basin)**

An experiment situated in the Romanche and Chain Fracture Zones, conducted in order to ascertain bottom water transport from the western to eastern basins of the equatorial Atlantic Ocean. Bottom water was defined as water with a potential temperature less than 1.9°C (Mercier et al. 1994; Mercier and Speer, 1998).

### **ACM25/26 (Subduction)**

This small-scale experiment was conducted in order to study the subduction process, whereby water forming in the mixed layer of the upper ocean moves downward into the thermocline, near the Bermuda/Azores high. The clockwise atmospheric

circulation present in this area makes the subtropical North Atlantic a good region to study this phenomenon (WOCE 2002).

#### **ACM27/28 (Morena)**

This experiment was designed to measure slope and shelf currents, heat and salt fluxes, and the seasonal variability of both along the Iberian continental margin. The Morena region ranges from 40°N to 43°N and lies between the coast and 11°W. Some distance from the wide continental shelf there is a complex bottom topography with several submarine canyons abutting the slope of this region (WOCE 2002).

#### **ACM29 (Labrador Sea)**

The Labrador Sea experiment was designed to obtain current and physical property data. This data will be analyzed to better understand Labrador Sea Water formation and its associated variability due to interannual variations in heat and salt fluxes (WOCE 2002).

#### ***3.1.1.2 Pre-WOCE Data Set***

The pre-WOCE North Atlantic Ocean dataset is a compilation of a number of datasets which were made available by the OSU Buoy Group at Oregon State University in order to augment the later collected WOCE data. This dataset includes current speed and temperature data from the following components itemized in Table 3.2 (ABCIRC = Abyssal Circulation (northwest Atlantic); BIO = Bedford Institute of Oceanography moorings; Conslex = experiment of Institute of Oceanographic Sciences; Gulf Stream = Gulf Stream Extension; LLWODP = Low Level Waste Ocean Disposal Program; LocalDyn = Local Dynamics Experiment; Lotus (northwest Atlantic); Nares = Subseabed Disposal Project, Nares Abyssal Plain; Neads = British experiment in North Atlantic; Polymode; Rise Array).

Table 3.2 Spatial & Temporal Details of pre-WOCE Components

<i>Experiment Name</i>	<i>Latitude Range</i>	<i>Longitude Range</i>	<i>Dates</i>	<i>Number of Records</i>
ABCIRC	35.6 – 41.2N	58.3 – 65.0W	03/20/83–08/24/84	23
BIO	37.7 – 40.5N	42.1 – 56.1W	11/05/76–04/30/80	23
Conslex	51.9 – 60.2N	9.2 – 19.9W	03/19/82–07/05/83	14
Gulf Stream	37.0 – 40.4N	42.0 – 46.9W	10/24/79–11/24/80	27
LLWODP	32.3 – 36.4N	70.7 – 71.8W	09/16/80–09/03/84	26
LocalDyn	30.5 – 31.4N	69.1 – 69.9W	05/01/78–07/23/79	22
Lotus	33.7 – 34.1N	69.7 – 70.1W	05/06/80–05/05/84	35
Nares	23.2 – 23.3N	63.9 – 64.1W	08/15/83–11/03/86	12
Neads	52.4 – 52.5N	17.7 – 17.8W	06/29/82–07/03/83	5
Polymode	28.2 – 41.5N	53.7 – 60.1W	08/04/74–07/07/77	58
Rise Array	36.4 – 39.2N	69.0 – 70.6W	04/11/74–12/15/74	27
<b>TOTAL</b>	23.2 – 60.2N	9.2 – 71.8W	04/11/74–11/03/86	272

The Conslex, Gulf Stream Extension, Local Dynamics, Low Level Waste Ocean Disposal Program, Nares, Neads, Polymode, and Rise Array datasets had an initial time increment of 15 minutes and were later subsampled to 1 hour time increments at OSU. The Abyssal Circulation, Bedford Institute of Oceanography, and Lotus datasets were filtered at OSU with a time increment of 24 hours (WOCE 2002).

This data consists of 272 records located between 23.2°N and 60.2°N latitude and 9.2°W and 71.8°W longitude, with depths ranging from 15 to 5800 meters below sea level. Calculations are based on means for the period April 11, 1974 to November 3, 1986.

### ***3.1.1.3 Data Processing at WOCE***

All of the records in the above two datasets were examined by the Current Meter Data Assembly Center (CMDAC), uniformly-processed and brought up to a uniform standard in which improbable spikes were removed and sections of data that were clearly in error due to instrument malfunctions were deleted (WOCE 2002).

Both original current meter data supplied by the Principal Investigator and altered versions that were cleaned are available in the data base. Cleaned data has been flagged by CMDAC and brief comments as regard to the nature of the changes is made available.

### 3.1.2 Stranger Format

The OSU Buoy Group has provided current meter data to other organizations in a simple ASCII format that has been named the Stranger format - "Stranger" because any stranger can easily understand and use it (WOCE 2002). This format is easily readable by both humans and computers. Following is a portion of the Stranger format:

```

22 header lines
11831 data lines
(i4,3i3,f8.2,f7.1,2f8.2,f8.3,f8.1,i6)
Experiment name:      BEST (ACM4)
Mooring name:        BEST 4
Mooring position:    30.003 deg S,   5.996 deg E
Instrument depth:    210 meters
Seafloor depth:      5180 meters
Instrument type:      Aanderaa RCM8
CMDB accession number: 1000
Parameters:
  hour
  day
  month
  year
  speed (cm s-1)
  dir (deg true)
  u (cm s-1) - zonal component
  v (cm s-1) - meridional component
  temp (deg C)
  pressure (db)
  line count

1800 23 6 92 16.61 283.0 -16.19 3.74 14.352 232.0 1
1900 23 6 92 15.75 289.0 -14.89 5.13 14.477 231.2 2
2000 23 6 92 17.19 286.0 -16.52 4.74 14.139 231.2 3
2100 23 6 92 20.35 282.0 -19.91 4.23 14.050 230.5 4
2200 23 6 92 18.34 275.0 -18.27 1.60 14.103 230.5 5
2300 23 6 92 18.91 276.0 -18.81 1.98 13.935 230.5 6
  0 24 6 92 19.20 276.0 -19.10 2.01 14.094 230.5 7
  100 24 6 92 19.20 275.0 -19.13 1.67 13.855 230.5 8
  200 24 6 92 20.06 272.0 -20.05 0.70 13.563 230.5 9
  300 24 6 92 15.46 261.0 -15.27 -2.42 13.837 230.5 10
...

```

The file begins with metadata. Following the metadata, each line represents one sampling cycle and contains hour, day, month, year, speed, direction, eastward component, northward component, temperature, pressure and a line count.

Microsoft Excel proved to be a straight forward tool to prepare the data for analysis in this thesis. Using the text import wizard one need only provide the row to begin importing, which is one more than the number of header lines, and the data format, which is space delimited. In this manner all the data can be processed for individual time series.

### **3.1.3 Spatial Coverage of Current Meters in the North Atlantic Ocean**

Appendix 8.1 gives a detailed synopsis of both the WOCE and pre-WOCE datasets. The appendix includes information on the 3-dimensional location with respect to latitude, longitude and instrument depth, as well as the water depth in which the data were taken. The dates the current meter recorded data and the instrument type used are also given. In addition there is a brief description of how the data were filtered, and a close-up map of the location of the current meters.

A two-dimensional summary of spatial coverage is shown in Figure 3.1, while a three-dimensional summary is depicted in Figure 3.2.

**WOCE Current Meters in the North Atlantic Ocean Categorized by Depth of Meter**

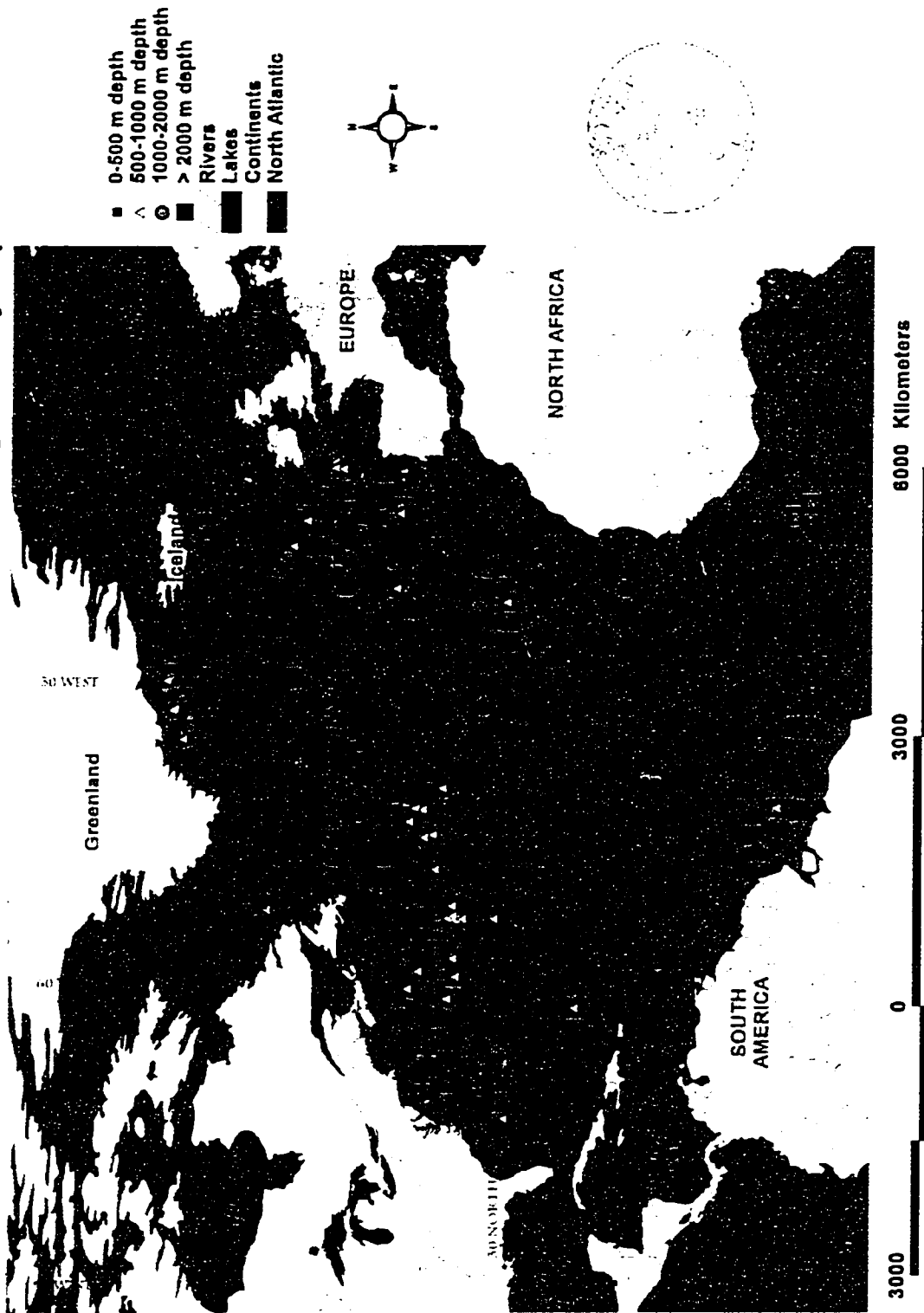


**Figure 3.1 WOCE Current Meter Moorings in the North Atlantic Ocean Categorized by Depth of Current Meter**



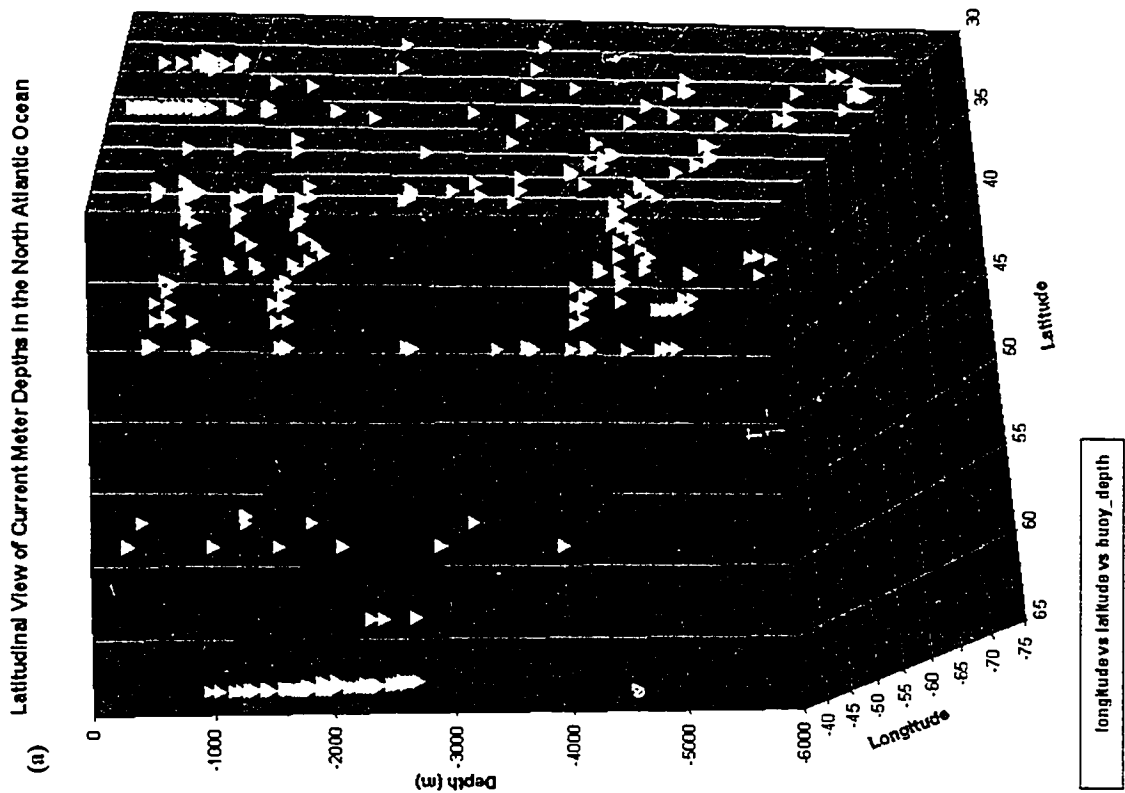
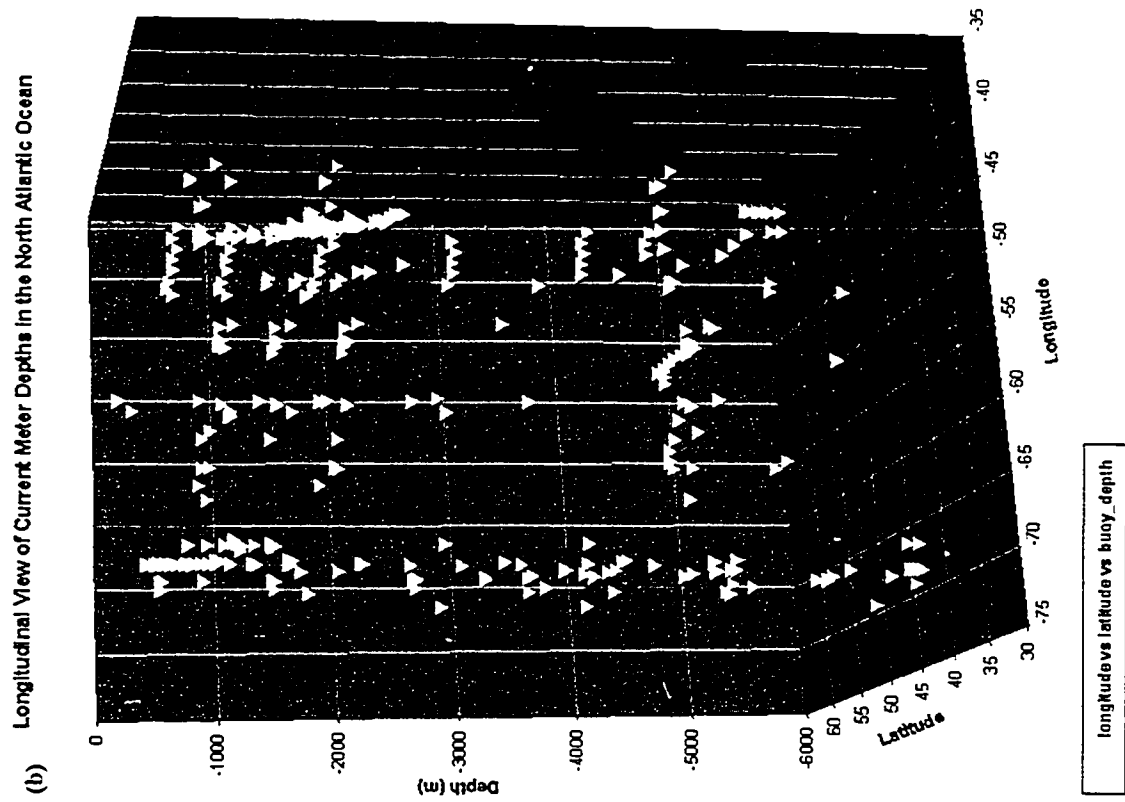


Figure 3.2 Three-dimensional representation of North Atlantic Ocean Current Meters located between 30°N and 65°N latitude and 35°W and 75°W longitude (a) Latitudinal View, (b) Longitudinal View

### **3.2 Surfer7 Gridding Procedures**

The software used in mapping much of the data is Surfer7, created by Golden Software, Inc. of Golden Colorado. The powerful 3-dimensional visual capability of Surfer7, as well as the ease of use and availability of the software made it a better choice than any of the competing GIS packages. The WOCE data set is made up of numerous data points that include data “rich” sites, at certain key locations where individual oceanographic studies have been conducted, and a huge gap over much of the ocean where data is missing. The gridding process allows for irregularly spaced xyz data to be converted into a regularly spaced, rectangular array of z values by extrapolating and/or interpolating z values at locations where there is no data.

#### **3.2.1 Duplicate Data Points**

One of the gridding issues that arise due to the nature of acquiring data through buoyed current meters is that a large number of duplicate data points are generated. This can be illustrated in cases where there are a large number of current meters placed at the same x- and y-coordinates but at a variety of depths (z-coordinates).

Duplicate data points are problematic when carrying out the gridding process. This is especially true for the kriging, natural neighbour, radial basis function, and triangulation with linear interpolation methods available in Surfer7.

Kriging is a geostatistical gridding method that attempts to illustrate the trends in the data, an example would be the interconnectivity of high points along a ridge rather than plotting them in isolation (Golden Software 1999). The equation used for Ordinary Kriging is

$$F(x, y) = \sum_{i=1}^n w_i f_i, \quad (3.1)$$

where  $n$  is the number of scatter points in the set,  $f_i$  are the values of the scatter points, and  $w_i$  are weights assigned to each scatter point. The natural neighbour gridding method shrinks some of the neighbouring polygons when interpolating new points and modifies these areas in order to implement this interpolation. The interpolation algorithm uses a weighted average of neighbouring observations in which the weights are proportional to these modified areas (Golden Software 1999). The radial basis function method of interpolation is the method used in this thesis and will be described in more detail in the next section. Finally, the triangulation with linear interpolation method uses the optimal Delaunay triangulation, in which the algorithm creates triangles by drawing lines between data points (Golden Software 1999).

A case in point of the problems inherent with duplicate data points is shown with the ACM25 Southeast Mooring data, particularly the Southeast 3 mooring with data collected between 07 October 1992 and 19 June 1993. As can be seen in Table 3.3, the mooring consists of sixteen instruments placed at varying depths at the same  $x$ - and  $y$ -coordinates.

When it comes to duplicate data points Surfer7 gives you the option of keeping: none, first, last, min\_x, max\_x, median\_x, min\_y, max\_y, median\_y, min\_z, max\_z, median\_z, sum, average, midrange, or a random data point (Golden Software 1999). Therefore in using any of the gridding methods listed above, only one data point will be kept while the remaining fifteen data points are deleted. The resulting statistical point is a fair compromise if the variation in depths is not great, but in some instances an “average” data point will be used for readings at 100, 2000, and 5000 meters below mean sea level. This compromise is not conducive to revealing any variation between depths.

**Table 3.3 Data Summary for WOCE ACM25 Southeast Mooring**

Mooring name	lat	lon	instr depth (meters)	water depth (meters)	instr type	dates
Southeast 3	17.995	-22.005	1	3297	Brancker Temp Recorder	07 Oct 92 - 07 Jun 93
Southeast 3	17.995	-22.005	10	3297	VMCM	07 Oct 92 - 19 Jun 93
Southeast 3	17.995	-22.005	30	3297	VMCM	07 Oct 92 - 19 Jun 93
Southeast 3	17.995	-22.005	50	3297	VMCM	07 Oct 92 - 19 Jun 93
Southeast 3	17.995	-22.005	60	3297	Brancker Temp Recorder	07 Oct 92 - 07 Jun 93
Southeast 3	17.995	-22.005	80	3297	Brancker Temp Recorder	07 Oct 92 - 19 Jun 93
Southeast 3	17.995	-22.005	90	3297	Brancker Temp Recorder	07 Oct 92 - 19 Jun 93
Southeast 3	17.995	-22.005	110	3297	Brancker Temp Recorder	07 Oct 92 - 19 Jun 93
Southeast 3	17.995	-22.005	130	3297	Brancker Temp Recorder	07 Oct 92 - 19 Jun 93
Southeast 3	17.995	-22.005	150	3297	Brancker Temp Recorder	07 Oct 92 - 19 Jun 93
Southeast 3	17.995	-22.005	200	3297	Brancker Temp Recorder	07 Oct 92 - 19 Jun 93
Southeast 3	17.995	-22.005	300	3297	Brancker Temp Recorder	07 Oct 92 - 19 Jun 93
Southeast 3	17.995	-22.005	400	3297	Brancker Temp Recorder	07 Oct 92 - 19 Jun 93
Southeast 3	17.995	-22.005	580	3297	Brancker Temp Recorder	07 Oct 92 - 07 Jun 93
Southeast 3	17.995	-22.005	750	3297	Brancker Temp Recorder	07 Oct 92 - 19 Jun 93
Southeast 3	17.995	-22.005	1500	3297	Brancker Temp Recorder	07 Oct 92 - 07 Jun 93

### 3.2.2 Appropriate Gridding Methods

In constructing the current flow fields for the North Atlantic Ocean a much larger number of interpolated points will be created from a fairly small number of control points. There are many gridding algorithms available in Surfer7, however these are dependent on the size of the data set. In looking at the North Atlantic Ocean it would appear that the data set is quite extensive, however due to the problem of duplicate data points, the data set is reduced by a large factor.

In gridding small data sets of fewer than 250 data points, or larger data sets ranging from 250 to 1000 data points the kriging using the linear variogram algorithm or the radial basis function using the multiquadric function produce good data representations (Golden Software 1999).

Both kriging using the linear variogram and the radial basis function using the multiquadric function generate high-resolution maps that reveal the flow pattern of the data. In addition these methods are able to extrapolate grid values beyond the data sets z range.

In experimenting with both gridding algorithms it was found that either one produces satisfactory results. The radial basis function using the multiquadric function is the method employed in this study, due in large part to the success found in many studies when using this procedure (Hardy 1971, Franke 1982, Saunderson 1992, 1994, Nuss 1994, Nuss and Titley 1994 and Sinha et al. 2002). The equation used by Surfer7 for the multiquadric function is

$$B(h) = \sqrt{h^2 + R^2} \quad (3.2)$$

where  $h$  is the anisotropically rescaled, relative distance from the point to the node and  $R^2$  is the smoothing factor specified by the user.

Franke 1982 evaluated a number of methods of scattered data interpolation, with regards to fitting ability, and visual smoothness, Hardy's multiquadric method was deemed the most impressive and gave the most accurate results of all tested methods. In equation 3.2 above, the  $B(h)$  denote the upper sheet of a hyperboloid of revolution, and the parameter  $R$  is specified by the user and is a shaping or smoothing factor (Franke 1982). The larger the  $R$  shaping factor, the smoother the contour lines appear. There is no universally accepted method for computing an optimal value for  $R$ , and indeed research in this area is ongoing, however a good compromise is somewhere between the distance between sample points and one-half the average distance between sample points (Golden Software 1999).

### 3.2.3 The Use of Exact and Smoothing Interpolators

Although one of the strengths of the multiquadric method is that it may be used for scattered points, the gridding algorithm employed by Surfer7 is necessary to maximize the number of available data points captured by the software. When using the

interpolation algorithms in Surfer7, coincident data points are assigned a weight of 1.0 while all other data points carry a weight of zero (Golden Software 1999). If data points do not line up exactly with the specified grid nodes, specific data points will not be registered by the software. Increasing the number of grid lines in both x- and y-coordinates increases the number of data values that are captured by the software. Smoothing interpolators are used to reduce small-scale variability effects between neighbouring data points by assigning weighting factors to all coincident data points. The radial basis function using the multiquadric function defines the optimal set of weights to apply to the data points when interpolating a grid node.

### ***3.3 Generation of Maps in Surfer7***

#### **3.3.1 Generation of Vector Plots**

Traditional vector plots are drawn so that the direction of the arrow represents the direction of the vector and the length of the arrow represents the magnitude being measured. In this research vector plots have been superimposed on contour plots, wire-frame plots and base maps to ascertain as much information as possible from the data.

Two separate grid files can be used to determine the vector direction and magnitude by Surfer7. The WOCE dataset includes both u- and v-components of current velocity, with positive numbers indicating the eastern and northern magnitude of flow respectively, and negative numbers indicating western and southern magnitudes respectively. Both grid files must have the same grid line geometry in order to be merged together (Golden Software 1999).

Head to tail addition of the u- and v-components of current velocity gives the direction of the resultant vector, while the magnitude of the vector is determined by the x- and y-coordinates of the head of the resultant vector as follows:

$$|\text{Magnitude}| = \sqrt{x^2 + y^2} \quad (3.3)$$

determined analytically by summing the respective components to obtain the resultant vector for current speed.

### **3.3.2 Generation of Contour Maps**

A grid file is read into the plot window as an array of x, y, z grid nodes, which consist of rows and columns of z values. Rows contain grid nodes with the same y-coordinate, and columns contain grid nodes with the same x-coordinate. Contour lines are drawn as a series of straight line segments between adjacent grid lines, and the point a contour line intersects a grid line is determined by interpolation between z values at adjacent grid nodes (Golden Software 1999).

### **3.3.3 Generation of Wire-Frame Maps**

Wire-frame maps are three-dimensional representations of a grid file or digital elevation model (DEM), created by joining z values along lines of constant x, y values.

Earth Topography – 5 Minute (ETOPO5) digital average seafloor bathymetry was compiled by the U.S. Naval Oceanographic Office and made available by the United States Geological Survey (USGS) and is composed of a gridded dataset with a grid spacing of 5 minutes of latitude by 5 minutes of longitude.

In analyzing near-bottom currents, the effect of the seafloor on current flow can be understood by visualizing current vectors overlain on a wire-frame mesh showing bathymetry.

### ***3.4 North Atlantic Bathymetry***

Figure 2.1 shows some of the major topographic features in the North Atlantic Ocean. The main characteristic to note is the main division of the North Atlantic Ocean into eastern and western basins surrounding the Mid-Atlantic Ridge. In addition there are numerous smaller basins, abyssal plains, and plateaus throughout the study area.

### ***3.5 Location of WOCE and pre-WOCE Data***

The location of the WOCE North Atlantic Ocean experiments are shown in Figure 3.3 and includes the current meter components described in Table 3.1. Data rich areas are found in the Irminger Basin, in the Newfoundland Basin off the Grand Banks, in the Iberian Basin off the coast of Europe, in the Guiana Basin along South America, and throughout the Bermuda Rise.

Locations of current meters for the pre-WOCE North Atlantic Ocean experiments are illustrated in Figure 3.4. This map includes the current meter components described in Table 3.2. The data rich areas are predominately located between 45°W and 75°W longitude and between 30°N and 40°N latitude. There is a good concentration of data along the Newfoundland Basin, the Sohm Abyssal Plain, and along the continental slope off of Cape Hatteras extending into the Nores Abyssal Plain and Bermuda Rise.



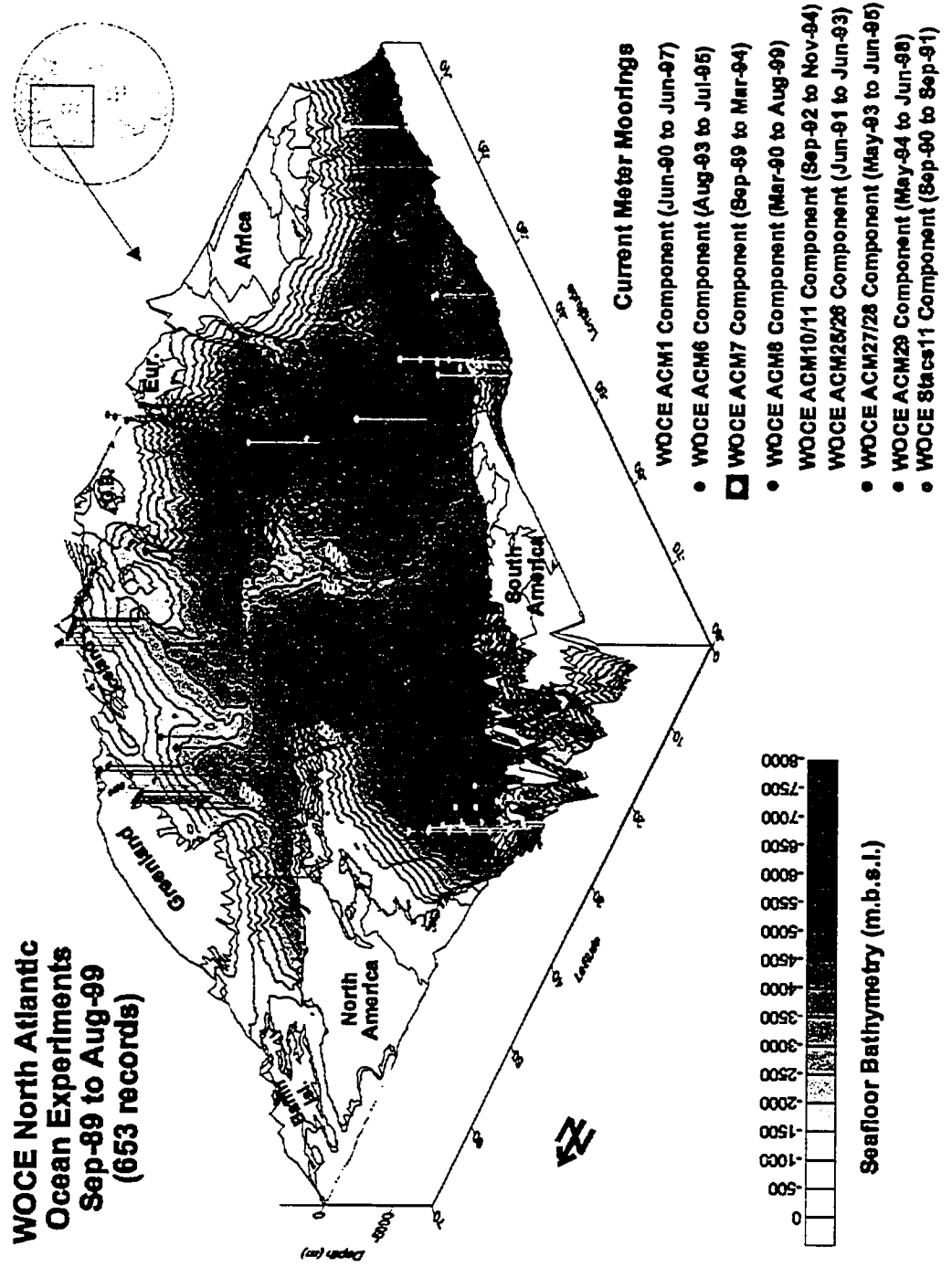


Figure 3.3 WOCE North Atlantic Ocean Experiments, Sep-89 to Aug-99. Note that the current meter moorings are denoted by elongated tacks, the tops of which indicate latitude/longitude position and the bottom which points to the depth at which the current meter is situated.

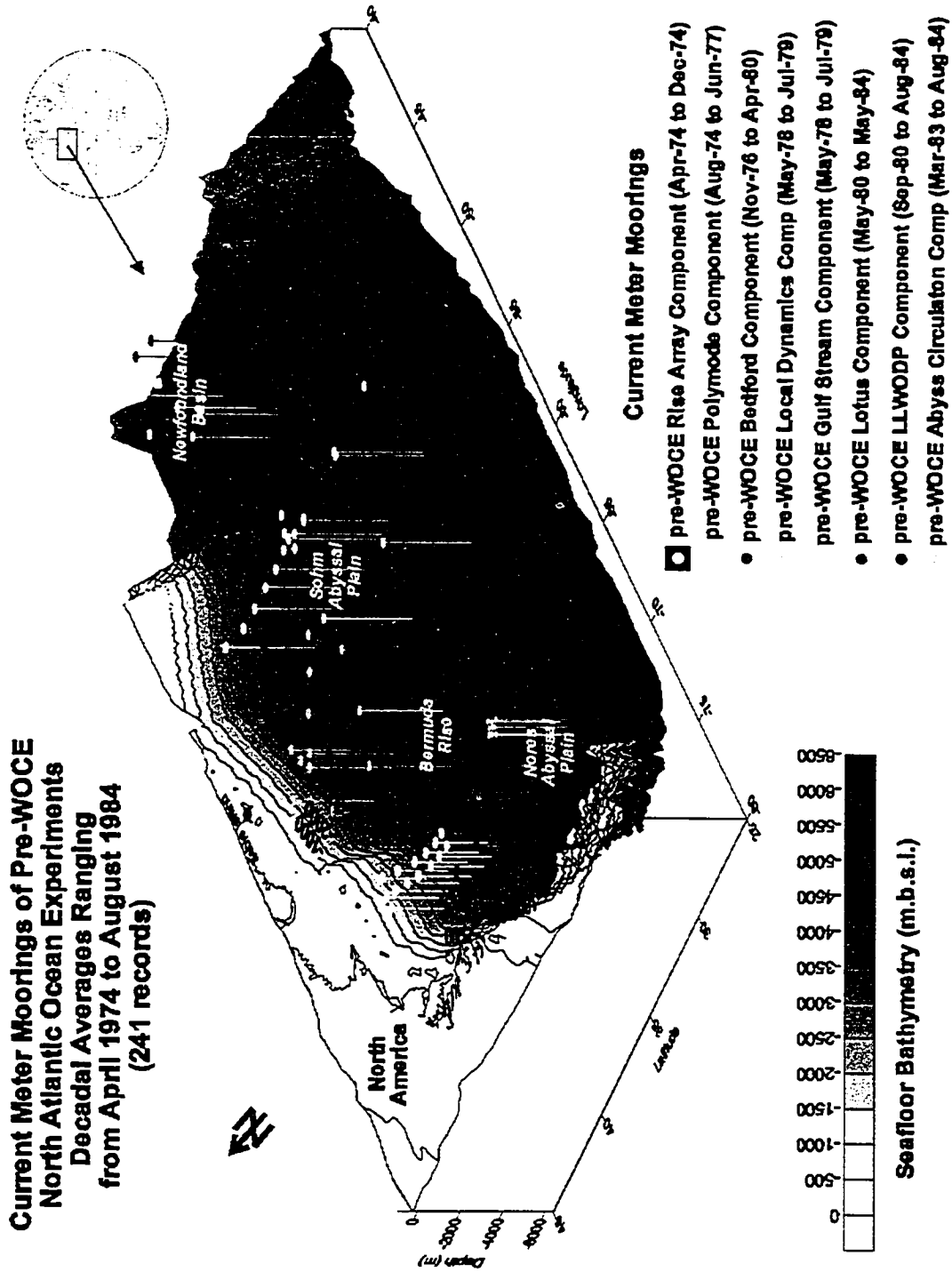


Figure 3.4 Current Meter Moorings of Pre-WOCE North Atlantic Ocean Experiments Decadal Averages from April 1974 to August 1984. Note, current meter moorings are denoted by elongated tacks – tops of which indicate latitude/longitude position and bottoms which point to depth at which current meter is situated.

### 3.6 Preliminary Analysis of Surfer 7.0 Vector Plots

The vector plots created in this study were all derived using the radial basis function interpolation gridding system and the multiquadric basis kernel type (as described in the methodology). Surfer allows for both Cartesian co-ordinates (x- and y-values) and polar co-ordinates (angle and length values) as inputs in order to generate 2-grid vector plots. Observation of Figure 3.5 (page 63) shows that the resulting interpolated vectors appear to differ somewhat with respect to both size and direction. The constancy of vectors situated at the data points appear to differ slightly in their orientation and magnitude.

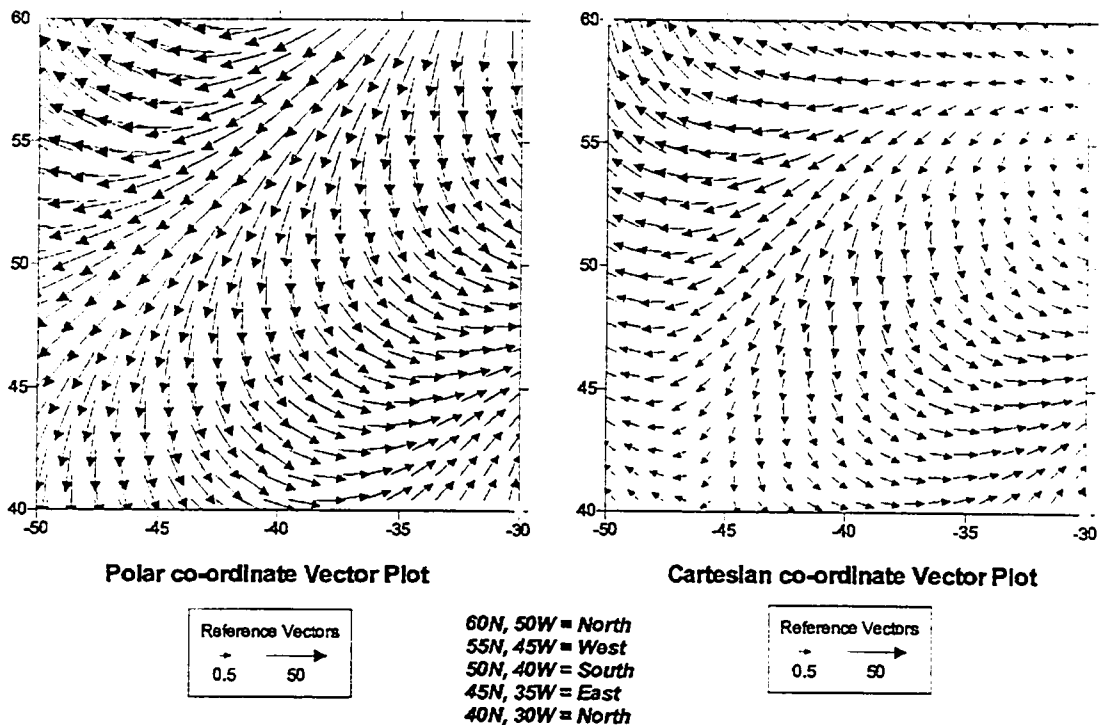
The plots for Figure 3.5 were generated from the following sample data, which were synthesized in order to test the two procedures.

Table 3.4 Synthesized Sample Data

<i>speed</i>	<i>dir_num</i>	<i>dir_text</i>	<i>lat</i>	<i>long</i>	<i>u</i>	<i>v</i>
10	0	N	40	-30	0	10
20	90	E	45	-35	20	0
30	180	S	50	-40	0	-30
40	270	W	55	-45	-40	0
50	360	N	60	-50	0	50

Note that the data consisted of four cardinal directions plus the inclusion of a second northing with increasing speed, and position north and west. The map produced using the polar co-ordinates of speed (length) and *dir\_num* (angle) appears to show a more symmetrical pattern in a line from the north-east to south-west corners of the plot, with magnitudes nearly equal to the values at the 50N, 40W data point. Vector dimensions to the north-west exceedingly increase in magnitude towards the 60N, 50W data point, and those in the south-east diminish towards the 40N, 30W data point.

## Variation in Interpolation of Vector Plots Polar (angle, length) co-ordinates vs. Cartesian (x, y) co-ordinates



Location of synthetic data

Figure 3.5 Variation in Interpolation of Vector Plots between Polar (angle, length) co-ordinates and Cartesian (x, y) co-ordinates

The map created by using the Cartesian, u and v, co-ordinates gives a different result to the interpolation algorithm. In the north-western sector of the plot there is a more northerly component in the flow direction, while in the north and north-east a more westerly flow than the southerly flow depicted in the polar co-ordinate plot. In general the north-west and south-east corners of the plot are similar to the polar plot, whereas the north-east and south-west sectors differ greatly in both direction and magnitude. An analysis of the data filter report produced by Surfer reveals the way apparently small differences in the data can result in some major variation in the processing of the interpolation algorithm.

In the relatively small synthetic dataset above, the standard deviation of the z-variable (which is the directional speed component) ranges from 19.60 for the u-component to 25.77 for the v-component, with the variance being 384 and 664 respectively. The final gridding summary gives a value for z-variables ranging from -26.87 to 13.19 for the u-component, and between -19.8 and 41.3 for the v-component. Alternatively for the polar co-ordinate gridding process the standard deviation for direction is 127.3 with a variance of 16200, while the speed variable has a standard deviation of 14.14 with a variance of 200. The corresponding ranges are 15.68 to 344.32 for direction and a range of 11.74 to 48.26 for speed.

Various sample sizes and locations were tried in order to determine the closest coincidence of pattern given by the two methods. Nearly all of the datasets tested showed similar differences between the two methods. One of the pitfalls of the Polar Grid method is that within the gridding technique chosen to interpolate the data, negative values may appear in the magnitude variable. There are a number of ways around this problem that involve regridding the magnitude data and consequently the angular data as well (Golden Software 1999).

Having acknowledged this, it would appear that the use of the Cartesian co-ordinate system gives a better approximation of the prevailing current flows and temperature regimes. The main reason for selecting the Cartesian data is that it reduces the pre-preparation necessary to analyze the data. Indeed, if both Cartesian and Polar co-ordinates are available for a dataset, it is far more expedient to use the Cartesian co-ordinate system.

### 3.6.1 The Relevance of Anisotropy

Another factor to consider is the usage of an anisotropy ratio in order to avoid clustering around data points. Anisotropy is the characteristic of an object in which its physical properties differ when measured in different directions (Golden Software 1999). Figure 3.6 illustrates the difference in changing the anisotropy ratio from 1.0 to 2.0.

When looking at the general pattern of current flow in the North Atlantic Ocean, anisotropy is not important since the distance between current meters is large enough to prevent clustering around data points. However in the analysis of some of the vertical profiles, such as in WOCE Component ACM7 which looks at a narrow band of ocean through a series of different depths, then the use of an anisotropy ratio is appropriate (Golden Software 1999). The rationale in this case is that data may vary greatly with respect to depth, but not so much between horizontal sample locations. Therefore the use of an anisotropy ratio will result in contours that give a better representation of the data.

Anisotropy is also useful when data sets use fundamentally different units in the x and y dimensions (Golden Software 1999). In the case of Figure 3.6, the solid gray vectors represent the original gridding process with anisotropy set to 1.0 (with vector magnitudes ranging from 0.37 to 41.80), while the red vectors indicate the new interpolation with anisotropy set to 2.0 and vector magnitudes now ranging from 2.56 to 45.69. Note the difference in vector orientation, which gets exaggerated at points further away from known data values, and in some instances approaches a directional change of 180°.

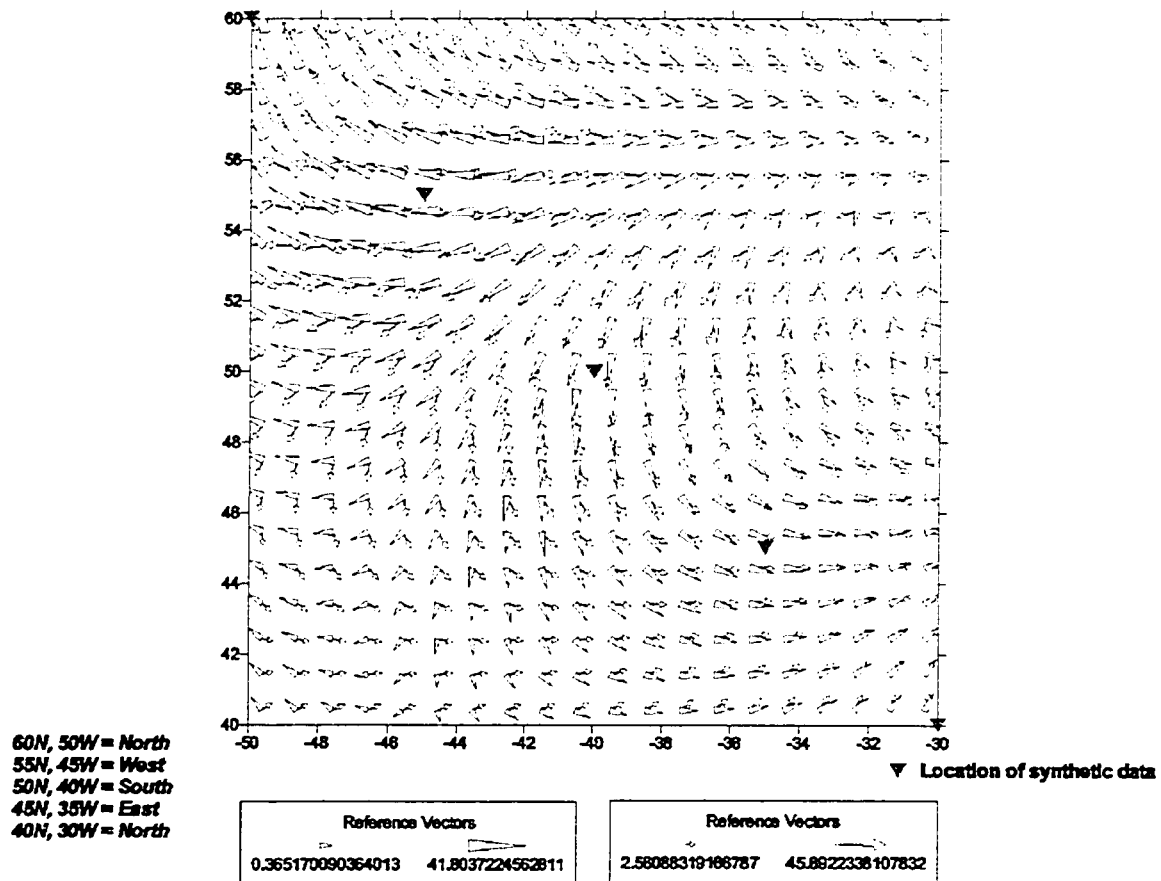


Figure 3.6 Variation in Interpolation of Vector Plots by using an Anisotropy Ratio

In Surfer7, anisotropy is controlled by both ratio and angle settings. The ratio is the primary range divided by the secondary range (considered mild if less than two and severe if greater than four), and the angle is the orientation of the primary axis (Golden Software 1999).

### 3.6.2 Are We Really Going to Get it Right?

The result of all this preliminary analysis is simply to underscore the reality of what the data, and more importantly the interpolated results, reveal about the actual physical processes that are occurring in the North Atlantic Ocean. As mentioned in the Introduction of this research, much of the WOCE data was made available to the research

community from a series of more localized studies that were conducted for very specific purposes. Therefore in using this data to observe patterns in the entire North Atlantic Basin a certain level uncertainty exists. Yet, a broad picture of the dynamics of current flow can be portrayed using current vector plots, and can then be compared to what is known about the general circulation of the North Atlantic Ocean.

### ***3.7 A Note on Interpreting Current Flows***

One important distinction to note when interpreting the text is that ocean currents are depicted in the direction they are flowing to, as opposed to winds, which are shown in the direction they are coming from. Therefore a south flowing current flows towards the south, whereas a southerly wind is blowing from the south and moving northwards.



## **4. Analytical Results and Visualization of pre-WOCE and WOCE Data**

### ***4.1 Introduction***

Chapter four is a comprehensive look at the results obtained from the mapping and statistical analysis of the WOCE data set. An analysis of the pre-WOCE data set includes an overview of the dataset, an analysis of the dynamics of current flow, and depth profiles showing the distribution of current speed and temperature with depth. A look at two sub-basin components, the Gulf Stream Extension and the Low Level Waste Ocean Disposal Program (LLWODP) are also included. As with the pre-WOCE dataset, an extensive mapping analysis was conducted on the entire WOCE dataset.

The results presented here begin with a look at the temporal and spatial distribution of the current meter data. Analysis of current flow is divided into surface water current vectors along with the associated mean surface wind data; shallow water current vectors, intermediate water current vectors, deep water current vectors, and near-bottom current vectors. Near-bottom is defined as being within 500 meters of the seafloor and ranges in depth from 250 meters below mean sea level, for areas along the continental margins, to the maximum depths in the dataset. Three dimensional plots of current vectors and temperature contours are included as an aid in comparing the flows at various depths. Additional analysis of the WOCE data set includes current speed depth profiles vs. latitude and longitude; and water temperature depth profile vs. latitude and longitude. A comparison of the two datasets is undertaken with the sets of data overlain to observe the two decadal flows. A section on whether fresh water discharges along the

continental margins of the ocean effect current flows is presented. Then the WOCE data is revisited in order to look at the annual mean circulation in the 1990s – particularly the flows between 1991 and 1993 which are data rich throughout the study region. Finally flow statistics of eddy kinetic energy in the North Atlantic Ocean is presented for the two decadal time periods.

## **4.2 Pre-WOCE Dataset**

These data are a compilation of a number of datasets made available by the Current Meter Data Assembly Center. The compilation includes current speed and temperature data from the pre-WOCE period as described in Table 3.2.

Means, minima, maxima, and standard deviations have been calculated at all moorings for the variables of interest. These are current speed, u-component and v-component of current speed, and temperature. Only 46 (19.1%) moorings had pressure data available and none of the moorings had salinity or conductivity data available, therefore density calculations were not possible.

The minimum number of days recorded at any one mooring was 73.3 days, the maximum 523.0 days, the mean was 319.5 days, and the median 300 days. Only 90 (37.3%) of the 241 records had data for 365 days or longer, 141 (58.5%) records had data for nine months or more, and 228 (94.6%) had data for six months or longer.

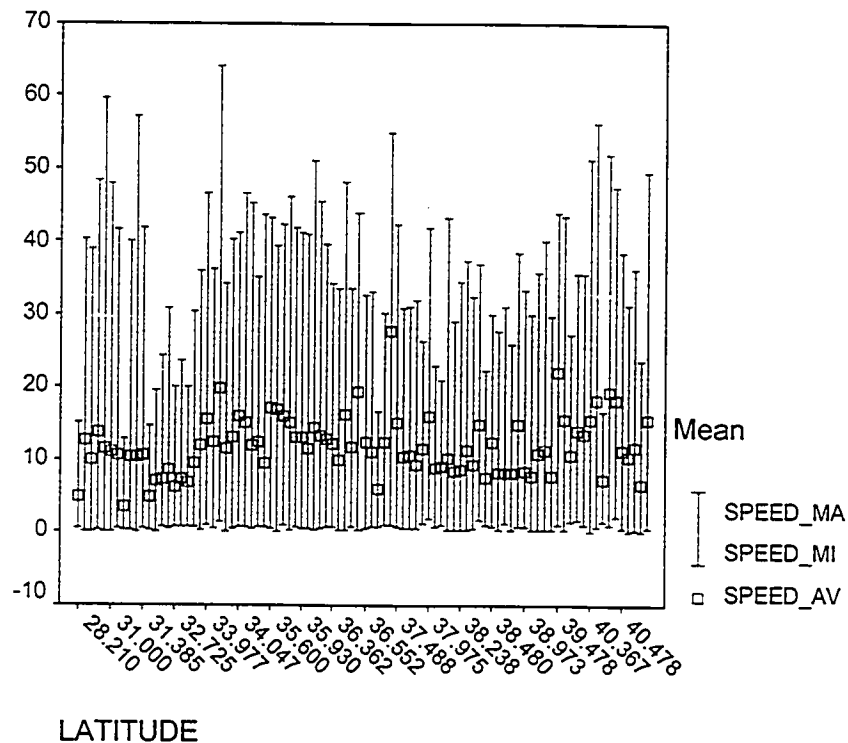
Table 4.1 Current Meter Recording Days for pre-WOCE Dataset

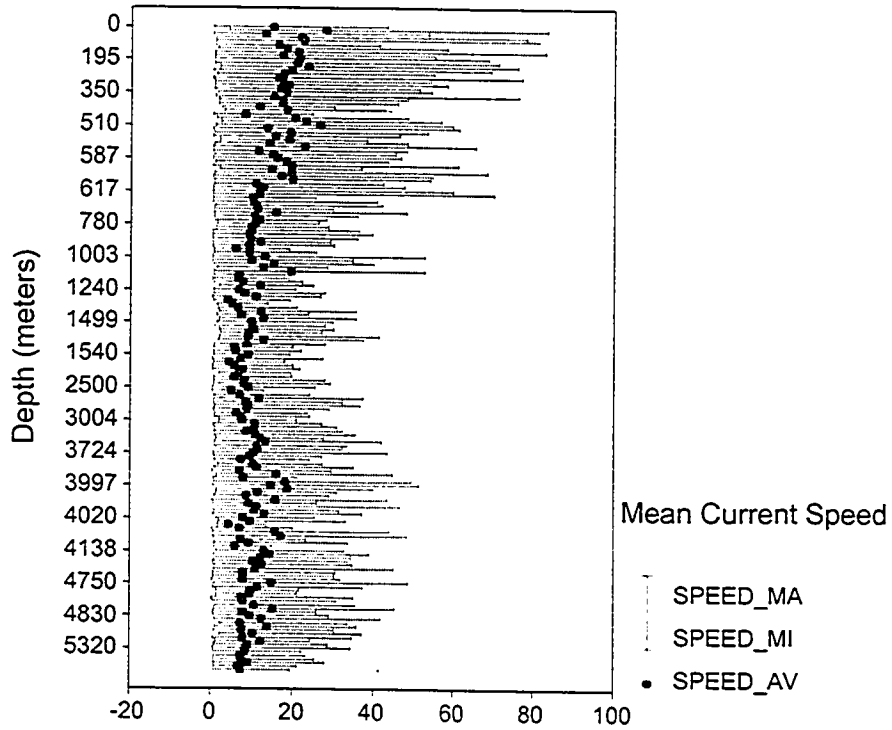
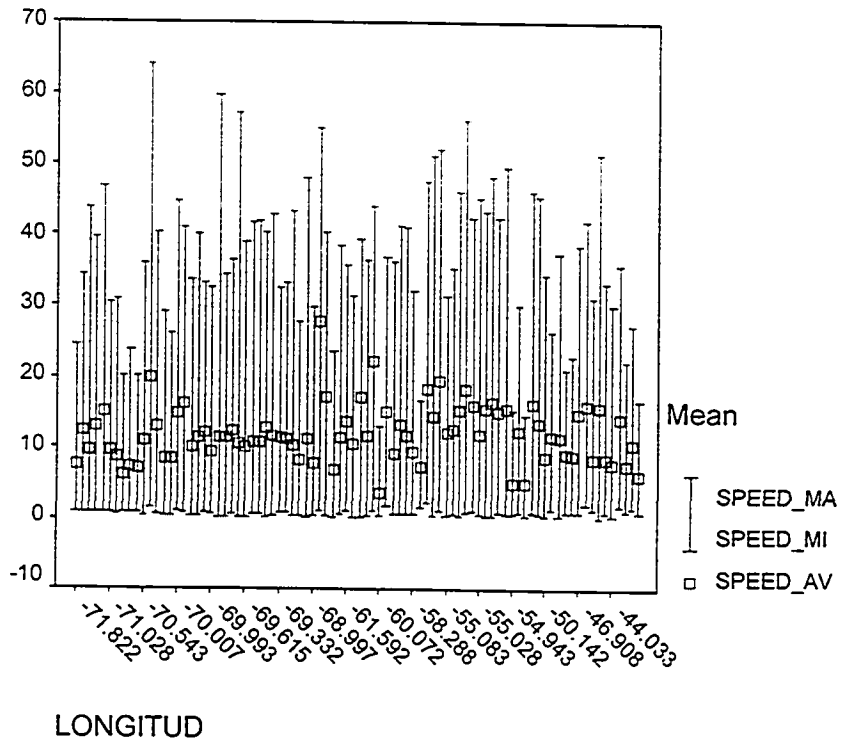
<i>Experiment Name</i>	<i>Minimum days</i>	<i>Mean days</i>	<i>Maximum days</i>
Rise Array	233.8	239.2	243.8
Polymode	73.3	239.6	307.0
Bedford	79.0	223.0	285.0
Local Dynamics	139.0	377.4	446.0
Gulf Stream	166.0	380.2	397
Lotus	166.0	326.9	387.0
LLWODP	289.5	378.8	493.9
Abyssal Circulation	320.0	499.2	523.0

The Rise Array experiment had no data collected between December 16 and April 10, and so is missing winter seasonal data. Data for the Polymode experiment were collected over a period of three years with only six of the moorings collecting data for fewer than 213 days. The calculated means are largely a representation of two or three seasons, therefore any variability in the means for this experiment could be related to seasonal differences rather than annual variations. The Bedford data were also collected over a long time period with only one mooring having data collected for fewer than six months, the same precautions for variability are extended to this data. Five of the moorings for the Local Dynamics Experiment have time series of less than one year. seven Lotus experiments are in this category, and only one of the moorings from the Gulf Stream Extension. Five moorings of the LLWODP dataset have time series of less than nine months. The Abyssal Circulation moorings had the most extensive and complete record of data of all the pre-WOCE experiments and so a more thorough analysis was undertaken on this data. The tabular and graphical results of this analysis are presented in Appendix 8.2. Geographically this dataset occupies the mid-western area of the North Atlantic Ocean including the Nores Abyssal Plain, Bermuda Rise, Sohm Abyssal Plain, Newfoundland Basin, and the Grand Banks (Figure 3.4).

### 4.2.1 Variation in Range of Variables for the pre-WOCE Dataset

The graphs in Figure 4.1 indicate no relationship between mean current speed and either latitude or longitude. However with regard to depth, the increased speed and the increased variability of speed are seen in the upper layers of the ocean, particularly above approximately 600 meters. The temperature curve shows the warm temperatures in the upper 500 meters of water, along with the thermocline of rapidly decreasing temperatures below that to about 1500 meters, and then a fairly consistent pattern to the seafloor.





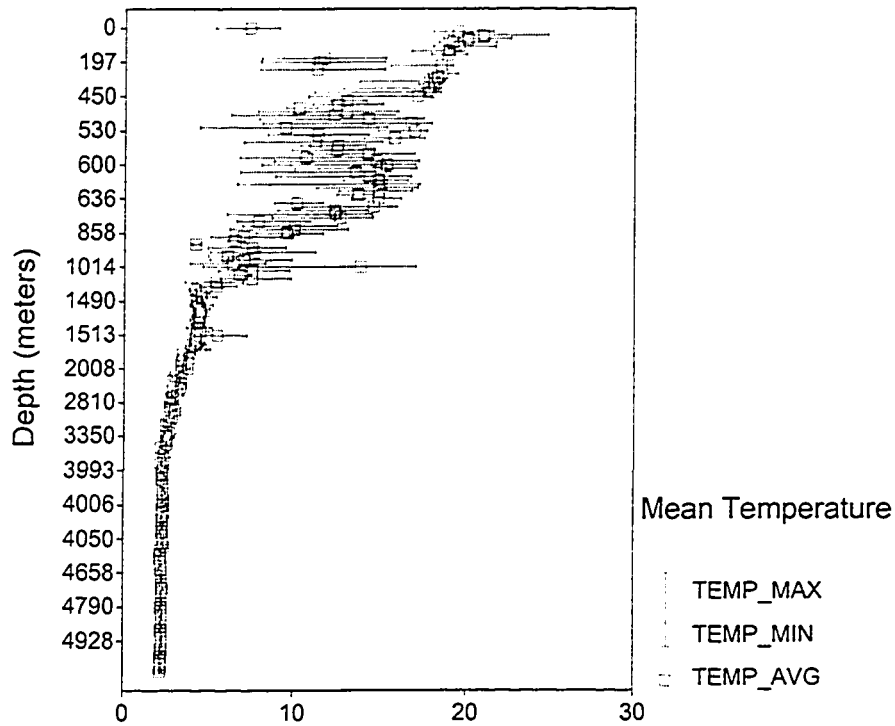


Figure 4.1 Variable Plots of Min, Mean, and Max Values for Current Meter Speed ( $\text{cm s}^{-1}$ ) vs. Latitude, Longitude and Depth and for Mean Temperature ( $^{\circ}\text{C}$ ) vs. Depth

#### 4.2.2 Dynamics of the pre-WOCE Data

Four sets of current vector plots were produced for the pre-WOCE dataset, shallow water, surface to 530 meters depth (Figure 4.2); intermediate water, 550 to 1,030 meters depth (Figure 4.3); deep water, 1,200 to 5,430 meters depth (Figure 4.4); and two near-bottom plots for moorings found between 2,512 and 5,430 meters situated less than 10% from the seafloor (Figures 4.5 & 4.6). Also 3-dimensional plots of current vectors and of temperature and current vectors were produced showing the three different levels of water depth – shallow, intermediate, and deep (Figures 4.7 & 4.8).

The shallow water vector plot (Figure 4.2) shows the fastest currents between  $50^{\circ}\text{W}$  and  $65^{\circ}\text{W}$  - north of  $35^{\circ}\text{N}$ . These currents are oriented in an easterly direction, corresponding roughly to the location of the Gulf Stream, and begin to alter direction to the south at about  $48^{\circ}\text{W}$ . Currents to the west of  $62^{\circ}\text{W}$  flow westward towards North America. A mass of slow moving water can be seen near  $40^{\circ}\text{N}$  and  $65^{\circ}\text{W}$ . Intermediate depth water (Figure 4.3) shows a more varied pattern with relatively rapid eastward flowing water from the Labrador Current north of  $40^{\circ}\text{N}$ , meeting up with southern flowing water from the East Greenland Current. Masses of slower moving water are seen near the Middle Atlantic Bight at  $70^{\circ}\text{W}$ , between  $33^{\circ}\text{N}$  and  $40^{\circ}\text{N}$ . Deep water (Figure 4.4) gives a clearer picture of the actual current conditions due to the larger number of current meter records that are available. A gyre is noticeable near  $37^{\circ}\text{N}$  and  $55^{\circ}\text{W}$  with a clock-wise flow of water around this area.

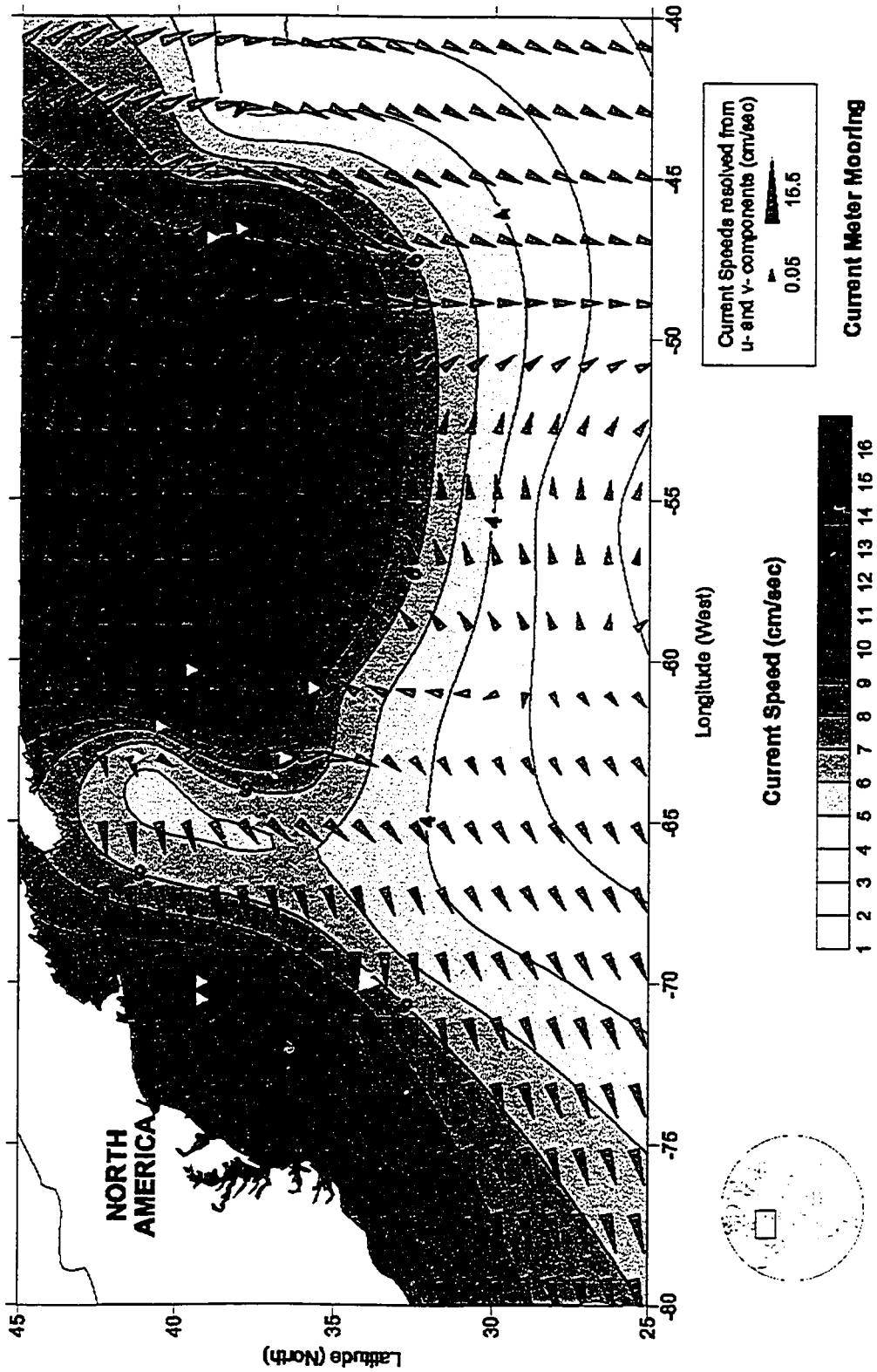


Figure 4.2 Pre-WOCE North Atlantic Ocean Components Shallow Water Current Vector Plots recorded from Apr-11-1974 to Aug-12-1984 for depths  $\leq$  530 meters



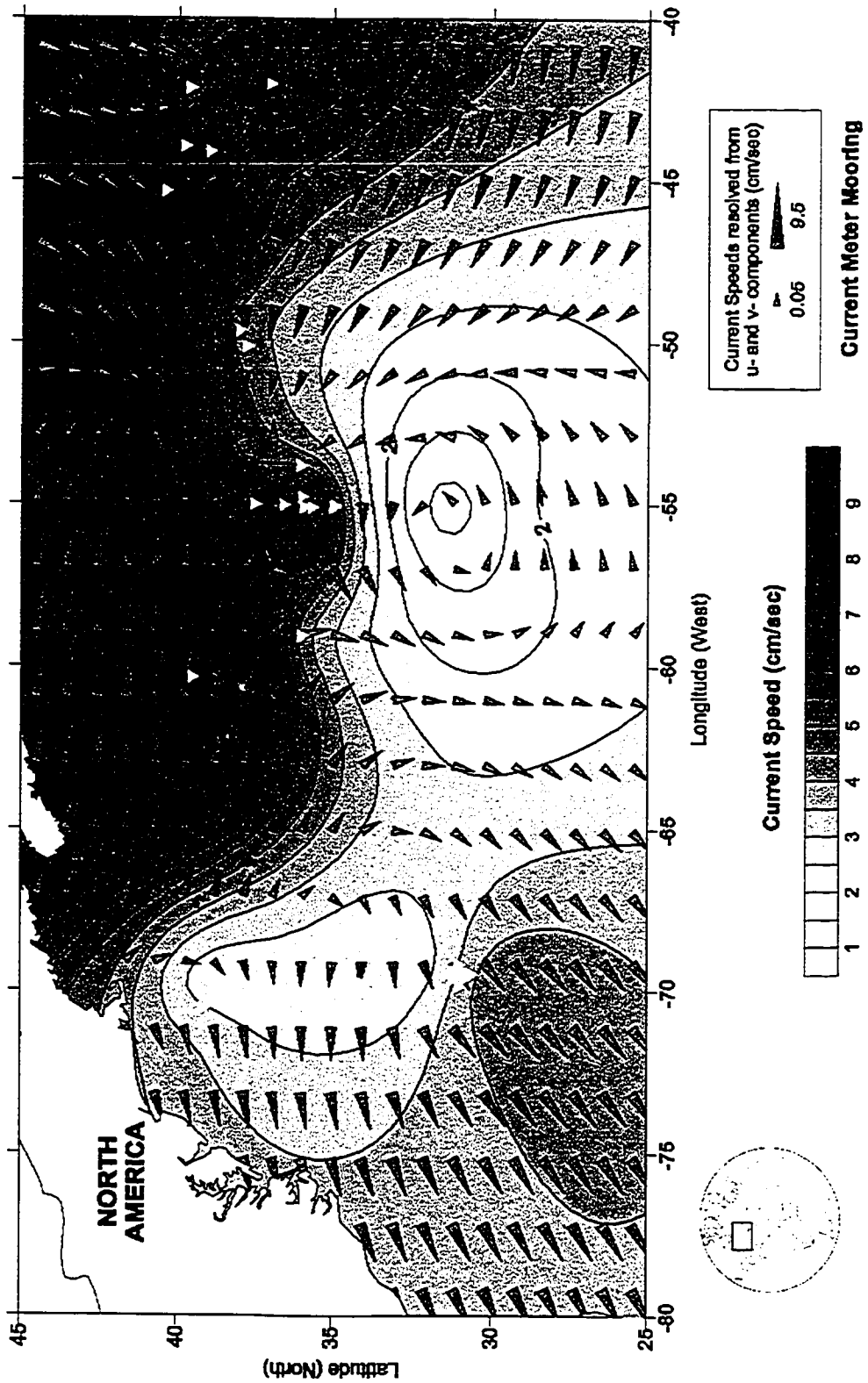


Figure 4.3 Pre-WOCE North Atlantic Ocean Components Intermediate Depth Water Current Vector Plots recorded from Apr-11-1974 to Aug-09-1984 for depths of 550 to 1,030 meters

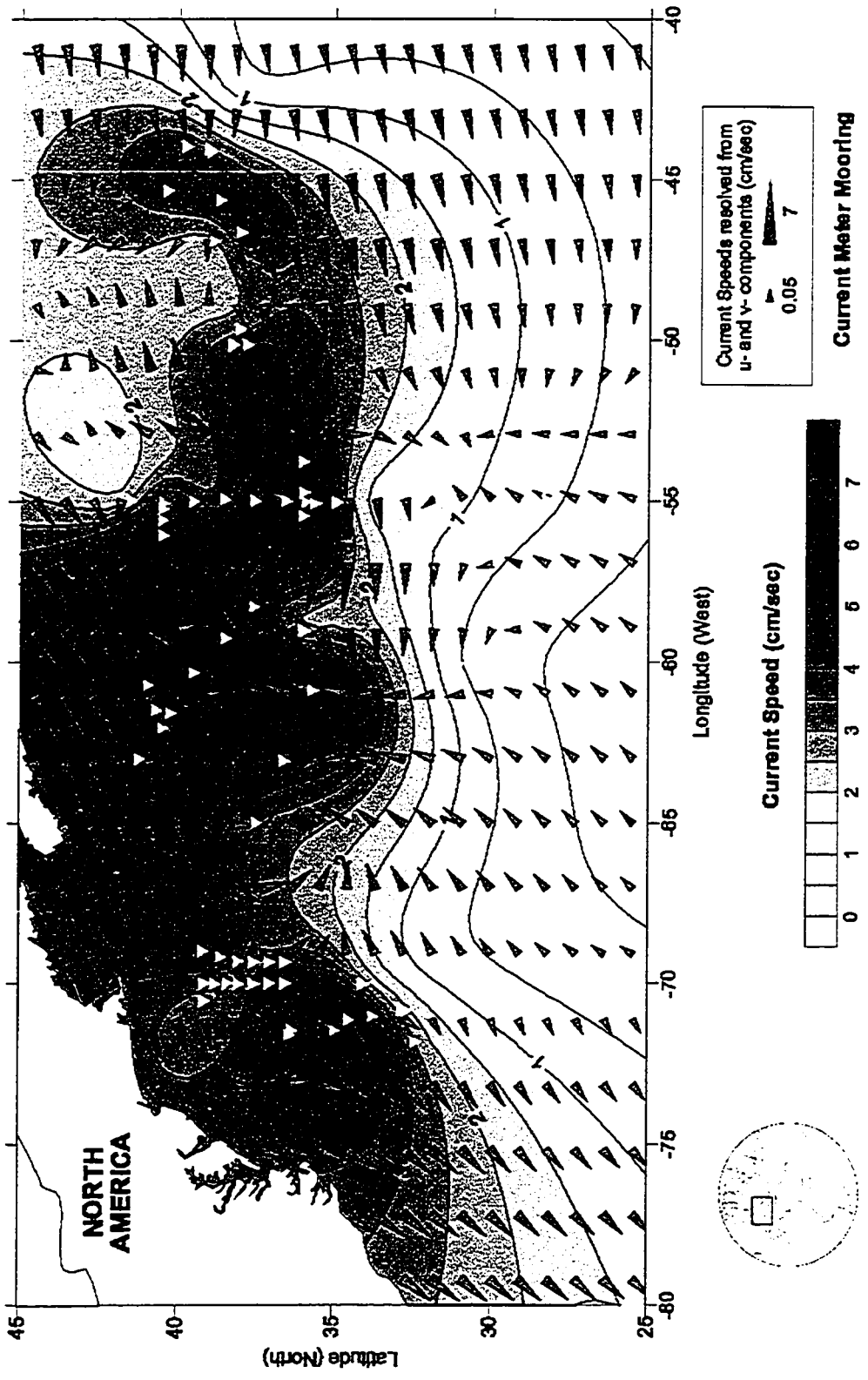


Figure 4.4 Pre-WOCE North Atlantic Ocean Components Deep Water Current Vector Plots recorded from Apr-11-1974 to Sep-03-1984 for depths of 1,200 to 5,430 meters

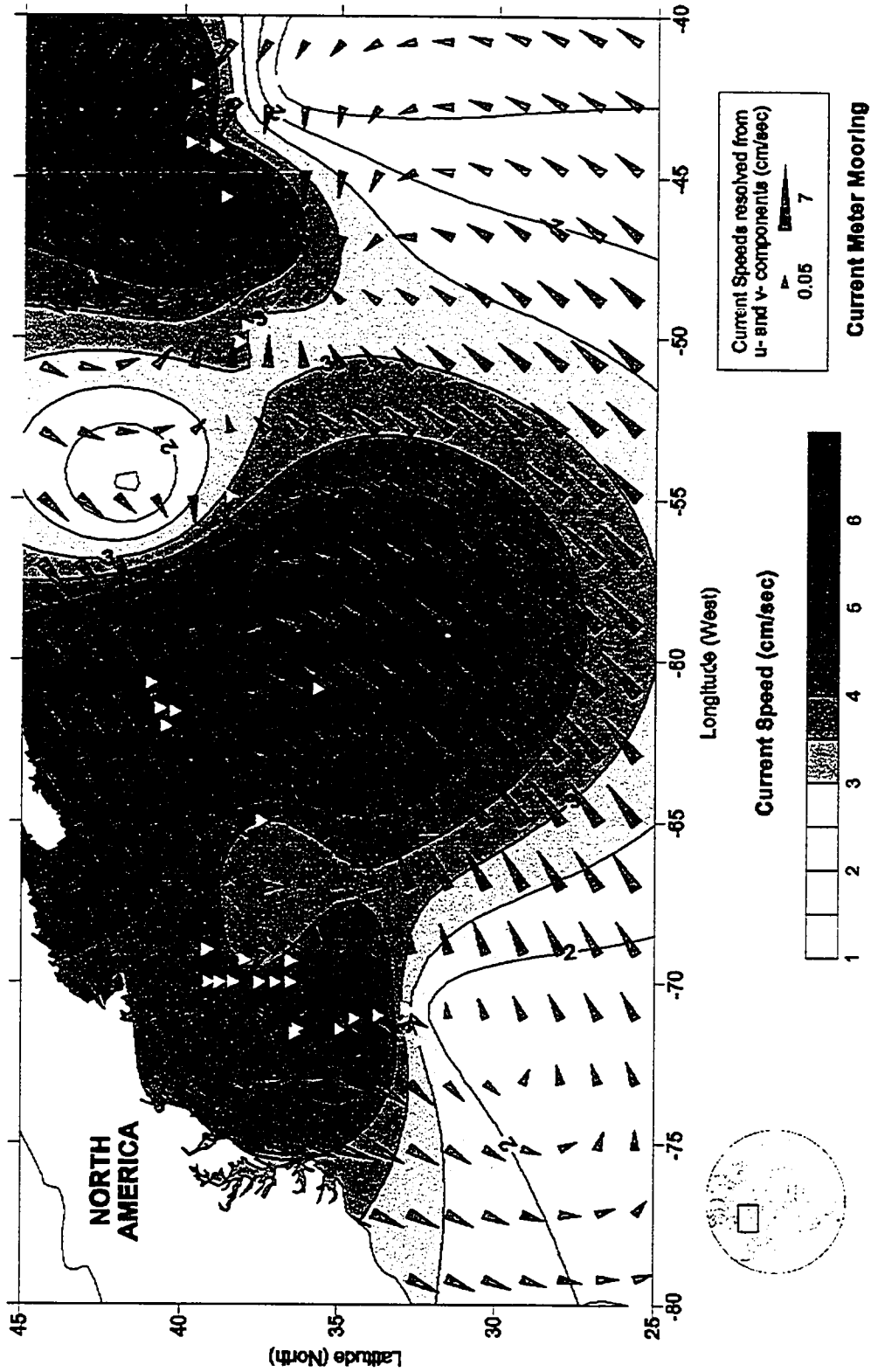


Figure 4.5 Pre-WOCE North Atlantic Ocean Components Near-Bottom Water Current Vector Plots recorded from Apr-11-1974 to Sep-03-1984 for depths within 10% of the Seafloor (2,512 to 5,430 meters depth)

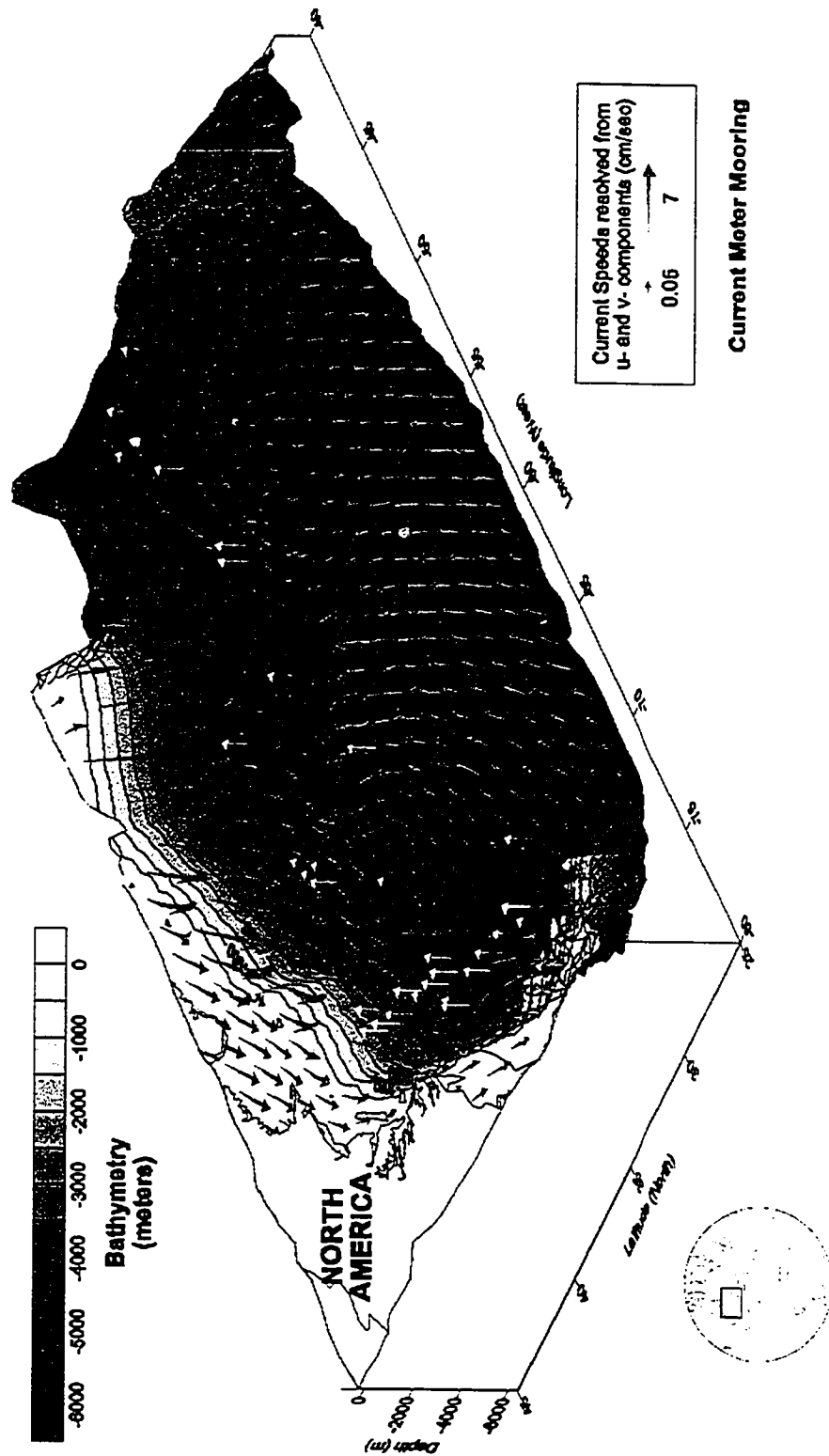
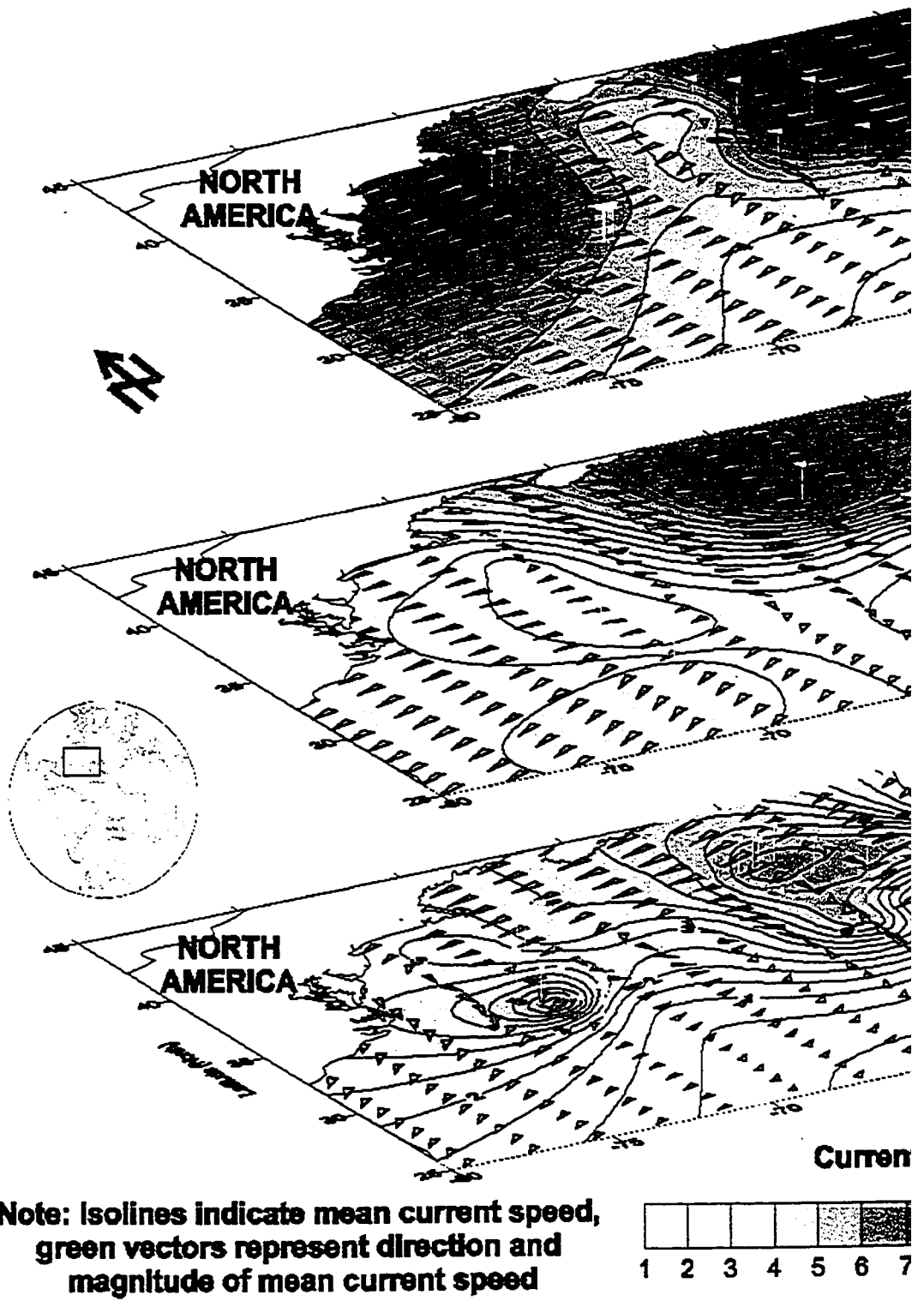
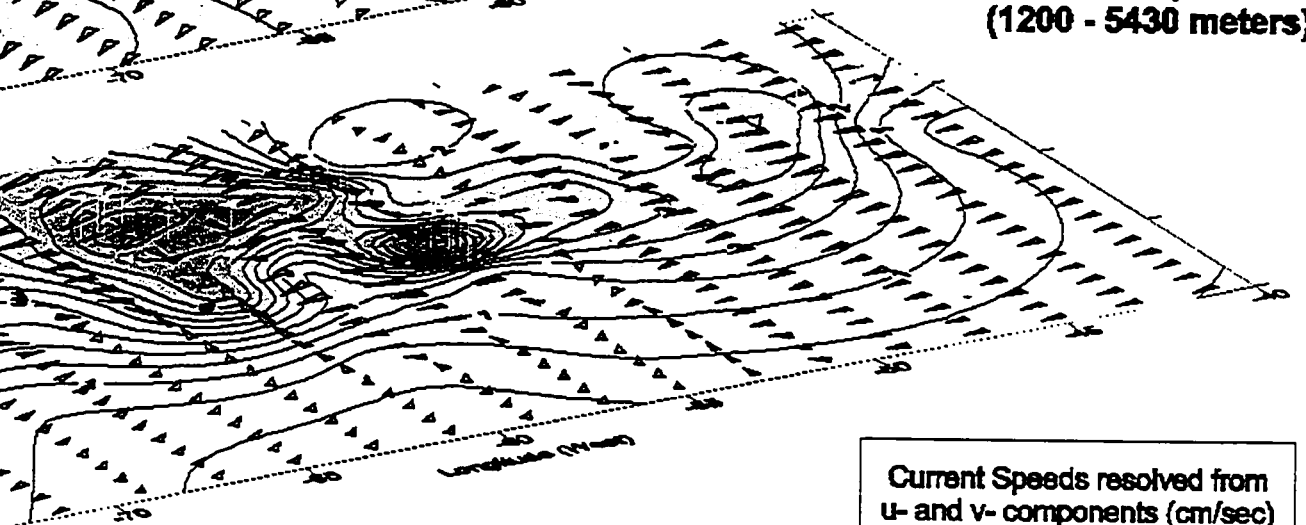
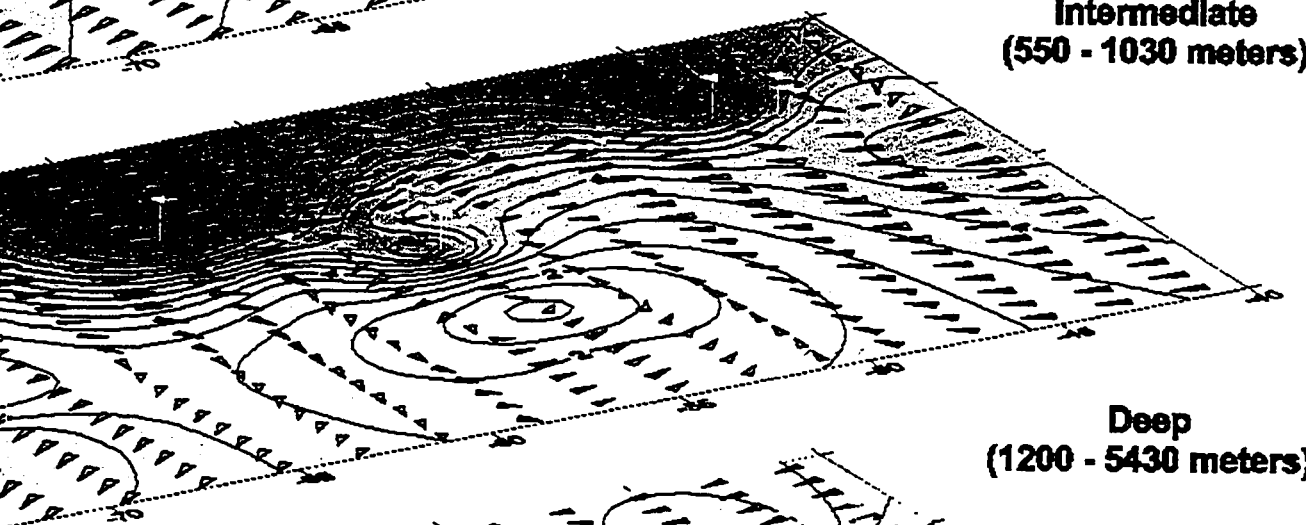
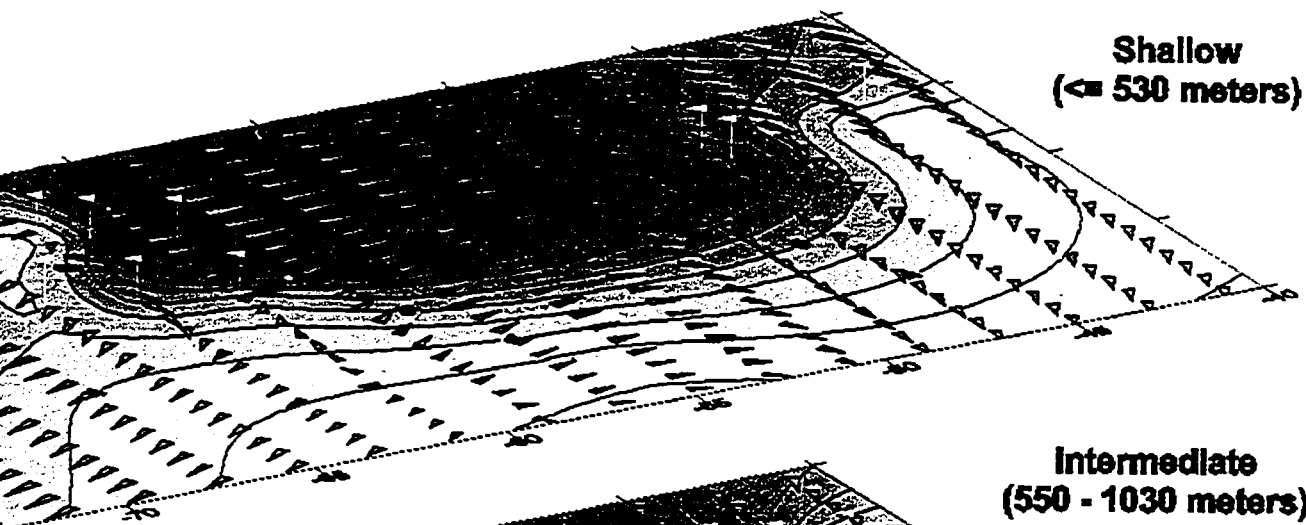


Figure 4.6 Interpolated Mean Current Vectors with Location of Current Meter Buoys and ETOPO-5 Bathymetry of the North Atlantic Ocean during the pre-WOCE Study Period of Apr-11-1974 to Sep-03-1984 for Near Bottom Depths

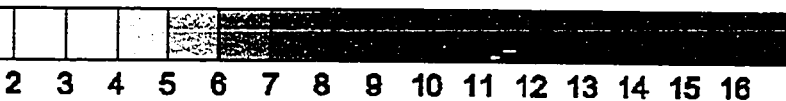
Figure 4.7 Three-Dimensional pre-WOCE North Atlantic Ocean Components Mean Current Speed Vector Plots for Shallow, Intermediate and Deep Depth Regimes of Figures 4.2 to 4.4



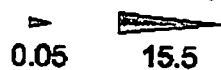




**Current Speed (cm/sec)**



Current Speeds resolved from  
u- and v- components (cm/sec)

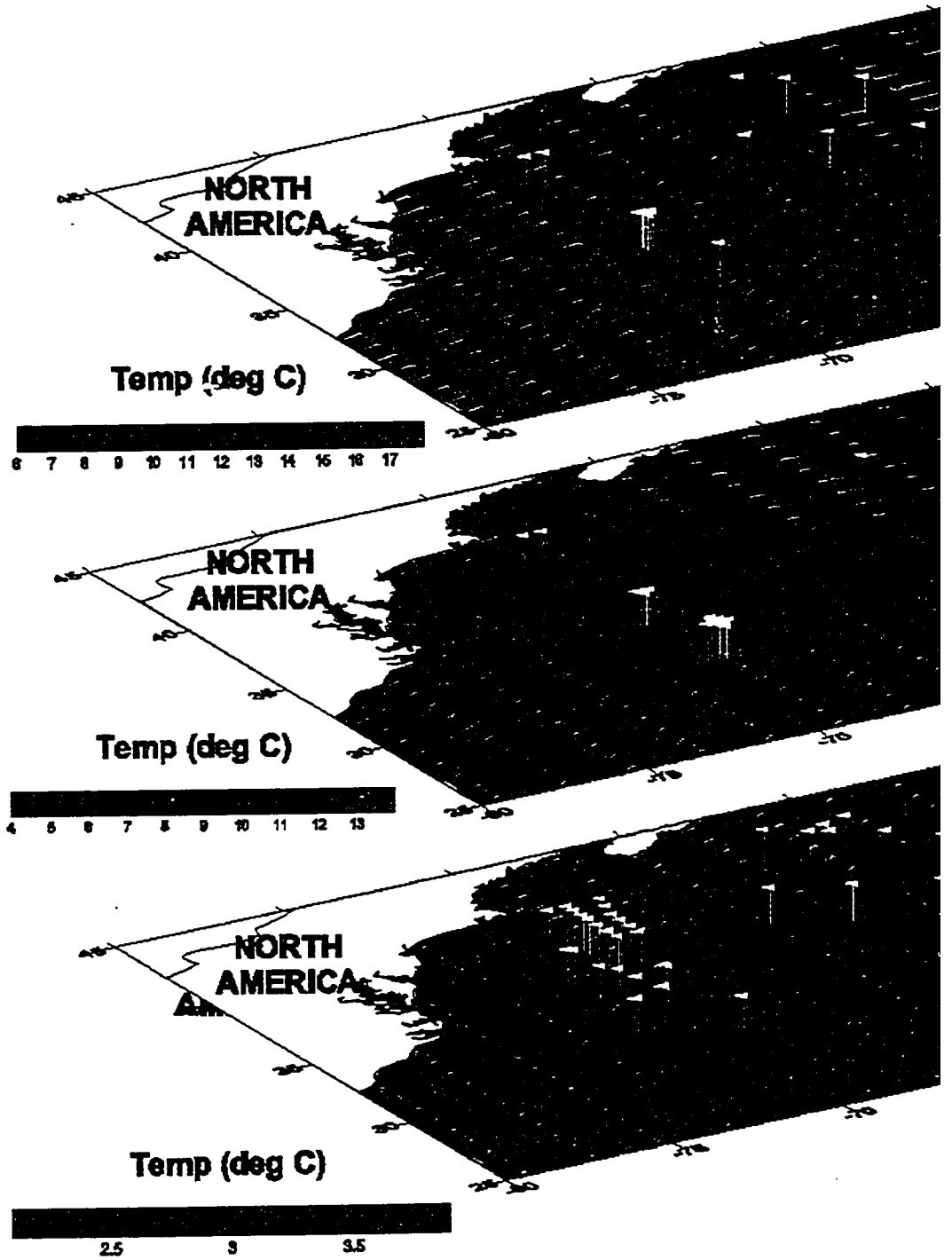


**Current Meter Mooring**



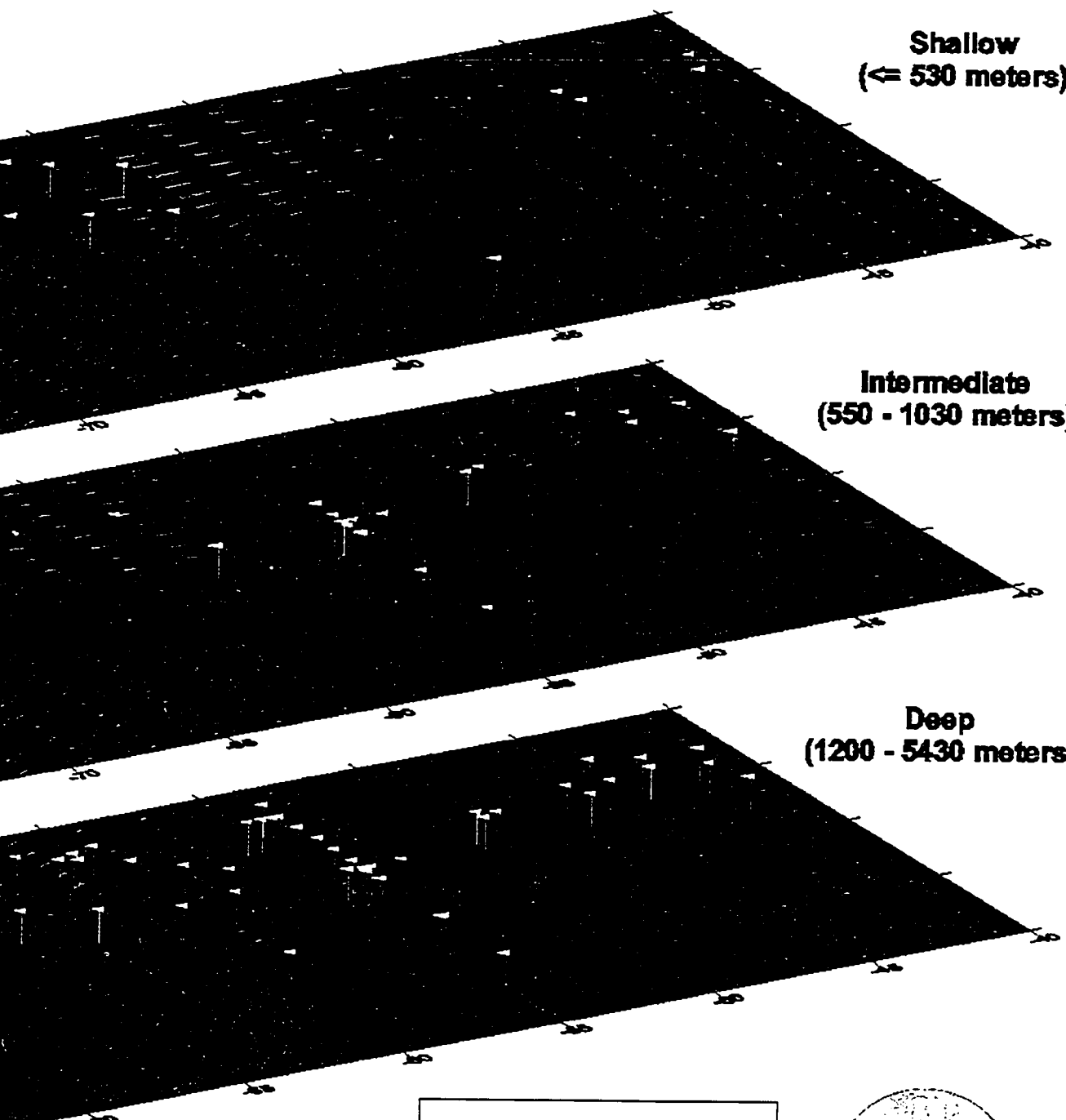


Figure 4.8 Three-Dimensional pre-WOCE North Atlantic Ocean Components Mean Current Speed Vector Plots superimposed on Mean Temperature Contour Map for Shallow, Intermediate and Deep Depth Regimes



**Note: Isolines indicate mean temperature, green vectors represent direction and magnitude of mean current speed**

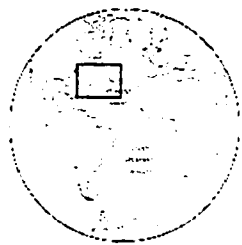
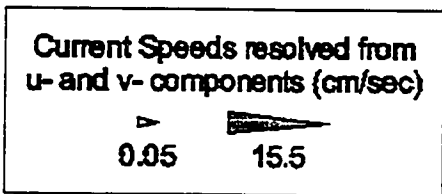




**Shallow**  
 ( $\le 530$  meters)

**Intermediate**  
 (550 - 1030 meters)

**Deep**  
 (1200 - 5430 meters)



seen vectors  
 current speed

**Current Meter Mooring**



Near-bottom water (Figures 4.5 and 4.6) shows a pattern of more spiraling water movement with southern flowing water near the continental margin, fed by southeast flowing water from the north, veering to an easterly flow and then moving northeast. Figure 4.6 shows the movement of NADW water making its way down the continental slope, while a counter-clockwise gyre is evident near 38°N and 60°W.

Figures 4.7 and 4.8 are 3-dimensional views of the data with shallow, intermediate and deep water layers overtop one another. The upper layer shows a zone of rapidly changing water temperature near 65°W, which corresponds to the mixing of warm Gulf Stream water with cold water from the Labrador Current. A more stable temperature stratification is seen toward the central North Atlantic Ocean and along the North American continental margin, with the exception of a warm water mass in the south-west sector of the map. Warm water masses are observed in the intermediate layer at three distinct locations – the mass located at 45°W can be attributed to MIW; the warm water mass located at 55°W is situated along the North Atlantic Current and may be due to the presence of warm core rings which are found north of the Current (Garrison 1996, Summerhayes and Thorpe 1996); the warm water in the south-west sector of the map is due to the North Equatorial Current flow. Though the range of water temperature is only about 2°C for deep water, there are some interesting areas of dense isotherms found at 35°N, 50°W and another near 35°N between 65°W and 75°W. Both these regions are in areas where current flow diverges.

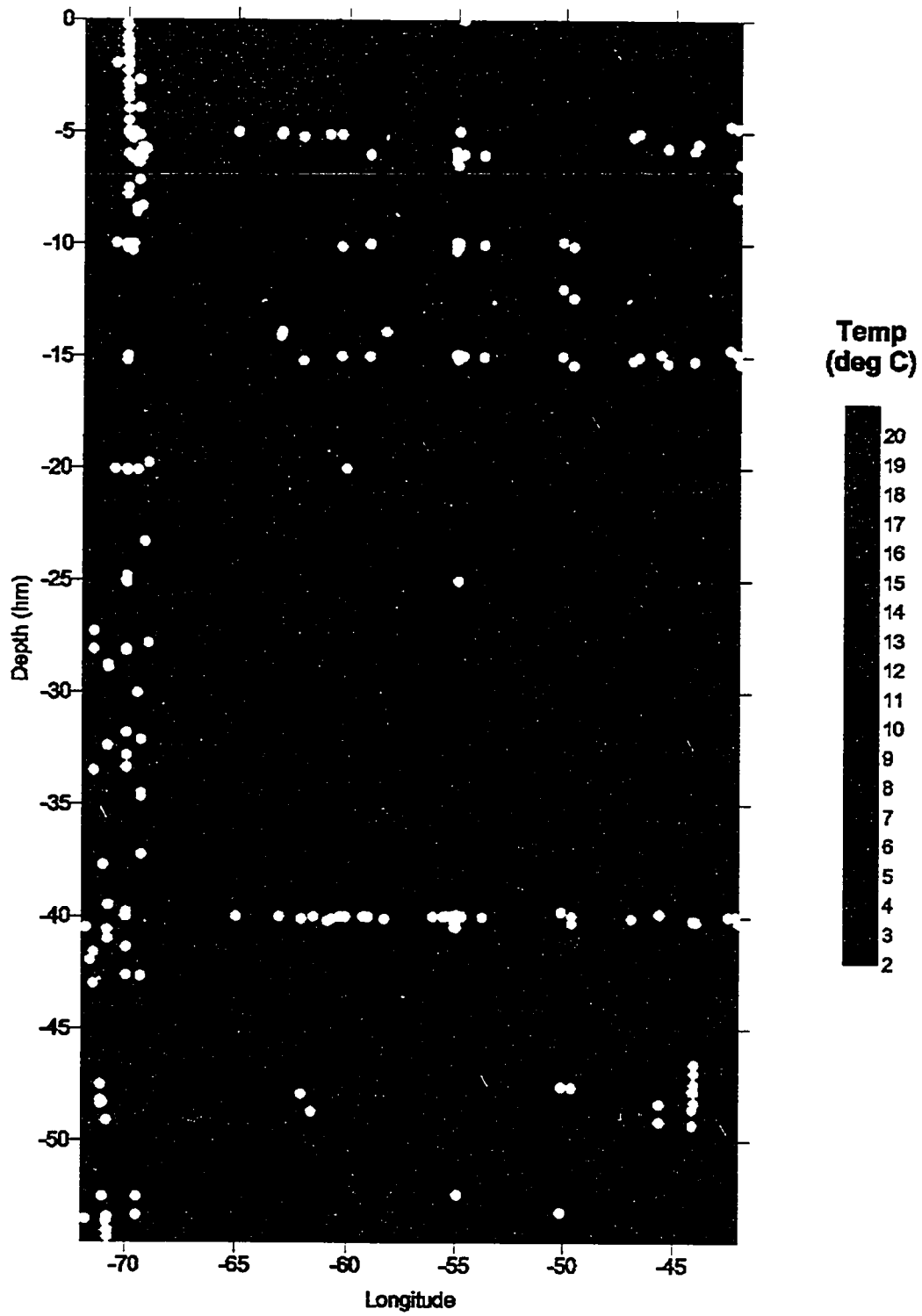
### **4.2.3 Pre-WOCE Depth Profiles**

Figures 4.9 and 4.10 show mean temperature depth profiles for longitude and latitude, while Figure 4.11 shows the mean current speed depth profile. The temperature

depth profile with respect to longitude in Figure 4.9 shows the thermocline extending from about 500 to 1,300 meters depth, and below about 2,500 meters temperatures are less than 3°C. Temperatures near the surface, in the upper 500 meters, are warmer in the western portion of the study area, possibly as a result of the warm water mass extending northward as seen in Figure 4.8.

Figure 4.10 illustrates the effect of anisotropy in smoothing out the isotherms for a more realistic temperature profile. As discussed in Section 3.6.1 (pages 69 to 70), the rationale with respect to depth profiles is that the data vary greatly with respect to depth, but not so much between horizontal sample locations. Therefore the use of an anisotropy ratio will result in contours that give a better representation of the data.

The ultimate goal of producing the depth profiles of Figures 4.8 to 4.11 is to observe the mean temperature gradients at depth throughout the North Atlantic Ocean (with regard to Figures 4.8 to 4.10), and the mean current speed gradients at depth (with respect to Figure 4.11). Since there was a dearth of salinity and pressure data, the rationale behind these plots is to try to gain some understanding of the thermohaline circulation by combining mean temperature and mean current speed. The aspiration inherent in this exercise was to create a three-dimensional plot whereby one could view a volumetric slice through the ocean. Various processes and combinations of software were tried to achieve this affect but they were all to no avail. Therefore the intent of these profiles is for the reader to envision both latitude and longitude plots as a cohesive whole in order to view the water masses flowing through the ocean. For example, in Figure 4.11 there is a water mass flowing at greater than  $12 \text{ cm s}^{-1}$  which is vertically located at 4,000 meters depth and is situated at 35°N and 55°W.



**Current Meter Moorings**

**Figure 4.9 Pre-WOCE North Atlantic Mean Temperature Depth Profiles vs. Longitude for Moorings sampled between April 11, 1974 and August 28, 1984**

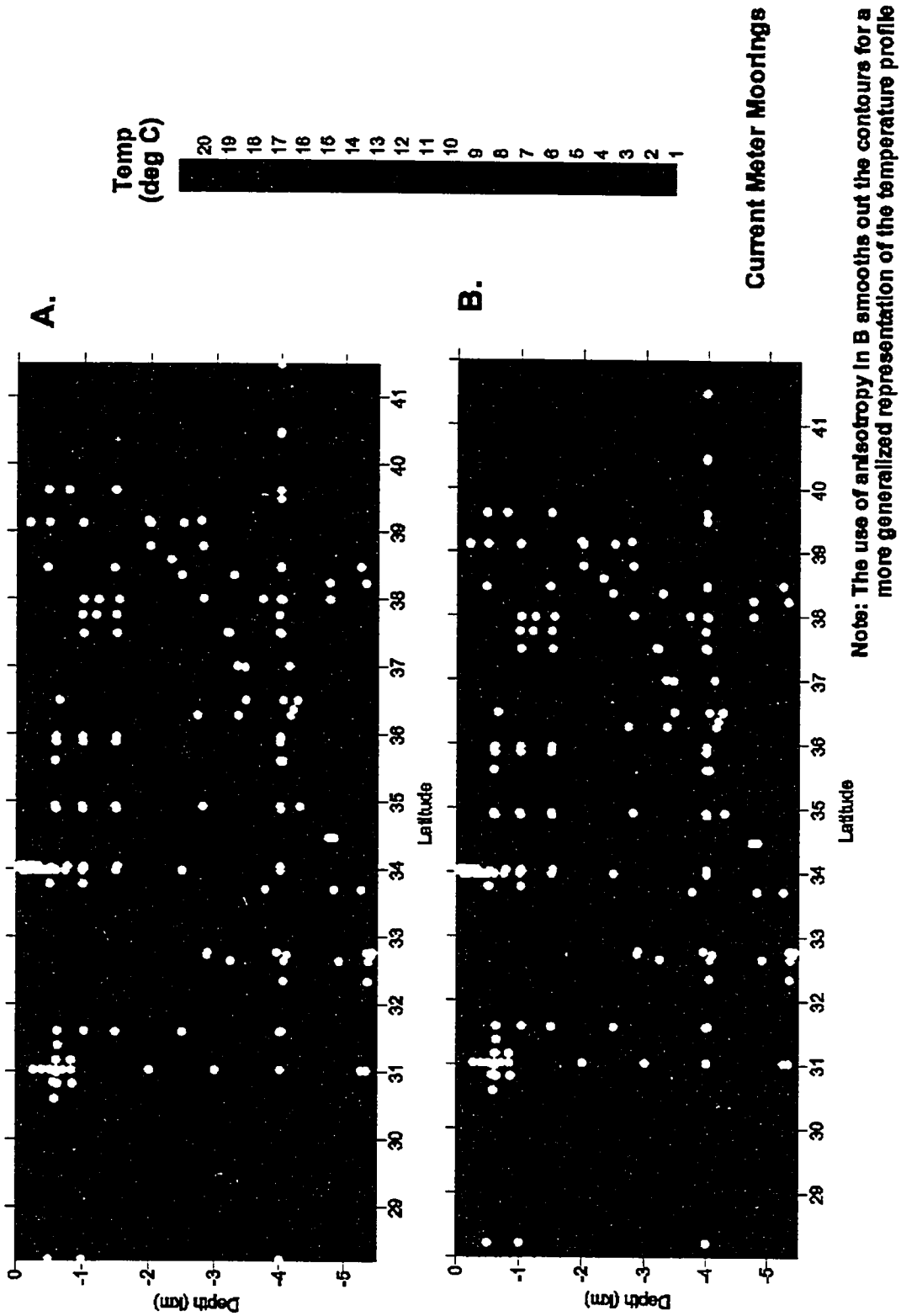
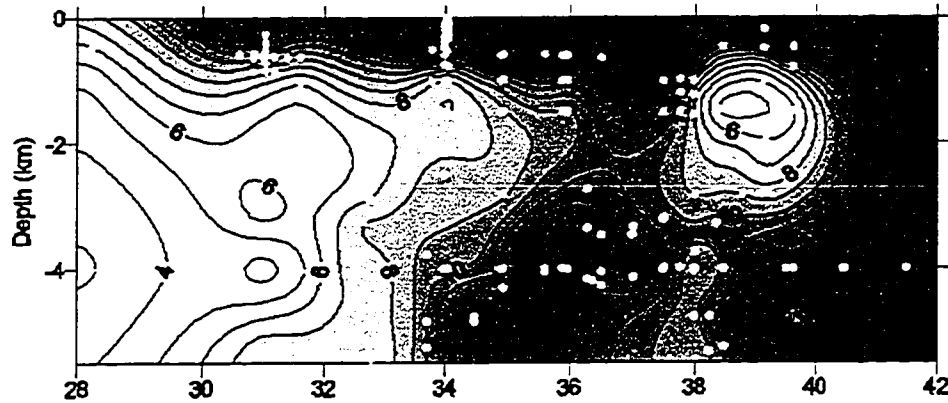
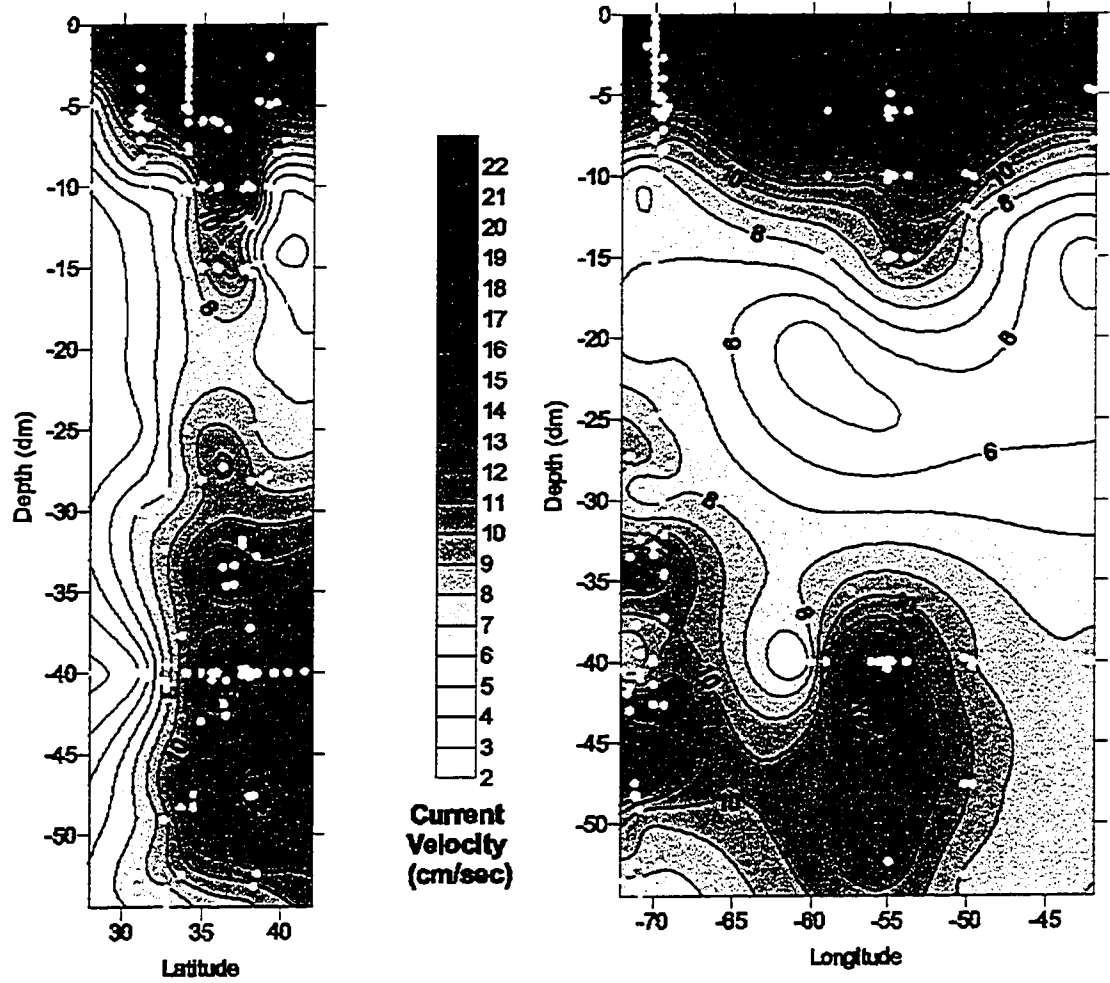


Figure 4.10 Pre-WOCE North Atlantic Mean Temperature Profiles vs. Latitude for Moorings sampled between April 11, 1974 and August 28, 1984





**A. Latitude vs. Depth in kilometers**



**B. Latitude vs. Depth in hectometers**

**C. Longitude vs. Depth in hectometers**

**Current Meter Moorings**

**Figure 4.11 Pre-WOCE North Atlantic Ocean Mean Current Velocity Depth Profiles for Current Meter Moorings sampled between April 11, 1974 and August 28, 1984 (Red square denotes homogeneous water mass – see discussion on page 90)**

The surface temperature profile appears to follow the latitudinal pattern of decreasing temperature northward, with the exception of a warm water area near 37°N and a cold water area near 39°N. When Figure 4.10 is viewed in conjunction with Figure 4.9 these appear to be a result of the warm water mass between 70°W and 75°W and the cold water mass between 65°W and 70°W. Using kilometers as the scale of depth it is difficult to get a precise location of the thermocline layers - more will be said on this in looking at Figure 4.11.

Figure 4.11 shows the mean current speed depth profile, which is given in both kilometers and decameters for latitude. The selection of different measurement scales affects the appearance of the map and any interpretation that can be done on the map. With a depth scale of kilometers, the mean current differences at varying latitudes can be discerned. Using a depth scale of decameters the depth differences are apparent, but the subtle variations in latitude are lost. The end result is dependent on the range of values for each variable. This is noticeable in Figure 4.11.C which gives a fairly good resolution for both depth and longitude. The main point to note in manipulating the x- and y-axes is that stretching one axis at the exclusion of the other skews the data in that direction and detracts what one can visualize from this representation of the data.

Figure 4.11.A shows a plume of slower moving water surrounded by faster water at a depth between 1000 and 2000 meters between 38°N and 40°N, and a larger region of slow moving water between 28°N and 33°N. Figure 4.11.C shows that this slower water lies across the entire longitudinal area between 42°W and 72°W. The former would appear to be water lying to the north of the North Atlantic Current, while the latter is the presence of the Sargasso Sea south of the North Atlantic Current.

### **4.3 Pre-WOCE Individual Components**

In an effort to include some results of local current conditions an analysis was conducted on two sets of pre-WOCE data. The Gulf Stream Extension, due to its relationship with the Gulf Stream Current, and the Low Level Waste Ocean Disposal Program (LLWODP) dataset due to the nature of the original study, which will be explained in Section 4.3.2.

#### **4.3.1 Gulf Stream Extension**

This dataset consists of 27 records located between 37.002°N and 40.367°N latitude and 42.007°W and 46.908°W longitude ranging in depths from 506 to 4,928 meters below sea level (Figure 4.12). This results in a study area that is roughly 159,000 square kilometers, or 703,500 cubic kilometers encompassing an area at the terminus of the Gulf Stream and at the start of the North Atlantic Current (Figure 4.13). The mean values calculated are annual means for the period October 1979 to November 1980.

The Gulf Stream begins upstream of Cape Hatteras and leaves the North American coast at various positions throughout the year, shifting north in the fall and south in the winter and early spring (Frankignoul et al. 2001).

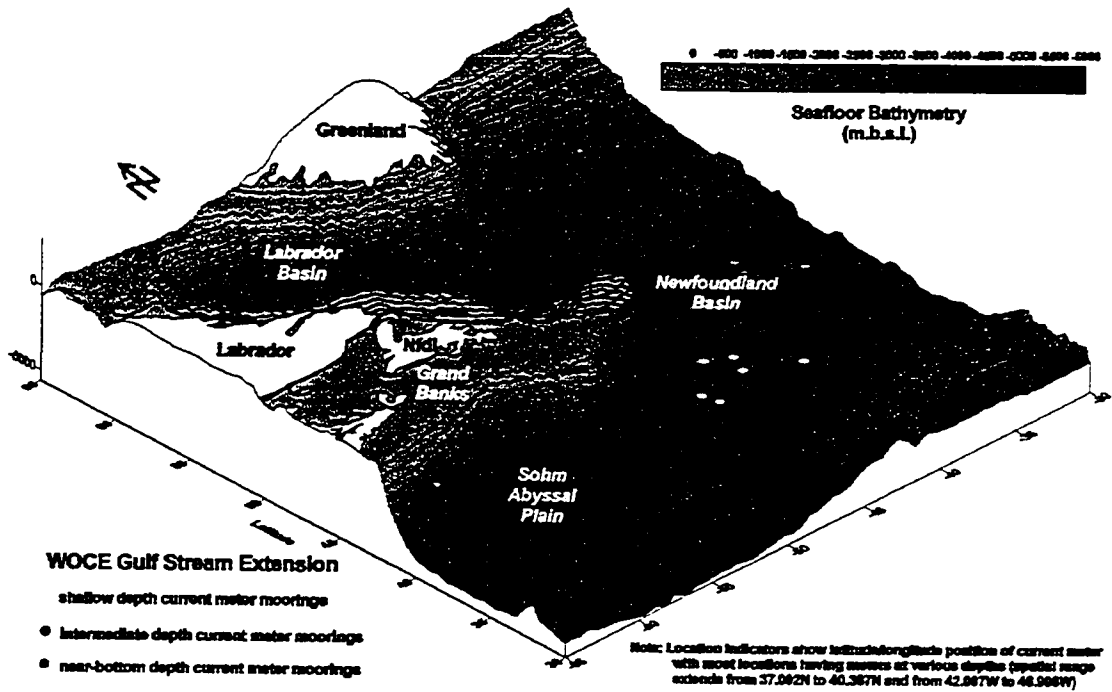


Figure 4.12 Site Map for the pre-WOCE Gulf Stream Extension in the North Atlantic Ocean (30°N to 65°N latitude, 30°W to 65°W longitude) showing Bathymetry and Landmasses

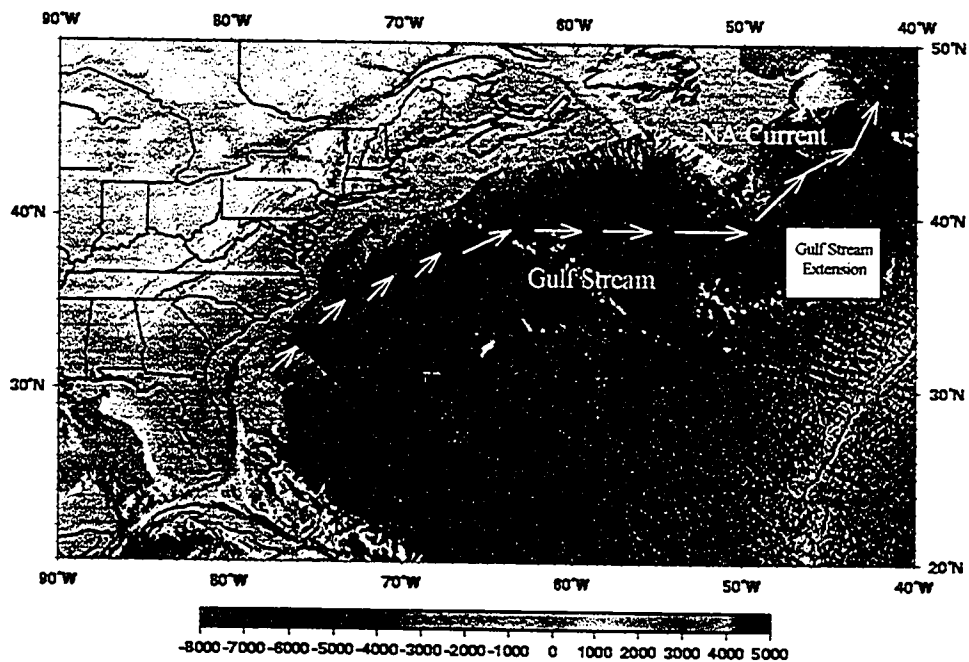


Figure 4.13 Location of Gulf Stream, North Atlantic Current and Gulf Stream Extension (Source: adapted from [http://oceancurrents.rsmas.miami.edu/atlantic/img\\_topo2/gulf-stream2.jpg](http://oceancurrents.rsmas.miami.edu/atlantic/img_topo2/gulf-stream2.jpg))

### 4.3.1.1 Variation in Range of Variables

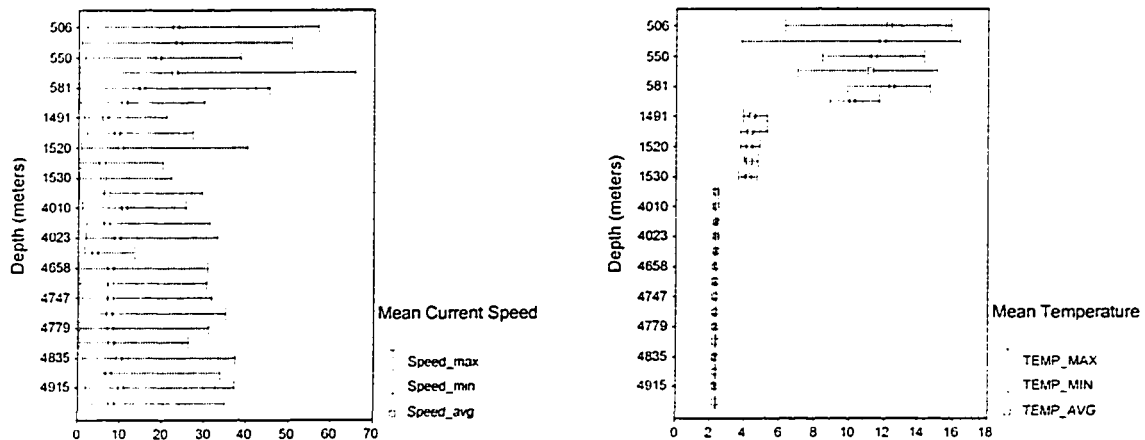


Figure 4.14 Variable Plots of Min, Mean, and Max Values versus Current Meter Depth for Current Speed ( $\text{cm s}^{-1}$ ) and Temperature ( $^{\circ}\text{C}$ )

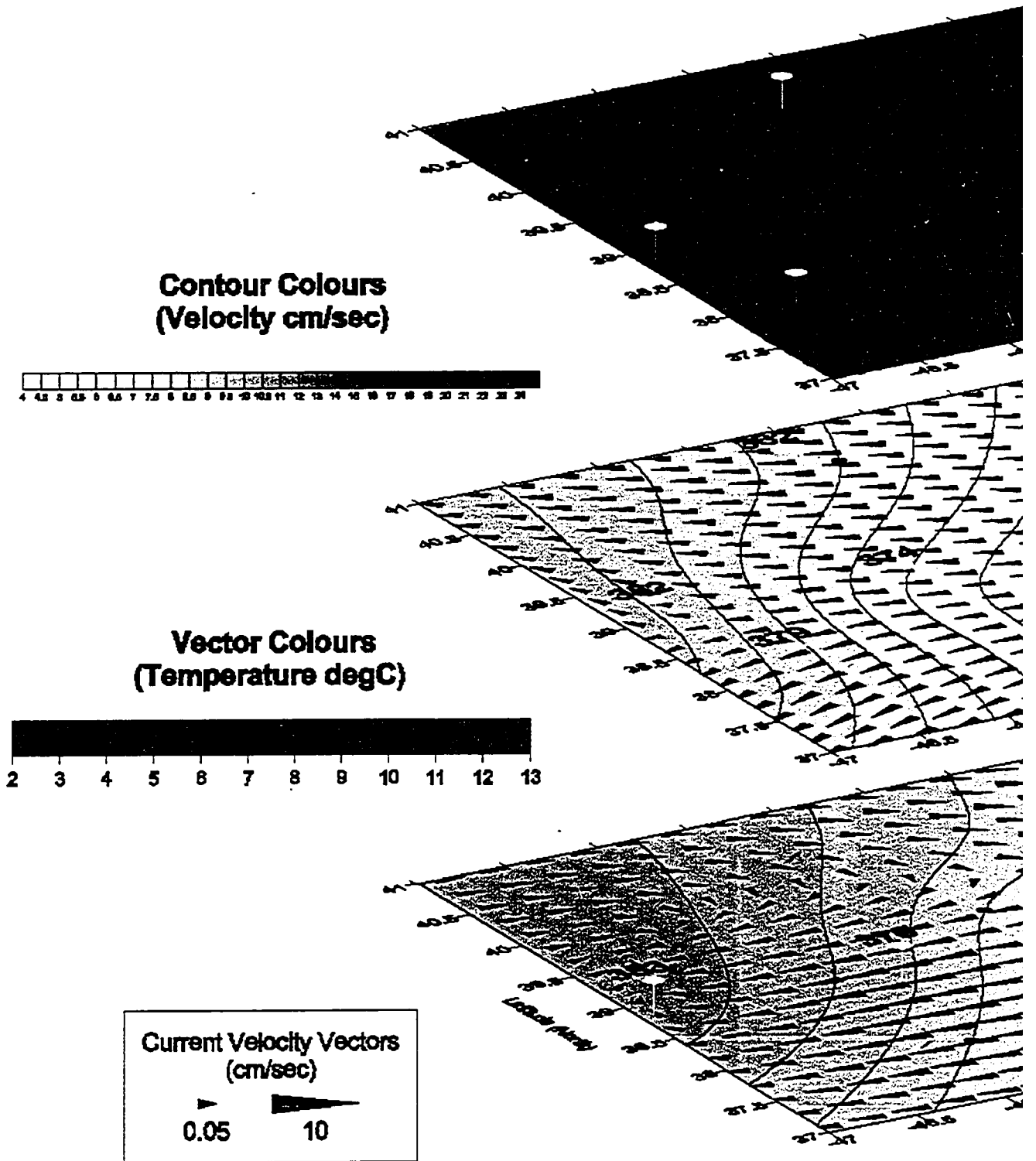
The above two charts illustrate the trends in the two variables of main concern, mean current speed and mean temperature. Mean current speed shows greater values and greater variability near the surface especially above 600 meters.

Mean temperatures follow the recognized pattern of decreasing values with depth until stabilizing at approximately  $2^{\circ}\text{C}$  at 4,000 meters depth. The range of each record also decreases by an approximate magnitude of 10 at each break in water depth, from a range of 10 degrees for shallow waters, 1 degree for intermediate water and 0.1 degree for deep water.

### 4.3.1.2 Dynamics of the Gulf Stream Extension

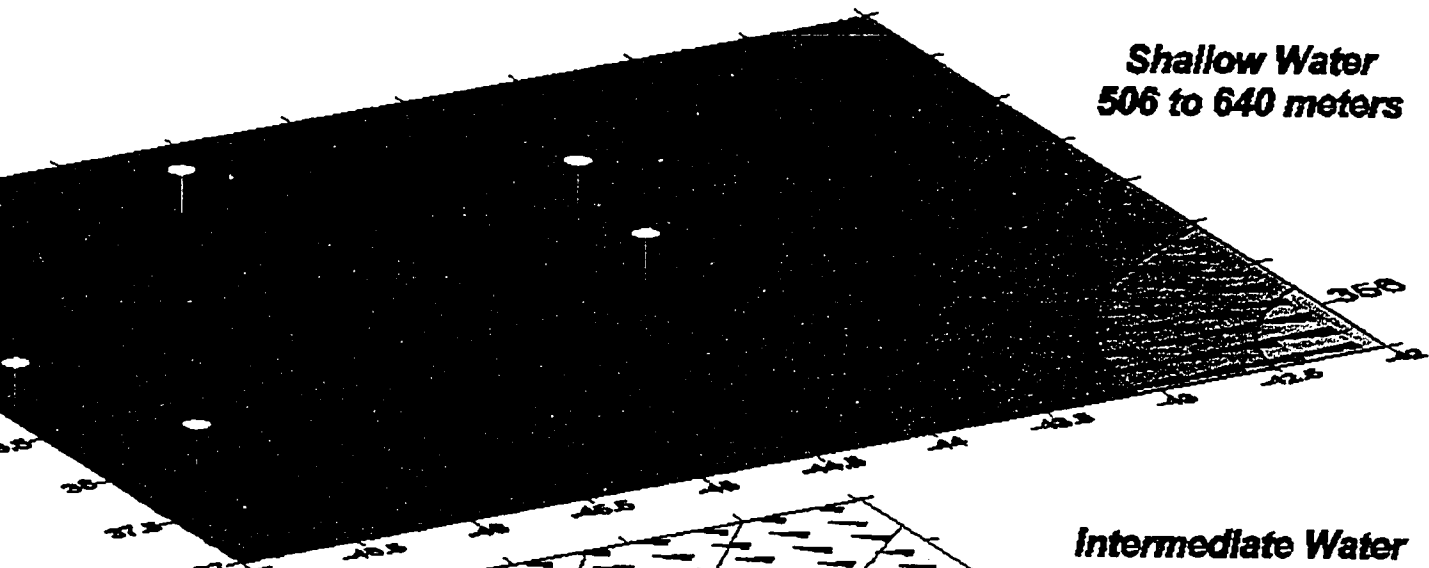
Three-dimensional plots of current velocity for shallow, intermediate, and deep water are shown in Figure 4.15. The shallow water plot includes current meters lying between 506 to 640 meters, intermediate water is for those between 1,491 and 1,530 meters, and deep water is for those between 3,989 to 4,928 meters. The magnitude of the vectors is equivalent to current velocity, while vector colours show changes in water temperature.

Figure 4.15 Pre-WOCE Gulf Stream Extension Experiment – Three-Dimensional View of Shallow, Intermediate and Deep Water (10/24/79 – 11/24/80)

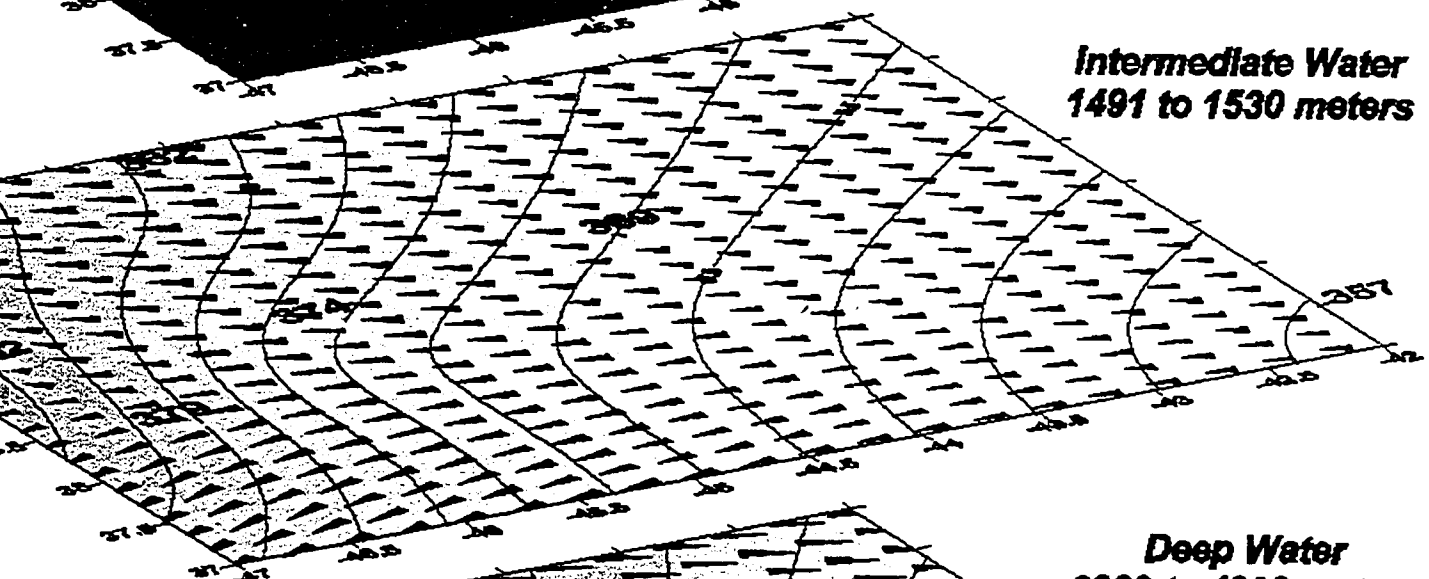




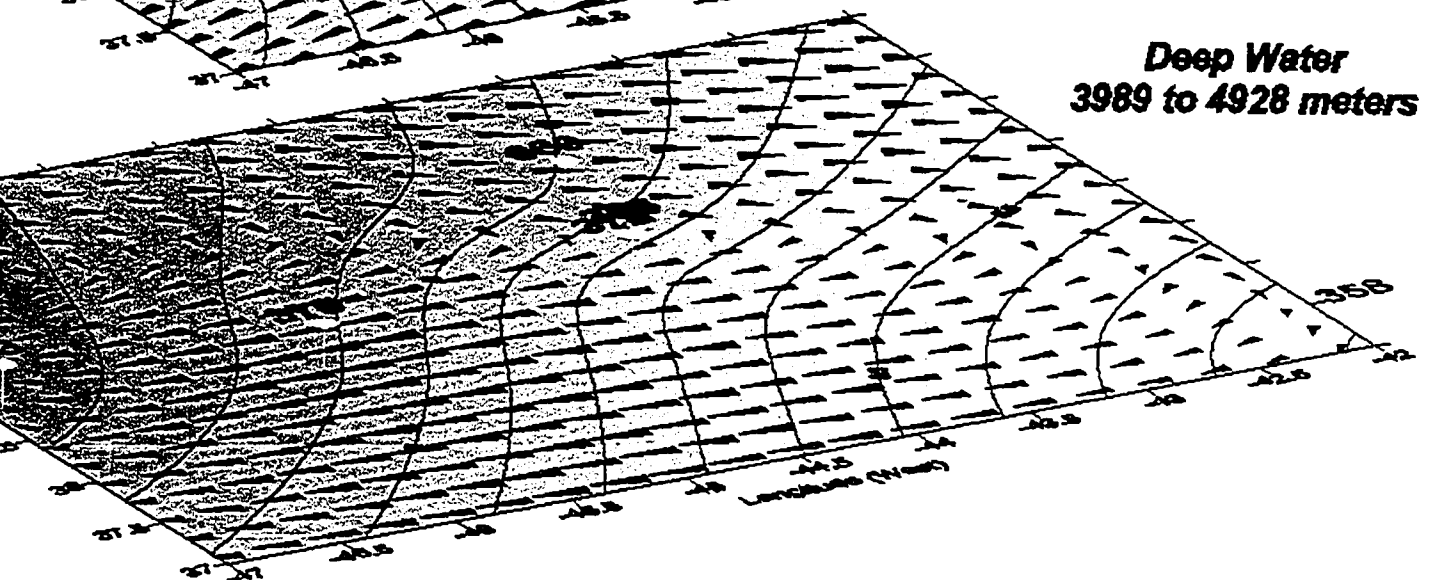
**Shallow Water  
506 to 640 meters**



**Intermediate Water  
1491 to 1530 meters**



**Deep Water  
3989 to 4928 meters**



**Current Meter Locations**





The plots of mean current speed need to be interpreted carefully due to the sparse placements of the current meter moorings. Greater certainty can be gleaned in the area circumscribed by 37.5°N and 40°N latitude and 44.5°W and 47°W longitude. In this 2.5° x 2.5° grid, shallow water shows a south to south-west flow west of 45°W. East of here the flow north of 38°N begins to spiral northward. The south-west flow from accession 361 (number adjacent to current meter location) becomes southerly near accession 381 and returns to a south-west flow at accession 378. The data rich areas of accessions 359 and 368 cause the interpolation algorithm to make the flow pattern veer to the north-east. Average current speed increases in a north-westerly direction. Intermediate water flow patterns seem more consistent with all current meters showing a general westerly flow and mean current speed increasing to the north-west as in the shallow water plot.

Current flow patterns in the deep water plot indicate a westerly flow south of 39°N. North of this area water tends to flow in an easterly direction with the indication of a rotational gyre. The easterly flow at depth is contiguous with the tail-end of the eastern flowing Gulf Stream at about 40°N. However, the north-east flow of the North Atlantic Current does not appear to be captured by the vector plot. This probably is a result of the absence of current meters in the north-east quadrant of the study area.

The general pattern across volumetric space shows a steady increase in mean current speeds to the north-west with consistent flows in the intermediate layer, spiraling flows in the deep layer, and a break in the south-west flow pattern near accession 368.

#### *4.3.1.3 Gulf Stream Extension Depth Profiles*

The locations of different water masses are difficult to identify based only on current speed and temperature because these data contain an incomplete record on salinity, making density calculations impossible. Therefore only general trends are discussed to determine the main patterns found in the depth profiles (Figures 4.16 & 4.17).

The temperature profile (Figure 4.16) shows temperatures greater or equal to 12°C at depths above 500 meters, which corresponds roughly to the surface zone. Temperatures then begin dropping rapidly from this depth to about 1,800 meters, where they reach 4°C, giving the thermocline a depth of roughly 1,300 meters for this area. Below about 2,000 meters temperatures remain steady below 3°C.

Current profiles (Figure 4.17) portray similar patterns for both mean and maximum current speeds. With respect to latitude (Figure 4.17.a.), surface speeds are greater than speeds at depth. However an area of faster currents at depth are found north of 40°N which coincides with the inflow from the Gulf Stream. These current speeds are especially pronounced at a depth below 4,000 meters. Faster current speeds are found between 38.5°N and 39.5°N at 4,500 to 5,000 meters depth. These should be considered as accurate due to the density of current meters at these locations which allow for a better representation of the data.

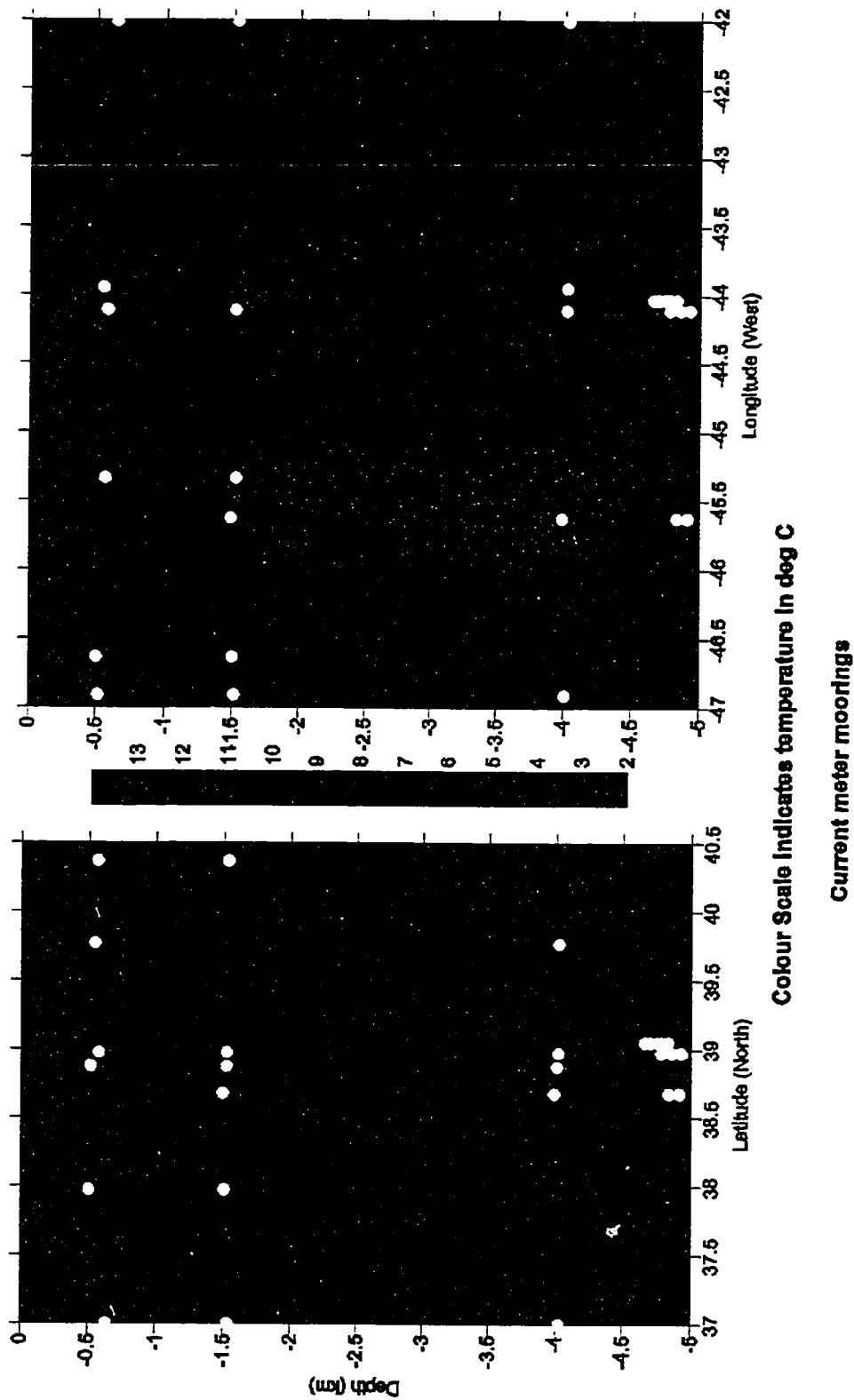
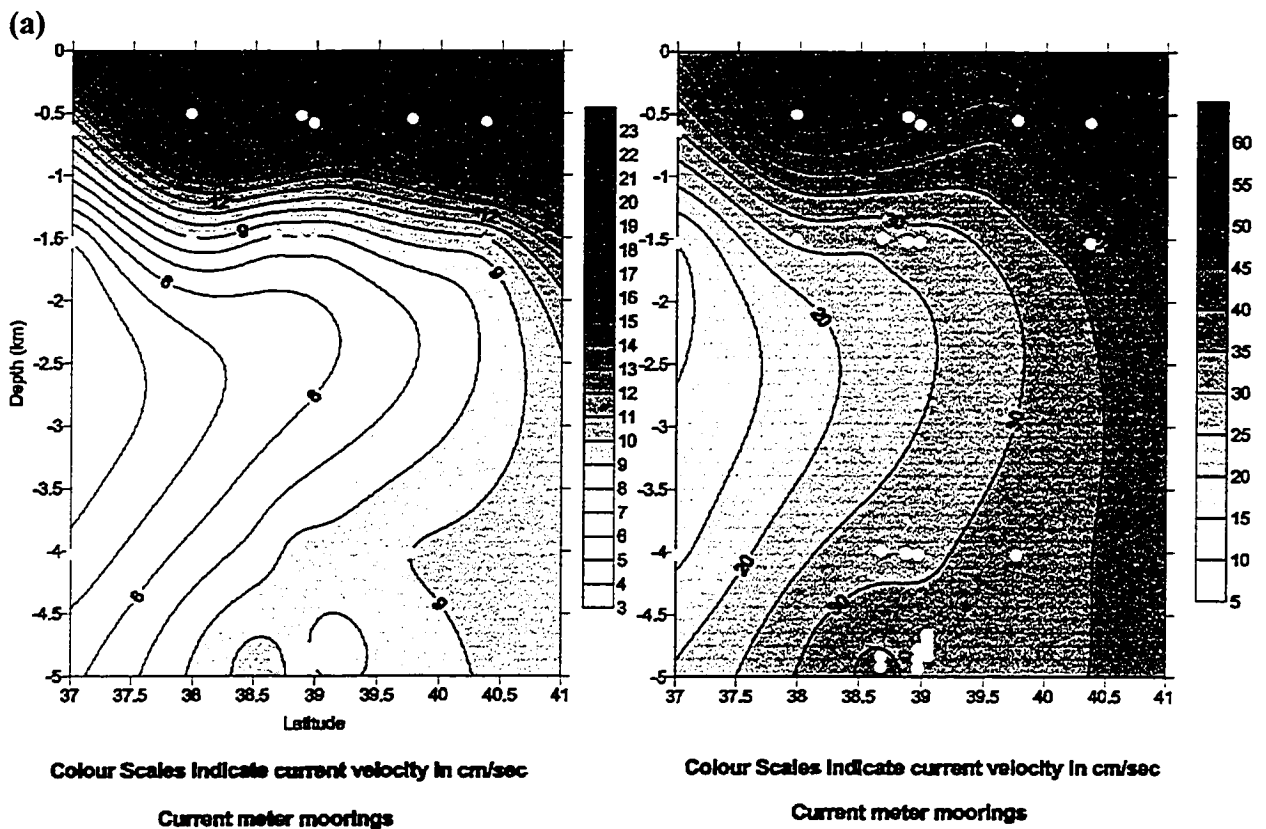
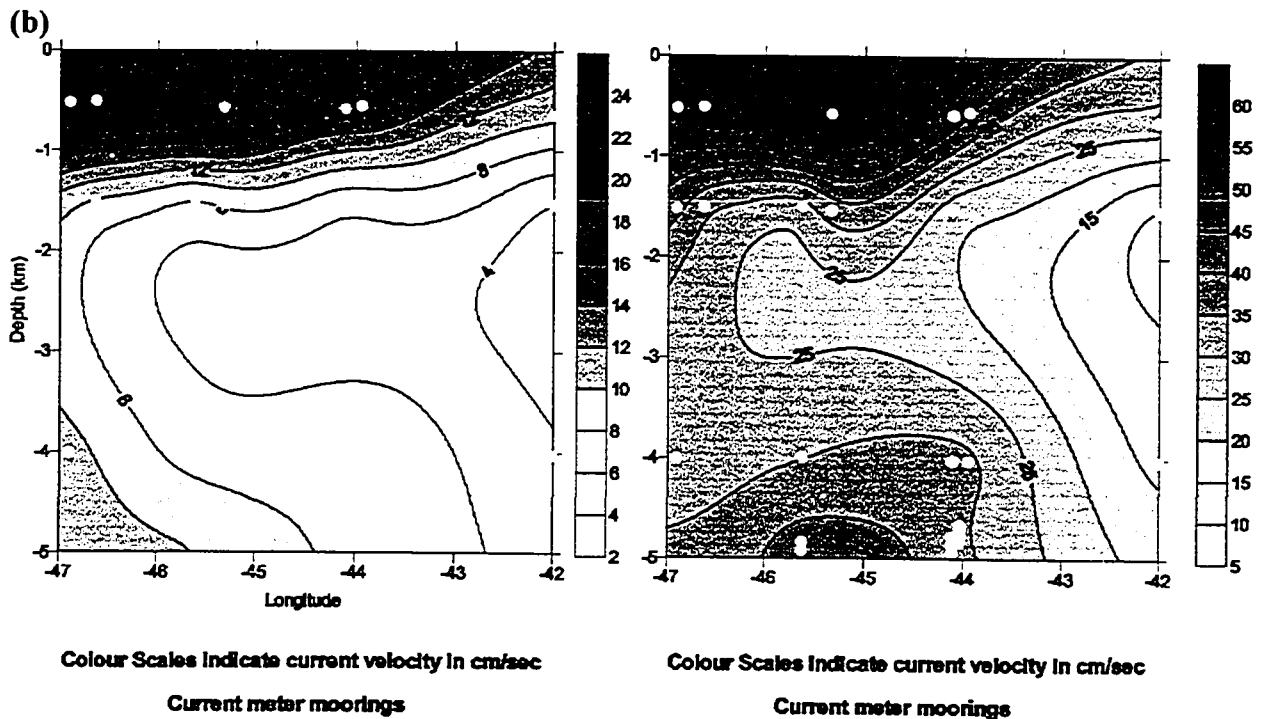


Figure 4.16 Pre-WOCE Gulf Stream Extension Component in the North Atlantic Ocean Depth Profile indicating Mean Temperature with Latitude and Longitude (October 1979 – November 1980)

Looking at longitude versus depth (Figure 4.17.b), the main features to note are the faster surface currents, and what appears to be a plume of slower moving water intruding into the faster water at a depth of 2,000 to 3,000 meters. Figure 2.4 indicates the movement of water masses along different latitudes and shows NADW making up the majority of the water between 37.0°N and 40.5°N beginning at a depth of approximately 1,200 meters. Above this depth there is an inflow of MIW from the Strait of Gibraltar. Taking this water mass into account, and the nature of the westward flowing surface water, the narrow contours of decreasing current speed above 1,500 meters could be related to the presence of this water mass.





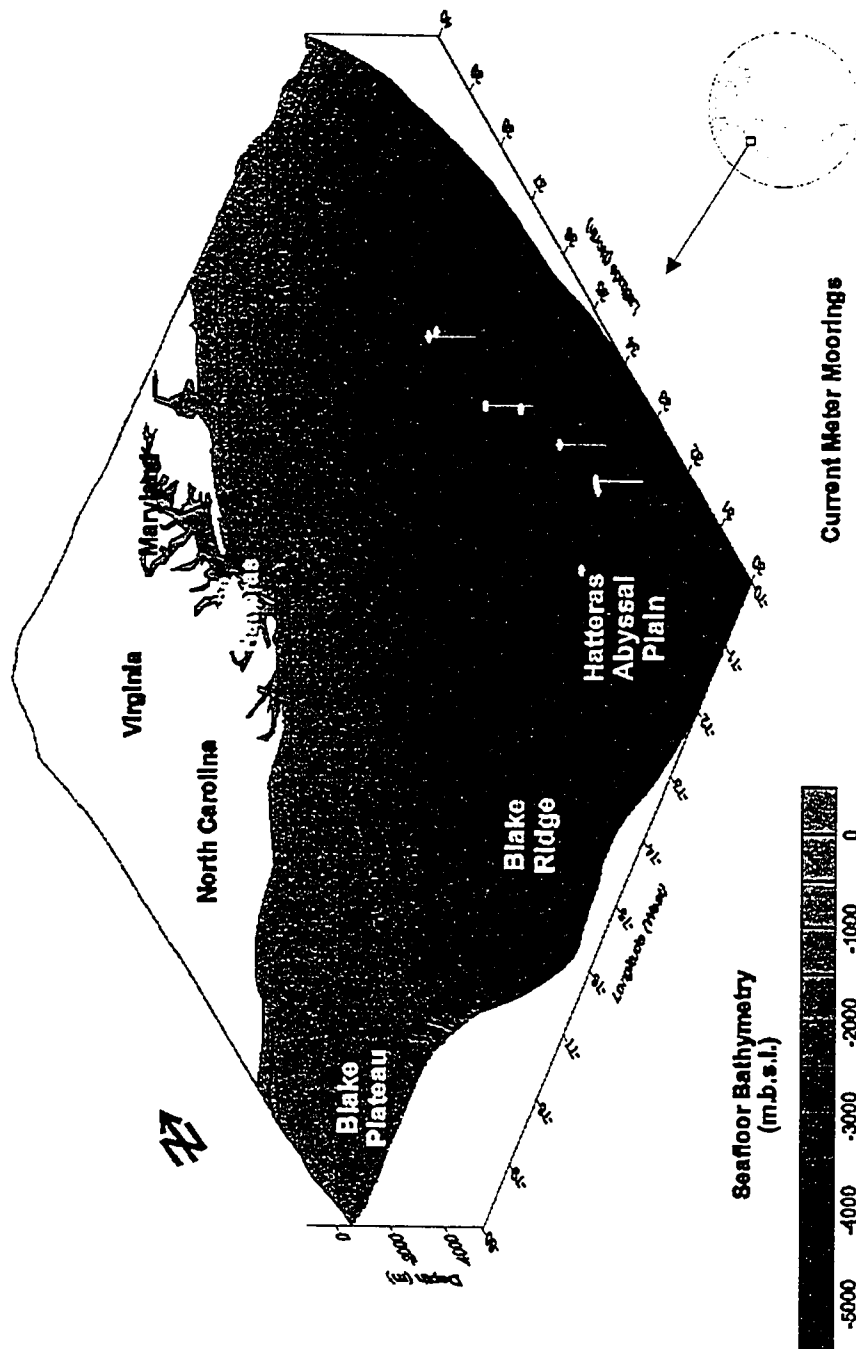
**Figure 4.17 Pre-WOCE Gulf Stream Extension Component in the North Atlantic Ocean Depth Profile indicating Mean and Maximum Current Velocity with (a) Latitude and (b) Longitude (October 1979 – November 1980)**

### 4.3.2 Pre-WOCE Low Level Waste Ocean Disposal Program (LLWODP)

These data are included as an example of a deep water set of current meters. The dataset includes 29 records, 26 of which are deep water moorings located between 32.342°N and 36.362°N latitude and 70.787°W to 71.822°W longitude, at depths ranging from 2,730 to 5,430 meters below sea level. The extent of the study area is approximately 42,400 square kilometers, or 114,500 cubic kilometers. Mean values are annual means for the period September 16, 1980 to September 3, 1984.

The current meters are located south-east of the origin of the Gulf Stream (Figure 4.18), and though no study has been found to confirm this, it would appear that they were initially deployed in order to determine if the absence of currents at depth was conducive for a possible abyssal waste dump. This has been presumed since grant money was

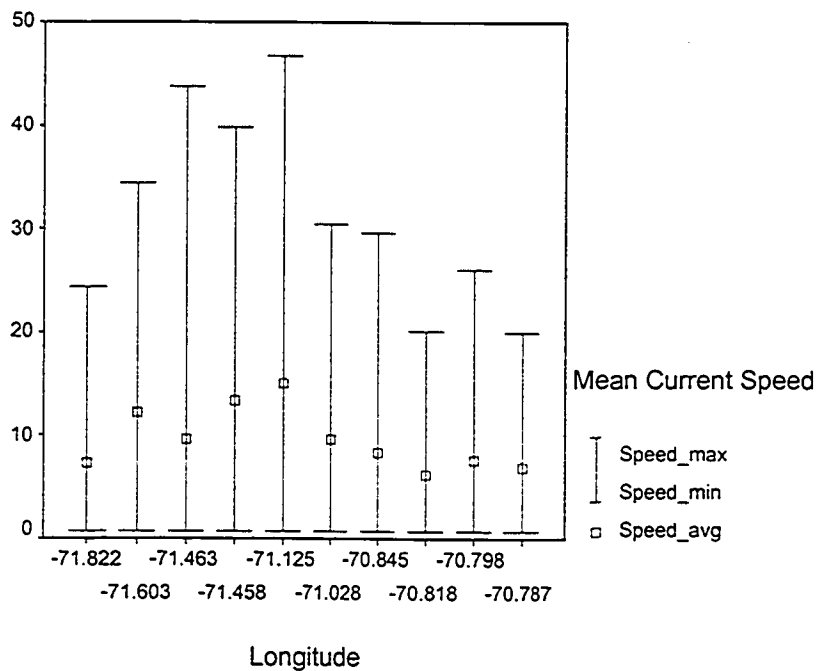
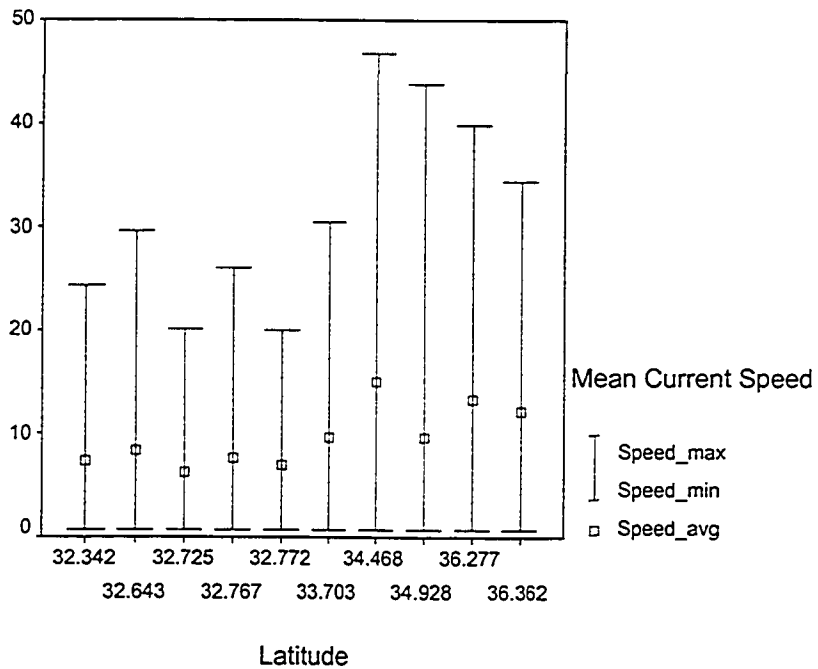
awarded to researchers implementing LLWODP by Sandia National Laboratories, who specialize in nuclear waste (<http://sheff.caeds.eng.uml.edu/hazwaste/ocean.htm>).



**Figure 4.18 Pre-WOCE Low Level Waste Ocean Disposal Program (LLWODP) Component in the North Atlantic Ocean – Current Meters Deployed Sep-16-1980 to Sep-03-1984**

### 4.3.2.1 Variation in Range of Variables

Figure 4.19 shows that mean current speed is faster north of about 34°N and west of roughly 71°W. Mean current speed versus depth shows no discernable pattern, while temperature indicates the usual pattern with temperatures stabilizing at approximately 2°C below 4,000 meters.





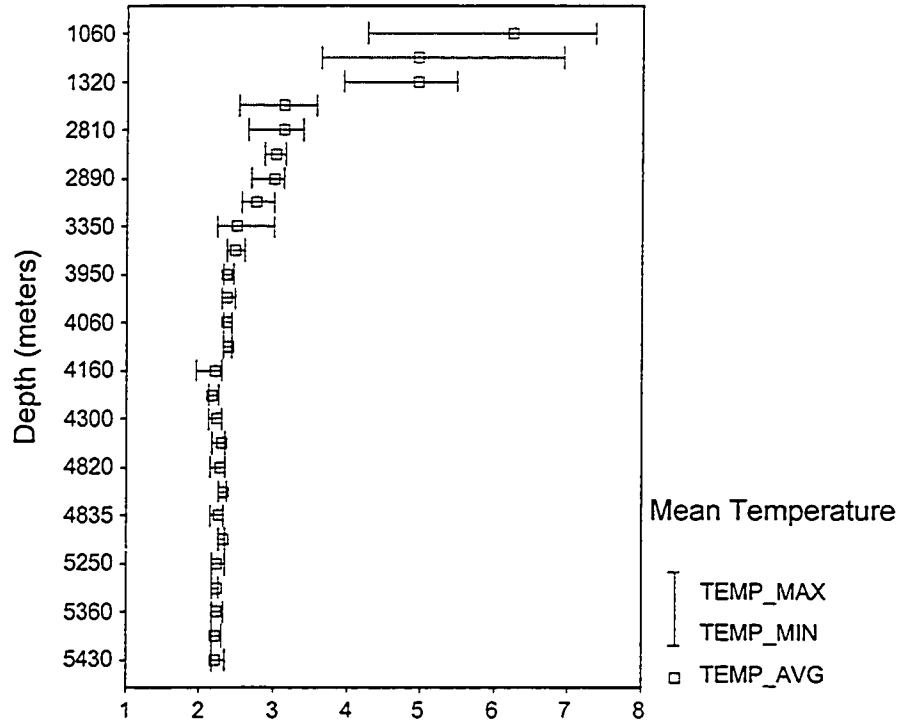
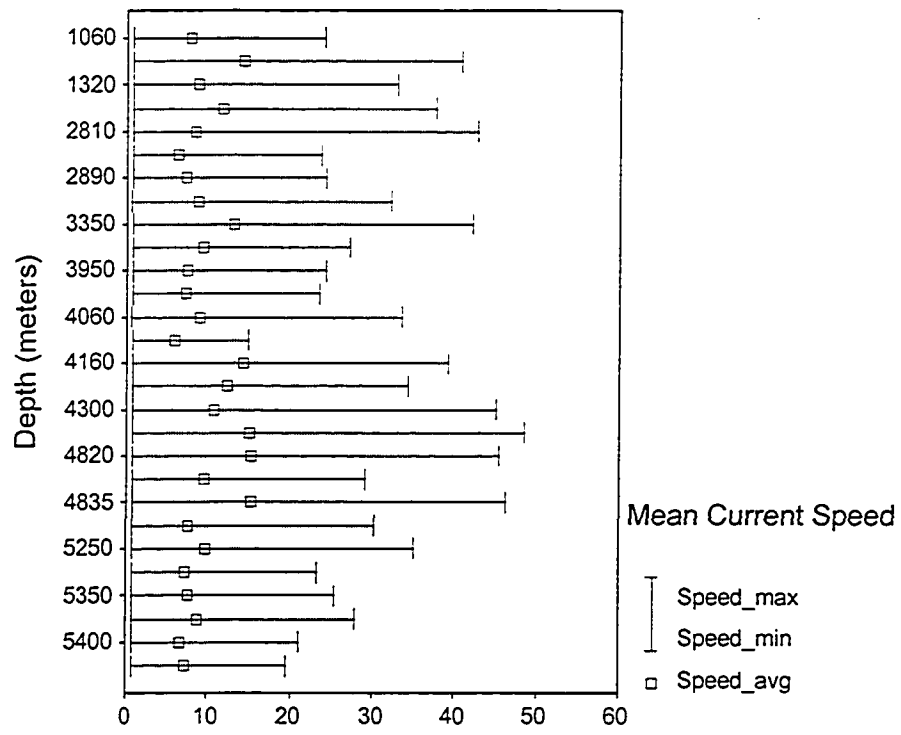


**Figure 4.19 Variable Plots of Min, Mean, and Max Values for Current Meter Speed ( $\text{cm s}^{-1}$ ) vs. Latitude, Longitude and Depth and for Mean Temperature ( $^{\circ}\text{C}$ ) vs. Depth**

### 4.3.2.2 Dynamics of LLWODP

The Low Level Waste Ocean Disposal Program focused on deep water, with 26 of the 29 data records being for depths below 2,700 meters. When looking at the near-bottom current vector plot (Figure 4.20) and the near-bottom bathymetric current vector plot (Figure 4.21), the current meters appear to be located in part of a gyre, with current speeds greatest between 34° and 36°N, spiraling in a south-east to south-west clockwise direction. South of 34°N current speeds slow down and flow direction becomes more chaotic with a westerly flow west of 71°W, and a southerly flow east of 70.5°W. The deeper waters south of 34°N, within the Hatteras Abyssal Plain, where current speeds are much slower, and where the majority of current meters were deployed, would appear to be the array which was under consideration for waste disposal.

### 4.3.2.3 LLWODP Depth Profiles

The depth profiles (Figure 4.22) mirror the current vector plots in showing a faster current speed regime north of 34°N and slower speeds over the Hatteras Abyssal Plain. This same tendency occurs east of 71°W, again over the Hatteras Abyssal Plain.

The depth profiles also shed some light on the nature of the current flow with some of the faster speeds and highest variability occurring between 4,500 and 5,500 meters depth, and some of the slowest speeds between 2,500 and 3,000 meters depth in the area over the Hatteras Abyssal Plain.

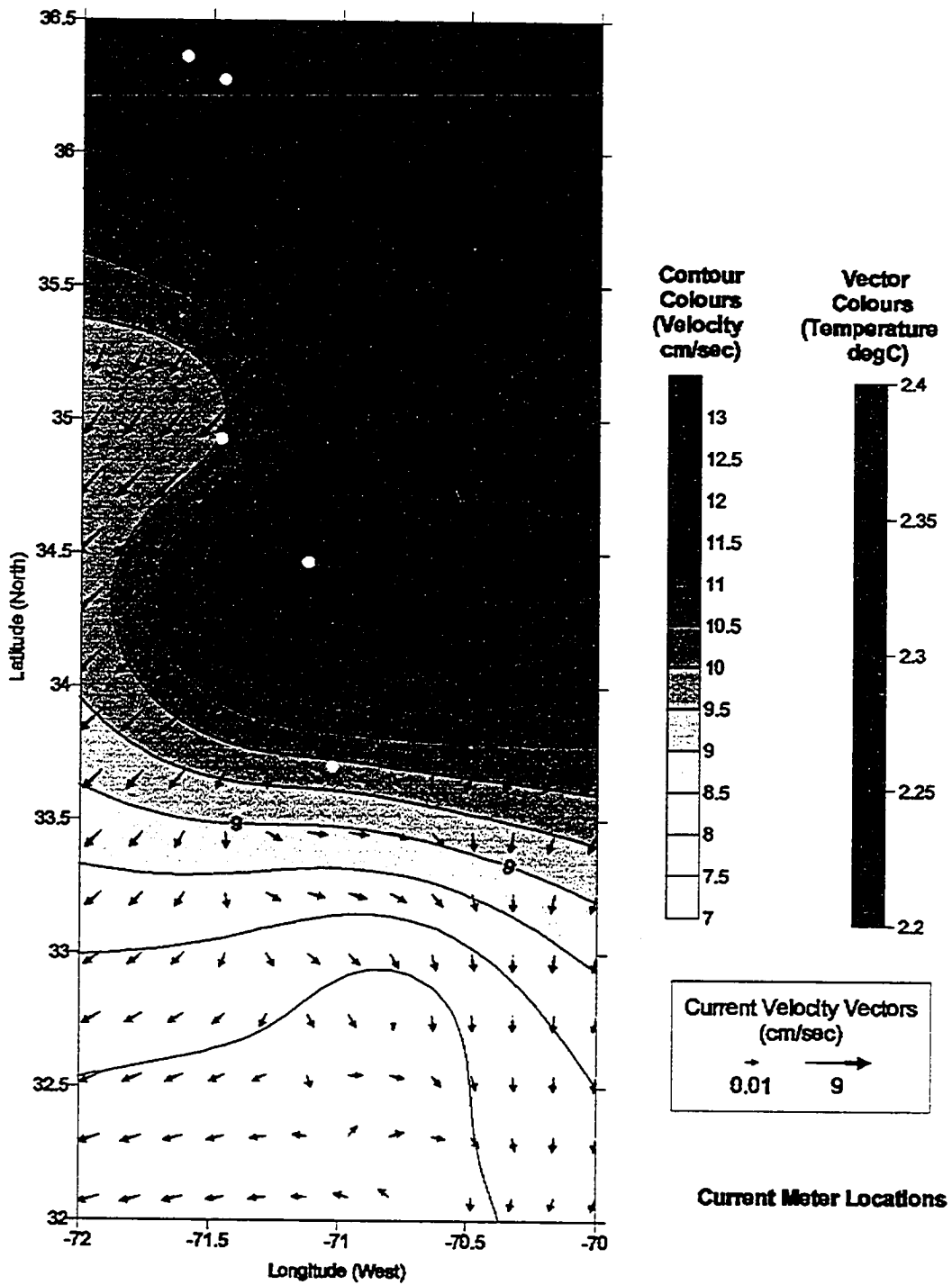


Figure 4.20 Pre-WOCE LLWODP East Experiment Near-bottom Current Vector Plots  
2,370 to 5,430 meters depth (09/16/80 – 09/03/84)

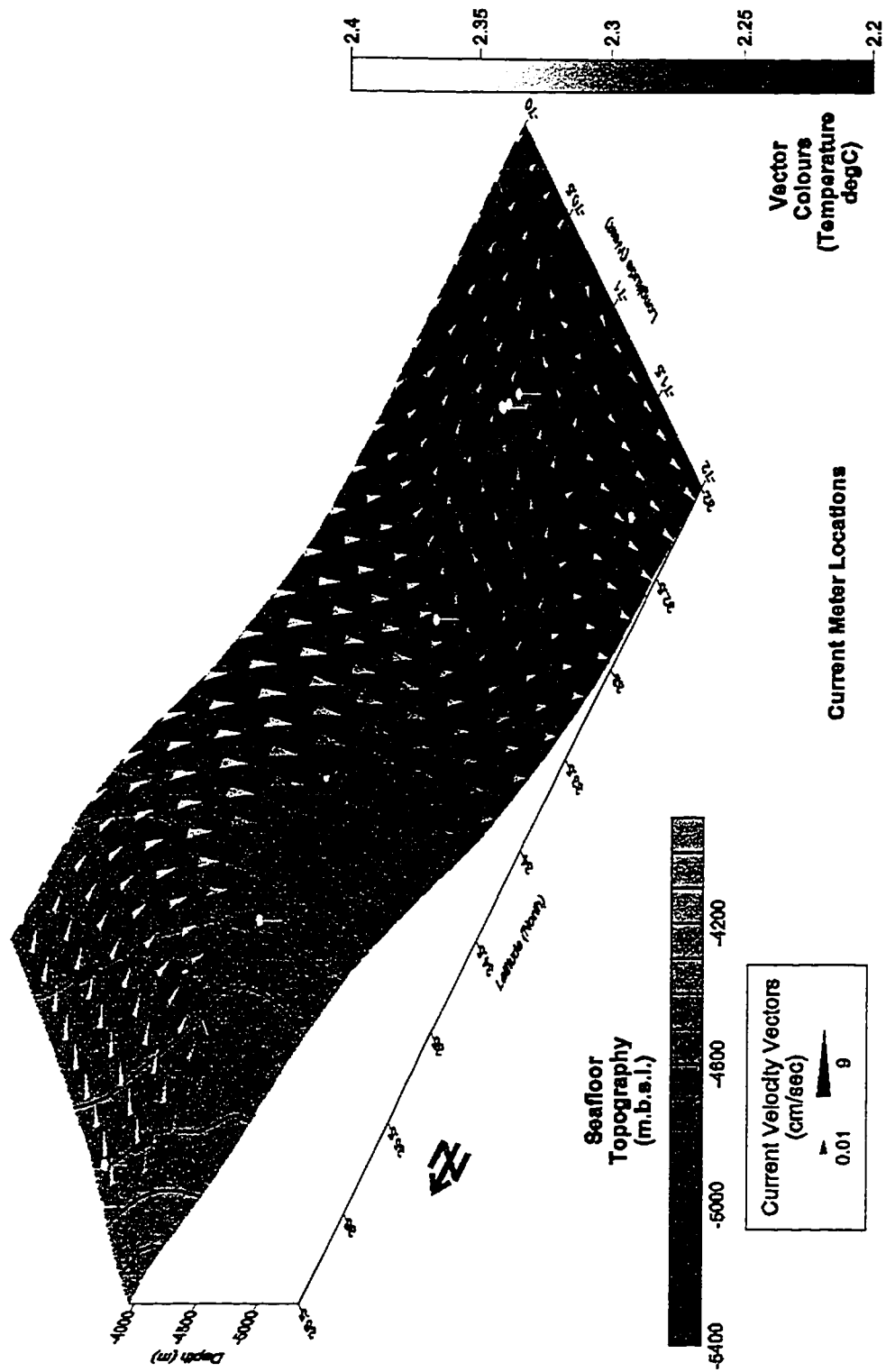


Figure 4.21 Pre-WOCE LLWODP East Experiment Near-bottom Current Vector Plots with Deployment at 2,370 to 5,430 meters depth (09/16/80 – 09/03/84) showing Local Bathymetry

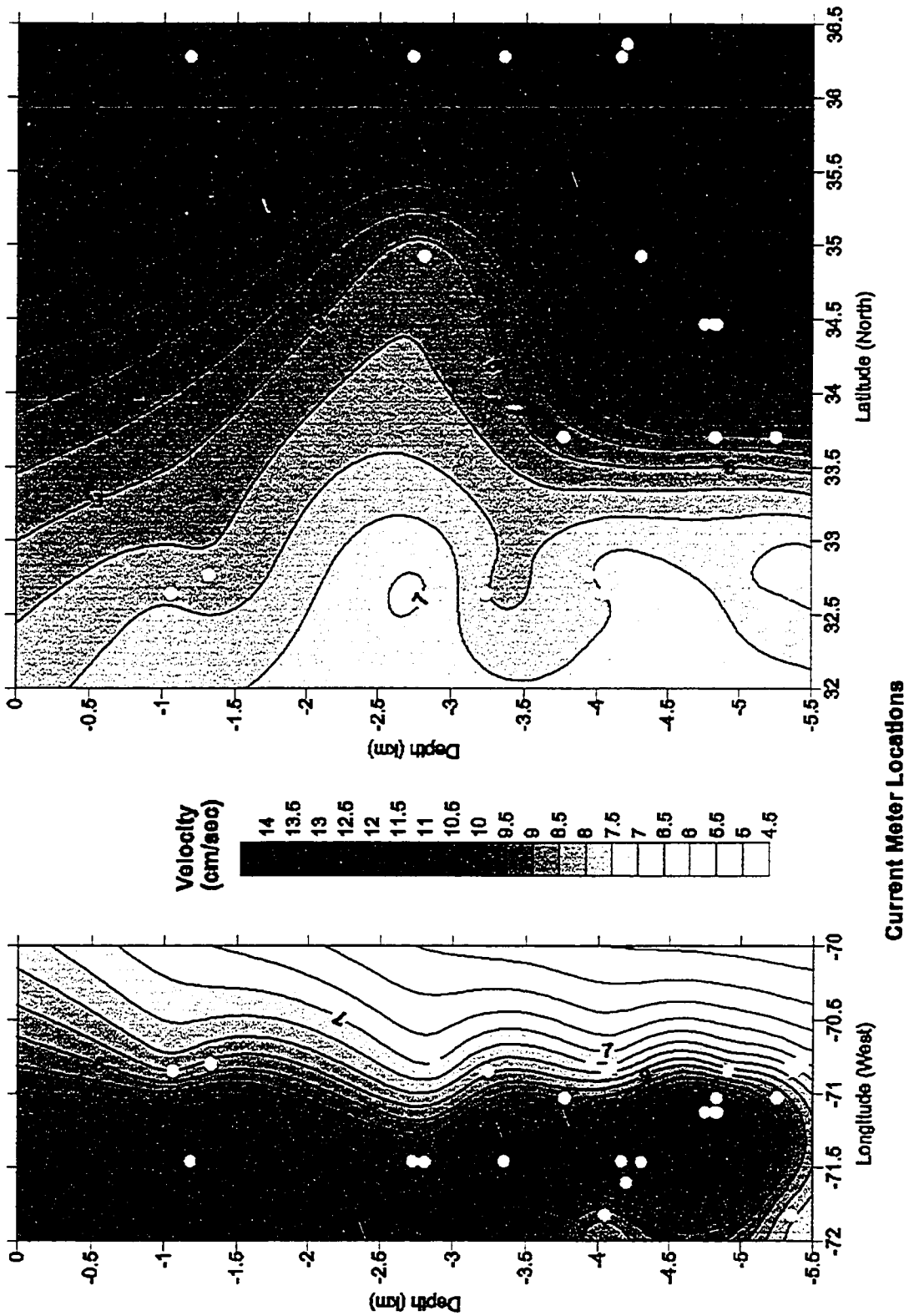


Figure 4.22 Pre-WOCE LLWODP East Experiment Depth Profiles Longitude vs. Depth and Latitude vs. Depth (09/16/80 – 09/03/84)

#### ***4.4 1990's WOCE Data and Patterns in the General Circulation***

The WOCE dataset for the 1990s includes 653 records comprising 285 deep water current meters (at depths below 1,000 meters), 151 intermediate depth current meters (at depths of 200 to 1,000 meters), and 217 shallow water current meters (to a depth of 200 meters). In addition two subsets were generated which looked at surface water (to a depth of 60 meters) and 114 records of near-bottom water, which consisted of water varying in depth from 250 to 5,500 meters. The main constraint for near-bottom water is that it followed the contours of seafloor topography in order to determine the impact of bathymetry in the movement of the deep water masses.

The spatial extent of the entire dataset extends from 0.087°N to 65.298°N latitude and from 9.475°W to 76.850°W longitude (Figure 3.3), while the temporal domain stretches from March 9, 1990 to August 19, 1999. A large portion of the WOCE dataset comprising 101 records for the Strait of Gibraltar was not included for two reasons. Firstly, it is not part of the Atlantic Basin per se, and more importantly the data set consisted of only 4 actual data points for this study since the experiment was based on a variety of different depth regimes over the Strait of Gibraltar (re: Section 3.2.1 on duplicate data points).

Shallow, intermediate and deep water were selected based on established depth profiles of the mixed surface layer (descending to 200 meters), the pycnocline extending to 1,000 meters (an area of rapid change in temperature, salinity and therefore density with increasing depth), and the deep layer below the pycnocline which comprises 80% of ocean water.

In addition to the individual plots of these different depth regimes (Figures 4.24 to 4.29), two three-dimensional maps are presented (Figures 4.30 – 4.31) in order to describe the variation in flows amongst the different layers. It is hoped that the combined visualization of these layers can shed some light on the variation which exists at different depths.

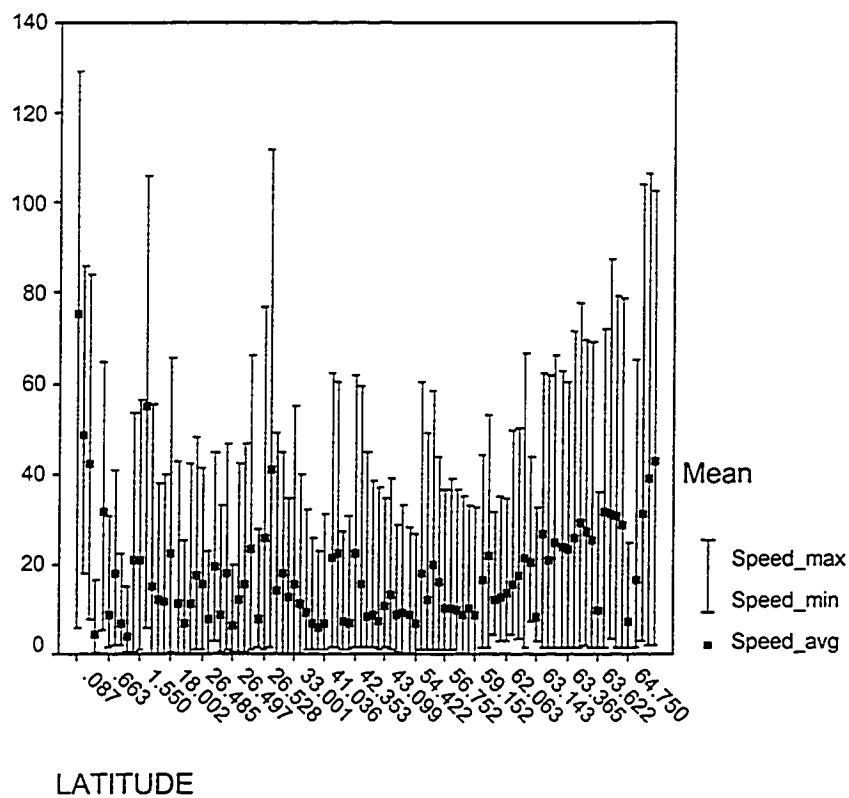
#### **4.4.1 Variation in Range of Variables**

As was the case for the pre-WOCE data, Figure 4.23 shows no apparent relationship between mean current speed and either latitude or longitude. It is interesting to note the absolute difference in current speeds with pre-WOCE data having values between 0 and 20 cm s<sup>-1</sup> and the WOCE data shown in Figure 4.23 having values extending to 40 cm s<sup>-1</sup>, though the largest proportion still fall between 0 and 20 cm s<sup>-1</sup>. The pattern of current speed vs. depth is similar to the pre-WOCE data in Figure 4.1, with increased speed and variability in speed in the upper 500 meters. Distribution of the mean temperature shows the thermocline roughly running between 500 and 1,500 meters, as was the case in Figure 4.1.

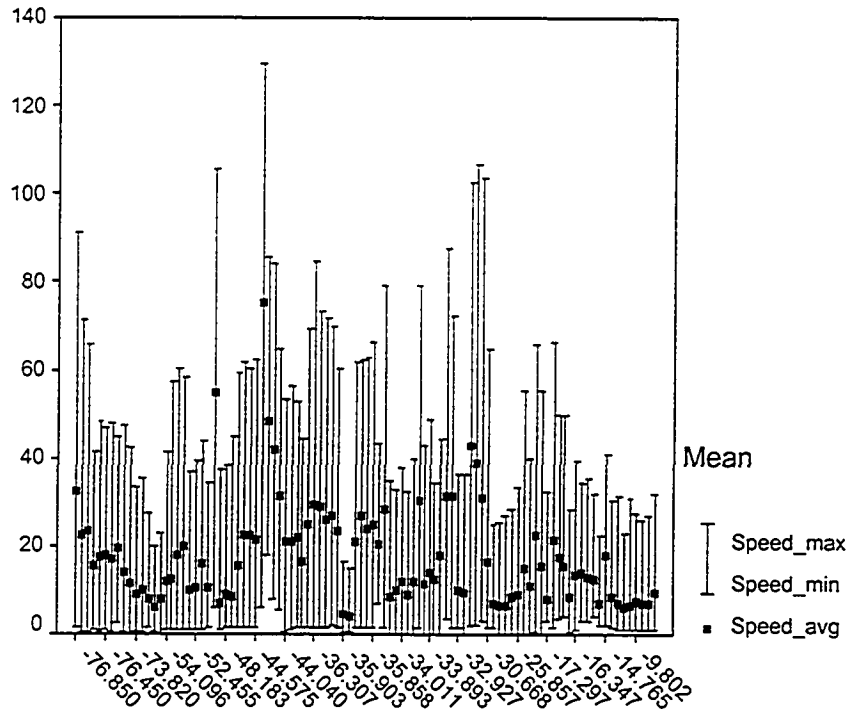
#### **4.4.2 WOCE Data Dynamics**

Surface wind data were available for the period March-1991 to December-1994 and therefore a map of surface water current vectors is produced to show the relationship between wind and surface flow (Figure 4.24). The data used for current speed were limited to the period Sep-25-1990 to Apr-16-1995 in order to better coincide with the range of data for wind speeds. The data for surface currents was limited to records with depths of up to 60 meters, in order to acquire a sufficient number of data points. In

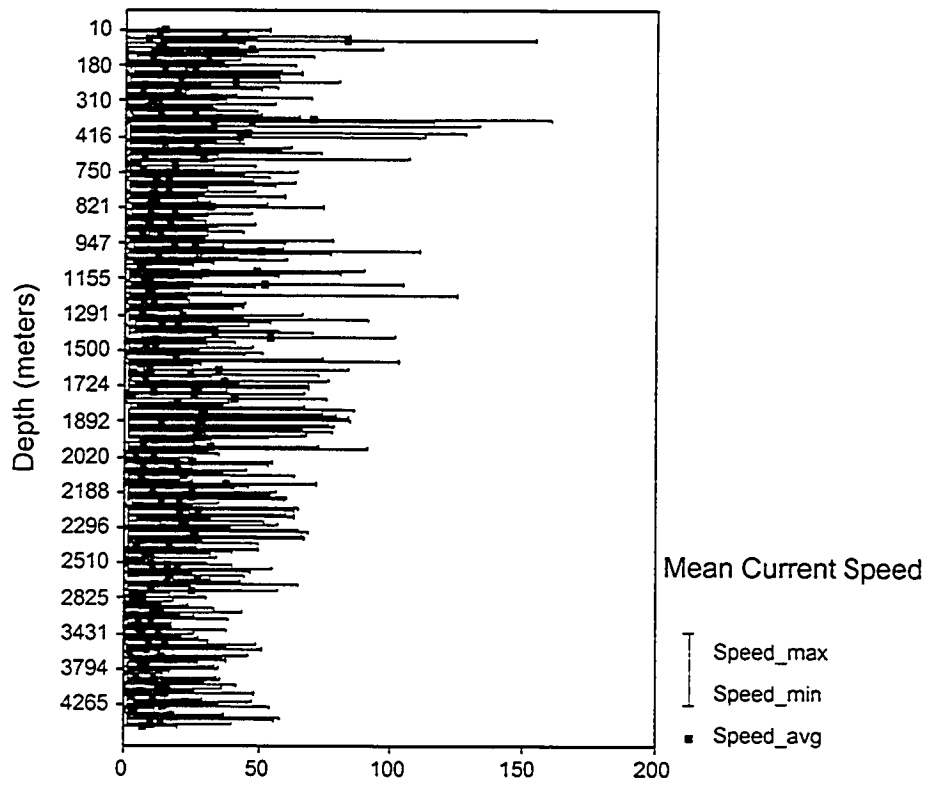
addition maps were created for shallow water current flows – to a depth of 210 meters (Figure 4.25), intermediate water current flows – 250 to 1,000 meters depth (Figure 4.26), deep water current flows – 1,108 to 5,483 meters depth (Figure 4.27), and near-bottom current flows – defined as depths within 500 meters from the seafloor and ranging between 250 and 5,483 meters in depth (Figures 4.28 and 4.29). Three-dimensional plots were developed as in the case of the pre-WOCE data analysis to better visualize the vertical differences in current flows (Figures 4.30 and 4.31).







Longitude



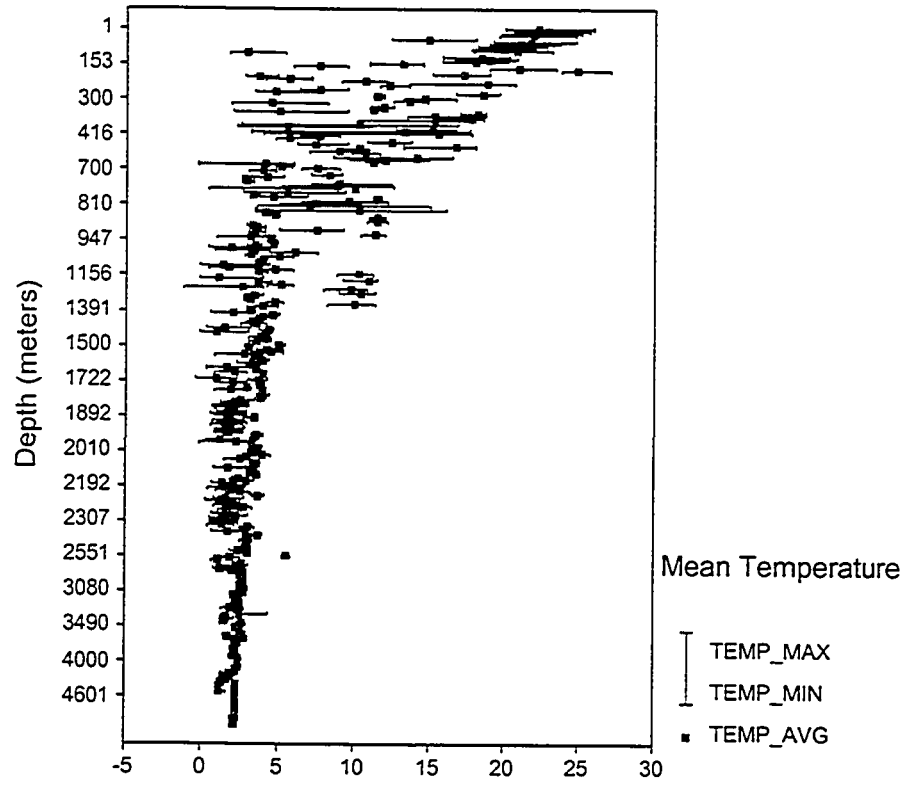


Figure 4.23 Variable Plots of Min, Mean, and Max Values for Current Meter Speed ( $\text{cm s}^{-1}$ ) vs. Latitude, Longitude and Depth and for Mean Temperature ( $^{\circ}\text{C}$ ) vs. Depth

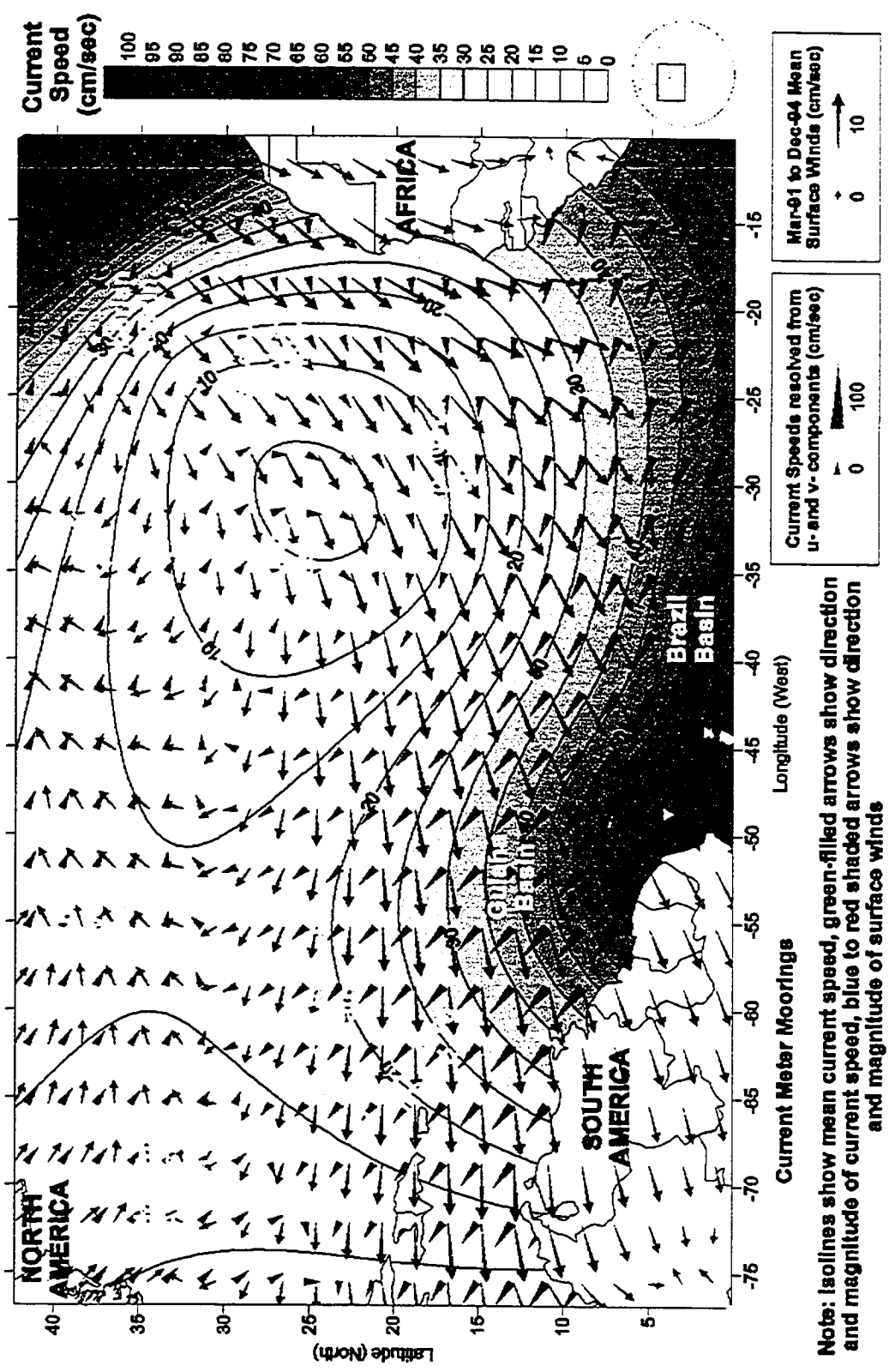


Figure 4.24 WOCE North Atlantic Ocean Surface Water Current Vector Plots recorded from Sep-25-1990 to Apr-16-1995 for depths  $\leq 60$  meters with Mar-1991 to Dec-1994 Mean Surface Wind Data Included

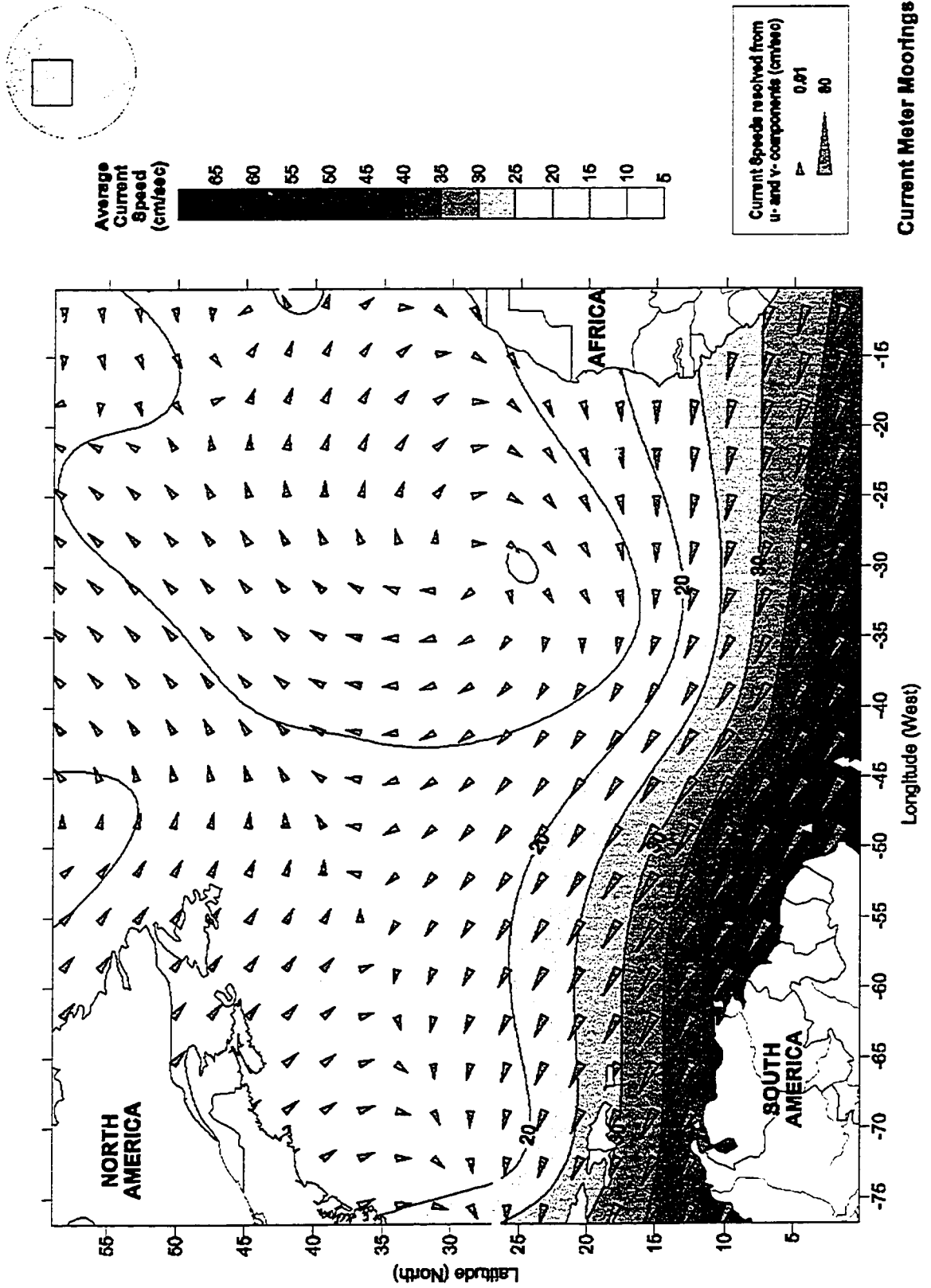


Figure 4.25 WOCE North Atlantic Ocean Shallow Water Current Vector Plots recorded from Aug-1989 to Aug-1999 for depths  $\leq 210$  meters

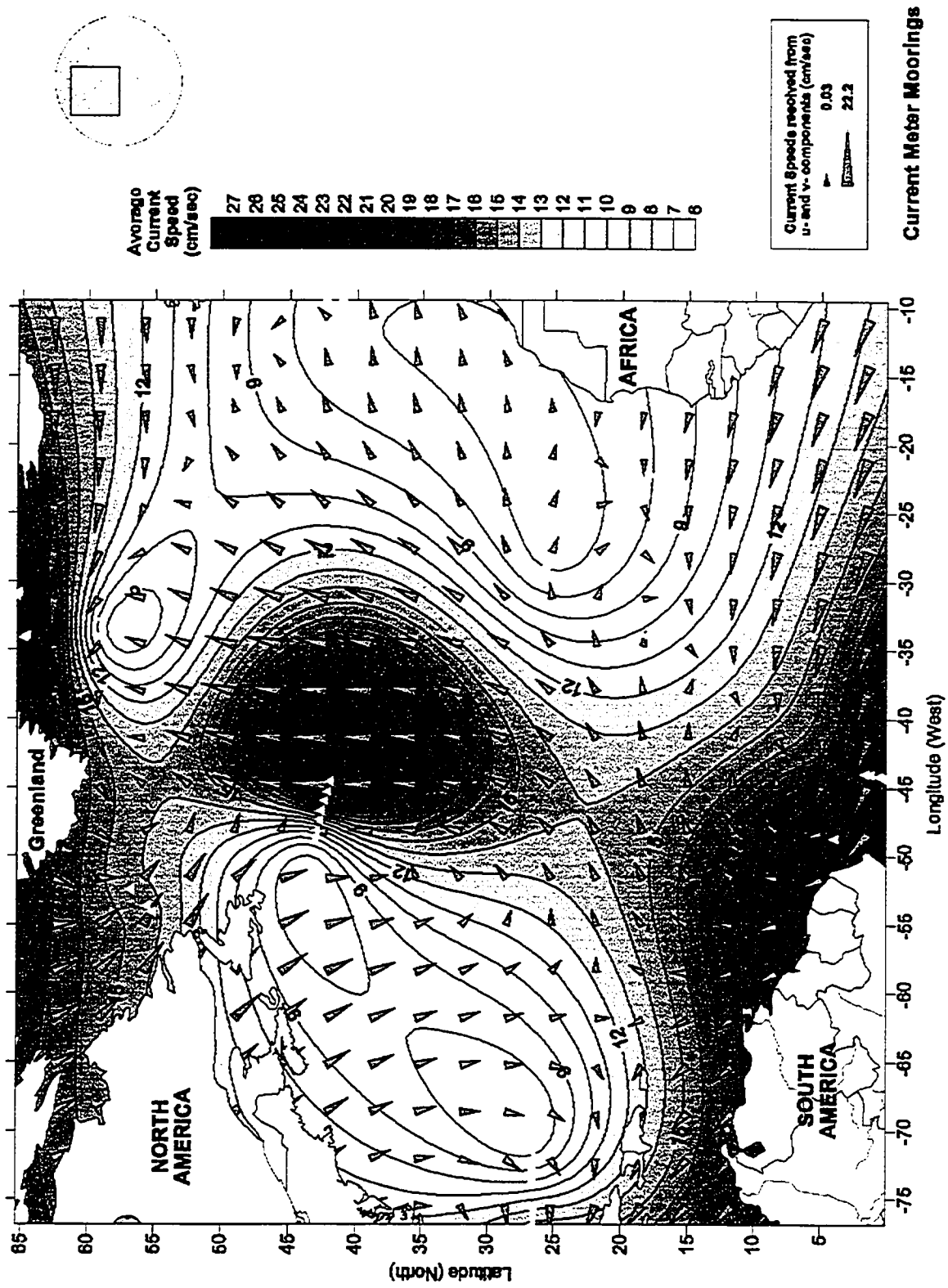


Figure 4.26 WOCE North Atlantic Ocean Intermediate Depth Current Vector Plots recorded from Aug-1989 to Aug-1990 for depths of 250 to 1,000 meters

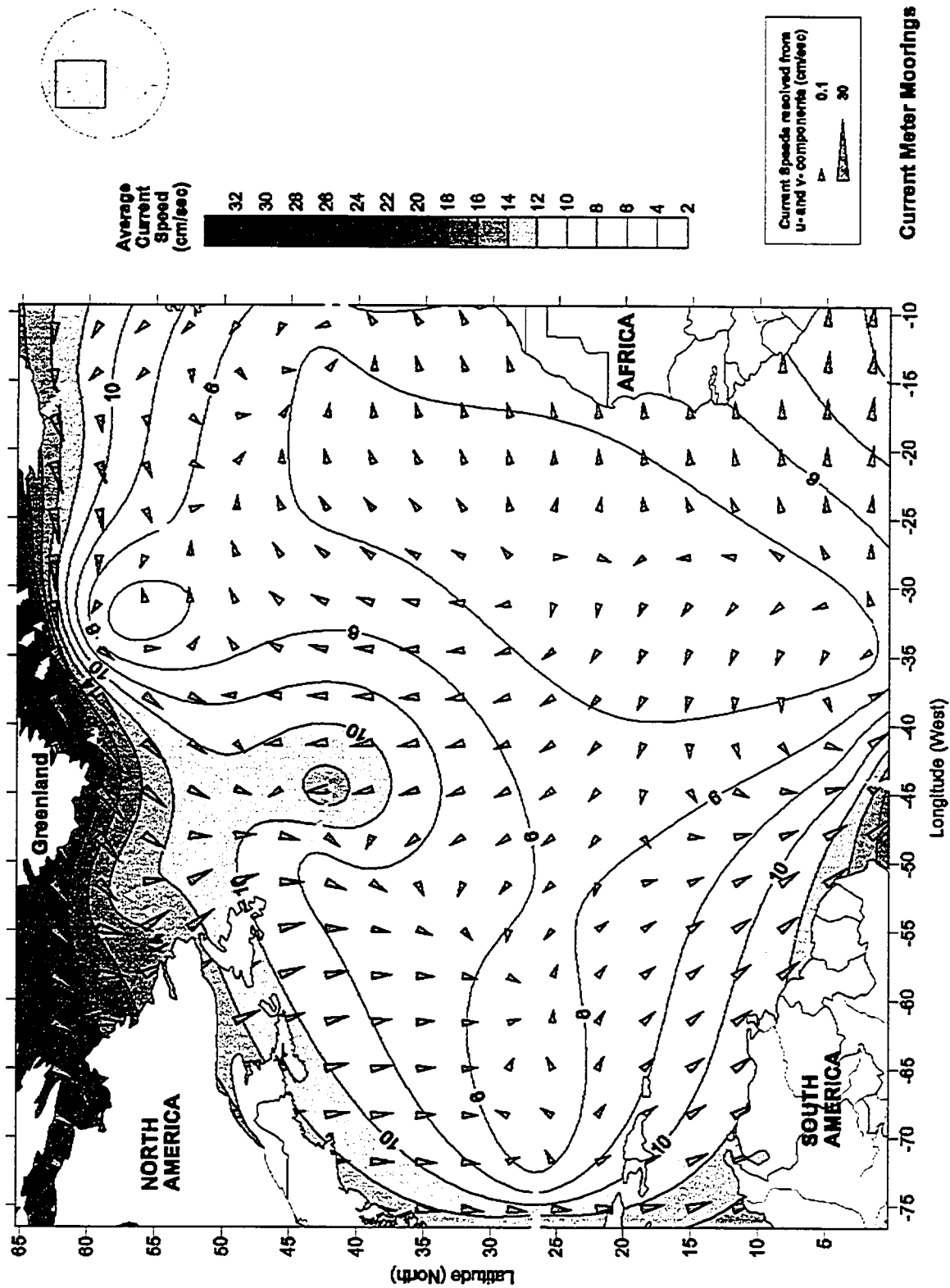


Figure 4.27 WOCE North Atlantic Ocean Deep Water Current Vector Plots recorded from Aug-1989 to Aug-1999 for depths of 1,108 to 5,483 meters

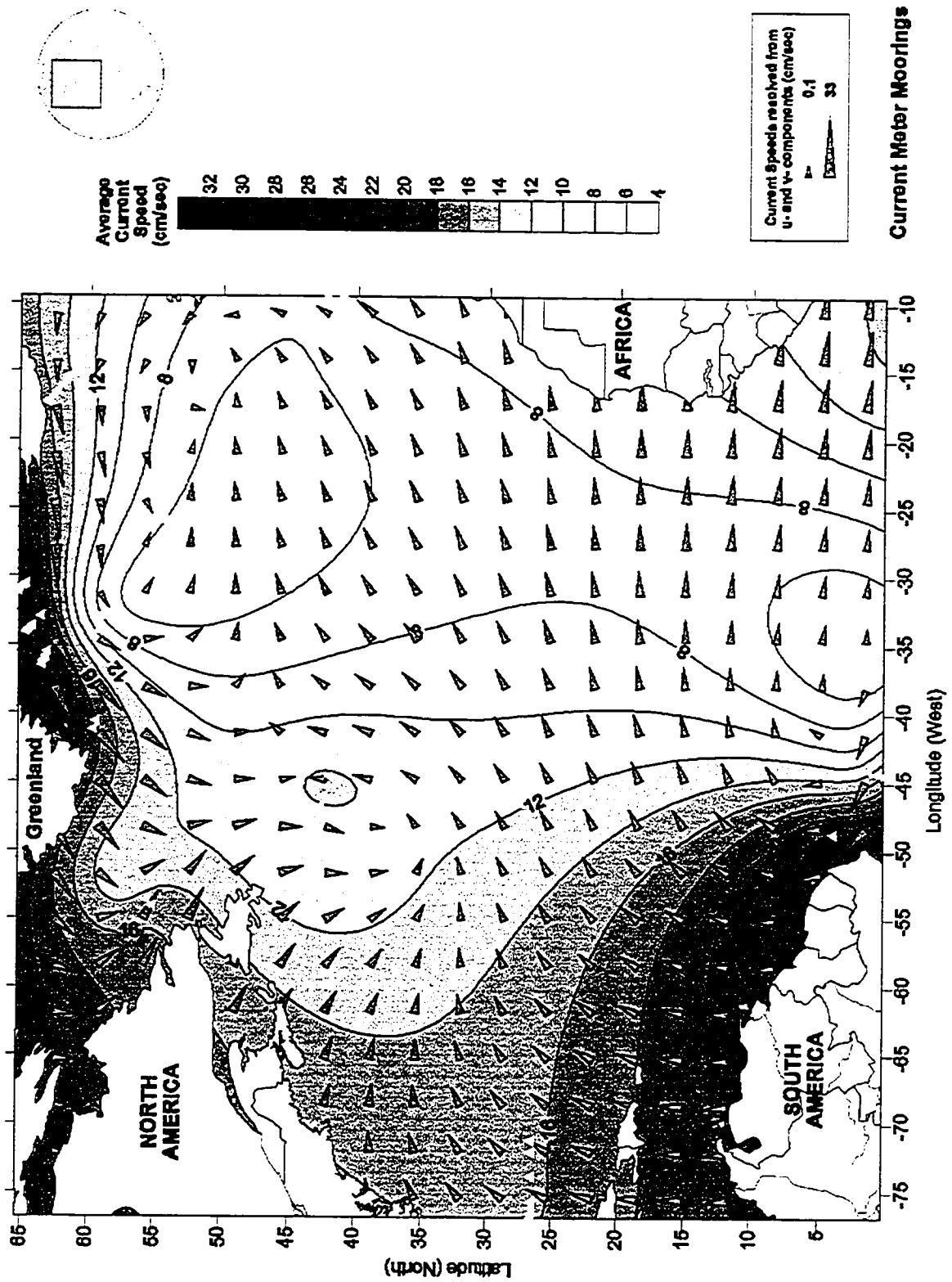
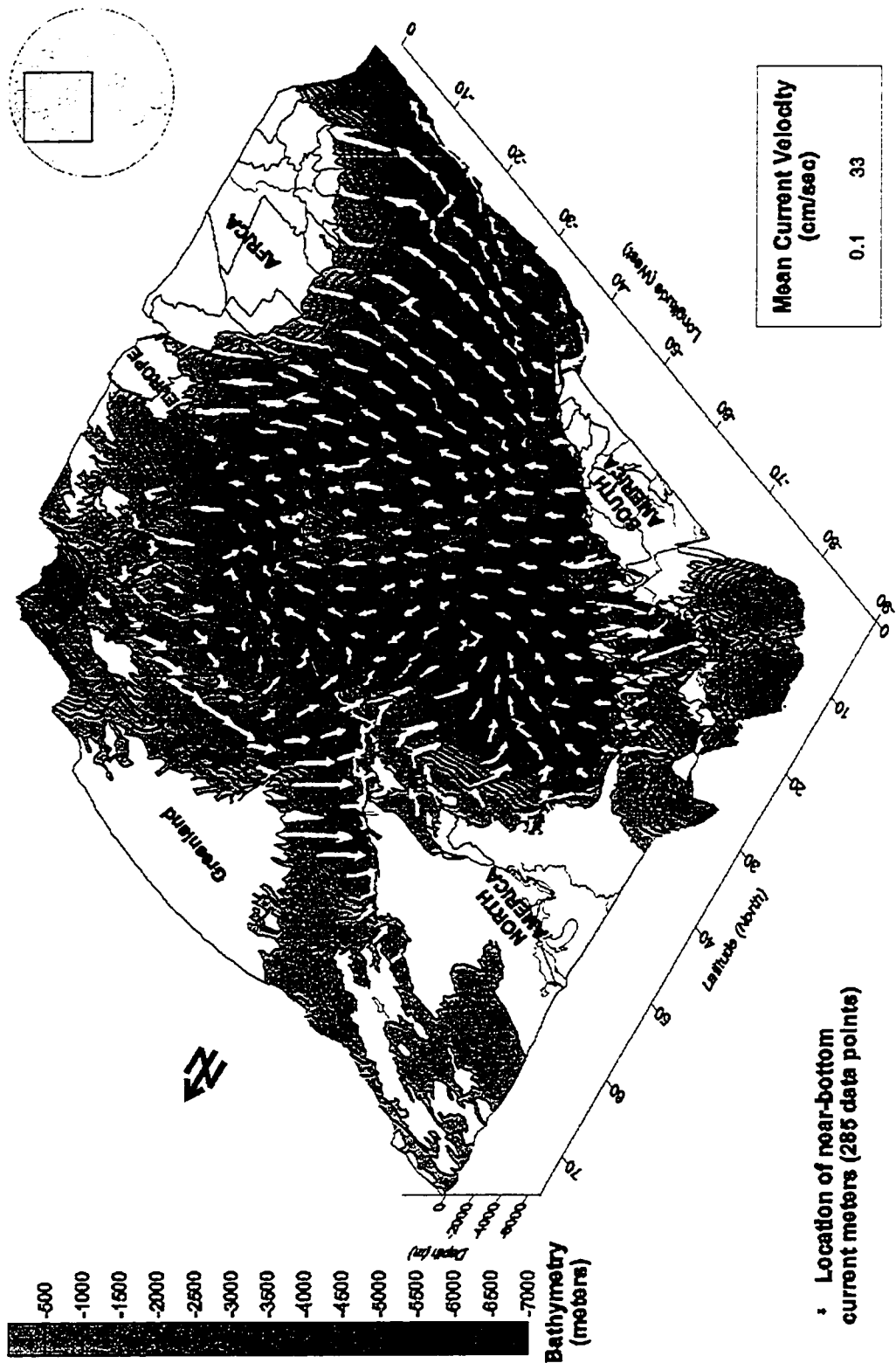


Figure 4.28 WOCE North Atlantic Ocean Near-Bottom Water Current Vector Plots recorded from Aug-1989 to Aug-1999 for depths less than 500 meters from the Seafloor (ranging in depth from 250 to 5,483 meters depth)



**Figure 4.29 Interpolated Mean Current Vectors with Location of Current Meter Buoys and ETOPO-5 Bathymetry of the North Atlantic Ocean during the WOCE Study Period of Aug-1989 to Aug-1999 for Near Bottom Depths**



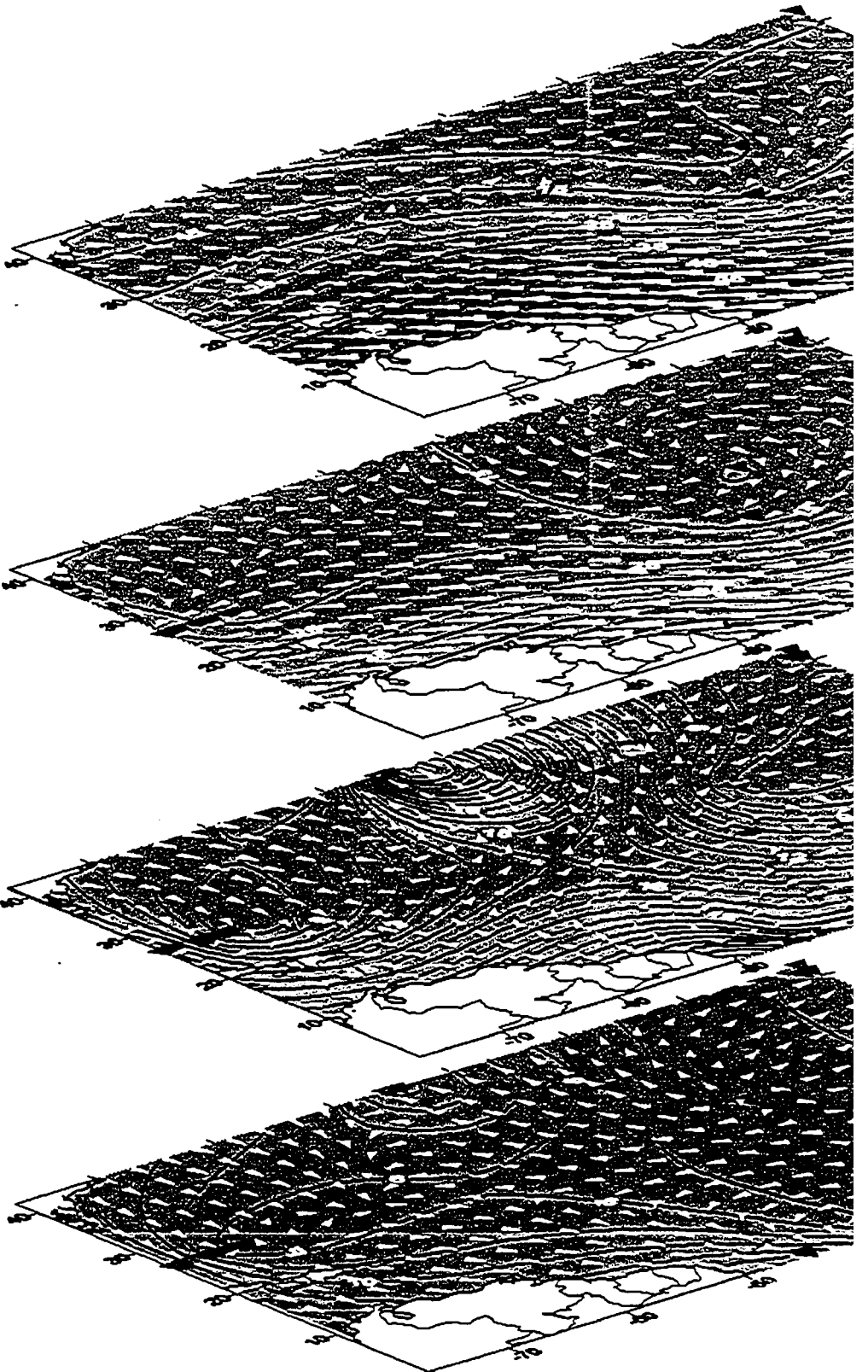
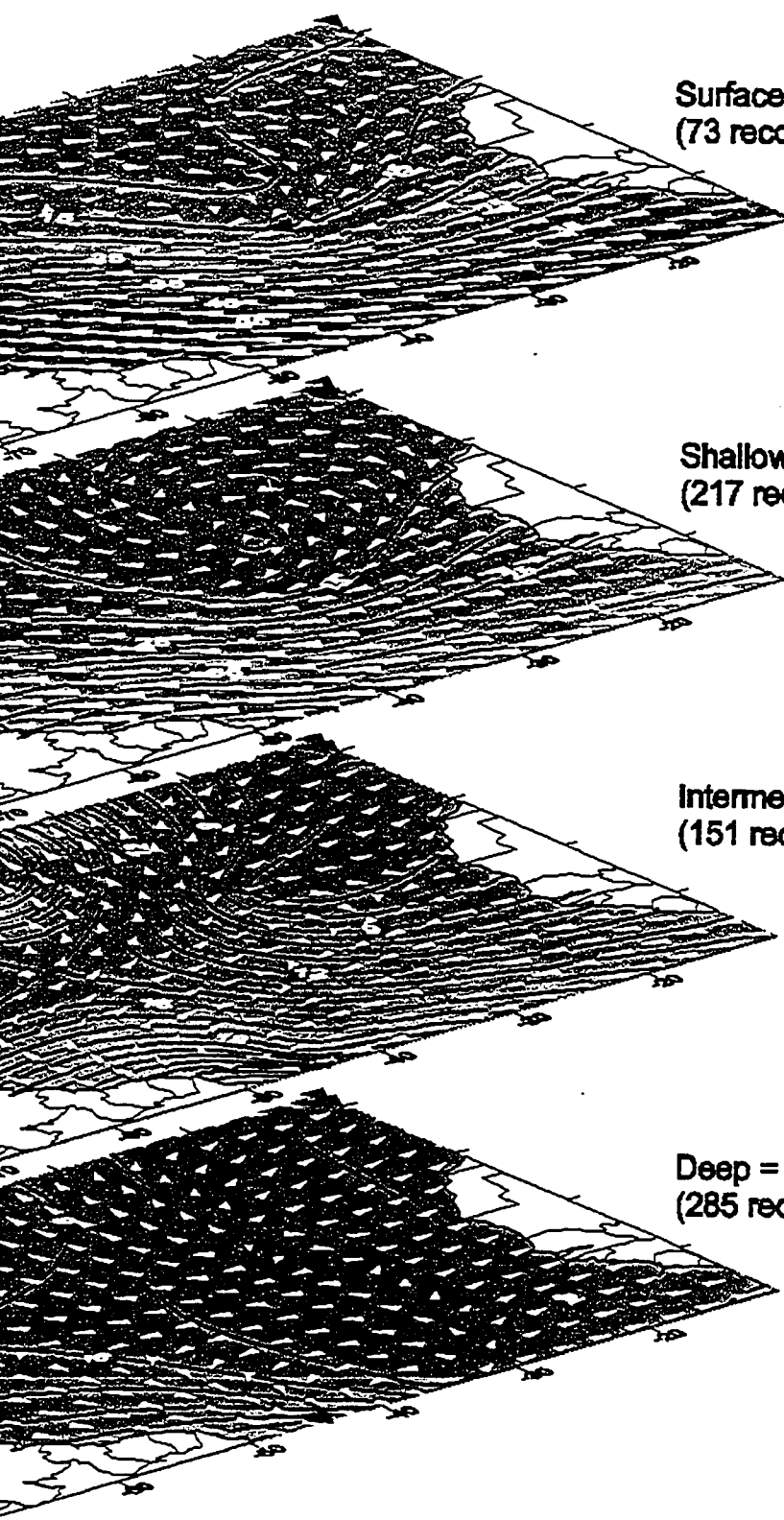


Figure 4.30 Three-Dimensional WOCE North Atlantic Ocean Mean Current Speed Vector Plots for Surface, Shallow, Intermediate and Deep Water Depths of Figures 4.24 to 4.27





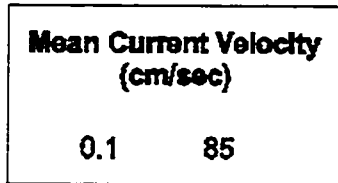
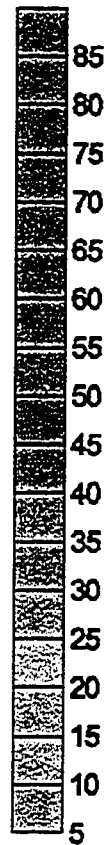
Surface = depth to 60 m  
(73 records)

Shallow = depth to 210 m  
(217 records)

Intermediate = 250 m to 1000 m  
(151 records)

Deep = 1000 m to seafloor  
(285 records)

Mean  
Current  
Velocity  
(cm/s)



▼ Current Meter Locations



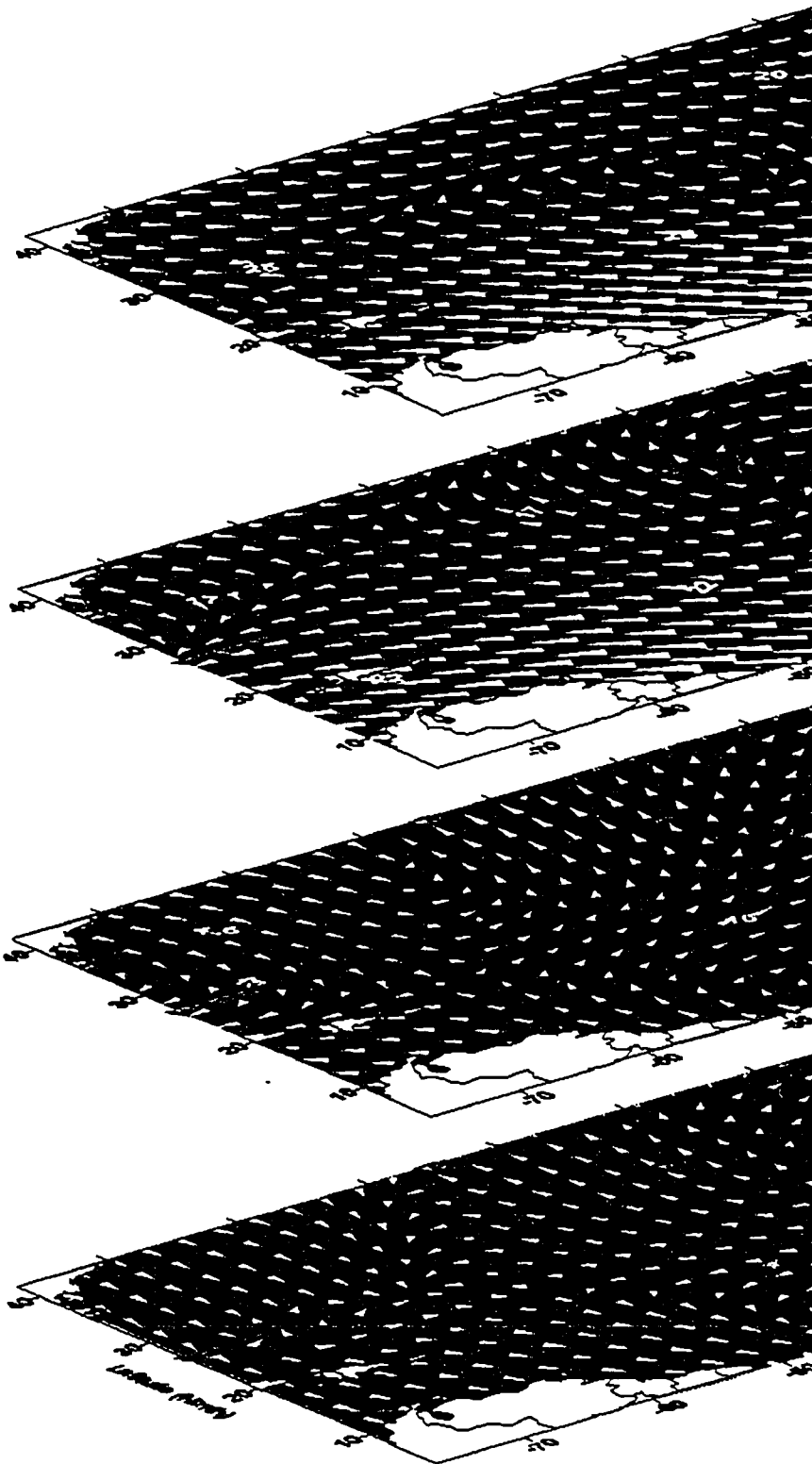
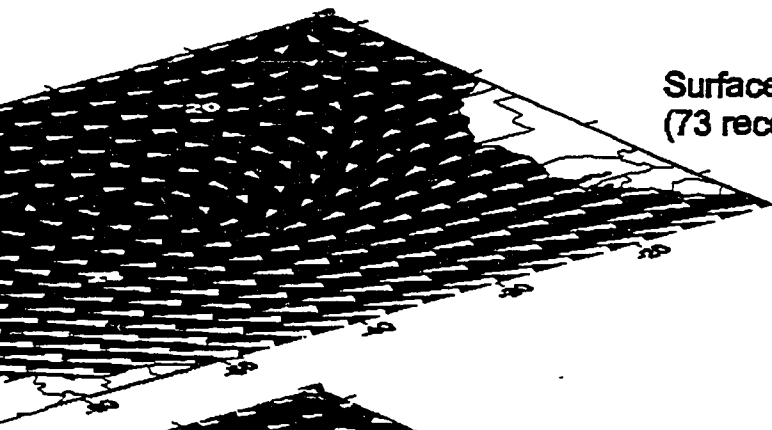
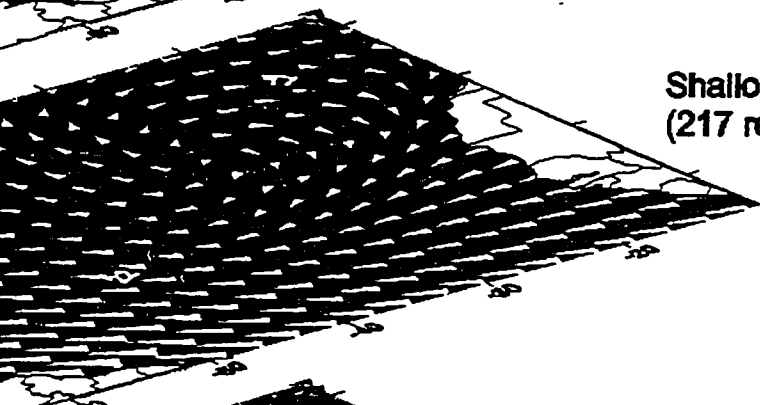


**Figure 4.31 Three-Dimensional WOCE North Atlantic Ocean Mean Current Speed Vector Plots superimposed on Mean Temperature Contour Map for Surface, Shallow, Intermediate and Deep Water Depths**

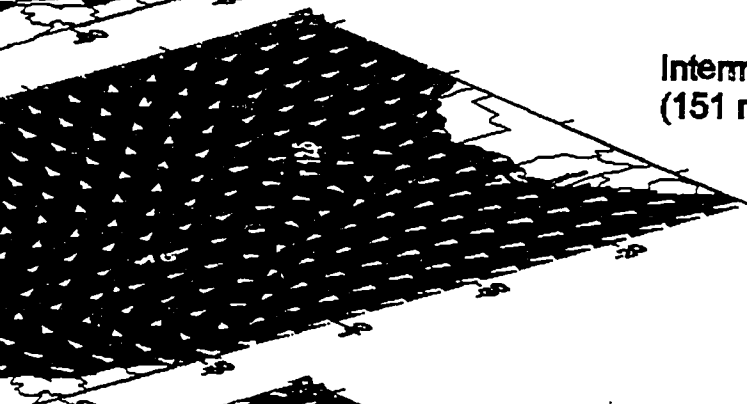




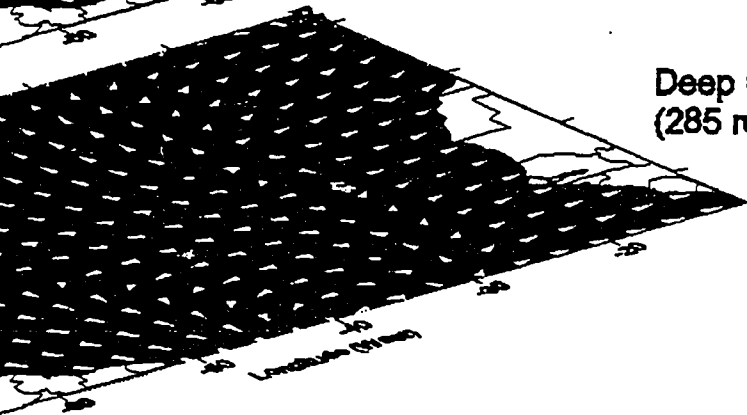
Surface = depth to 60 m  
(73 records)



Shallow = depth to 210 m  
(217 records)

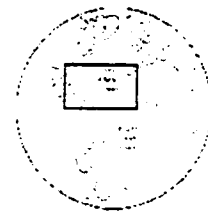
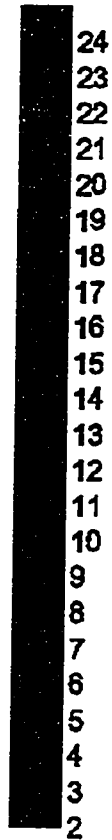


Intermediate = 250 m to 1000 m  
(151 records)



Deep = 1000 m to seafloor  
(285 records)

Water  
Temperature  
(deg C)



Current Velocity  
(cm/sec)

0.1      85

▼ Current Meter Locations





For the majority of the study area, the plot of surface currents and surface wind data (Figure 4.24) shows a strong relationship between the directional flow. The surface current flows at right angles to the mean surface wind field, which is in agreement with the principle of Ekman transport for the Northern Hemisphere, whereby current flow direction is affected by a combination of Coriolis deflection and wind stress. Of primary interest is the clock-wise flowing Sub-tropical gyre of the North Atlantic Ocean, clearly visible in both the current vector plots and the mean current speed contours.

The map of shallow water current flow (Figure 4.25) shows that the faster currents lie south of 20°N and tend to a westerly flow, this is in sharp contrast to the pattern that was seen in Figure 4.2. In addition, a clockwise rotating gyre is evident between 15° and 40°N and 10° to 50°W, associated predominately with a large mass of slower moving water. The intermediate water (Figure 4.26) shows an area of faster moving water near 40°N and 45°W which is associated with the Gulf Stream Extension and largely shows up due to the dense array of current meters situated in the area. The large patch of slower moving water located near the Middle Atlantic Bight and which was discussed with regards to Figure 4.4 is evident in the 1990s dataset as well. The deep water plot (Figure 4.27) is characterized by large distances between clusters of current meter arrays. The resulting current vectors show the southward flow of NADW from the Irminger Basin, which is superseded by the northerly flow of AABW near the mid-latitudes of the map. This is primarily a result of the lack of current meters throughout the mid-latitudes and the tendency of the interpolation algorithm to weigh more heavily on flows adjacent to the current meter arrays. Near the equator the cross-equatorial movement of NADW is evident especially near the WOCE ACM7 array near 45°W.

The plots of near-bottom water (Figures 4.28 and 4.29) give a good representation of the flow of bottom water. Beginning in the north-west, the flow of water from the Labrador Basin into the North Atlantic is evident, along with its mixing with NADW originating from the Irminger Basin. AABW water which has crossed the equator and made its way into the Caribbean Sea can be seen flowing into the abyssal plains of the North Atlantic. One discrepancy to note is the apparent flow of deep water over the Mid-Atlantic Ridge. In reality the flow of deep water is impeded by this structure and tends to flow towards and through gaps in the bottom topography. However, since this plot included water of shallower depths (with distance from seafloor being the only determinant), then the mixture of various water masses tends to generalize the flow.

The 3-dimensional plots shown in Figure 4.30 illustrate the differences in both magnitude and direction. A large part of these discrepancies are due to the spatial distribution of the current meters, whereby points close to the instrumentation give a good account of the data, and points further away are less reliable. When the current vectors are coupled with temperature contours, Figure 4.31, some of the main patterns that emerge are predominately northward flowing water transporting warm equatorial waters – particularly in the upper two plots; and the areas of warm water in the intermediate plot, which would seem to be associated with the formation of warm-core rings due to the Gulf Stream (Summerhayes 1996, Brown et al. 1989a, 1989b), but which should be found further west than 35°W.

#### **4.4.3 WOCE Depth Profiles**

Depth profiles for mean temperature vs. latitude and longitude, and for mean current speed vs. latitude and longitude are shown in Figures 4.32 and 4.33. Both plots of

mean temperature vs. latitude and longitude do not show a characteristic representation of the upper warm layer and the thermocline. In Figure 4.32 (a) this is due to the lack of current meters between 50° and 70°W and for Figure 4.32 (b) it is due to the lack of current meters between 5° and 15°N and the lack of surface data between 60° and 70°N. By excluding these ranges from any interpretation of the data, a regular pattern emerges which corresponds to the characteristic surface layer to 500 meters in depth, and a thermocline varying between 1,000 and 1,800 meters in depth for Figure 4.32 (a). With regards to Figure 4.32 (b) the effect of latitude causes a much sharper gradient with a homogenous cold layer developing at about 1,500 meters depth north of 15°N and the thermocline disappearing and giving way to warmer surface waters as one proceeds south. Of primary interest is the uniform distribution of current meters at 75°W longitude which clearly defines the boundaries of surface water, thermocline and deep water and the corresponding uniform distribution of current meters at 27°N latitude which does likewise. It is evident at these locations that the thermocline extends down to about 1,000 meters depth, with water of 4° to 6°C between 1,000 and 1,600 meters depth, and temperatures between 2° and 4°C from 1,600 meters depth down to the seafloor. The general pattern to be observed are the presence of two thermoclines, a long-term thermocline from the equator to about 30°N which is deeper, and a short-term seasonal thermocline north to 55°N which is shallower.

In Figure 4.33 large masses of homogenous water are evident in areas which are lacking data points. In these areas the homogeneity is an effect of the interpolation algorithm as discussed in Section 3.2.3 on page 57 (Golden Software 1999). Focusing on the areas which are data rich and comparing these patterns with Figure 2.5 of the Atlantic

Ocean water masses the patterns which emerge with respect to Figure 4.33 (a) are the presence of slow moving NADW at depth, and the influx of faster moving MIW near the surface between the equator and 40°N latitude. Figure 4.33 (b) shows the results of mean current speed vs. longitude after applying an anisotropy ratio of 3.0 to smooth out the contours and eliminate some of the noise (Golden Software 1999). Deep pockets of faster moving water found between 30° and 50°W longitude are associated with the Gulf Stream jet which reaches speeds in excess of 100 cm s<sup>-1</sup> on a regular basis (Garrison 1996, Ross 1988). The phenomenon of the Gulf Stream jet is also apparent in the fast moving zone of water evident at the surface between 45° and 50°W. These observations are made without the luxury of having any salinity or pressure data which would give a much better understanding of the composition of the various water masses and allow a more detailed undertaking of locating the deep water masses.

One further observation is the mass of faster moving water shown in Figure 4.33 (a) between 65° and 70°N. This water mass is shown in Figure 4.33 (b) between 30° and 35°W at a depth of 1,000 to 1,500 meters. This would appear to be related to the convergence of the Irminger Current with the East Greenland Current (Figure 2.3) and is corroborated by the flow of fast moving water in the intermediate water plot of Figure 4.27 around Greenland. This is an example of how observation of all relative plots can give a good indication of the location and characteristics of various water masses.

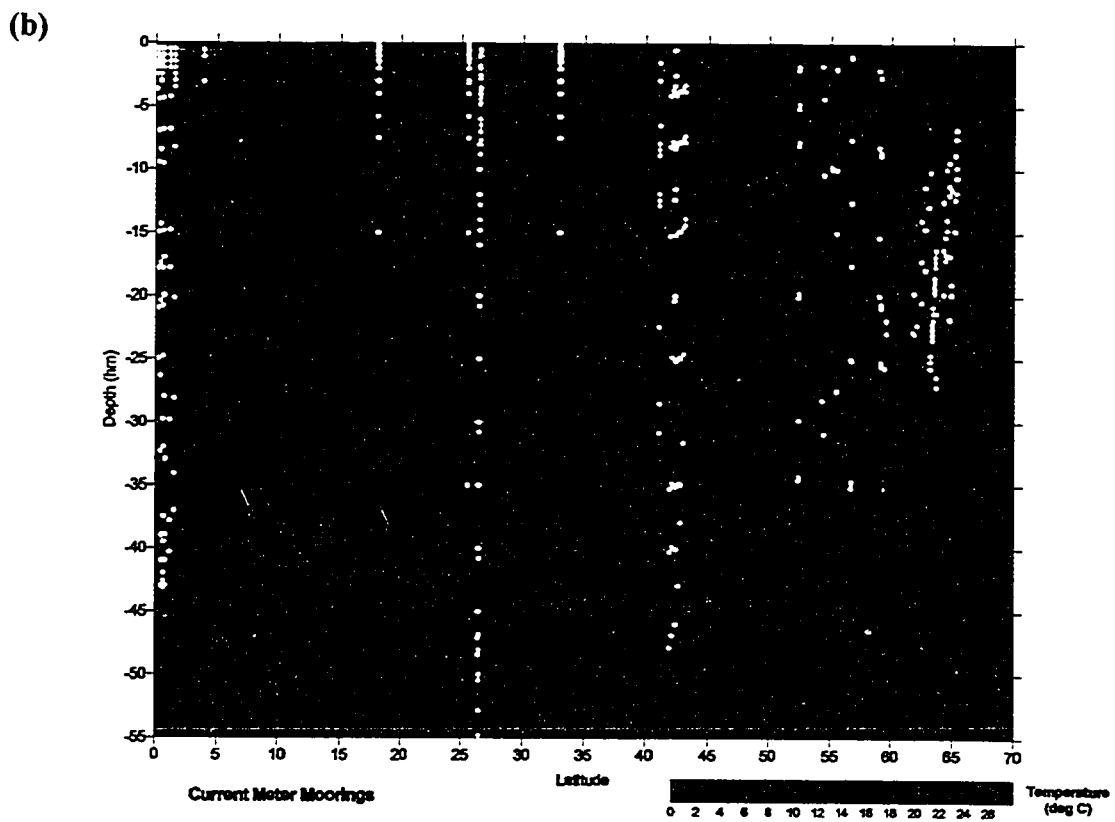
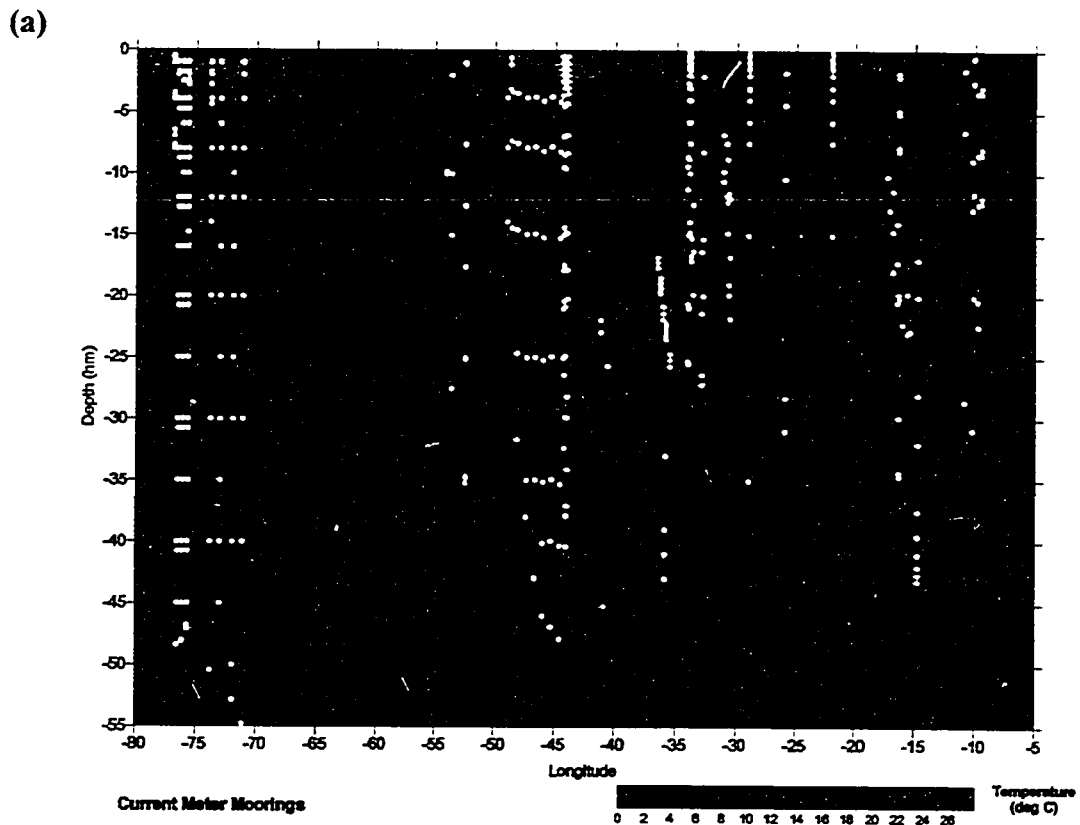


Figure 4.32 WOCE North Atlantic Ocean Depth Profiles of (a) Mean Temperature vs. Longitude and (b) Mean Temperature vs. Latitude for Period Mar-1990 to Aug-1999

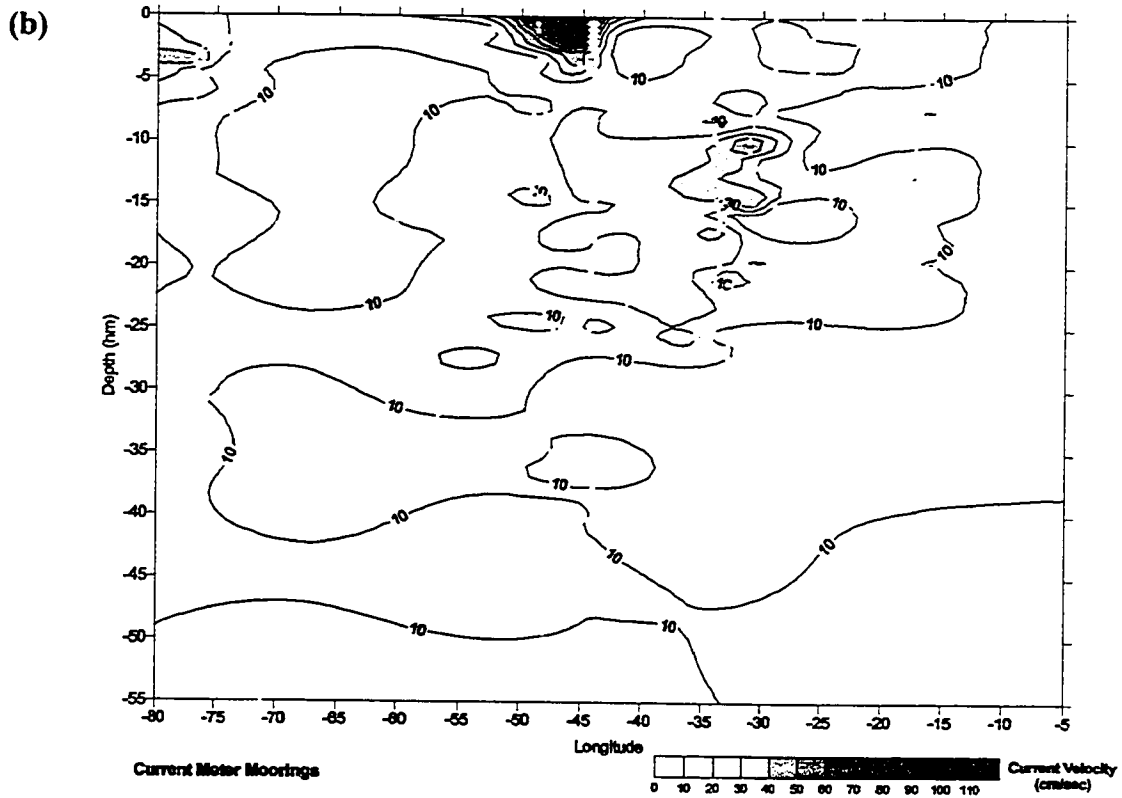
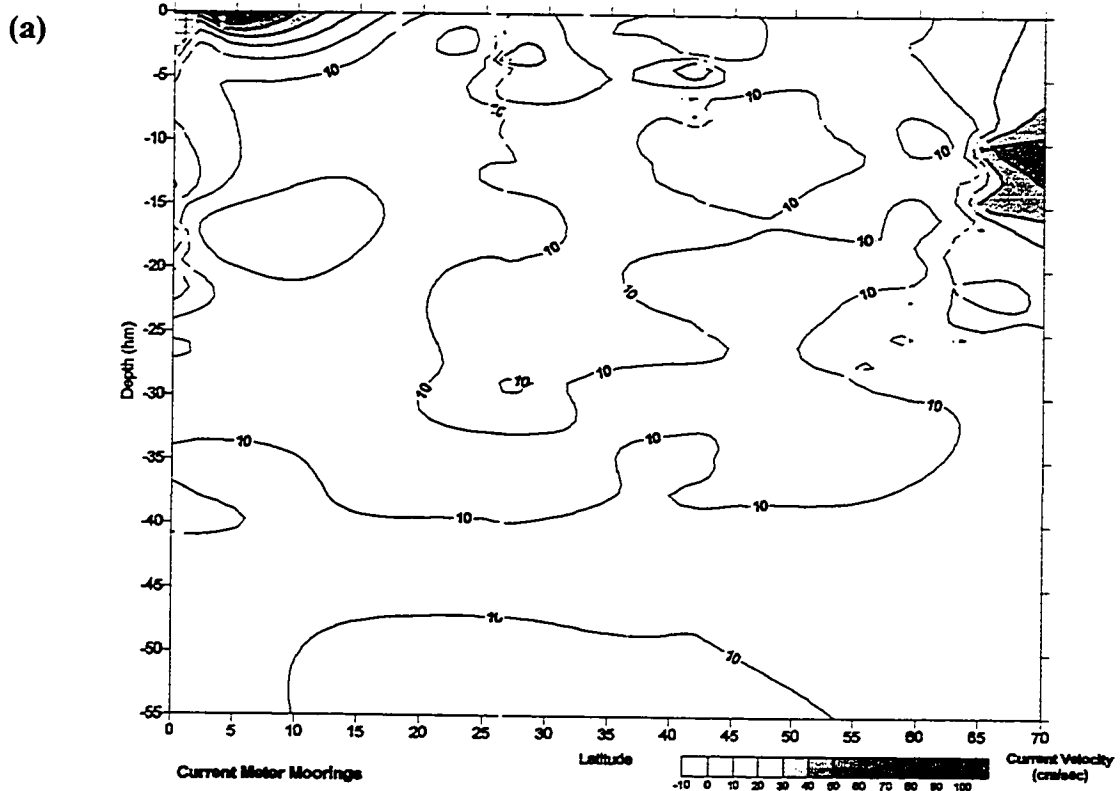


Figure 4.33 WOCE North Atlantic Ocean Depth Profiles of Mean Current Velocities for (a) Latitude vs. Depth and (b) Longitude vs. Depth for Period Mar-1990 to Aug-1999 (Note: Longitude vs. Depth plotted using an anisotropy ratio of 3.0 to smooth out the contours)

## ***4.5 Comparison of pre-WOCE and WOCE General Circulation***

Figures 4.34 to 4.37 are overlays of the pre-WOCE and WOCE datasets in order to see the differences in the general circulation of the North Atlantic Ocean between the two time periods of 1974 to 1984 and 1990 to 1999. There are a few items of note when interpreting the current flows on these maps. Firstly due to the vertical distribution of current meters during both time periods, the comparison depths do not agree with one another. Secondly, the spatial scale of the analysis was set at 25° - 45°N latitude and 40° - 80°W longitude (Western North Atlantic) since this was the spatial scale used for the analysis of the pre-WOCE dataset in section 4.2 and therefore common to both sets of data. Thirdly, the locations of current meters for the pre-WOCE dataset are all inclusive on these views.

On the other hand, the current meter locations for the WOCE dataset extends beyond the map boundaries, since the spatial extent of this analysis was from the equator to roughly 65°N latitude, and from 10° - 75°W longitude. For the pre-WOCE data, current flows in areas not adjacent to current meter sites are a result of the interpolation algorithm of the software; whereas for much of the WOCE data, current flows are affected by the position of current meters not in the map boundary. For example, for the shallow water plot there are a series of current meters situated at 25°N, 35°W and 35°N, 35°W which are just off the right of the map boundary in Figure 4.34 that determine the direction of flow for the edge of the map. In addition, since the spatial extent of the WOCE data was limited to 75°W longitude, notice that there the red current flow vectors for the WOCE data end abruptly just west of 75°W. It should also be noted that these differences may very well be real differences in the decadal mean flow over time.

The shallow water depth current vector plots (Figure 4.34), have pre-WOCE depths are 530 meters and WOCE depths to 210 meters. The degree of association between the two datasets is not very close, with the general flow of the North Atlantic Sub-tropical gyre evident in the pre-WOCE plot (green vectors), compared to more local peculiarities, such as the southern flow of the Labrador Current near the coastline and the strong North Equatorial Current flow below 30°N in the WOCE plot (red vectors). Where both pre-WOCE and WOCE instrumentation are spatially adjacent to one another the flow regimes are similar to one another, i.e. pre-WOCE meters located between 31° and 34°N, 70°W and WOCE meters located between 27°N, 72° and 77°W. However in many areas of the map the current flows are 180° in the opposite direction, i.e. south of 35°N and running from 50° to 60°W, as well as flows 90° opposed to one another east of 48°W.

The intermediate depth plots (Figure 4.35) show stronger association with respect to current direction, especially west of 55°W longitude and south of 37°N latitude. In general the current speeds are greater for the 1990 dataset. Even though the comparison depths are not the same, the depths are deep enough to not be influenced by surface conditions. The pre-WOCE plot (green vectors) appears to be picking up various flow regimes, such as the Gulf Stream Extension and North Atlantic Current flows to the north-center of the map, including some of the turbulence that results in eddies about the Gulf Stream. The WOCE plot (red vectors) are characteristic of flows from the Labrador Current and the Slope Current around the coast near Cape Hatteras, as well as the more complex intermediate water flows of the NACW which flows counter to the Gulf Stream.



The deep water current vector plots (Figure 4.36) show quite a few areas of agreement, and here the comparisons are generally over the same water depth. The complexity of the cold and warm core eddies about the Gulf Stream are in evidence in the vicinity of the pre-WOCE current meters (blue stations). In addition, with current meters arrayed between a gap of 4,230 meters there is a wide range of intermediate and deep current data that the pre-WOCE instruments obtain. Both the southerly flow of NADW and the northerly flow of AABW is apparent, thus explaining the rather complex flow patterns throughout the map. These seemingly contradictory flows are due to the distance between stations, both in horizontal and vertical terms, and in the interpolation algorithm of the software. The south-west and north-east corners of the map are where the WOCE instruments are located. In the north-east sector, where there is also a dense concentration of pre-WOCE current meters, the WOCE circulation is offset some  $45^\circ$  to the right of the pre-WOCE flow but also shows current flows directly opposed to the pre-WOCE flow.

The near bottom circulation shown in Figures 4.37 and Figure 4.38 reveal opposing flows adjacent to the North American coast, with WOCE data following the flow of the deep Gulf Stream along the coast, while pre-WOCE flow is predominately equatorward along and down the continental slope. This discrepancy between pre-WOCE and WOCE data in the area of New England and Nova Scotia could be due to edge effects, or it can be a true reflection of differences in near-bottom flow over the two time periods. East of  $70^\circ\text{W}$  and south of  $35^\circ\text{N}$  the two flows are more in agreement with each other, with WOCE circulation offset to the right of the pre-WOCE flow. Both datasets, particularly the pre-WOCE current vectors, show a somewhat counterclockwise rotational cell near the bottom of the Western North Atlantic Ocean.

The bathymetric view of Figure 4.38 shows quite plainly the flow of water down the continental slope into the Hatteras Abyssal Plain, Nores Abyssal Plain and Sohm Abyssal Plain and the flow of water over the Bermuda Rise. Also evident is the acceleration of flow down the continental slope, due to the combined additive effects of slope and water density. The mixing of NADW and AABW throughout the abyssal plains is evident, and towards the eastern sector of the map there would appear to be MIW making its way westward. Just past the boundary of the north-east sector of the map, lies the Gibbs Fracture Zone which allows the passage of cold NADW through the Mid-Atlantic Ridge mountain chain. Therefore, in addition to MIW water heading westward, much of this flow could be water that has been diverted through the Gibbs Fracture Zone and into the abyssal plains.

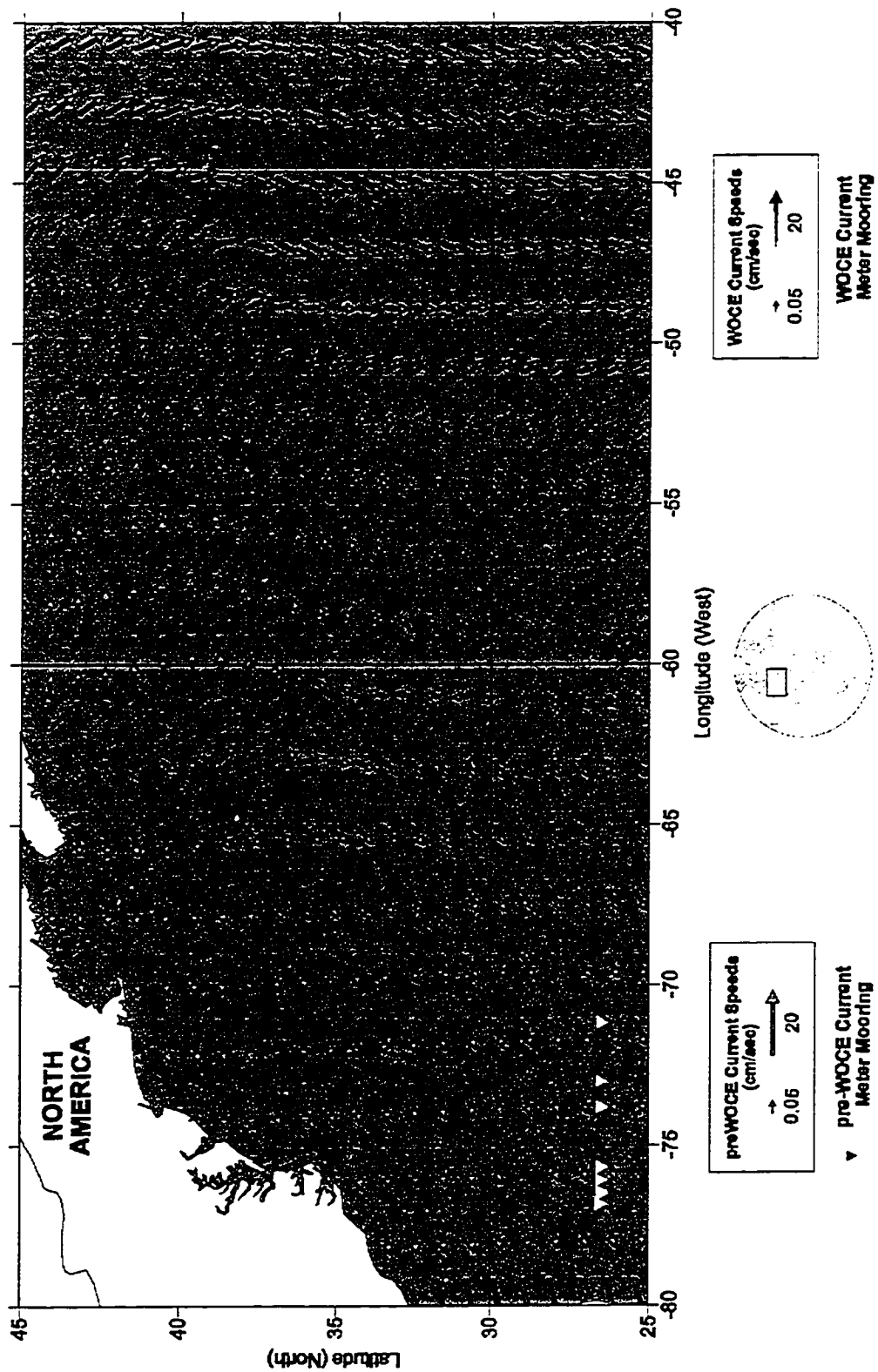


Figure 4.34 Comparison of pre-WOCE and WOCE North Atlantic Ocean Current Vector Plots for Shallow Water Currents (pre-WOCE depths  $\leq$  530 meters, WOCE depths  $\leq$  210 meters)

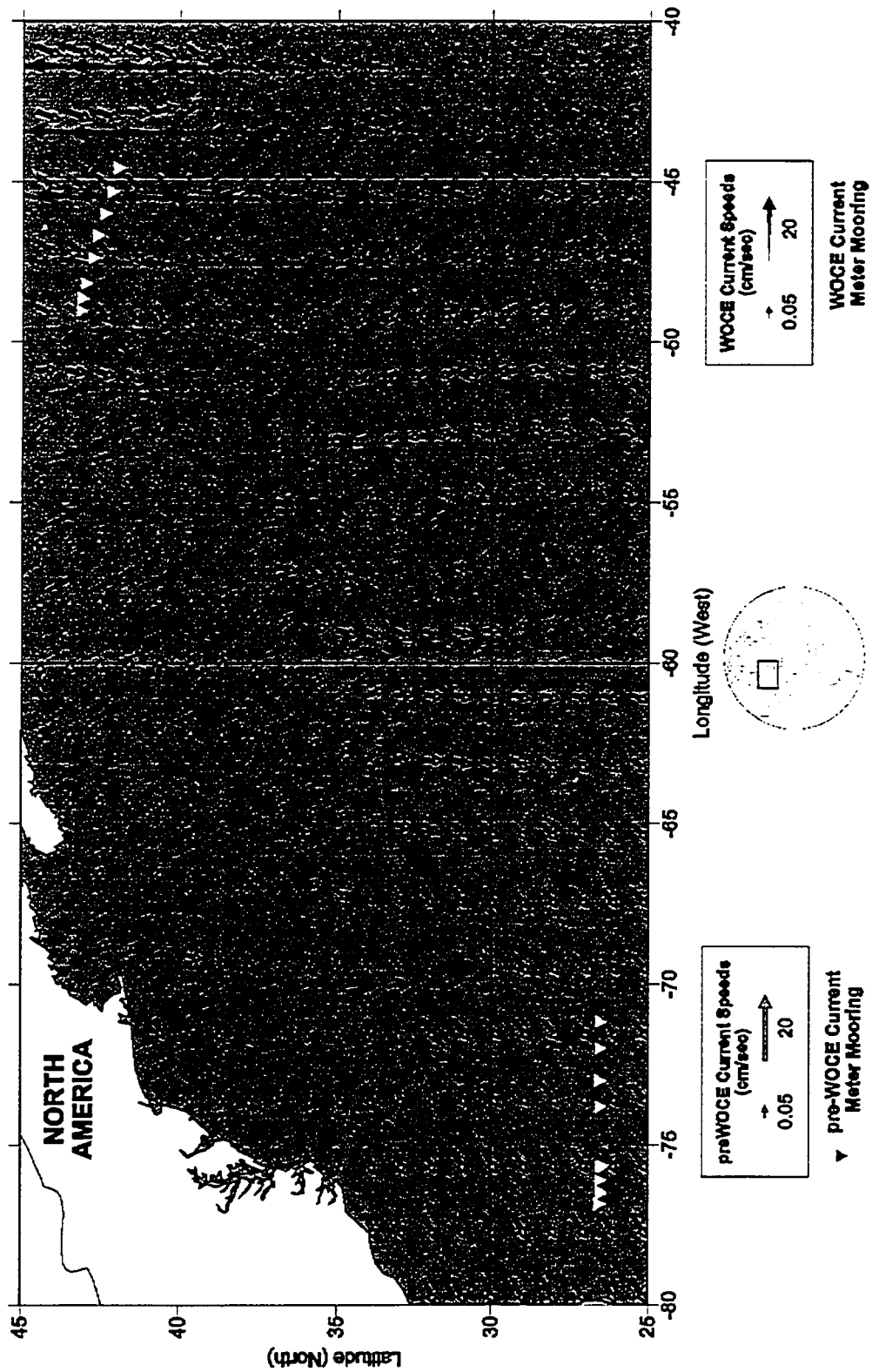


Figure 4.35 Comparison of pre-WOCE and WOCE North Atlantic Ocean Current Vector Plots for Intermediate Depth Water Currents (pre-WOCE: depths 550 to 1000 meters, WOCE depths: 250 to 1000 meters)

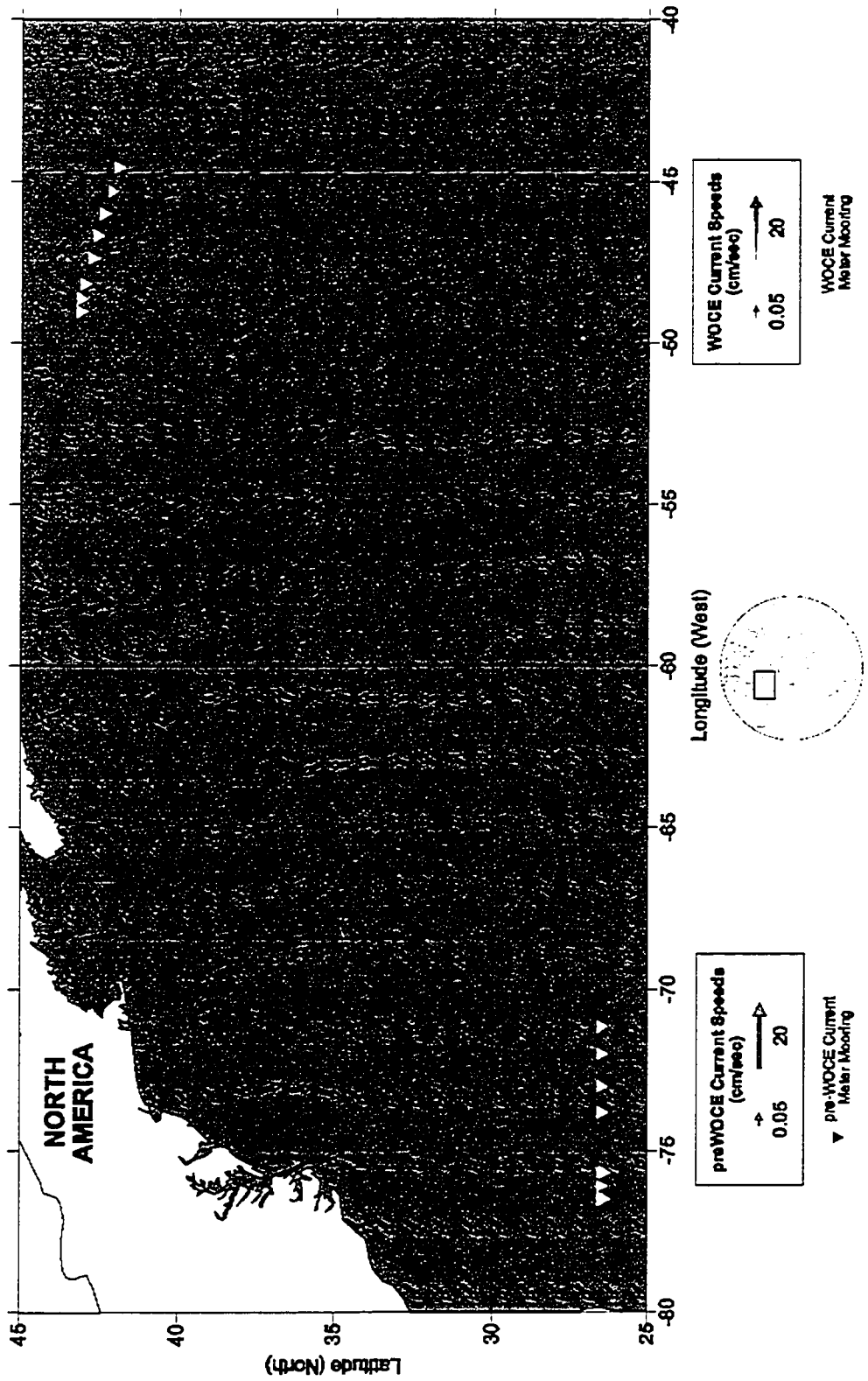


Figure 4.36 Comparison of pre-WOCE and WOCE North Atlantic Ocean Current Vector Plots for Deep Water Currents (pre-WOCE depths: 1200 to 5430 meters, WOCE depths: 1108 to 5483 meters)

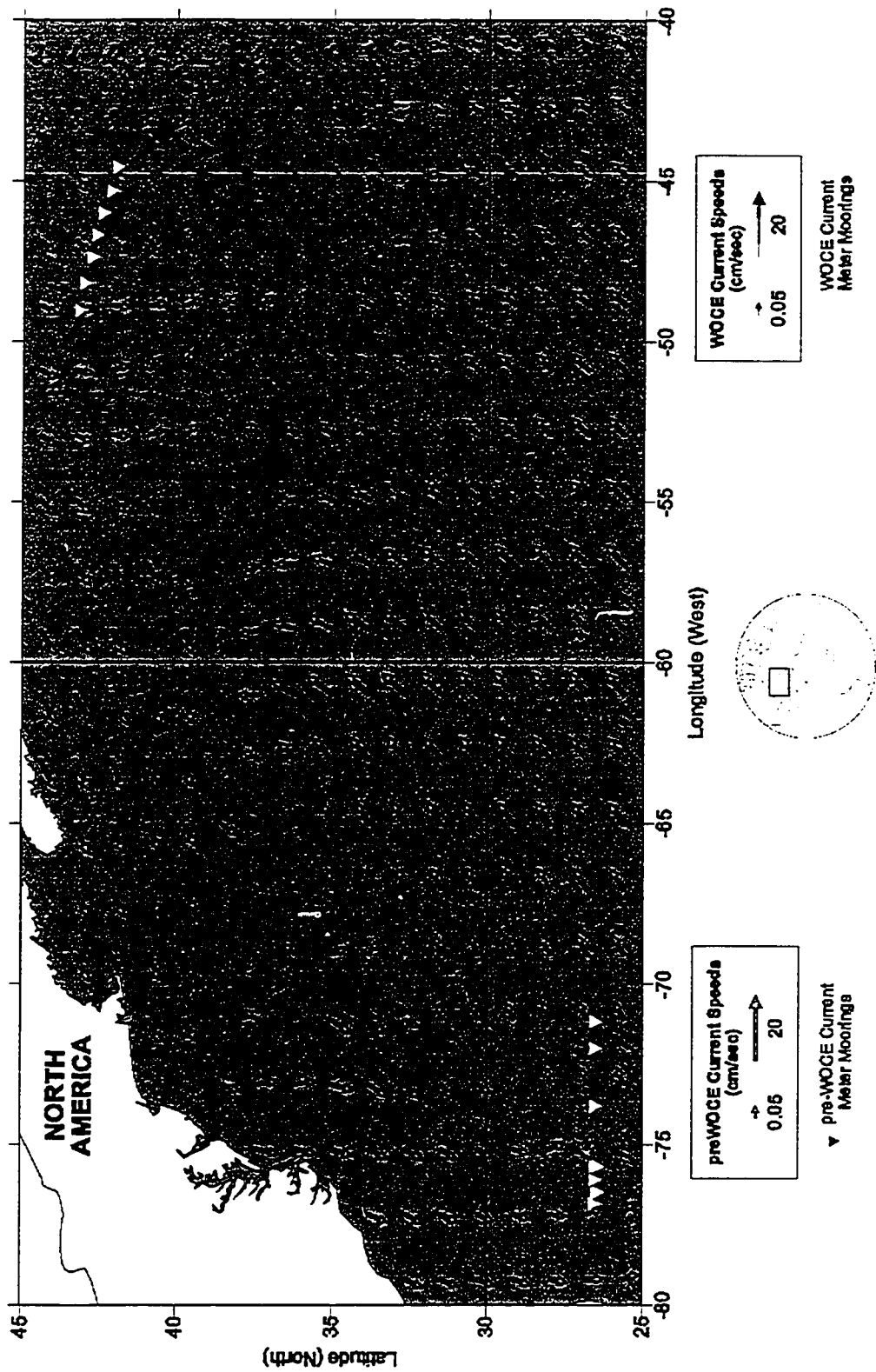


Figure 4.37 Comparison of pre-WOCE and WOCE North Atlantic Ocean Current Vector Plots for Near-Bottom Water Depth Water Currents

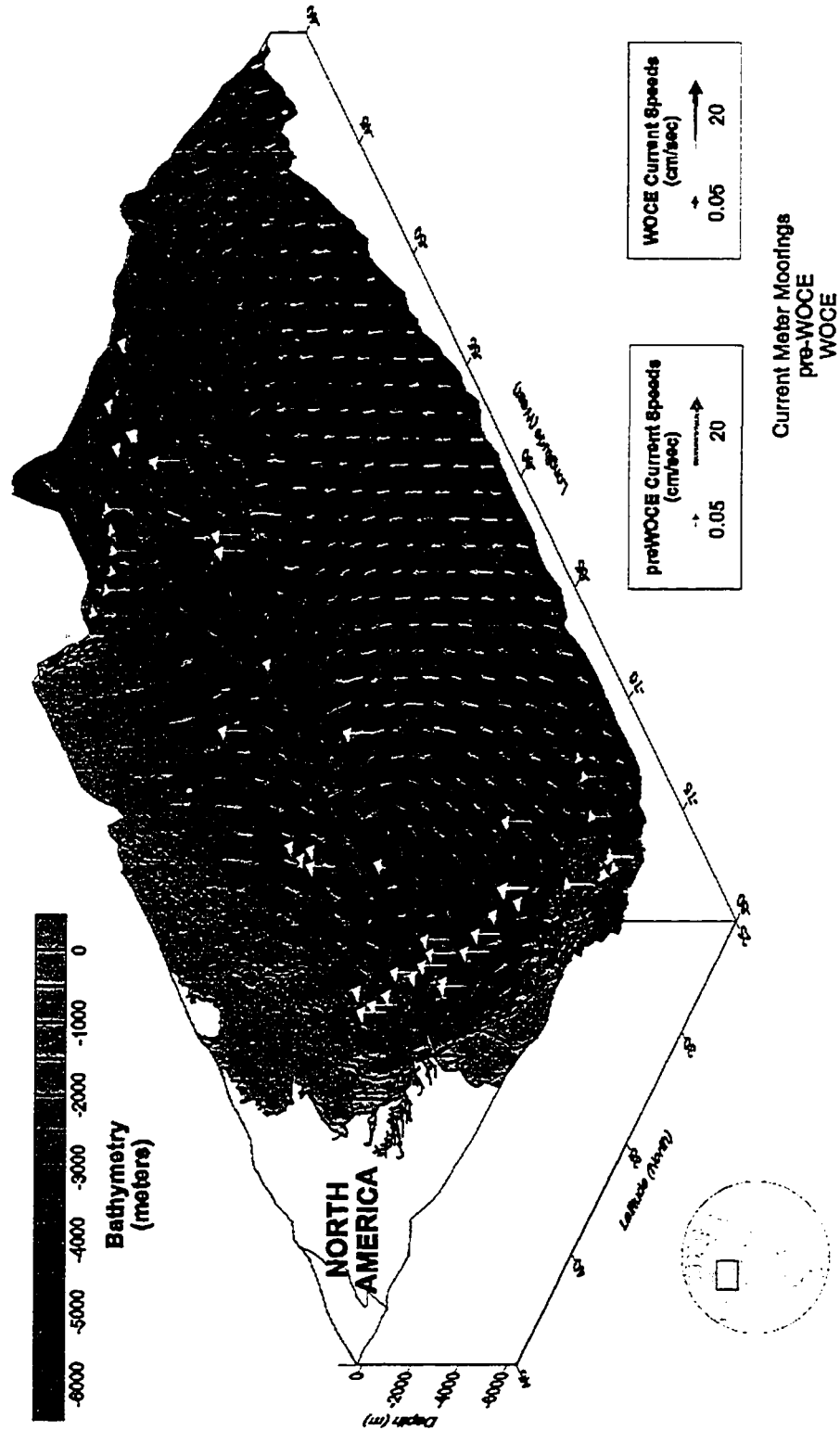


Figure 4.38 Interpolated Mean Current Vectors with Location of Current Meters and ETOPO-5 Bathymetry of the North Atlantic Ocean during the pre-WOCE and WOCE Study Periods for Near-Bottom Depths

## ***4.6 Does River Discharge Affect Current Flow along the Continental Margins?***

Current flow is typically measured in millions of  $\text{m}^3 \text{s}^{-1}$  and is denoted in Sverdrup (Sv) units, where  $1 \text{ Sv} = 1 \times 10^6 \text{ m}^3 \text{ s}^{-1}$ . The Gulf Stream transports greater than 150 million  $\text{m}^3 \text{ s}^{-1}$  (150 Sv), while smaller currents such as the deep western boundary currents transport 10 to 20 million  $\text{m}^3 \text{ s}^{-1}$  (10 to 20 Sv). Overflows, which contribute to the general circulation, such as that coming from the Mediterranean, are in the range of 1 to 3 million  $\text{m}^3 \text{ s}^{-1}$  (1 to 3 Sv). In comparison, all rivers flowing into the Atlantic Ocean transport approximately 0.6 million  $\text{m}^3 \text{ s}^{-1}$  (0.6 Sv). The largest of these is the Amazon River which transports 0.2 million  $\text{m}^3 \text{ s}^{-1}$  (0.2 Sv), while the Mississippi River only transports 0.02 million  $\text{m}^3 \text{ s}^{-1}$ , about  $1/10,000^{\text{th}}$  of the Gulf Stream's transport (Garrison 1996, Tomczak & Godfrey 1994).

Figure 4.39 shows the major river discharges into the North Atlantic Ocean and includes the Amazon River since it is the largest fresh water source (though it technically feeds into the South Atlantic Ocean). The data were obtained from the Oak Ridge National Laboratory Distributed Active Archive Center and consisted of monthly average discharge records. The mapped data indicate the mean discharge over all the records.

In terms of fresh water discharge into the Atlantic Ocean the Amazon River is the only major river with any significant impact. Figure 4.40 combines the location and impact of the Amazon River, as well as the location lesser impact of the St. Lawrence and Magdelana Rivers (which each have roughly 5% the discharge output of the Amazon River). Mean current velocity vectors and contours for shallow water were derived from the WOCE data (as in Figure 4.25).





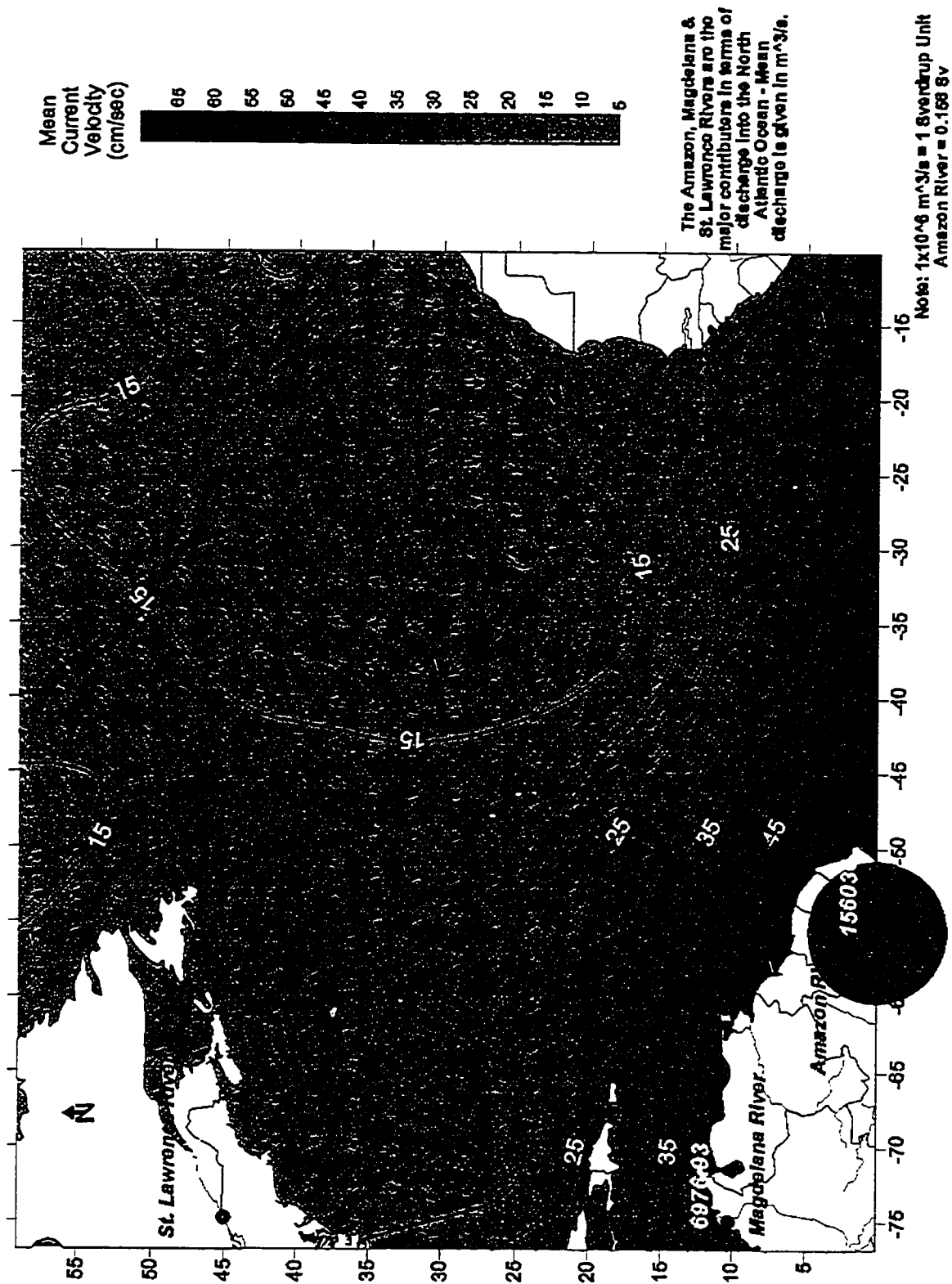


Figure 4.40 WOCE North Atlantic Ocean Mean Current Velocity Vectors for Shallow Water showing Relative Magnitude of Mean Fresh Water Discharge from Major Rivers

The time interval of the Amazon River discharge data differs from the data used to plot the current flow for the North Atlantic Ocean. The current flow record comprises a ten-year period between 1990 and 1999, while the Amazon discharge records consist of a 55-year period between 1928 and 1983. Though discharge data were not available for the Amazon River for the past twenty years, it can be assumed that the impact of the river has only increased during that time frame owing to the massive deforestation which has taken place in the Amazon (Zeng 1999, Muller-Krager et al. 1988).

The reason for undertaking this analysis is due to the observation of the increase in velocity along the South American coast in proximity to the Amazon River outflow. Is this a result of salinity changes due to the fresh water being added to the coastline? Or is it just a matter of the additive effects of water from the North Equatorial Current flow and cross-equatorial flow from the South Atlantic funneling into the Caribbean Current?

Research on large-scale buoyancy driven circulation on the continental shelf has shown that freshwater plumes and coastal currents are produced from freshwater discharges of rivers and estuaries (Narayanan and Garvine, 2002). The extent to which this water infiltrates into the ocean is dependent on scaled inlet volume transport, scaled breadth and scaled diffusivity (Narayanan and Garvine, 2002). Indeed, fresh water discharge from the Amazon River can be found in surface waters at a distance of some 1000 to 1200 kilometers from the coast (Fedorov and Ginsburg 1992). Behaving much like the eddies which emanate from the Gulf Stream, these fresh water “lenses” have salinity values some 3 to 5‰ lower than the surrounding waters and effecting upwelling (Fedorov and Ginsburg 1992). Therefore it would appear that the outflow of fresh water from the Amazon does have an impact on the current velocities we are observing.

## **4.7 WOCE Data Revisited – A Look at the Annual Mean Circulation in the 1990s**

### **4.7.1 Mean Current Flows (1990 – 1997)**

A further analysis of the annual mean circulation was carried out on the WOCE data from 1990 – 1997. These are the years in which a sufficient number of data points were available to plot the mean circulation. Both 1998 and 1999 lacked sufficient data points to implement any sort of interpolation regime, indeed the 1999 dataset contained only 6 stations all located at the southern tip of Greenland (Figure 4.41).

Figure 4.42 extends from pages 130 to 133 with each vector plot representing the mean current flow for that year. The plots were produced by using the entire data available for each year of WOCE data. In the case of duplicate data, data with the same x-, y-co-ordinates, selection was based on the point closest to the surface. This was done in order to better approximate surface conditions for the year in question. In addition to these plots a CD-ROM is included with this thesis that includes animations compiled in Microsoft PowerPoint. There are three animations included,

- i) one to show the yearly circulation from the data available, these plots include water temperatures in order to visualize the changes in water temperature through the decade;
- ii) the second animation has the same current vector plots but without the temperature contours in order to better focus on the circulation pattern;
- iii) the final animation shows surface current flows combined with the wind field in order to visualize both parameters

It should be noted that the first two animations each contain nine frames, spanning from 1990 to 1998 - note the absence of data points throughout the study region for the years 1996 to 1998. These years were included to show the extreme change in circulation based on an incomplete spatial sample. The third animation contains only four frames since wind field data was only available for the years 1992 to 1995.

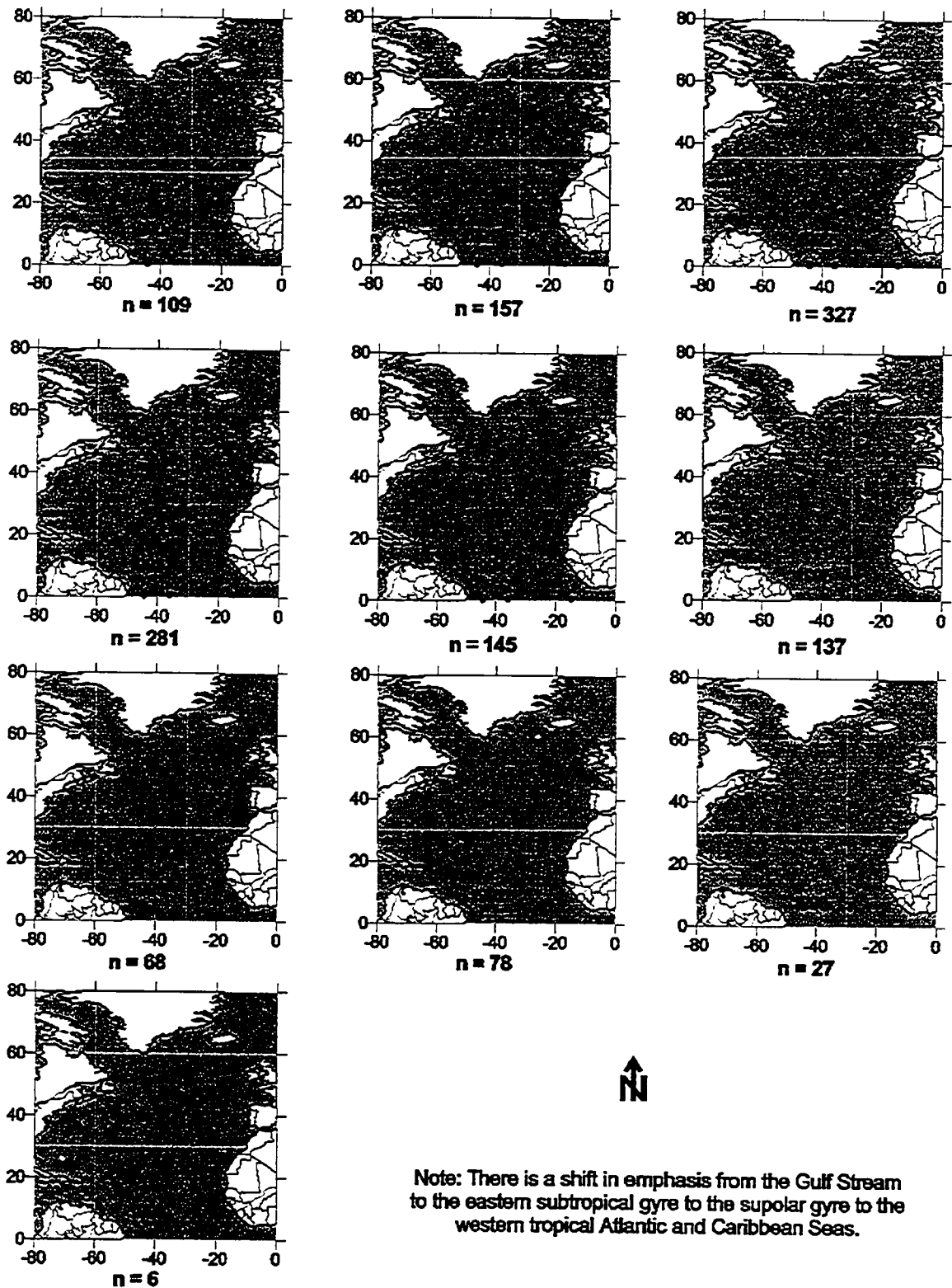
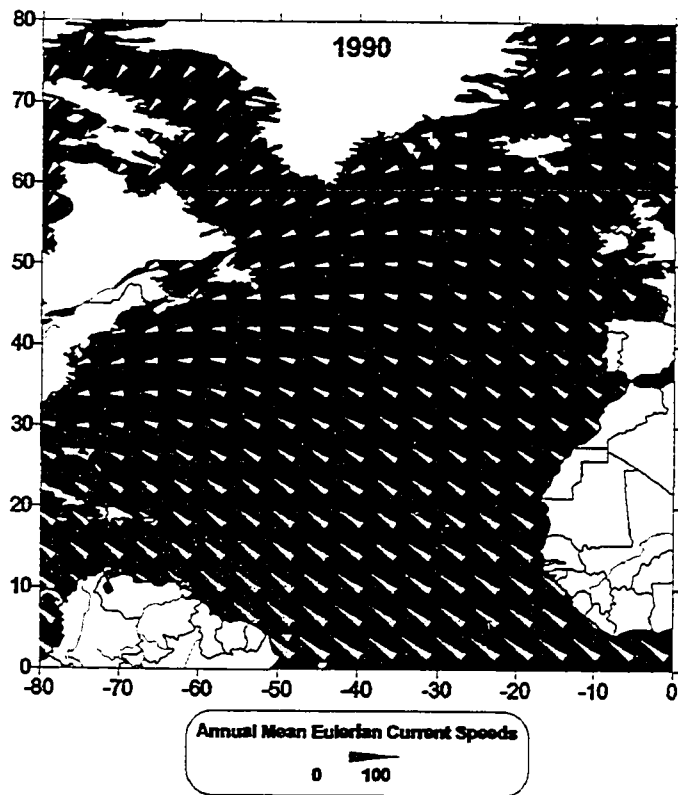


Figure 4.41 Temporal and Spatial Distribution of Current Meter Moorings for the WOCE Period of 1990 to 1999 (n = number of current meter moorings)

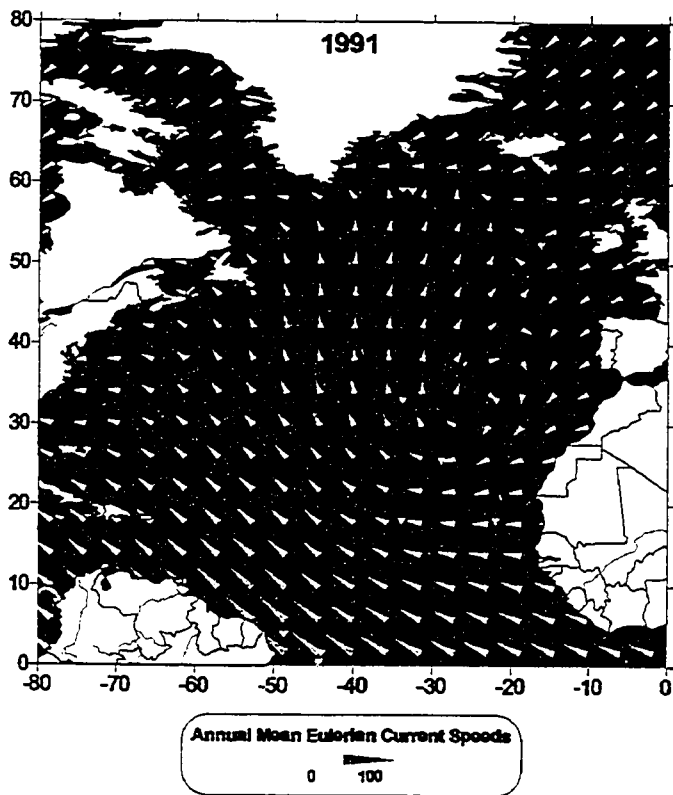


Annual Mean Temperature



Radial Basis Function Interpolation  
using Multiquadric Kernel Method  
26 of 102 data points retained

- Current Meter Locations



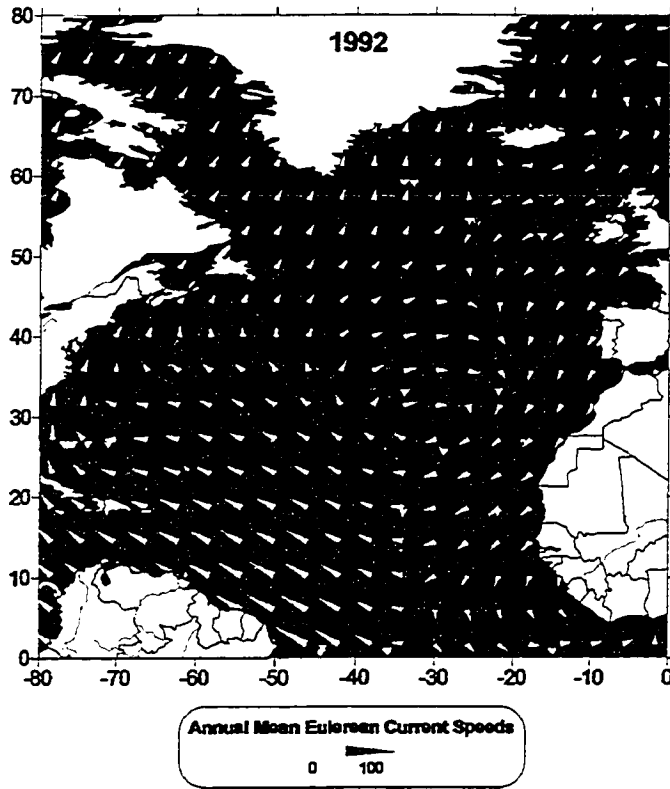
Annual Mean Temperature



Radial Basis Function Interpolation  
using Multiquadric Kernel Method  
29 of 116 data points retained

- Current Meter Locations

Figure 4.42 Annual Mean Eulerian Current Speeds in the North Atlantic Ocean (Figure continues over the next three pages, i.e. 145-148 inclusive)

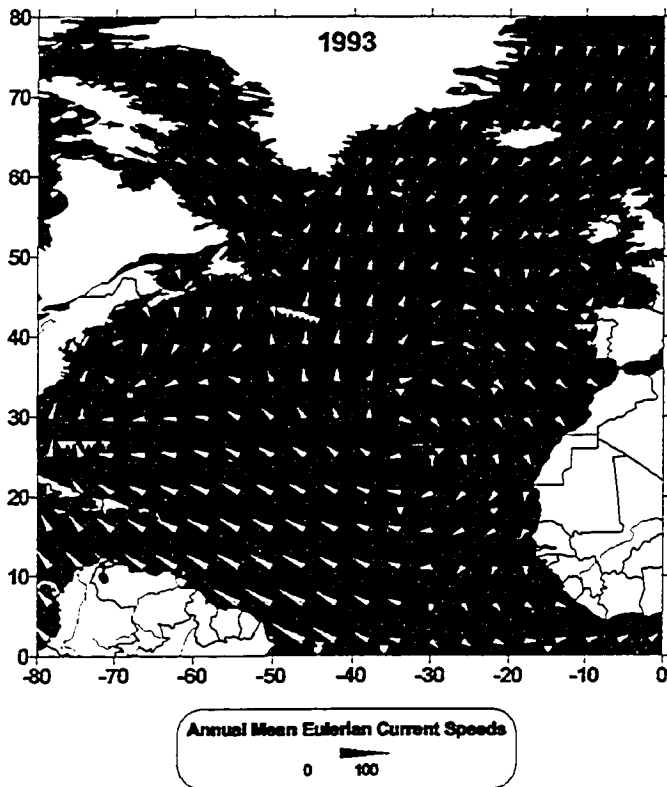


Annual Mean Temperature



Radial Basis Function Interpolation  
using Multiquadric Kernel Method  
32 of 203 data points retained

- Current Meter Locations

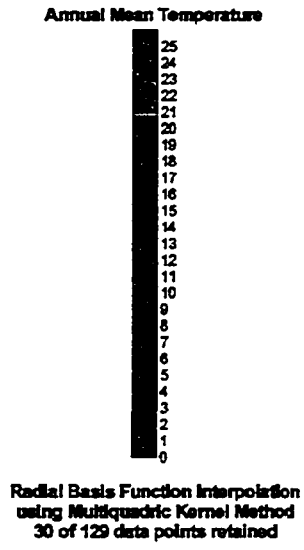
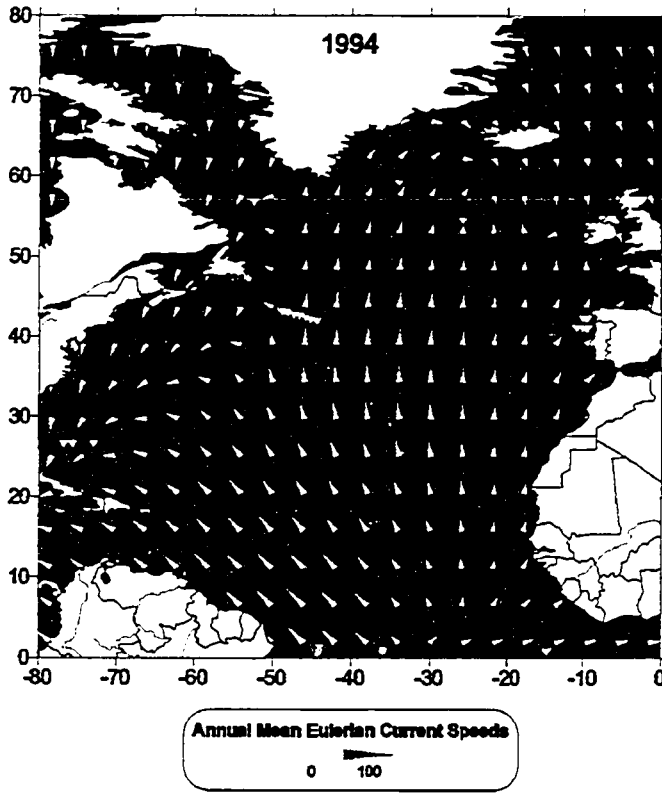


Annual Mean Temperature

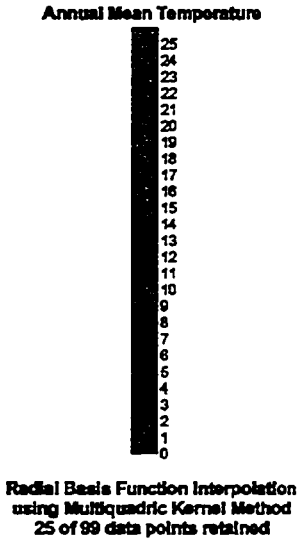
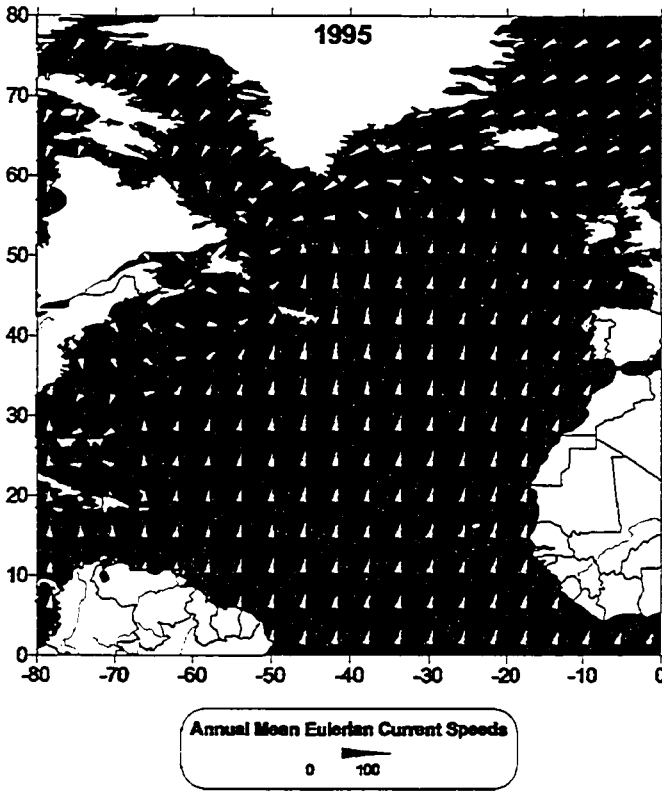


Radial Basis Function Interpolation  
using Multiquadric Kernel Method  
38 of 200 data points retained

- Current Meter Locations

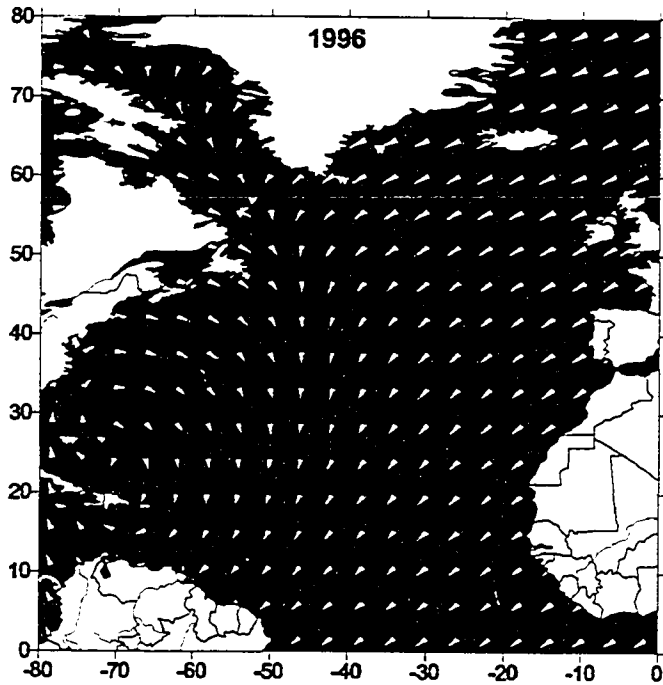


- Current Meter Locations



- Current Meter Locations



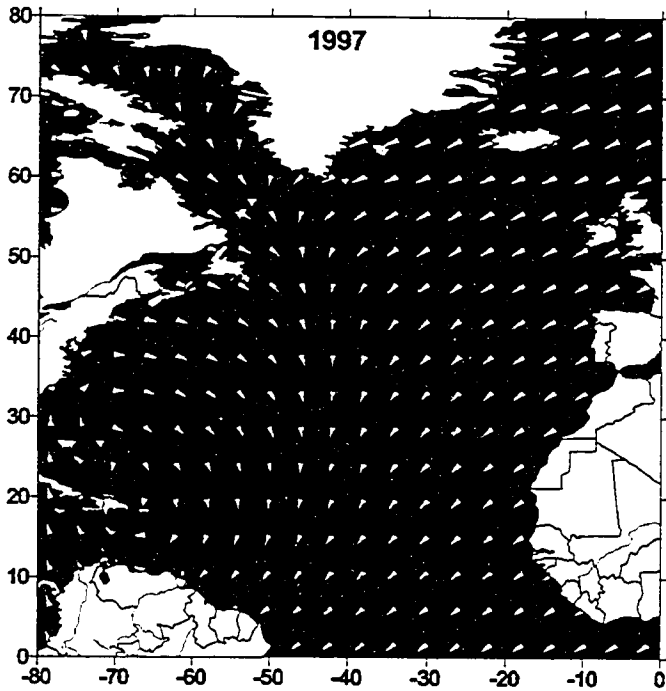


Annual Mean Temperature



Radial Basis Function Interpolation  
using Multiquadric Kernel Method  
14 of 45 data points retained

Current Meter Locations



Annual Mean Temperature



Radial Basis Function Interpolation  
using Multiquadric Kernel Method  
17 of 53 data points retained

Current Meter Locations

The current vector plots were produced in Surfer7 with radial basis function interpolation using the multiquadric kernel method. Next to each annual plot the number of data points that were retained in implementing the interpolation are given. Note that there was a significant loss of data necessary in producing the current vector plots. Though the data retained is sufficient to give some general circulation patterns.

Between 1990 and 1991 the annual mean circulation diverges northward with temperatures increasing throughout the North Atlantic. This observation is largely due to the inclusion of current meters along the eastern portion of the study area that were not present in 1990. Therefore a more accurate circulation and temperature distribution appears in 1991.

Moving forward through to 1993 the same patterns appear as in the 1991 plot. The flow of the sub-tropical gyre is clearly evident in these three plots, though a lack of current meters in the Labrador Sea results in no indication of the sub-polar gyre. It is also interesting to note the eastward movement of the large warm water core that is centered near 25°N, 40°W in 1991 positioning itself near 20°N,30°W by 1993. Also a smaller warm water core forms and moves north to center itself around 50°N, 15°W, following the path of the Gulf Stream and North Atlantic Drift. These observations appear to coincide with the expansion and compression of the sub-tropical gyre, and the changes in current flow between 1991 and 1993 are tied to the transfer of heat westward towards the Caribbean and north-eastward toward the United Kingdom.

The loss of key current meter moorings in the south-east North Atlantic by 1994 causes a loss of information regarding both the sub-tropical gyre flow and the temperature distribution, resulting in an apparent northward shift to 40°N of a somewhat

cooler warm core by 1995. The extreme loss of data points by 1996, with only a few northern current meters, results in the loss of current and temperature information.

#### **4.7.2 Shallow Mean Current Flows and the Mean Wind Field (1992 – 1995)**

Figure 4.43, on the next two pages, shows four current vector plots of annual mean Eulerian current speeds for shallow water (less than 60 meters depth) overlaid with annual mean wind field vectors and annual mean temperature contouring.

The mean wind field gridded dataset was obtained on-line from the French Processing and Archiving Facility (CERSAT 2002). The annual mean wind field for all four years is very consistent, with most of the variance occurring north of 30°N in the area of the subtropical high. The annual mean current flow shows some wildly fluctuating patterns with a predominate south-east flow in 1992 near the equator turning into a north-west flow in 1993 and maintaining this direction in 1994. The plot for 1995 does not give much information since the current meters situated near the equator at 45°W are gone and the result is a generalized western flow based on the current meters near 25°N, 75°W. An interesting pattern to note is that the annual mean north-west current flow of 1993 and 1994 match up quite well with the WOCE decadal mean flow of shallow water in the 1990s shown in Figure 4.34.

The 1993 to 1994 maps are similar to Figure 4.24 on page 106 with the mean current flow at right angles to the wind. The predominate flow for 1992 in the opposite direction of the 1993 and 1994 plots, could be a factor of current reversals or perhaps some discrepancy in the data. The 1995 map shows a general south-east flow due to the absence of instrumentation.

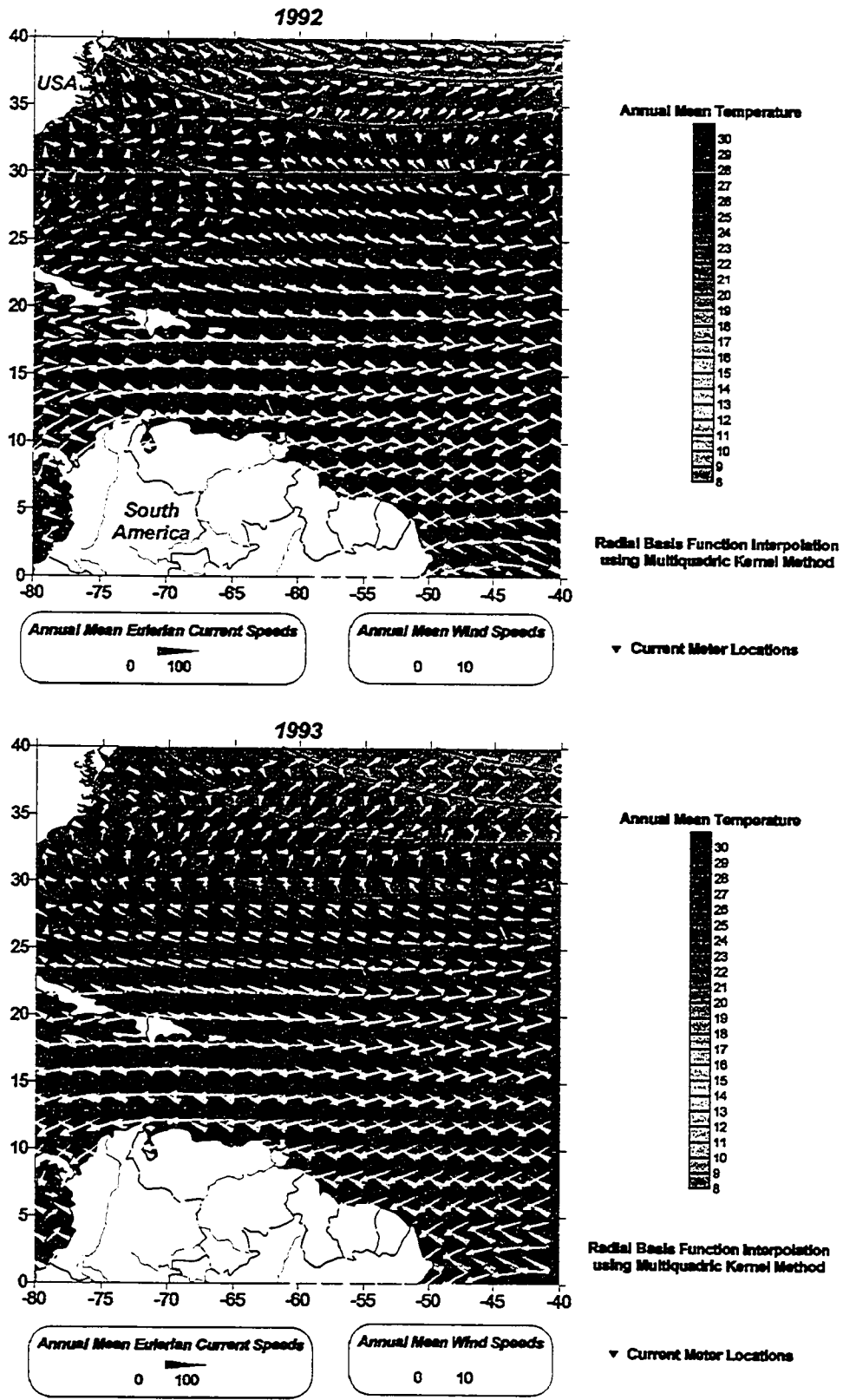
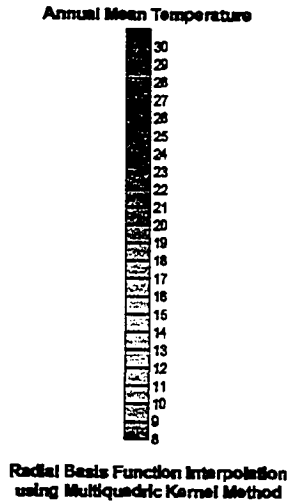
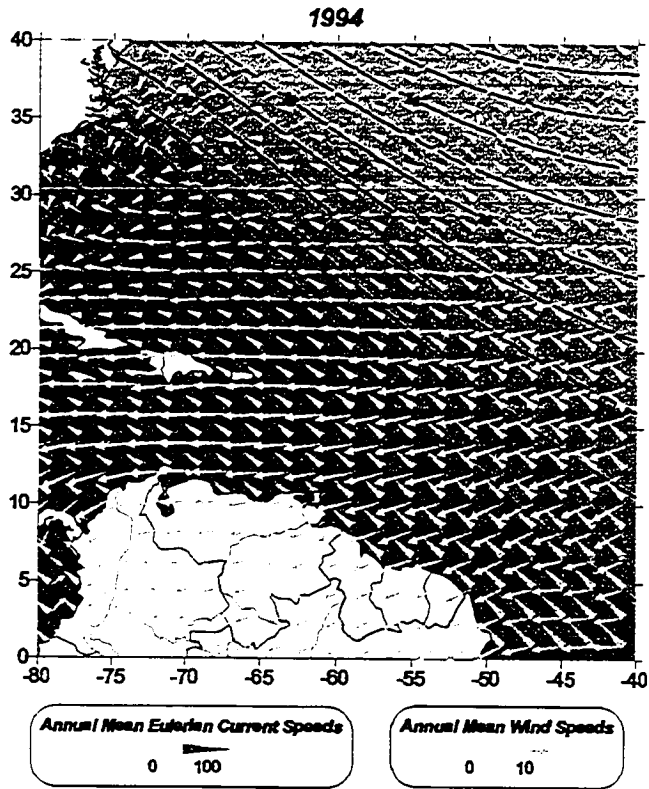
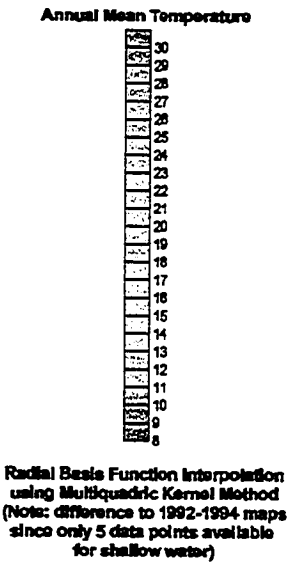
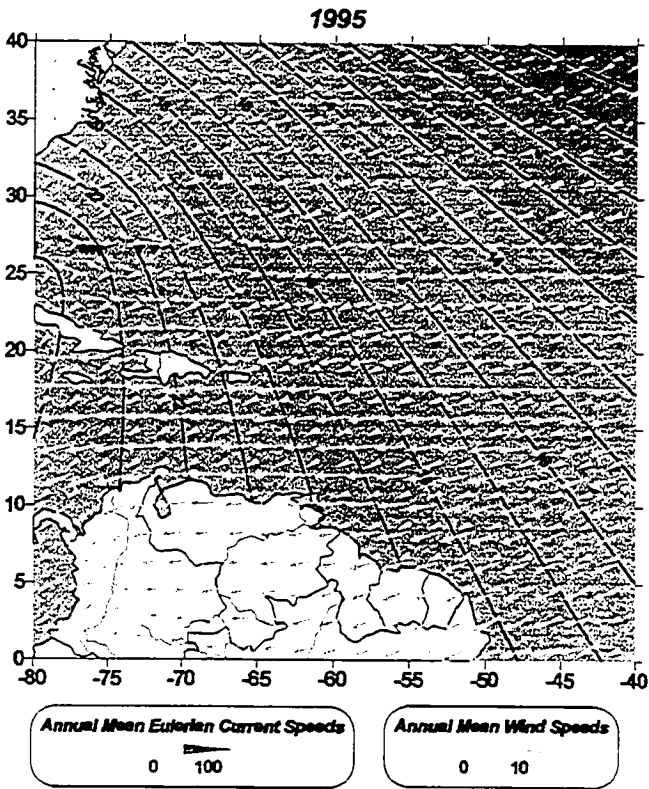


Figure 4.43 Annual Mean Eulerian Current Speeds for the North Atlantic Ocean with Annual Mean Wind Speeds superimposed for Comparison Purposes



▼ Current Meter Locations



▼ Current Meter Locations

## 4.8 Eddy Kinetic Energy Flow Data in the North Atlantic Ocean

### 4.8.1 Introduction

Data made available through the WOCE initiative included global datasets for eddy kinetic energy per unit mass, kinetic energy of the mean flow, and the covariance of east with north, i.e. distance with respect to direction, for both the pre-WOCE and WOCE periods (Dickson and Medler 1998). The pre-WOCE flow statistics include data collected up to January 1989. Descriptive statistics of the flow from experiments that ended prior to January 1989 are shown in Table 4.1, with extreme values highlighted. Depths are given in meters, and KE denotes eddy kinetic energy per unit mass and has cgs units of  $\text{cm}^2 \text{s}^{-2}$ ; KM is the energy per unit mass of the mean flow with units  $\text{cm}^2 \text{s}^{-2}$ ; and UV is the mean eddy momentum flux ( $\text{cm}^2 \text{s}^{-2}$ ) calculated as the mean value of  $(u - u_{\text{mean}})(v - v_{\text{mean}})$ .

**Table 4.1 pre-WOCE Flow Statistics for Shallow (< 500 meters depth), Intermediate (500 – 2000 meters depth), and Deep (>2000 meters depth) Water**

Pre-WOCE Period	Latitude	Longitude	Water Depth	Instr Depth	KE	KM	UV	Days
Min(shallow)	0.00	-79.98	-6015	-499	4.8	0.0	-610.8	28
Mean(shallow)	34.74	-54.18	-2204	-218	252.8	901.5	65.9	259
Median(shallow)	32.52	-69.98	-992	-200	144.5	45.5	19.3	201
Max(shallow)	79.02	-0.92	-75	-7	1765.7	29153.4	830.9	3204
Min(intermediate)	0.00	-79.58	-6015	-2000	1.0	0.0	-168.2	31
Mean(intermediate)	40.75	-40.67	-3597	-1045	70.8	64.4	0.8	333
Median(intermediate)	36.17	-35.71	-4250	-1000	33.2	3.8	0.2	330
Max(intermediate)	79.01	-2.98	-521	-500	1044.8	1796.0	208.1	3204
Min(deep)	4.02	-76.77	-6015	-5800	0.2	0.0	-53.3	35
Mean(deep)	41.62	-35.07	-4397	-3698	25.5	13.4	0.0	321
Median(deep)	41.7	-25.14	-4335	-3943	8.2	1.9	0.0	327
Max(deep)	79.02	-0.92	-2045	-2002	280.5	312.7	36.0	2057

The ranges of values for the three key statistics are as follows:

Shallow	$\Delta\text{KE} = 1760.9$	$\Delta\text{KM} = 29153.4$	$\Delta\text{UV} = 1441.7$
Intermediate	$\Delta\text{KE} = 1043.8$	$\Delta\text{KM} = 1796.0$	$\Delta\text{UV} = 376.3$
Deep	$\Delta\text{KE} = 280.3$	$\Delta\text{KM} = 312.7$	$\Delta\text{UV} = 89.3$

In most cases KE, KM, and UV were calculated from filtered data, from which the diurnal tides and higher frequencies were removed (Dickson and Medler 1998). For the pre-WOCE data above there were 3,090 values available (984 shallow, 1,037 intermediate, and 1,069 deep).

The WOCE period flow statistics include data collected up to May 1998. In table 4.2 gives the descriptive statistics for the WOCE period include 1,628 values (606 shallow, 452 intermediate, and 570 deep).

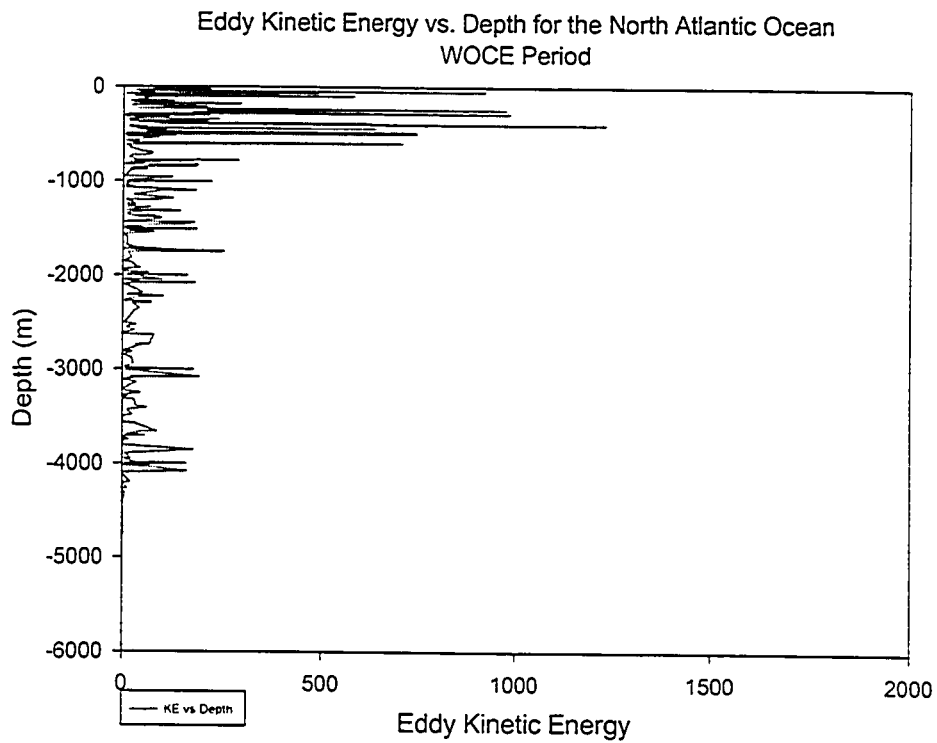
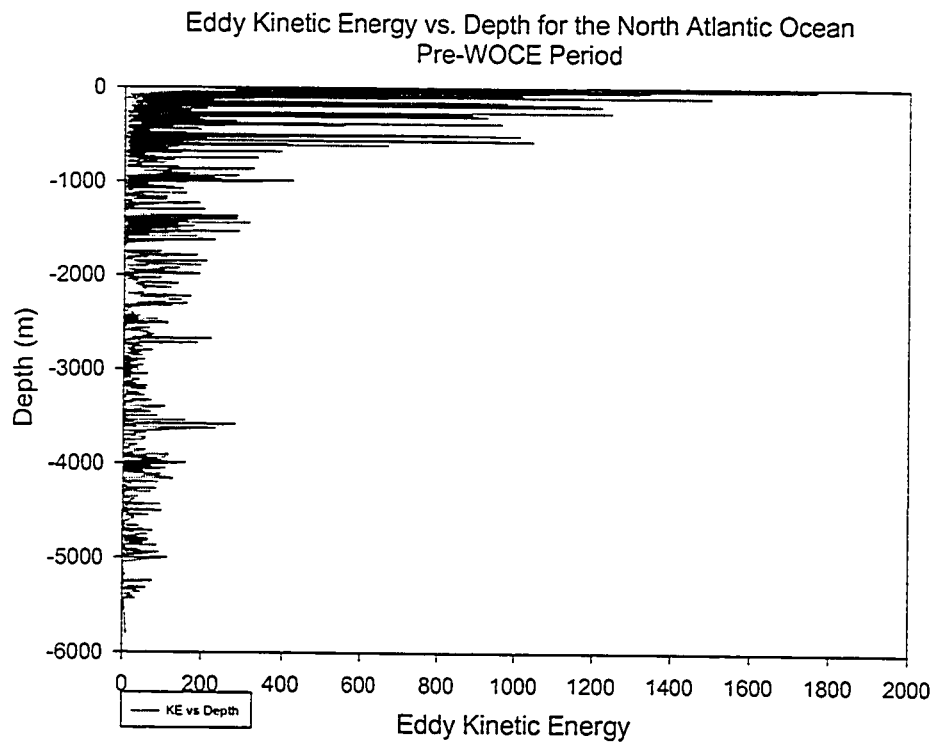
**Table 4.2 WOCE Period Flow Statistics for Shallow (<500 meters depth), Intermediate (500 – 2000 meters depth), and Deep (>2000 meters depth) Water**

WOCE Period	Latitude	Longitude	Water Depth	Instr Depth	KE	KM	UV	Days
Min(shallow)	0.09	-76.85	-5670	-499	2.9	0.0	-218.3	92
Mean(shallow)	43.56	-32.62	-3365	-212	146.7	158.4	-1.9	334
Median(shallow)	39.49	-28.95	-3481	-181	70.7	10.8	2.9	316
Max(shallow)	75.57	-0.80	-198	-10	1229.2	6675.0	473.7	701
Min(intermed)	0.42	-76.85	-5670	-2000	2.0	0.0	-167.0	94
Mean(intermed)	47.19	-32.13	-3054	-1162	69.4	49.4	-0.7	391
Median(intermed)	47.91	-20.01	-2920	-1192	29.8	7.0	1.2	357
Max(intermed)	75.48	-0.80	-506	-500	705.8	2628.1	74.5	712
Min(deep)	0.42	-76.52	-5670	-4758	0.3	0.0	-82.4	150
Mean(deep)	35.00	-37.09	-3998	-3309	39.8	20.9	3.8	441
Median(deep)	37.87	-35.9	-4235	-3409	22.6	4.0	1.1	373
Max(deep)	75.06	-5.45	-2056	-2020	193.8	292.6	68.2	712

The ranges of values for the three key statistics are as follows:

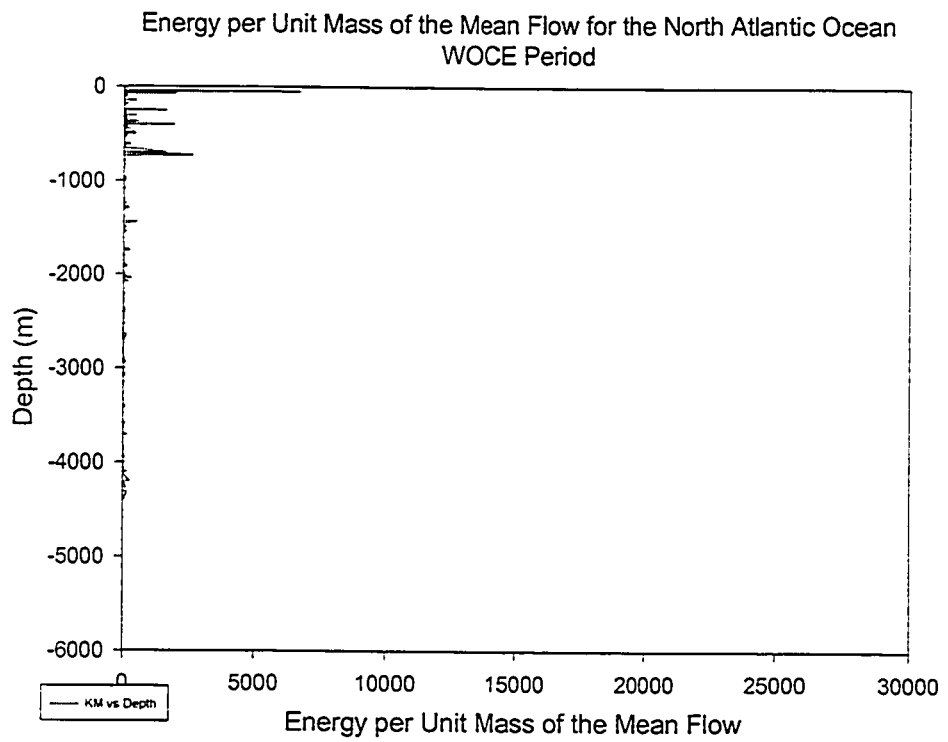
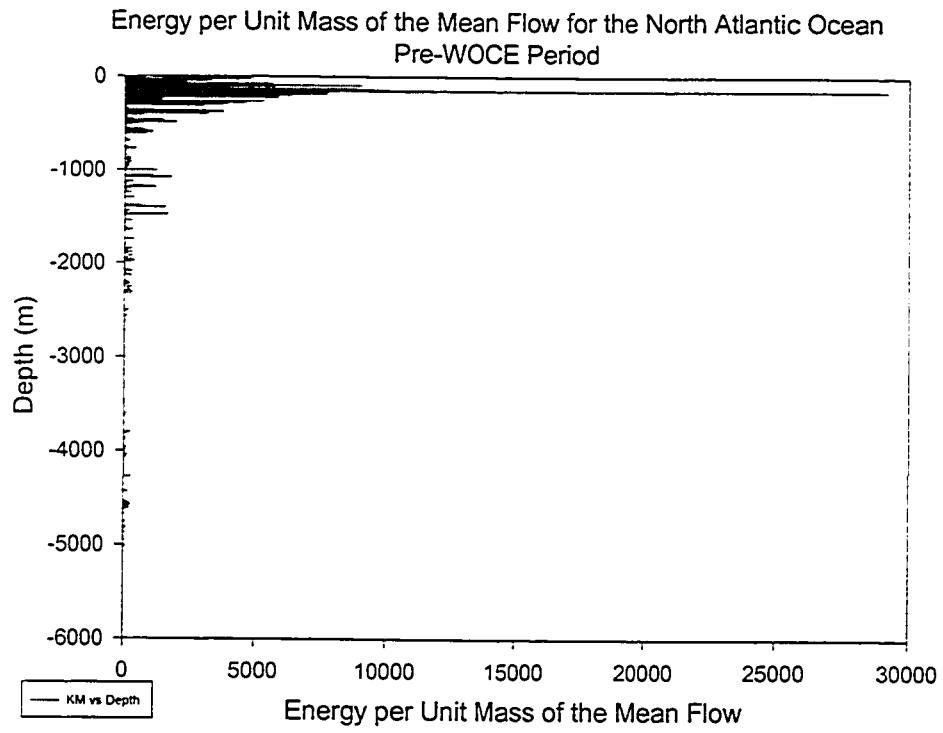
Shallow	$\Delta KE = 1226.3$	$\Delta KM = 6675.0$	$\Delta UV = 692.0$
Intermediate	$\Delta KE = 703.8$	$\Delta KM = 2628.1$	$\Delta UV = 241.5$
Deep	$\Delta KE = 193.5$	$\Delta KM = 292.6$	$\Delta UV = 150.6$

Figure 4.45 plots KE, KM and UV against depth for both the pre-WOCE and WOCE datasets in order to discern the differences between study periods and within study periods at different depths.

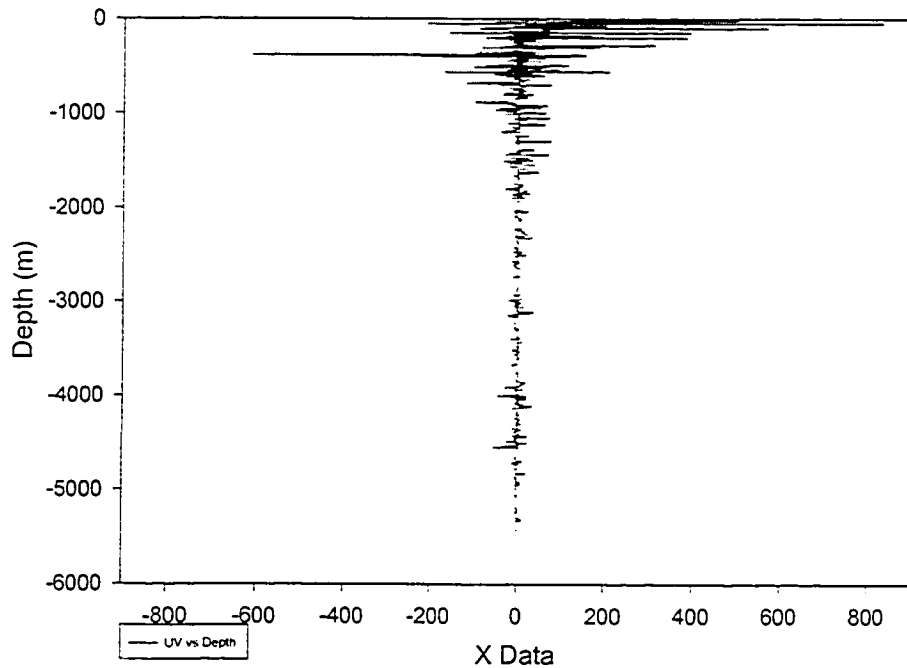


**Figure 4.44** Plots of Eddy Kinetic Energy (KE), Energy per Unit Mass of the Mean Flow (KM), and Mean Eddy Momentum Flux (UV) against Depth for the North Atlantic Ocean for pre-WOCE (left) and WOCE (right) Period Datasets

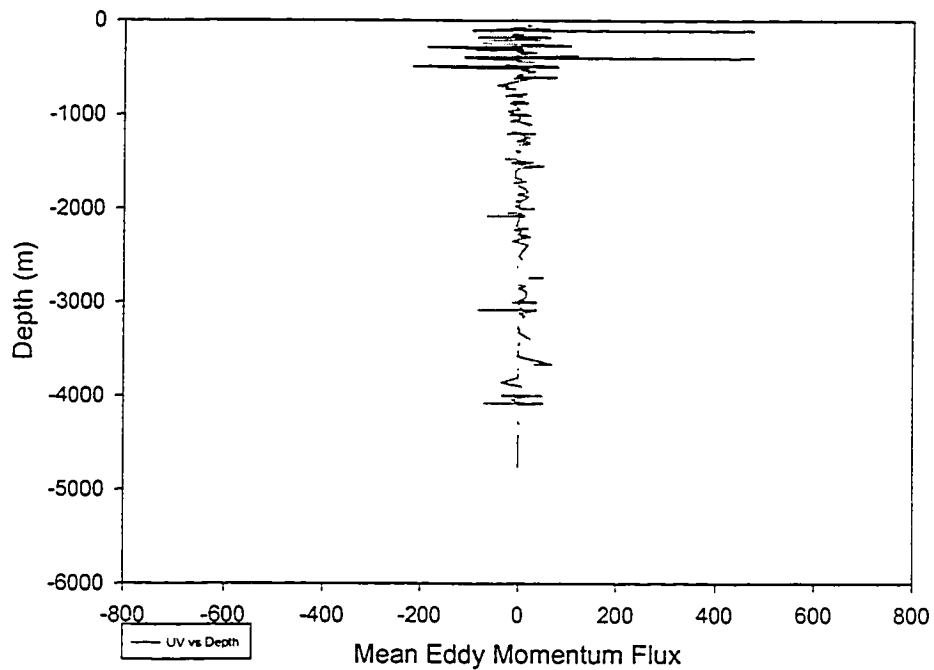




Mean Eddy Momentum Flux for the North Atlantic Ocean  
Pre-WOCE Period



Mean Eddy Momentum Flux for the North Atlantic Ocean  
WOCE Period



First, note that energy is much greater in the upper 500 meters of the ocean, and shows much more variability than at greater depths. Values for pre-WOCE are generally much larger than for the WOCE period, with the exception of  $\Delta KM_{\text{intermediate}}$  and  $\Delta UV_{\text{deep}}$ . KE for the pre-WOCE period was generally much higher than for the WOCE period, as was KM. With respect to UV, there appears to be greater eddy momentum flux in the upper 500 meters for the pre-WOCE period, but slightly greater fluxes (though very much smaller in actual size) at depth for the WOCE period.

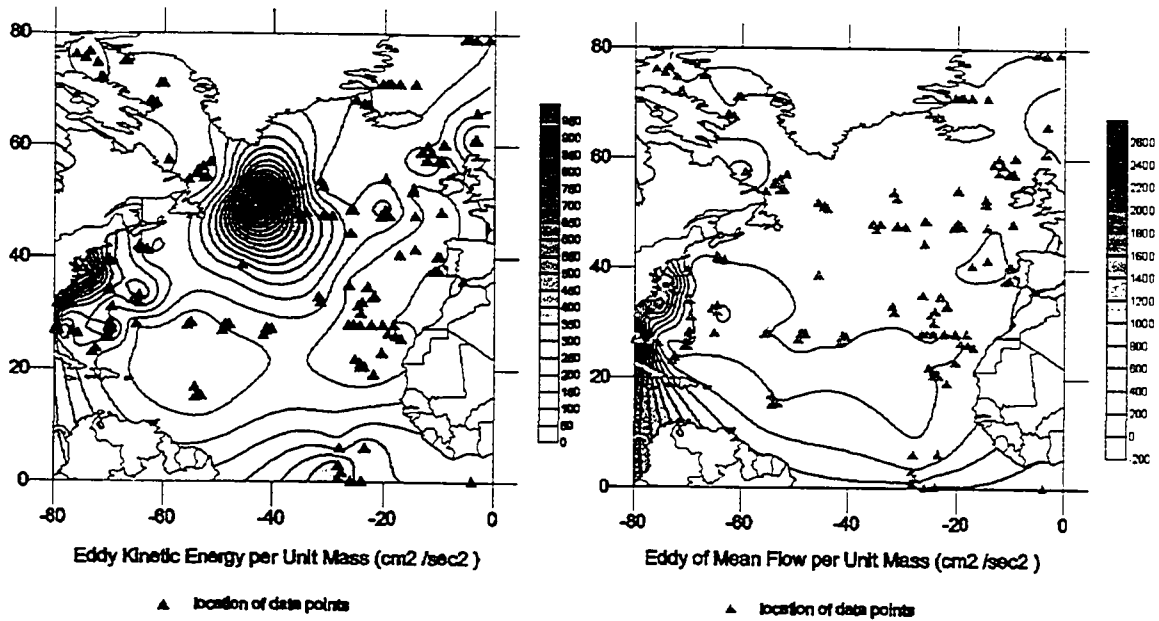
#### **4.8.2 Eddy Kinetic Energy Plots**

Using the data from these two periods, plots were constructed for eddy kinetic energy per unit mass ( $\text{cm}^2 \text{s}^{-2}$ ) and for the kinetic energy of the mean flow ( $\text{cm}^2 \text{s}^{-2}$ ).

Figure 4.45 (a) shows the eddy kinetic energy per unit mass and the kinetic energy of the mean flow for the North Atlantic Ocean pre-WOCE and WOCE periods at shallow depths (0 – 499 meters); Figure 4.45 (b) shows the same flow statistics for the North Atlantic pre-WOCE and WOCE periods at intermediate depths (500 – 2,000 meters); and Figure 4.45 (c) shows the same flow statistics for the North Atlantic pre-WOCE and WOCE periods at deep depths (2,000 – 5,000 meters).

An intense region of eddy kinetic energy in the western portion of the North Atlantic Ocean off the coast of North America and roughly analogous to the position of the western boundary currents, particularly the Gulf Stream is evident in the pre-WOCE plot of Figure 4.45 (a), extremely high values of KM are also observed indicating the large amount of energy still present in the mean flow. Another intense area is situated where cold water from the Irminger Basin mixes with warm water from the Gulf Stream.

(a) Flow Statistics for pre-WOCE and WOCE Shallow Water (0 to 500 meters depth)



pre-WOCE (above) / WOCE (below)

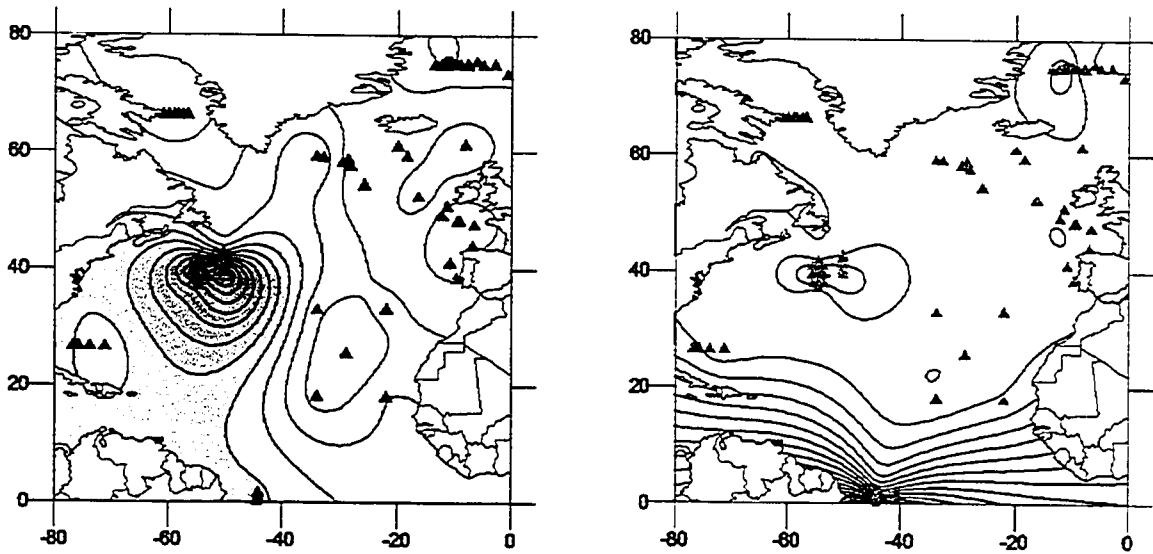
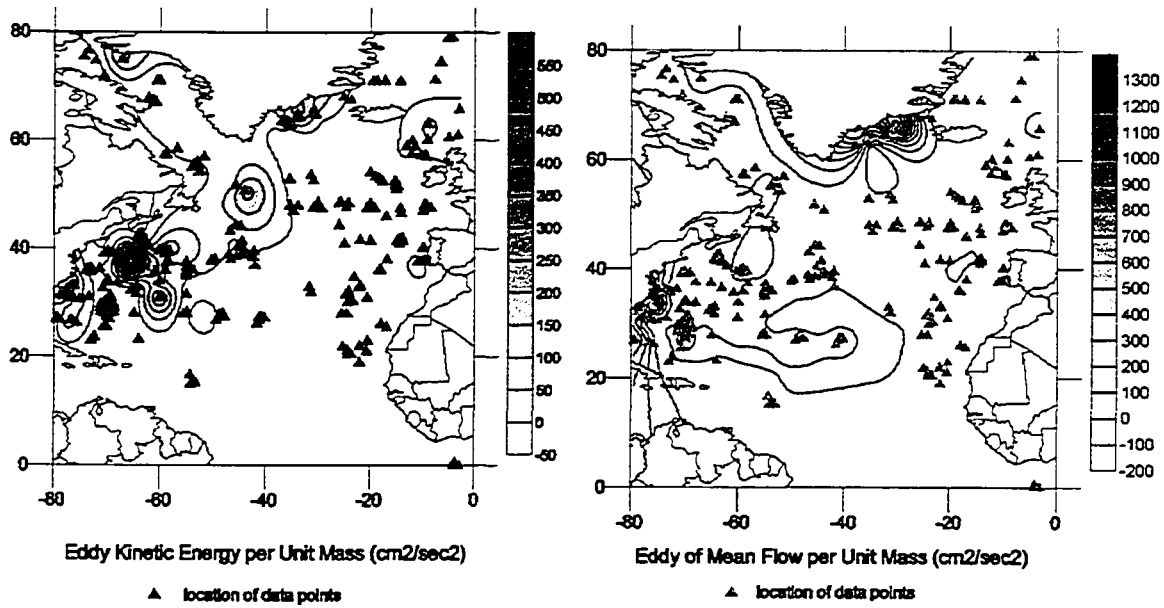
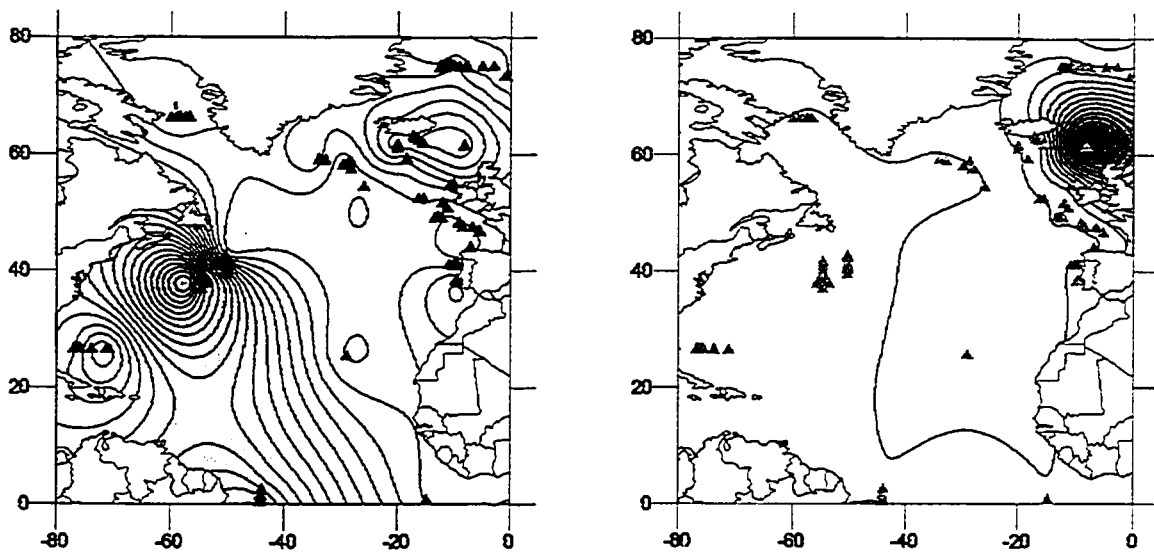


Figure 4.45 (a) – (c) Pre-WOCE Flow Statistics to January 1989 and WOCE Period Flow Statistics to May 1998 for Shallow, Intermediate and Deep Waters in the North Atlantic Ocean (Shallow = 0 to 500 meters, Intermediate = 500 to 2000 meters, Deep = >2000 meters)

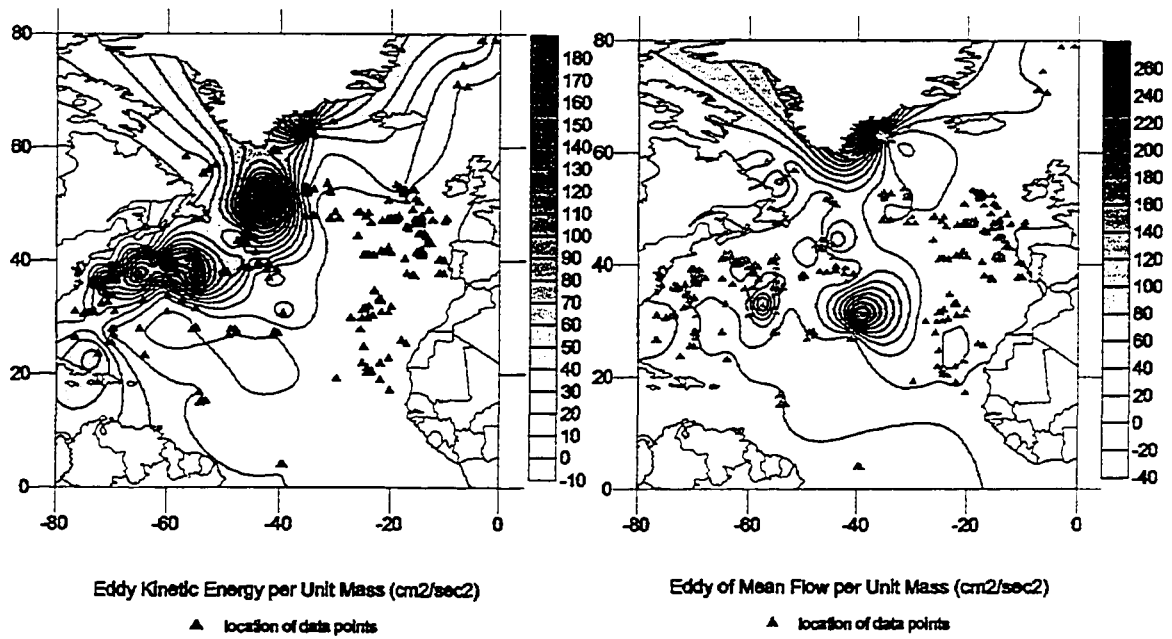
(b) Flow Statistics for pre-WOCE and WOCE Intermediate Water (500 to 2,000 meters)



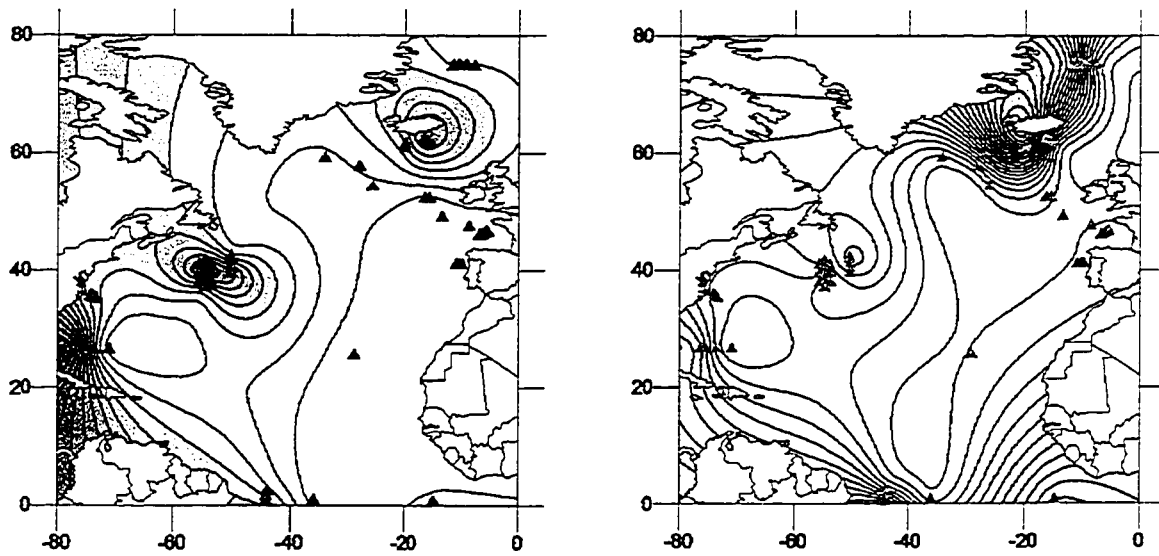
pre-WOCE (above) / WOCE (below)



(c) Flow Statistics for pre-WOCE and WOCE Deep Water (> 2,000 meters depth)



pre-WOCE (above) / WOCE (below)



The WOCE portion of Figure 4.45 (a) illustrates a localized high energy area along the Gulf Stream, though of a magnitude of some 50% of that of the pre-WOCE period. The highest values of KM occur around the coast of South America, near the Amazon River delta with values approximately 30% that of pre-WOCE levels.

Intermediate depth water for the pre-WOCE period, Figure 4.46 (b), show high eddy kinetic energy levels in through the Bermuda Rise with more moderate KE levels further north where the Gulf Stream and Labrador Current meet. High KM values lie along the East Greenland Current and just off Cape Hatteras. Maximum values which are some three times less intense than pre-WOCE levels, are observed in the WOCE portion of Figure 4.45 (b) along the North American continental shelf where the Gulf Stream and Labrador currents converge. North of the United Kingdom where warm North Atlantic Drift water collides with colder Irminger Current water, high KM values, some 2.5 times greater than for the pre-WOCE time period, are revealed.

Figure 4.45 (c) shows maximum KE values in the Gulf Stream along 40°N and at the terminus of the cold East Greenland Current and Labrador Currents and warm Gulf Stream waters. High KM areas are found along the southern tip of Greenland and in two areas south of 40°N. The last two maps of WOCE deep water in Figure 4.45 (c) are associated with the lowest maximum levels of both KE and KM for all study areas with local maxima of KE observed around the terminus of the Caribbean Current, in the Gulf Stream and surrounding Iceland. These same locations are localized maxima for KM, with the addition of an area adjacent to the Amazon delta.

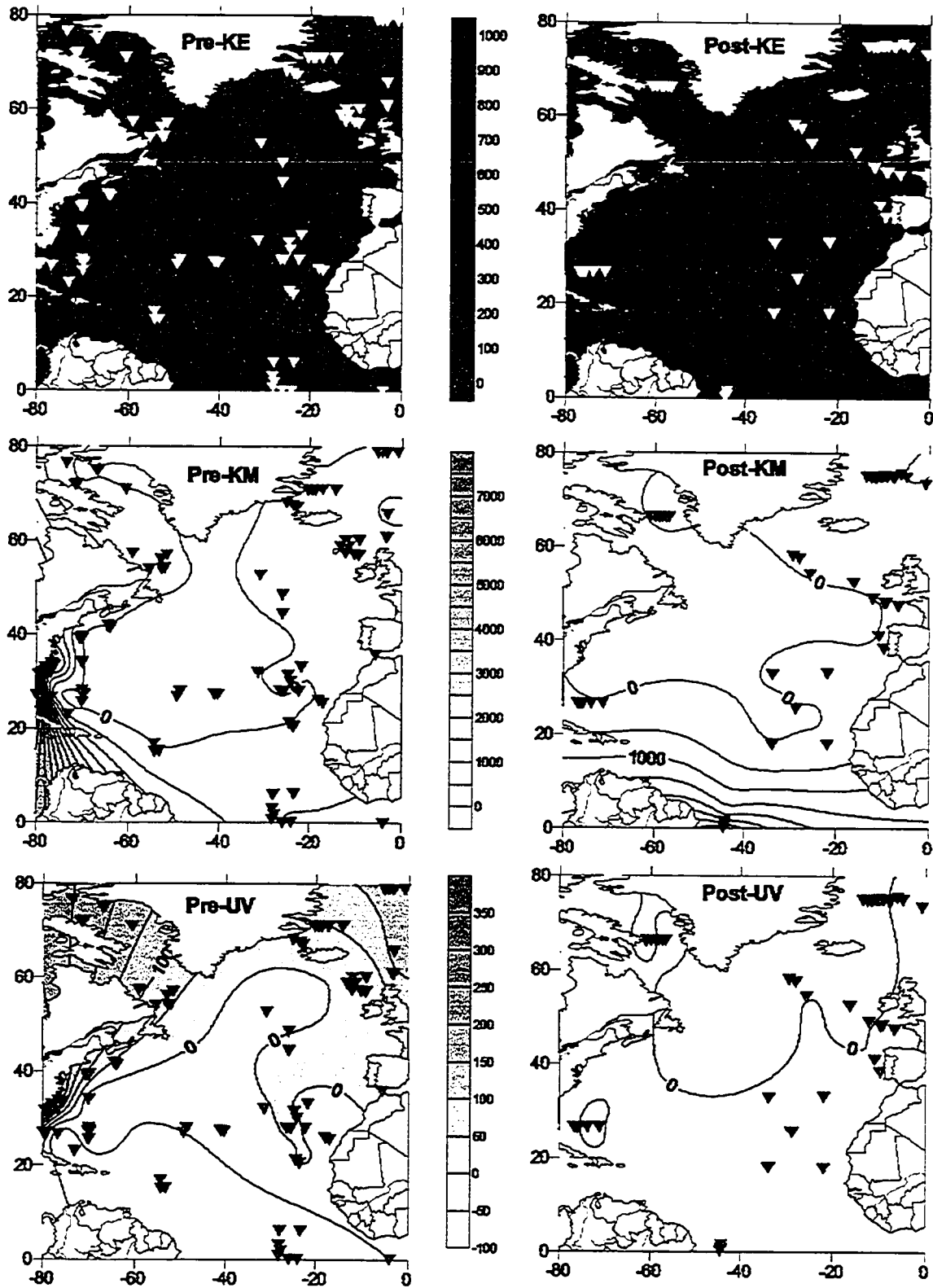


Figure 4.46 Surface Water Flow Statistics of KE, KM, and UV for the pre- and WOCE Periods of Study for Waters that are 0 to 60 meters below mean sea level.



Figure 4.46 differs from Figure 4.45 and attempts to shed some light on surface conditions of the North Atlantic Ocean by looking at KE, KM and UV (all having units  $\text{cm}^2 \text{s}^{-2}$ ) for surface waters of 60 meters or less below mean sea level. The feature that makes these plots unique from the shallow water plots in Figure 4.45 (a) is the effect of wind incorporated into the kinetic energy statistics. Many of the high energy areas associated with the Gulf Stream show up at these depths, with the pre-WOCE levels (left plots) having far greater values than WOCE levels (right plots). The pre-WOCE eddy kinetic energy per unit mass plot shows a maximum KE value around Cape Hatteras but this area does not appear in the WOCE plot to the right. However also shown are generally higher levels of energy during the WOCE period, with large homogenous areas near the Caribbean and north-east coast of South America.

Values of KM are low throughout most of the North Atlantic Ocean with higher values through the Caribbean Sea in pre-WOCE years and towards the equator in the WOCE years. Mean eddy momentum flux, UV, shows largely no activity during the WOCE years and has maximums through the Labrador Sea in the pre-WOCE plot. The general energy profile that is revealed is a movement of energy from the Gulf Stream, Caribbean Sea and Labrador Sea during the pre-WOCE period to a more central position north of the equator (as evidenced by the post-KE and post-KM plots of Figure 4.46).

## 5. Discussion

### 5.1 Regional Patterns

An examination of the various regional characteristics of the general North Atlantic Ocean circulation the current vector plots reveal some interesting phenomena. Though the dataset is not exhaustive in terms of its spatial coverage of the area, in terms of latitude and longitude, it does give a good representation of current flow at various depths. This is one aspect of the general circulation that is missing from studies that look at only surface currents by means of Lagrangian surface drifters and satellite altimetry.

First, the Gulf Stream and North Atlantic Current mean flow along and ultimately away from, the coastline is somewhat evident, especially in the shallow current plots (Figures 4.2 and 4.25). The current vector plots (especially Figures 4.7 and 4.30) do a good job of picking up the counterflows that are due to the southern recirculation gyre (Hogg 1992). In addition, the intermediate depth current vectors (Figures 4.3 and 4.26) and the energy plots (Figures 4.45 and 4.46) for both the pre-WOCE and WOCE data, clearly indicate a region of instability and high energy which is part of the Gulf Stream Jet.

The near-bottom circulation contains an anticyclonic gyre, evident in the Newfoundland Basin, near 43°N and 45°W (Figures 4.28 and 4.29) which has been associated with seafloor topography (Lazier 1994). Indeed one of the strengths of these visualizations is the ability to view the current flow superimposed on the seafloor

bathymetry; as generalized paths and flows can be traced which follow the topography. If one were to expand the spatial range of this study and include the northern Mediterranean seas and South Atlantic Ocean, and also isolate and focus on some of the fracture zones through the Mid-Atlantic Ridge, one would get a clear picture of the through-flow of water at depth and the meandering necessary in the global circulation.

North of the Gulf Stream along the continental shelf there is a general equatorward flow, which is reinforced by the Labrador Current. This is assumed to be a continuous current spanning from the southern coast of Greenland to the Mid-Atlantic Bight (Chapman and Beardsley 1989). This general flow is most pronounced in the vector plots associated with both intermediate and deep water, and is clearly more evident in the WOCE data, Figures 4.26 and 4.27, due to the greater amount of sampling points available for the interpolation.

The flows of water originating around Greenland are due to the effects of the East and West Greenland Currents as they mix with the Labrador Current which merges into them. An anticyclonic flow has been shown to exist at the confluence of this area (Lavender et al. 2000) and is apparent in the intermediate and deep water plots constructed for the WOCE data.

Other studies have observed an area of instability in the region surrounding the Labrador Sea, especially around the area of Cape Farewell, at the southern tip of Greenland (Figure 2.1). The coastline in this area shows an abrupt change in slope topography which can possibly aid in destabilizing the West Greenland Current (Pickart, 2000). Figure 4.29, page 107, illustrates this abrupt slope change and shows how the current is thrust southward due to this topography.

As the North Atlantic Current proceeds eastwardly through the North Atlantic Ocean it must pass through a constriction connecting the Mid-Atlantic Ridge with the Reykjanes Ridge. This area is shown in Figure 2.1 as the deep passageway located at about 52-53°N and 30-32°W adjacent to the Iceland Basin. Once through the gap the North Atlantic Drift Current proceeds northeasterly toward Iceland (Garrison 1996). The current vector plots show this relatively fast flowing water (especially some of the deep water vectors that show up in Figure 4.29), however the actual flow directions are somewhat misleading. This is in large part due to the vector plots combining the effects of this current flow with the flow of NADW originating from the area of the Norwegian Sea. The depth profiles in Figures 4.32 and 4.33 help in distinguishing between these two water masses with the warmer, faster flowing water being typical of the North Atlantic Drift Current. The presence of high energy witnessed in Figure 4.46 (e-f) also gives us another clue in tracing this water mass.

Figure 4.33 (a) shows an abundance of slower moving water (the green water with current velocity ranging between 0 and 20 cm s<sup>-1</sup>). The blue water nearer the surface can be associated with the North Atlantic Current. In Figure 4.33 (b) this faster moving water can be seen extending to 2500 meters depth between 30° and 45°W longitude, which is generally in agreement with the location of the gap through the Mid-Atlantic Ridge. More certainty could have been ascertained with respect to these water masses by having had a record of salinity.

The Caribbean Current connects the western tropical Atlantic Ocean with the Gulf of Mexico and is the process whereby warm waters are moved northward into the North Atlantic Ocean (Murphy et al. 1999, Richardson et al. 1994). Much of this warm water

originates from the North Brazil Current and continues along as a western boundary current eventually becoming the Gulf Stream. The flow of this cross-equatorial water is evident in Figures 4.24 to 4.26 for the decadal WOCE data and also in Figure 4.42 showing the mean annual circulation.

Surface velocities in the tropical North Atlantic (Figure 4.24) are highest along the coast of South America, approaching 70 to 75 cm s<sup>-1</sup>, and in close agreement with some previous studies (Gordon 1967, Johns et al. 2002). The plots of intermediate, deep and near-bottom current vectors show the deflection of the North Brazil Current into the North Atlantic, however the shallow water current vectors indicate the passage of this water along the South American coastline into the Caribbean Sea. The energy associated with this current flow has been associated with the North Brazil Current rings (Johns et al 1990, Richardson et al. 1994), and indeed Figure 4.46 (d-f) and 4.47 show this region as an area of high eddy kinetic energy.

## **5.2 The General Circulation**

Most of the research on flow variability has resulted from studies conducted with Lagrangian drifters (Fratantoni 2001, Reid 1994). The WOCE moored current meter dataset has a coarse spatial structure, due to the patching together of various smaller scale experiments, which nevertheless is able to capture detail on current circulation. The variability that has been discovered in the data shows the formation of eddies, the movement of deep water masses, sections of the flow of the sub-tropical and sub-polar gyre, and the highly dynamic state of the ocean. In particular the subtropical gyre's tendency to expand and contract in size (see especially Figure 4.42 – 1991 to 1993), helps in explaining some of the reverse flows that are observed in the current vector plots. Flow

statistics of eddy kinetic energy reveal the high energy areas of the North Atlantic and further help in delineating the various current flows.

An initial objective of this research was to determine the effect of the wind- and thermohaline-driven parts of the circulation. It is known that wind stress and thermohaline forcing do not act in a linear fashion in driving the general circulation. Furthermore, it has been suggested that the thermohaline-driven part of the circulation plays a far more significant role. Based on the observations gleaned from this research, particularly in the maps created for surface water velocity and surface winds (Figure 4.44 and animations) the wind stress does appear to play a large role in driving the North Atlantic circulation.

Even though the current flow is at an angle to the wind speed, it is apparent that the upper layer circulation is indeed influenced by the wind. Even though decadal and mean annual current flows were plotted in this study, the general circulation is not that variable that there is much loss of information from this. Perhaps a seasonal plotting of the current flows would have produced a better relationship between current flow and wind speed.

The combined effects of the zonal subtropical tradewinds and mid-latitude westerlies determines the wind stress curl and affects the general flow of surface waters (Garrison 1996, Gross 1993). Along with the Coriolis Force, due to Earth's rotation, the main effect is to drive water into the interior of the subtropical gyre and out of the subpolar gyre (Garrison 1996, Gross 1993). The equatorward movement of water in the subtropical gyre and poleward movement of water in the subpolar gyre tend to conserve momentum (Garrison 1996, Gross 1993).

With the addition of the ETOPO-5 bathymetry data to the WOCE current data, a comprehensive picture of the near-bottom circulation emerged. In general, near-bottom ocean currents appear to be influenced by their interaction with the underlying bottom topography. Looking at the bathymetric plots of current flow in combination with the eddy kinetic energy plots at depth gives an indication of the movement of water through fracture zones (Figures 4.6, 4.29, 4.38 and to a lesser extent Figure 4.45 (c)) and tends to give a more comprehensive picture of the thermohaline circulation.

While the WOCE dataset is an expansive collection encompassing the world oceans, it is not exhaustive. Though the WOCE plan was intended as a means of acquiring a large spatial and temporal chunk of data from throughout the World Ocean, the majority of individual datasets were implemented to research specific areas of ocean circulation and therefore spatial and temporal extents do not merge into a cohesive whole. However, by careful selection of appropriate temporal and spatial scales, a study of the general circulation can, and has, proven fruitful as described in this chapter.

### ***5.3 Average Temperature Depth Profile and Relation to El Nino***

The primary goals of this thesis were to visualize the general circulation of the North Atlantic Ocean, by means of mean current vector plots, mean temperature contours, and eddy kinetic energy plots. Though not examined and not of prime concern in this study, one question that has been asked by numerous researchers is if an El Nino originates in the Atlantic Ocean (Cook et al. 1998, Griffies and Bryan 1997, Rogers 1984). Analyses of historical data have shown that the dominant feature in tropical Atlantic Ocean large-scale variability is the annual cycle (Rogers 1984). From late May until October surface currents are driven by the tradewinds, while warm water along the

American coast is replaced by an upwelling of cold, deep water originating in the Gulf of Guinea (Tomczak and Godfrey 1994). As in the Pacific Ocean, though not reaching the scale of the El Nino phenomenon, warm waters appear in the Gulf of Guinea during these events, which are linked to equatorial dynamics and lasting along the time-scale of a few months. Though the mechanism involved is that they are either locally driven or forced by El Nino events in the Pacific Ocean, the results are that strong tradewinds in the tropical Atlantic Ocean tend to cause a buildup of warm water in the western Atlantic with a reciprocal flow a few months later (Rogers 1984). These patterns were observed in the Atlantic Ocean in 1984 and 1988 following the El Nino events of 1982-1983 and 1986-1987 respectively (Ross 1988). In the beginning of 1995 a similar pattern was observed in the Atlantic Ocean. Of concern in the 1995 event was the fact that the phenomenon continued growing well past the usual time period, resulting in the disruption of the fishing industry, droughts in the Sahel and floods in north-east Brazil (Lody 1995).

It was hoped that some of the mean annual circulation patterns in the North Atlantic Ocean would shed some light on these matters. The plots of Figure 4.42 would have certainly shed some light on this phenomenon. Unfortunately, 1991 to 1993 were the best years of data collection and 1994 to 1996 did not reveal any information due to the scarcity of current meters. However, just by analyzing the 1991 to 1993 plots one can see the expanse of warm water throughout the North Atlantic extending from the Gulf of Guinea to the South American coast in the 1991 plot.



## **6. Conclusion**

### ***6.1 Limitations of Research***

#### **6.1.1 Physical Limitations**

The biggest limitation in mapping out the current vector field of ocean circulation is the absence of important variables that can help in ascertaining the make-up and origins of various water masses. Most important of these would be to have salinity data in order to aid in determining the general pathways of water mass origin and destination.

Though these data were not available at the time this thesis commenced, the WOCE initiative has enabled access to a wealth of information in the past two years. Salinity and pressure records, though not corresponding perfectly in either spatial or temporal boundaries, is now available to complement the dataset used in this study.

Another important variable to include with the data would have been pressure. Measurements of pressure would have given us confidence that the data collected was actually for the spatial location intended. There is inherent instability in the oceanic environment, from extremes of storm surges to normal, everyday oceanic characteristics such as tides and the corroding effects of salt water, to mechanical failures in the instrumentation itself, to the intrusive effects of commercial shipping on the placement of current meters.

All of these factors lead to current meters being knocked out of commission or knocked out of their proper spatial orientation. Part of the verification procedure for data quality and control is the collection of pressure readings for a sample of current meters in order to determine if the readings match-up to the correct depth.

### **6.1.2 Computational Limitations**

The various pitfalls and comprises required in the use of any interpolation program have been mentioned in the body of this work. Whether devising a computational or mathematical model to simulate the oceanic circulation, or whether using interpolation to fill in data from the sampling measurements taken, the assumptions and methods chosen will invariably lead to some bias in the results obtained. However, if one takes these measures into account, a useful picture of the oceanic circulation can be obtained which can give us some understanding of the mechanisms at work. Appendix 8.2 gives a brief description on the rotor-type current meters used to collect data in this study.

## **6.2 Research Conclusions**

Much of the current literature focuses on the modeling of the general ocean circulation due to an inconsistency and sparse network of reliable data gathering (Willebrand and Hadivogel 2001). Recently, there has been much information obtained by a combination of surface drifters and remote sensing, which is giving us a clearer picture of surface flows (Fratantoni 2001). However, this thesis illustrates that moored current meter buoys can give an accurate picture of current flows.

This is especially important in lieu of the fact that surface drifters and remote sensing are only able to observe the surface and upper few meters of the shallow water circulation. Moored current meters are the only data collection method available in collecting characteristic variables for the deep water circulation.

This thesis adds to the body of literature by visualizing the general circulation of the North Atlantic Ocean and by relating this circulation to underlying assumptions in order to strengthen the validity of ocean general circulation models.

Current flow patterns in the North Atlantic Ocean were plotted for various depths. A comparison between the pre-WOCE dataset of the mid-1970s to mid-1980s versus the WOCE dataset of the 1990s was undertaken, but was limited due to the spatial variation of the two datasets. More specifically, the pre-WOCE dataset was a spatial subset of the much more encompassing WOCE experiment.

The addition of annual mean circulation to the decadal circulation revealed similar patterns in both flows. Also, the addition of eddy kinetic energy measurements helped isolate pockets of activity that were associated with such features as high-speed surface currents and high-speed thermohaline circulation due to the effects of bottom topography.

### ***6.3 Future Research***

The influence of freshwater inputs from rivers was briefly touched upon in Section 4.6 of this thesis. Existing research has shown that the North Atlantic Ocean circulation is indeed sensitive to these freshwater inputs (Garrison 1996, Wiffels 2001). There is room for much research into the full effects of freshwater discharge with the

availability and constant expansion of the WOCE dataset in the public domain, and with the availability of other datasets, such as the RivDis river discharge data used in this thesis.

When freshwater gets mixed into the North Atlantic the rate of the overturning process is slowed (Fedorov and Ginsberg 1988, Bowden 1983). Studies have shown that freshwater from land-based melting glaciers which drained into the North Atlantic Ocean at the end of the last ice age, would have shut down the NADW circulation system in a few hundred years (Chandler and Dybas 2001). It has been hypothesized that there is a linear relationship between the NADW and the addition of freshwater, with its effect being a largely less energetic Gulf Stream. Due to the effect of the wind stress on surface currents, the Gulf Stream would not be entirely shut down (Chandler and Dybas 2001).

To what depth the freshwater influence affects the circulation would be an interesting avenue to pursue (Weaver and Hughes 1994). As mentioned moored current meters would be the only data collection method to obtain information on the deeper parts of the ocean and to see the shifts that are occurring there.

The movement of surface water northward from the equator by the Gulf Stream results in this warm water cooling, and becoming denser due to evaporation which increases ocean salinity. Once this equatorial water reaches the Grand Banks, the Labrador Basin and the Norwegian Sea, it sinks due its increased density. This water then travels southward via the NADW completing the circulation. This thesis has touched on the expansion and contraction of the subtropical gyre. Further research on the effects of this change in circumference with respect to atmospheric heat transfers and therefore climate change would be a further avenue to pursue. Furthermore, an analysis of seasonal

circulation with the effects of the seasonal wind stress could possibly give us more information of the mesoscale changes in oceanic circulation.

One of the lessons learned from digging in to this massive dataset is that various other analyses could have been conducted and may have indeed shed more light on the circulation of the North Atlantic Ocean. For example, mean current speeds, mean temperatures, and mean wind speeds were used in gathering the vector and contour plots in this thesis. However, after having plotted this data and seen some of the discrepancies that are more than likely attributable to the spatial and temporal differences inherent in the two datasets, it would have perhaps been more beneficial to plot the variations in the above variables in order to see the degree of change during the two time periods. Having spent the better part of one year in cleaning and processing the data, the thought of what would lay down the road was not totally obvious. In hindsight, it would have been prudent and would be very beneficial in the future to analyse the variability in the data in order to get a better understanding of decadal changes.

## 7. References

- Aagard, K., J. H. Swift, and E. C. Carmack. 1985. Thermohaline Circulation in the Arctic Mediterranean Seas. Journal of Geophysical Research, 90:4833-4846.
- Bayev, S.A., and A.B. Polonskiy. 1991. Seasonal Variability of the Equatorial Countercurrent and the North Equatorial Current in the Central Tropical Atlantic. Oceanology, 31:155-159.
- Bersch, M. 1995. On the Circulation of the Northeastern North Atlantic. Deep Sea Research, 42(9):1583-1607.
- Bigg, G. R., and M. R. Wadley. 2001. Millennial-Scale Variability in the Oceans: An Ocean Modelling View. Journal of Quaternary Science, 16(4):309-319.
- Bishop, J. M. 1984. Applied Oceanography. John Wiley & Sons: New York.
- Borstad, G. A. 1982. The Influence of the Meandering Guyana Current and Amazon River Discharge on Surface Salinity Near Barbados. Journal of Marine Research, 40(x):421-434.
- Bowden, K. F. 1983. Physical Oceanography of Coastal Waters. Ellis Horwood: Chichester.
- Briggs, D., P. Smithson, T. Ball, P. Johnson, P. Kershaw, and A. Lewkowicz. 1993. Fundamentals of Physical Geography. Copp Clark Pitman: Toronto.
- Brown, J., A. Colling, D. Park, J. Phillips, D. Rothery, and J. Wright. 1989a. Ocean Circulation. Pergamon Press: Oxford.
- Brown, J., A. Colling, D. Park, J. Phillips, D. Rothery, and J. Wright. 1989b. Seawater: Its Composition, Properties and Behaviour. Pergamon Press: Oxford.
- Burkov, V. A. 1993. General Circulation of the World Ocean. A. A. Balkema: Brookfield.
- CERSAT. 2002. Mean Wind Fields Gridded Data (MWF/WOCE Product) – ERS-1 & ERS-2. CERSAT/Ifremer – French Processing and Archiving Facility. Available on-line [<http://www.ifremer.fr/cersat/en/data/overview/gridded/mwfers.htm>]

Chandler, L., C. Dybas. 2001. Ocean Circulation Shut Down by Melting Glaciers After Last Ice Age. Goddard Space Flight Center, 19 November 2001. Available on-line [<http://www.gsfc.nasa.gov/topstory/>]

Chapman, D. C., and R. C. Beardsley. 1989. On the Origin of Shelf Water in the Middle Atlantic Bight. Journal of Physical Oceanography, 19:384-391.

Chapman, P. 1998. The WOCE Data Resource. Bulletin of the American Meteorological Society, 79(6):1037-1042.

Chapman, M. R., and M. A. Maslin. 1999. Low Latitude Forcing of Meridional Temperature and Salinity Gradients in the Subpolar North Atlantic and the Growth of Glacial Ice Sheets. Geology, 27(10):875-878.

Clarke, A., J. Church, and J. Gould. 2001. Ocean Processes and Climate Phenomena in Ocean Circulation & Climate: Observing and Modelling the Global Ocean, G. Siedler, J. Church, and J. Gould, eds. Academic Press: San Diego.

Cook, E. R., R. D. D'Arrigo, and K. R. Briffa. 1998. A Reconstruction of the North Atlantic Oscillation Using Tree-ring Chronologies from North America and Europe. The Holocene, 8:9-17.

Cromwell, D., P. G. Challenor, A. L. New, and R. D. Pingree. 1996. Persistent Westward Flow in the Azores Current as Seen From Altimetry and Hydrography. Journal of Geophysical Research, 101(C5):11923-11933.

Cunningham, S. A. 2000. Circulation and Volume Flux of the North Atlantic Using Synoptic Hydrographic Data in a Bernoulli Inverse. Journal of Marine Research, 58(1):1-35.

Cuny, J., P. B. Rhines, P. P. Niiler, and S. Bacon. 2002. Labrador Sea Boundary Currents and the Fate of the Irminger Sea Water. Journal of Physical Oceanography, 32(2):627-647.

DeMers, M. N. 1997. Fundamentals of Geographic Information Systems. John Wiley & Sons: New York.

Dickson, R. R., and E. Gmitrowicz. 1990. Deep Water Renewal in the Northern North Atlantic. Nature, 344:848-850.

Dickson, R. R., and J. Brown. 1994. The Production of North Atlantic Deep Water: Sources, Rates, and Pathways. Journal of Geophysical Research, 99(C6):12319-12341.

Dickson, R., and K. Medler. 1998. Flow Statistics from Long-Term Current Meter Moorings. World Climate Research Program Report WMO/TD – No. 337.

- Doscher, R., C. W. Boning, and P. Herrmann. 1994. Response of Circulation and Heat Transport in the North Atlantic to Changes in Thermohaline Forcing in Northern Latitudes: A Model Study. Journal of Physical Oceanography, 24(11):2306-2320.
- Dyke, P. 1996. Modelling Marine Processes. Prentice Hall: London.
- Emery, W. J., and R. E. Thomson. 1997. Data Analysis Methods in Physical Oceanography. Pergamon: Oxford.
- Fedorov, K. N., and A. I. Ginsburg. 1992. The Near-Surface Layer of the Ocean. VSP: Utrecht.
- Fisher, N. I. 1993. Statistical Analysis of Circular Data. Cambridge University Press: New York.
- Flagg, C. N., R. L. Gordon, and S. McDowell. 1986. Hydrographic and Current Observations on the Continental Slope and Shelf of the Western Equatorial Atlantic. Journal of Physical Oceanography, 16(8):1412-1429.
- Foreman, S. J. 1990. The Ocean as a Component of the Climate System. Climate-Ocean Interaction, M. E. Schlesinger, ed. Kluwer Academic: Dordrecht.
- Franke, R. 1982. Scattered Data Interpolation: Tests of Some Methods. Mathematics of Computation, 38(157):181-200.
- Frankignoul, C., G. de Coetlogon, T. M. Joyce, and S. F. Dong. 2001. Gulf Stream Variability and Ocean-Atmosphere Interactions. Journal of Physical Oceanography, 31(12):3516-3529.
- Fratantoni, D. M. 2001. North Atlantic Surface Circulation During the 1990's Observed with Satellite-tracked Drifters. Journal of Geophysical Research, 106(C10):22067-22093.
- Fu, L. 2001. Ocean Circulation and Variability from Satellite Altimetry in Ocean Circulation & Climate: Observing and Modelling the Global Ocean, G. Siedler, J. Church, and J. Gould, eds. Academic Press: San Diego.
- Fuglister, F. G. 1951. Multiple Currents in the Gulf Stream System. Tellus, 3:230-233.
- Garrison, T. 1996. Oceanography: An Invitation to Marine Science. Wadsworth: Belmont.
- Golden Software. 1999. Surfer7 Users Guide: Contouring and 3D Surface Mapping for Scientists and Engineers. Golden Software: Golden.



- Gordon, A. L. 1967. Circulation of the Caribbean Sea. Journal of Geophysical Research, 72(24):6207-6223.
- Gowda, H. H., B. Manikiam, V. Jayaraman, and M. G. Chandrasekhar. 1993. Impact of Satellite Remote Sensing on Ocean Modelling – an Overview. International Journal of Remote Sensing, 14(17):3317-3331.
- Grassl, H. 2001. Climate and Oceans in Ocean Circulation & Climate: Observing and Modelling the Global Ocean, G. Siedler, J. Church, and J. Gould, eds. Academic Press: San Diego.
- Greatbatch, R. J., A. F. Fanning, A. D. Goulding, and S. Levitus. 1991. A Diagnosis of Interpentadal Circulation Changes in the North Atlantic. Journal of Geophysical Research, 96(C12):22009-22023.
- Gross, M. G. 1993. Oceanography: A View of the Earth. Prentice Hall: Englewood Cliffs.
- Hall, M. M., and N. P. Fofonoff. 1993. Downstream Development of the Gulf Stream from 68° to 55°W. Journal of Physical Oceanography, 23(2):225-249.
- Halliwel, G., P. Cornillon, and D. A. Byrne. 1991. Westward Propagating SST Anomaly Features in the Sargasso Sea. Journal of Physical Oceanography, 21(5):635-649.
- Han, G. 2000. Three-dimensional Modelling of Tidal Currents and Mixing Quantities Over the Newfoundland Shelf. Journal of Geophysical Research, 105(C5):11407-11422.
- Hardy, R. L. 1971. Multiquadric Equations of Topography and Other Irregular Surfaces. Journal of Geophysical Research, 76(8):1905-1915.
- Hogg, N. G. 1992. On the Transport of the Gulf Stream Between Cape Hatteras and the Grand Banks. Deep Sea Research, 39(7-8):1231-1246.
- Huthnance, J. M., H. M. Van Aken, M. White, E. D. Barton, B. Le Cann, E. F. Coelho, E. A. Fanjul, P. Miller, and J. Vitorino. 2002. Ocean Margin Exchange – Water Flux Estimates. Journal of Marine Systems, 32(1-3):107-137.
- Iselin, C. O. 1936. A Study of the Circulation of the Western North Atlantic. Papers in Physical Oceanography and Meteorology, 4(4):1-101.
- Ivey, G. N., and R. I. Nokes. 1989. Vertical Mixing Due to the Breaking of Critical Internal Waves on Sloping Boundaries. Journal of Fluid Mechanics, 204:479-500.

- Johns, W. E., T. N. Lee, F. A. Schott, R. J. Zantopp, and R. H. Evans. 1990. The North Brazil Current Retroflexion: Seasonal Structure and Eddy Variability. *Journal of Geophysical Research*, 95(C12):22103-22120.
- Johns, W. E., T. L. Townsend, D. M. Fratantoni, and W. D. Wilson. 2002. On the Atlantic Inflow to the Caribbean Sea. *Deep Sea Research*, 49(2):211-243.
- Kershaw, S., and A. Cundy. 2000. Oceanography: An Earth Science Perspective. Stanley Thornes: Cheltenham.
- Knauss, J. A. 1997. Introduction to Physical Oceanography, Second Edition. Prentice Hall: Upper Saddle River.
- Kovach Computing Services. 1994. Oriana for Windows, v. 1.06. KCS: Pentraeth.
- Lavender, K. L., R. E. Davis, and W. B. Owens. 2000. Mid-depth Recirculation Observed on the Interior Labrador and Irminger Seas by Direct Velocity Measurements. *Nature*, 407:66-69.
- Lazier, J. R. N., and D. G. Wright. 1993. Annual Velocity Variations in the Labrador Current. *Journal of Physical Oceanography*, 23(4):659-678.
- Leier, M. 2000. World Atlas of the Oceans. Key Porter: Toronto.
- Lindstrom, E. J., and D. M. Legler. 2001. Developing the WOCE Global Data System in Ocean Circulation & Climate: Observing and Modelling the Global Ocean, G. Siedler, J. Church, and J. Gould, eds. Academic Press: San Diego.
- Lody, C. 1995. Is an "El Nino" Born in the Atlantic. *Aviso*. Available on-line: [[http://www.Jason.oceanobs.com/html/applications/climat/nino\\_atl\\_uk.html](http://www.Jason.oceanobs.com/html/applications/climat/nino_atl_uk.html)]
- Mercier, H., K. Speer, and J. Honnorez. 1994. Flow Pathways of Bottom Water Through the Romanche and Chain Fracture Zones. *Deep Sea Research*, 41(10):1457-1477.
- Mercier, H., and K. Speer. 1998. Transport of Bottom Water in the Romanche Fracture Zone and Chain Fracture Zone. *Journal of Physical Oceanography*, 28(5):779-790.
- Mittelstaedt, E. 1991. The Ocean Boundary Along the Northwest African Coast: Circulation and Oceanographic Properties at the Sea Surface. *Progress in Oceanography*, 26(4):307-355.
- Muller-Krager, F.E., C.R. McClain, and P.L. Richardson. 1988. The Dispersal of the Amazon's Water. *Nature*, 333:56-59.

- Murphy, S. J., H. E. Hurlburt, and J. J. O'Brien. 1999. The Connectivity of Eddy Variability in the Caribbean Sea, the Gulf of Mexico, and the Atlantic Ocean. Journal of Geophysical Research, 104(C1):1431-1453.
- Narayanan, C., and R. W. Garvine. 2002. Large Scale Buoyancy Driven Circulation on the Continental Shelf. Dynamics of Atmospheres and Oceans, 36:125-152.
- New, A. L., Y. Jia, M. Coulibaly, and J. Dengg. 2001. On the Role of the Azores Current in the Ventilation of the North Atlantic Ocean. Progress in Oceanography, 48(2-3):163-194.
- Nuss, W. A. 1994. Three Dimensional Meteorological Analysis Using Multiquadric Interpolation. Journal of Applied Science and Computations, 1(2):350-374.
- Nuss, W. A., and D. W. Titley. 1994. Use of Multiquadric Interpolation for Meteorological Objective Analysis. Monthly Weather Review, 122:1611-1631.
- Pickart, R. S. 1992. Water Mass Components of the North Atlantic Deep Western Boundary Current. Deep Sea Research, 39(8):1553-1572.
- Pickart, R. S., 2000. Bottom Boundary Layer Structure and Detachment in the Shelfbreak Jet of the Middle Atlantic Bight. Journal of Physical Oceanography, 30:2668-2686.
- Reid, J. L. 1994. On the Total Geostrophic Circulation of the North Atlantic Ocean: Flow Patterns, Tracers, and Transports. Progress in Oceanography, 33(1):1-92.
- Reid, R. O. 1997. Dynamical Oceanography. Part I: Fundamental Principles. Available on-line [<http://stommel.tamu.edu/~baum/reid/book1/book/book.html>] from Steve Baum.
- Reynaud, T. H., A. J. Weaver, and R. J. Greatbatch. 1995. Summer Mean Circulation of the Northwestern Atlantic Ocean. Journal of Geophysical Research, 100(C1):779-816.
- Richardson, P. L., G. E. Hufford, R. Limeburner, and W. S. Brown. 1994. North Brazil Current Retroflexion Eddies. Journal of Geophysical Research, 99(C3):5081-5093.
- Rogers, J. C. 1984. The Association Between the North Atlantic Oscillation and The Southern Oscillation in the Northern Hemisphere. Monthly Weather Review, 112:1999-2015.
- Ross, D. A. 1988. Introduction to Oceanography. Prentice Hall: Englewood Cliffs.
- Rosby, T. 1996. The North Atlantic Current and Surrounding Waters: At the Crossroads. Reviews of Geophysics, 34(4):463-481.
- Rudels, B., H. J. Friedrich, and D. Quadfasel. 1999. The Arctic Circumpolar Boundary Current. Deep Sea Research II: Topical Studies in Oceanography, 46(6-7):1023-1062.

- Rudels, B., E. Fahrbach, J. Meincke, G. Budeus, and P. Eriksson. 2002. The East Greenland Current and its Contribution to the Denmark Strait Overflow. ICES Journal of Marine Science, 59(6):1133-1154.
- Saunders, P. M. 1996. The Flux of Dense Cold Overflow Water Southeast of Iceland. Journal of Physical Oceanography, 26(1):85-95.
- Saunderson, H. C. 1992. Multiquadric Interpolation of Fluid Speeds in a Natural River Channel. Computers and Mathematics with Applications, 24(12):187-193.
- Saunderson, H. C. 1994. Multiquadric Surfaces in C. Computers and Geosciences, 20(7/8):1103-1122.
- Schmidt, C., R. L. Molinari, and S. L. Garzoli. 2001. New Observations of the Intermediate Depth Circulation in the Tropical Atlantic. Journal of Marine Research, 59(2):281-312.
- Schmitt, R. W. 1996. If Rain Falls On the Ocean – Does It Make a Sound?: Fresh Water's Effect on Ocean Phenomena. Oceanus Magazine, 39(2):4-8.
- Schmitz, W. J., Jr., and M. S. McCartney. 1993. On the North Atlantic Circulation. Reviews of Geophysics, 31(1):29-50.
- Schott, F., J. Fischer, J. Reppin, and U. Send. 1993. On Mean and Seasonal Currents and Transports at the Western Boundary of the Equatorial Atlantic. Journal of Geophysical Research, 98(C8):14353-14368.
- Schott, F., J. Fischer, and L. Stramma. 1998. Transports and Pathways of the Upper Layer Circulation in the Western Tropical Atlantic. Journal of Physical Oceanography, 28(10):1904-1928.
- Sinha, S. K., M. Mahakur, and P. N. Mahajan. 2002. Meteorological Objective Analysis Using Multiquadric Interpolation Scheme Over India and Adjoining Region. Atmosfera, 15(4):209-222.
- Spokes, L. 2003. Consequences of Global Warming on Ocean Circulation. ESPERE Climate Encyclopaedia, Available at: <http://www.atmosphere.mpg.de/enid/p4.html>
- Stommel, H. M., and D. W. Moore. 1989. An Introduction to the Coriolis Force. Columbia University Press: New York.
- Stramma, L., and T. J. Muller. 1989. Some Observations of the Azores Current and the North Equatorial Current. Journal of Geophysical Research, 94(x):3181-3186.

- Stramma, L., J. Fischer, and J. Reppin. 1995. The North Brazil Undercurrent. Deep Sea Research, 42(5):773-795.
- Stramma, L., and F. Schott. 1999. The Mean Flow Field of the Tropical Atlantic Ocean. Deep Sea Research II: Topical Studies in Oceanography, 46(1-2):279-303.
- Summerhayes, C. P., and S. A. Thorpe. 1996. Oceanography: An Illustrated Guide. John Wiley & Sons: New York.
- Talley, L. D., D. Stammer, and I. Fukumori. 2001. Towards a WOCE Synthesis in Ocean Circulation & Climate: Observing and Modelling the Global Ocean, G. Siedler, J. Church, and J. Gould, eds. Academic Press: San Diego.
- Thiébaux, H. J. 1994. Statistical Data Analysis for Ocean and Atmospheric Sciences. Academic Press: San Diego.
- Tomczak, M. 1981. An Analysis of Mixing in the Frontal Zone of South and North Atlantic Central Water off North-West Africa. Progress in Oceanography, 10(3):172-192.
- Tomczak, M., and J. S. Godfrey. 1994. Regional Oceanography: An Introduction. Pergamon: Oxford.
- Trenberth, K. E., and C. J. Guillemot. 1995. Evaluation of the Atmospheric Moisture Budget as Seen from Analyses. Journal of Climate, 8(9):2255-2272.
- Verstraete, J. M. 1992. The Seasonal Upwellings in the Gulf of Guinea. Progress in Oceanography, 29(x):1-60.
- Vorosmarty, C. J., B. M. Fekete, and B. A. Tucker. 1998. Global River Discharge, 1807-1991, Version 1.1 (RivDIS). Data set. Available on-line [<http://www.daac.ornl.gov>] from Oak Ridge National Laboratory Distributed Active Archive Center, Oak Ridge, Tennessee, U.S.A.
- Weaver, A. J. and T. M. C. Hughes. 1994. Rapid Interglacial Climate Fluctuations Driven by North Atlantic Ocean Circulation. Nature, 367:447-450.
- West, N. 1996. Applied Statistics for Marine Affairs Professionals. Praeger: Westport.
- Wiffels, S. E. 2001. Ocean Transport of Fresh Water in Ocean Circulation & Climate: Observing and Modelling the Global Ocean, G. Siedler, J. Church, and J. Gould, eds. Academic Press: San Diego.

- Willebrand, J., and D. B. Haidvogel. 2001. Numerical Ocean Circulation Modelling: Present Status and Future Directions in Ocean Circulation & Climate: Observing and Modelling the Global Ocean, G. Siedler, J. Church, and J. Gould, eds. Academic Press: San Diego.
- Wilson, D. L. 2000. Introduction to Biology. Blackwell Science: Malden.
- Wilson, W. D., and W. E. Johns. 1997. Velocity Structure and Transport in the Windward Islands Passages. Deep Sea Research, 44(3):487-520.
- WOCE Data Products Committee. 2002. WOCE Global Data. Version 3.0. WOCE International Project Office, WOCE Report No. 180/02: Southampton, U.K.
- WOCE Current Meter Database maintained at Oregon State University by the Current Meter Data Assembly Center. Available at: <http://www.kepler.oce.edu/cmdac.html>
- Woodward, M. J., W. S. Huggett, and R. E. Thomson. 1990. Near-Surface Moored Current Meter Intercomparisons. Canadian Technical Report of Hydrography and Ocean Sciences, No. 125. Dept. of Fisheries and Oceans: Sydney.
- Wu, N. 1997. The Maximum Entropy Method Series: Springer Series in Information Sciences. Volume 32. Springer: New York.
- Wunsch, C. 2001. Global Problems and Global Observations in Ocean Circulation & Climate: Observing and Modelling the Global Ocean, G. Siedler, J. Church, and J. Gould, eds. Academic Press: San Diego.
- Xie, P., and P. A. Arkin. 1996. Analyses of Global Monthly Precipitation Using Gauge Observations, Satellite Estimates, and Numerical Model Predictions. Journal of Climate, 9(4):840-858.
- Zeng, N. 1999. Seasonal Cycle and Interannual Variability in the Amazon Hydrologic Cycle. Journal of Geophysical Research, 104(D8):9097-9106.
- Zhang, D., M. J. McPhaden, and W. E. Johns. 2003. Observational Evidence for Flow Between the Subtropical and Tropical Atlantic: The Atlantic Subtropical Cells. Journal of Physical Oceanography, 33(8):1783-1797.
- Zhou, M., J. D. Paduan, and P. P. Niiler. 2000. Surface Currents in the Canary Basin from Drifter Observations. Journal of Geophysical Research, 105(C9):21893-21911.

## 8. Appendices

### 8.1. WOCE in the Atlantic Ocean

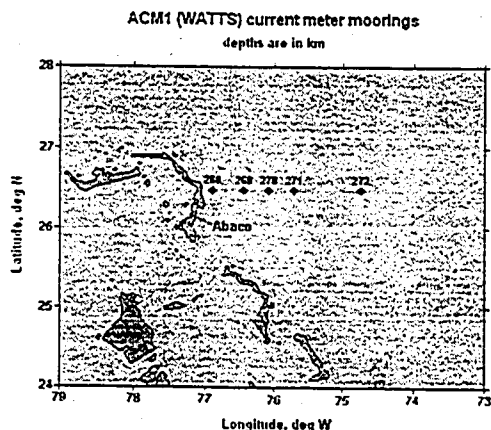
The World Ocean Circulation Experiment took place in the 1990's. This section looks at all the current meter records that were used in this thesis. These data were collected by the WOCE Current Meter Data Assembly Center, which was operated by the OSU Buoy Group.

WOCE component ACM1 (NW Atlantic near Abaco Island), 1990 - 1997  
WOCE component ACM6 (NW Atlantic), 1993 - 1995  
WOCE component ACM7 (Brazil continental slope), 1989 - 1994  
WOCE component ACM8 (North Atlantic), 1986 - 2000  
WOCE component ACM10 (Deep Basin), 1992 - 1994  
WOCE component ACM11 (Deep Basin), 1992 - 1994  
WOCE component ACM25/26 (Subduction), 1993 - 1995  
WOCE component ACM27 (MORENA), 1993 - 1994  
WOCE component ACM28 (MORENA), 1993 - 1995  
WOCE component ACM29 (Labrador Sea), 1994 - 1998

#### WOCE component ACM1

ACM1 included a series of current meter arrays deployed east of Abaco Island. The first was placed in June 1990 as part of the Western Atlantic Thermohaline Transport Study (WATTS). This was followed by three phases of the Atlantic Climate Change Program (ACCP). Also included is the STACS 10 array, which was deployed in the same area, in October 1988.

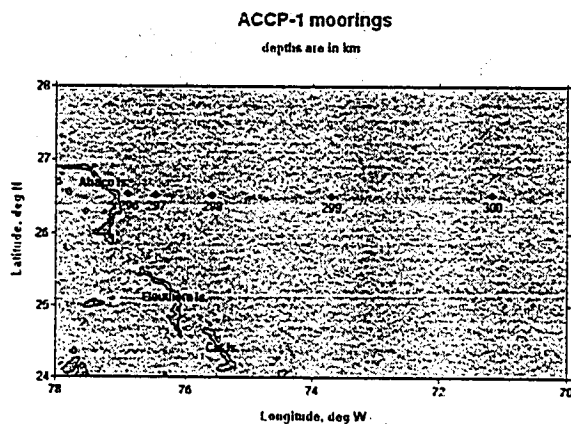
#### Western Atlantic Thermohaline Transport Studies (part of WOCE component ACM1)



Mooring name	lat	Lon	instr (meters)	depth water (meters)	depth instr type	dates
M268	26.528	-76.848	100	900	VACM	19 Jun 90 - 15 Nov 91
M268	26.528	-76.848	400	900	Aanderaa RCM	19 Jun 90 - 09 Feb 91
M268	26.528	-76.848	800	900	Aanderaa RCM	19 Jun 90 - 01 Jan 92
M269	26.496	-76.450	180	4838	VACM	20 Jun 90 - 09 May 91
M269	26.496	-76.450	480	4838	Aanderaa RCM	20 Jun 90 - 10 Feb 92
M269	26.496	-76.450	880	4838	Aanderaa RCM	20 Jun 90 - 10 Feb 92
M269	26.496	-76.450	1280	4838	Aanderaa RCM	20 Jun 90 - 02 Apr 91
M269	26.496	-76.450	2080	4838	VACM	20 Jun 90 - 10 Feb 92
M269	26.496	-76.450	3080	4838	VACM	20 Jun 90 - 10 Feb 92
M269	26.496	-76.450	4080	4838	VACM	20 Jun 90 - 10 Feb 92
M270	26.500	-76.100	180	4808	VACM	21 Jun 90 - 02 Feb 92
M270	26.500	-76.100	480	4808	Aanderaa RCM	21 Jun 90 - 02 Feb 92
M270	26.500	-76.100	880	4808	Aanderaa RCM	21 Jun 90 - 02 Feb 92
M270	26.500	-76.100	1280	4808	Aanderaa RCM	21 Jun 90 - 23 Mar 91
M270	26.500	-76.100	2080	4808	VACM	21 Jun 90 - 02 Feb 92
M270	26.500	-76.100	3080	4808	VACM	21 Jun 90 - 02 Feb 92
M270	26.500	-76.100	4080	4808	VACM	21 Jun 90 - 02 Feb 92
M271	26.500	-75.683	180	4685	VACM	22 Jun 90 - 09 Feb 92
M271	26.500	-75.683	280	4685	TD recorder	22 Jun 90 - 09 Feb 92
M271	26.500	-75.683	480	4685	Aanderaa RCM	22 Jun 90 - 09 Feb 92
M271	26.500	-75.683	880	4685	Aanderaa RCM	22 Jun 90 - 09 Feb 92
M271	26.500	-75.683	1280	4685	Aanderaa RCM	22 Jun 90 - 09 Feb 92
M271	26.500	-75.683	1480	4685	TD recorder	22 Jun 90 - 09 Feb 92
M271	26.500	-75.683	2080	4685	VMCM	22 Jun 90 - 09 Feb 92
M271	26.500	-75.683	3080	4685	VACM	22 Jun 90 - 24 Feb 91
M271	26.500	-75.683	4080	4685	VACM	22 Jun 90 - 09 Feb 92
M272	26.492	-73.820	180	4800	VACM	24 Jun 90 - 05 Feb 92
M272	26.492	-73.820	280	4800	TD recorder	24 Jun 90 - 04 Feb 92
M272	26.492	-73.820	440	4800	Aanderaa RCM	24 Jun 90 - 04 Feb 92
M272	26.492	-73.820	1200	4800	VMCM	24 Jun 90 - 04 Feb 92
M272	26.492	-73.820	1400	4800	TD recorder	24 Jun 90 - 04 Feb 92
M272	26.492	-73.820	2000	4800	VMCM	24 Jun 90 - 15 Dec 91
M272	26.492	-73.820	3000	4800	VACM	24 Jun 90 - 04 Feb 92
M272	26.492	-73.820	4000	4800	VACM	24 Jun 90 - 05 Feb 92

All of the time series from this experiment have been filtered and have a time increment of 12 hours. The diurnal tides and all higher frequencies have been removed.

### Atlantic Climate Change Program, Phase 1 (a part of WOCE component ACMI)



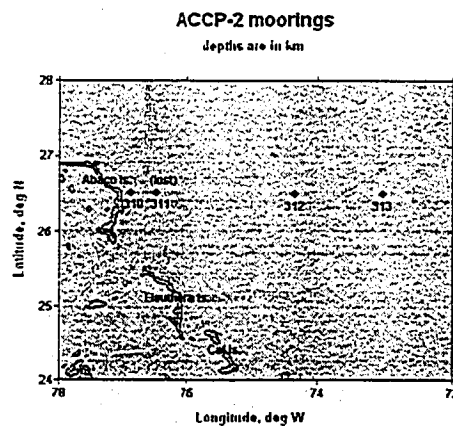


mooring name	lat	lon	instr (meters)	depth water (meters)	depth	instr type	dates
Mooring 296	26.528	-76.850	70	824		VACM	12 Feb 92 - 04 Apr 93
Mooring 296	26.529	-76.850	370	824		Aanderaa RCM	12 Feb 92 - 28 Sep 93
Mooring 296	26.529	-76.850	770	824		Aanderaa RCM	12 Feb 92 - 28 Sep 93
Mooring 297	26.485	-76.523	100	4849		VACM	11 Feb 92 - 27 Mar 92
Mooring 297	26.485	-76.523	200	4849		Benthos temp recorder	11 Feb 92 - 22 Jun 92
Mooring 297	26.485	-76.523	400	4849		Aanderaa RCM	11 Feb 92 - 02 Oct 93
Mooring 297	26.485	-76.523	800	4849		Aanderaa RCM	11 Feb 92 - 02 Oct 93
Mooring 297	26.485	-76.523	1200	4849		Aanderaa RCM	11 Feb 92 - 02 Oct 93
Mooring 297	26.485	-76.523	2000	4849		VACM	11 Feb 92 - 02 Oct 93
Mooring 297	26.485	-76.523	3000	4849		VACM	11 Feb 92 - 02 Oct 93
Mooring 297	26.485	-76.523	4000	4849		VACM	11 Feb 92 - 02 Oct 93
Mooring 297	26.485	-76.523	4840	4849		Seacat CTD	11 Feb 92 - 25 Sep 93
Mooring 298	26.490	-75.690	100	4685		VACM	10 Feb 92 - 15 Apr 93
Mooring 298	26.490	-75.690	200	4685		Benthos temp recorder	10 Feb 92 - 01 Oct 93
Mooring 298	26.490	-75.690	400	4685		Aanderaa RCM	11 Feb 92 - 01 Oct 93
Mooring 298	26.490	-75.690	800	4685		Aanderaa RCM	10 Feb 92 - 19 Apr 93
Mooring 298	26.490	-75.690	1200	4685		Aanderaa RCM	10 Feb 92 - 01 Oct 93
Mooring 298	26.490	-75.690	2000	4685		VACM	11 Feb 92 - 02 Oct 93
Mooring 298	26.490	-75.690	3000	4685		VACM	10 Feb 92 - 02 Nov 92
Mooring 298	26.490	-75.690	4000	4685		VACM	10 Feb 92 - 01 Oct 93
Mooring 298	26.490	-75.690	4680	4685		Seacat CTD	10 Feb 92 - 25 Sep 93
Mooring 299	26.498	-73.802	100	5050		VACM	09 Feb 92 - 30 Sep 93
Mooring 299	26.498	-73.802	200	5050		Benthos temp recorder	09 Feb 92 - 30 Sep 93
Mooring 299	26.498	-73.802	400	5050		Aanderaa RCM	09 Feb 92 - 04 Mar 93
Mooring 299	26.498	-73.802	800	5050		Aanderaa RCM	09 Feb 92 - 30 Sep 93
Mooring 299	26.498	-73.802	1200	5050		Aanderaa RCM	09 Feb 92 - 30 Sep 93
Mooring 299	26.498	-73.802	2000	5050		VACM	09 Feb 92 - 30 Sep 93
Mooring 299	26.498	-73.802	3000	5050		VACM	09 Feb 92 - 30 Sep 93
Mooring 299	26.498	-73.802	4000	5050		VACM	09 Feb 92 - 30 Sep 93
Mooring 299	26.498	-73.802	5045	5050		Seacat CTD	09 Feb 92 - 25 Sep 93
Mooring 300	26.487	-71.167	100	5488		VACM	06 Feb 92 - 16 Feb 93
Mooring 300	26.487	-71.167	200	5488		Benthos temp recorder	06 Feb 92 - 29 Sep 93
Mooring 300	26.487	-71.167	400	5488		Aanderaa RCM	04 Feb 92 - 26 Sep 93
Mooring 300	26.487	-71.167	800	5488		Aanderaa RCM	06 Feb 92 - 29 Sep 93
Mooring 300	26.487	-71.167	1200	5488		Aanderaa RCM	06 Feb 92 - 29 Sep 93
Mooring 300	26.487	-71.167	2000	5488		VACM	07 Feb 92 - 29 Sep 93
Mooring 300	26.487	-71.167	3000	5488		VACM	06 Feb 92 - 29 Sep 93
Mooring 300	26.487	-71.167	4000	5488		VACM	06 Feb 92 - 29 Sep 93
Mooring 300	26.487	-71.167	5483	5488		Seacat CTD	06 Feb 92 - 25 Sep 93

All of the time series from this experiment have been filtered and have a time increment of 12 hours. The diurnal tides and all higher frequencies have been removed.

## Atlantic Climate Change Program, Phase 2 (a part of WOCE component ACM1)

mooring name	lat	lon	instr (meters)	depth water (meters)	depth	instr type	dates
Mooring 310	26.528	-76.850	50	856		VACM	29 Sep 93 - 16 Apr 95
Mooring 310	26.528	-76.850	350	856		Aanderaa RCM	29 Sep 93 - 07 Jun 95
Mooring 310	26.528	-76.850	650	856		VACM	29 Sep 93 - 24 Dec 95
Mooring 312	26.498	-75.683	100	4689		VACM	02 Oct 93 - 29 Oct 95
Mooring 312	26.498	-75.683	250	4689		Seacat CTD	02 Oct 93 - 28 Oct 95
Mooring 312	26.498	-75.683	400	4689		VACM	02 Oct 93 - 29 Oct 95
Mooring 312	26.498	-75.683	600	4689		TSKA data recorder	02 Oct 93 - 29 Oct 95
Mooring 312	26.498	-75.683	800	4689		TSKA data recorder	02 Oct 93 - 29 Oct 95
Mooring 312	26.498	-75.683	1000	4689		TSKA data recorder	02 Oct 93 - 29 Oct 95
Mooring 312	26.498	-75.683	1200	4689		VACM	02 Oct 93 - 29 Oct 95
Mooring 312	26.498	-75.683	1600	4689		Seacat CTD	02 Oct 93 - 29 Oct 95
Mooring 312	26.498	-75.683	2000	4689		VACM	02 Oct 93 - 29 Oct 95
Mooring 312	26.498	-75.683	2500	4689		TSKA data recorder	02 Oct 93 - 29 Oct 95
Mooring 312	26.498	-75.683	3000	4689		VACM	02 Oct 93 - 29 Oct 95
Mooring 312	26.498	-75.683	3500	4689		TSKA data recorder	02 Oct 93 - 29 Oct 95
Mooring 312	26.498	-75.683	4000	4689		VACM	02 Oct 93 - 29 Oct 95
Mooring 312	26.498	-75.683	4688	4689		Seacat CTD	02 Oct 93 - 29 Oct 95
Mooring 313	26.508	-73.003	100	5000		VACM	01 Oct 93 - 05 Dec 93
Mooring 313	26.508	-73.003	400	5000		Aanderaa RCM	01 Oct 93 - 08 Aug 95
Mooring 313	26.508	-73.003	600	5000		TSKA data recorder	30 Sep 93 - 27 Oct 95
Mooring 313	26.508	-73.003	800	5000		TSKA data recorder	30 Sep 93 - 27 Oct 95
Mooring 313	26.508	-73.003	1200	5000		Aanderaa RCM	01 Oct 93 - 27 Oct 95
Mooring 313	26.508	-73.003	1600	5000		TSKA data recorder	01 Oct 93 - 27 Oct 95
Mooring 313	26.508	-73.003	2000	5000		VACM	01 Oct 93 - 27 Oct 95
Mooring 313	26.508	-73.003	2500	5000		TSKA data recorder	01 Oct 93 - 27 Oct 95
Mooring 313	26.508	-73.003	3000	5000		VACM	01 Oct 93 - 27 Oct 95
Mooring 313	26.508	-73.003	3500	5000		TSKA data recorder	01 Oct 93 - 27 Oct 95
Mooring 313	26.508	-73.003	4000	5000		VACM	01 Oct 93 - 27 Oct 95
Mooring 313	26.508	-73.003	4500	5000		TSKA data recorder	30 Sep 93 - 27 Oct 95



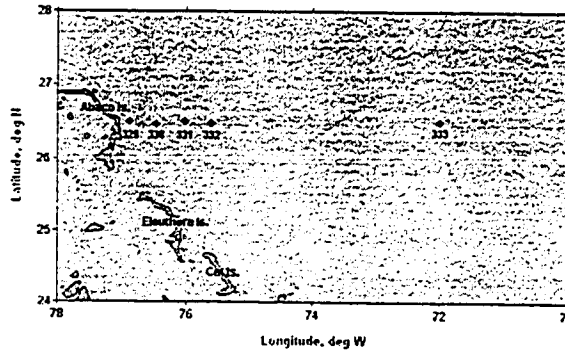
All of the time series from this experiment have been filtered and have a time increment of 12 hours. The diurnal tides and all higher frequencies have been removed.

**Atlantic Climate Change Program, Phase 3  
(a part of WOCE component ACM1)**

mooring name	lat	lon	instr (meters)	depth water (meters)	depth	instr type	dates
Mooring 329	26.507	-76.845	100	1006		Aanderaa RCM	31 Oct 95 - 12 Jun 97
Mooring 329	26.507	-76.845	400	1006		Aanderaa RCM	31 Oct 95 - 12 Jun 97
Mooring 329	26.507	-76.845	700	1006		VACM	31 Oct 95 - 27 Feb 96
Mooring 330	26.410	-76.500	1200	4840		Aanderaa RCM	31 Oct 95 - 12 Jun 97
Mooring 330	26.413	-76.503	1600	4840		TSKA data recorder	31 Oct 95 - 12 Jun 97
Mooring 330	26.413	-76.503	2000	4840		VACM	31 Oct 95 - 31 Jan 97
Mooring 330	26.413	-76.503	2500	4840		TSKA data recorder	31 Oct 95 - 12 Jun 97
Mooring 330	26.413	-76.503	3000	4840		VACM	31 Oct 95 - 12 Jun 97
Mooring 330	26.413	-76.503	3500	4840		TSKA data recorder	31 Oct 95 - 12 Jun 97
Mooring 330	26.413	-76.503	4000	4840		VACM	31 Oct 95 - 12 Jun 97
Mooring 330	26.413	-76.503	4500	4840		TSKA data recorder	31 Oct 95 - 12 Jun 97
Mooring 330	26.413	-76.503	4840	4840		Seacat CTD	31 Oct 95 - 12 Jun 97
Mooring 331	26.500	-76.100	100	4807		VACM	26 Oct 95 - 13 Jun 97
Mooring 331	26.500	-76.100	250	4807		TSKA data recorder	26 Oct 95 - 13 Jun 97
Mooring 331	26.500	-76.100	400	4807		Aanderaa RCM	26 Oct 95 - 13 Jun 97
Mooring 331	26.500	-76.100	600	4807		TSKA data recorder	26 Oct 95 - 13 Jun 97
Mooring 331	26.500	-76.100	800	4807		Aanderaa RCM	26 Oct 95 - 13 Apr 96
Mooring 331	26.500	-76.100	1000	4807		TSKA data recorder	26 Oct 95 - 13 Jun 97
Mooring 331	26.500	-76.100	1200	4807		Aanderaa RCM	26 Oct 95 - 13 Jun 97
Mooring 331	26.500	-76.100	1600	4807		TSKA data recorder	26 Oct 95 - 13 Jun 97
Mooring 331	26.500	-76.100	2000	4807		VACM	26 Oct 95 - 13 Jun 97
Mooring 331	26.500	-76.100	2500	4807		TSKA data recorder	26 Oct 95 - 13 Jun 97
Mooring 331	26.500	-76.100	3000	4807		VACM	26 Oct 95 - 13 Jun 97
Mooring 331	26.500	-76.100	3500	4807		TSKA data recorder	26 Oct 95 - 13 Jun 97
Mooring 331	26.500	-76.100	4000	4807		VACM	26 Oct 95 - 13 Jun 97
Mooring 331	26.500	-76.100	4500	4807		TSKA data recorder	26 Oct 95 - 13 Jun 97
Mooring 331	26.500	-76.100	4807	4807		Seacat CTD	26 Oct 95 - 13 Jun 97
Mooring 332	26.405	-75.678	800	4711		Aanderaa RCM	29 Oct 95 - 15 Jun 97
Mooring 332	26.405	-75.678	1000	4711		TSKA data recorder	29 Oct 95 - 15 Jun 97
Mooring 332	26.405	-75.678	1200	4711		Aanderaa RCM	29 Oct 95 - 15 Jun 97
Mooring 332	26.405	-75.678	1600	4711		TSKA data recorder	29 Oct 95 - 15 Jun 97
Mooring 332	26.405	-75.678	2000	4711		VACM	29 Oct 95 - 15 Jun 97
Mooring 332	26.405	-75.678	3000	4711		VACM	29 Oct 95 - 15 Jun 97
Mooring 332	26.405	-75.678	4000	4711		VACM	29 Oct 95 - 15 Jun 97
Mooring 332	26.405	-75.678	4500	4711		TSKA data recorder	29 Oct 95 - 15 Jun 97
Mooring 332	26.405	-75.678	4711	4711		Seacat CTD	29 Oct 95 - 15 Jun 97
Mooring 333	26.497	-72.004	800	5284		Aanderaa RCM	27 Oct 95 - 14 Jun 97
Mooring 333	26.497	-72.003	1000	5284		TSKA data recorder	27 Oct 95 - 14 Jun 97
Mooring 333	26.497	-72.004	1200	5284		Aanderaa RCM	27 Oct 95 - 22 Dec 96
Mooring 333	26.497	-72.003	1600	5284		TSKA data recorder	27 Oct 95 - 14 Jun 97
Mooring 333	26.497	-72.003	2000	5284		VACM	28 Oct 95 - 14 Jun 97
Mooring 333	26.497	-72.003	2500	5284		TSKA data recorder	27 Oct 95 - 14 Jun 97
Mooring 333	26.497	-72.003	3000	5284		VACM	28 Oct 95 - 14 Jun 97
Mooring 333	26.497	-72.003	4000	5284		VACM	28 Oct 95 - 14 Jun 97
Mooring 333	26.497	-72.003	5000	5284		VACM	28 Oct 95 - 14 Jun 97
Mooring 333	26.497	-72.003	5284	5284		Seacat CTD	27 Oct 95 - 14 Jun 97

**ACCP-3 current meter moorings**

depths are in km



All of the time series from this experiment have been filtered and have a time increment of 12 hours. The diurnal tides and all higher frequencies have been removed.

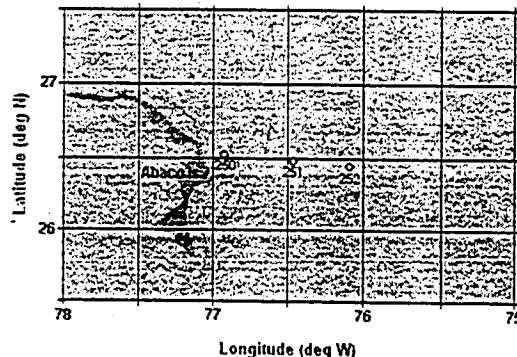
**Subtropical Atlantic Climate Studies (STACS)  
Component 10**

Note that STACS 10 can be considered a precursor to WOCE component ACM1, which occurred in the same area east of Abaco Island.

mooring name	lat	lon	instr (meters)	depth water (meters)	depth	instr type	dates
M250	26.510	-76.840	100	900		VACM	08 Oct 88 - 23 Apr 90
M250	26.510	-76.840	400	900		Aanderaa	08 Oct 88 - 28 Feb 90
M250	26.510	-76.840	800	900		VACM	08 Oct 88 - 28 Jun 89
M251	26.489	-76.448	100	4850		VACM	06 Oct 88 - 27 Apr 90
M251	26.489	-76.448	400	4850		Aanderaa	06 Oct 88 - 23 Feb 90
M251	26.489	-76.448	1200	4850		VACM	06 Oct 88 - 19 Jun 90
M251	26.489	-76.448	2400	4850		VACM	06 Oct 88 - 12 Mar 90
M251	26.489	-76.448	3800	4850		VACM	06 Oct 88 - 10 Mar 90
M252	26.475	-76.102	100	4810		VACM	06 Oct 88 - 17 Jul 89
M252	26.475	-76.102	400	4810		Aanderaa	06 Oct 88 - 16 Mar 90
M252	26.475	-76.102	800	4810		Aanderaa	06 Oct 88 - 05 Mar 90
M252	26.475	-76.102	1200	4810		VACM	06 Oct 88 - 20 Jun 90
M252	26.475	-76.102	2400	4810		VACM	06 Oct 88 - 13 Oct 89
M252	26.475	-76.102	3800	4810		VACM	06 Oct 88 - 10 Mar 90

**STACS-10 current meter moorings**

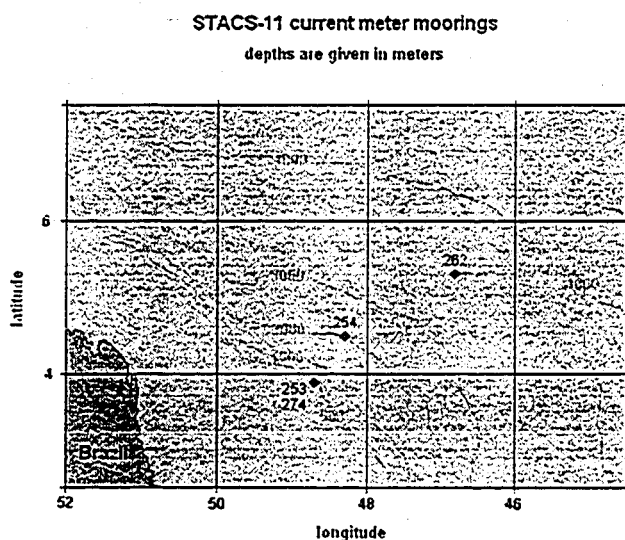
depth is given in meters



## Subtropical Atlantic Climate Studies (STACS) Component 11

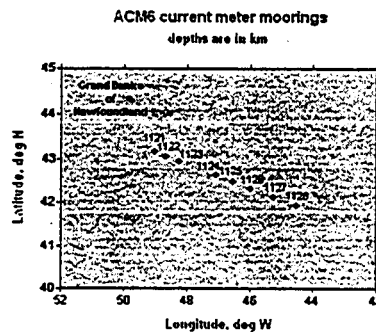
All of the STACS-11 time series are filtered and have a time increment of 12 hours. The diurnal tides and all higher frequencies have been removed. In the case of the ADCP the term "instr depth" below refers to bin depth. Note that only mooring 274 (the bottom three records) were used as part of the WOCE dataset.

mooring name	lat	lon	instr (meters)	depth water (meters)	depth	instr type	dates
Mooring 253	3.878	-48.724	60	483		VACM	09 Sep 89 - 24 Sep 90
Mooring 253	3.878	-48.724	110	483		Aanderaa	09 Sep 89 - 24 Sep 90
Mooring 253	3.878	-48.724	310	483		Aanderaa	09 Sep 89 - 24 Sep 90
Mooring 254	4.478	-48.308	50	2037		ADCP	09 Sep 89 - 21 Jan 91
Mooring 254	4.478	-48.308	100	2037		ADCP	09 Sep 89 - 21 Jan 91
Mooring 254	4.478	-48.308	150	2037		ADCP	09 Sep 89 - 21 Jan 91
Mooring 254	4.478	-48.308	200	2037		ADCP	09 Sep 89 - 21 Jan 91
Mooring 254	4.478	-48.308	250	2037		ADCP	09 Sep 89 - 21 Jan 91
Mooring 254	4.478	-48.308	300	2037		ADCP	09 Sep 89 - 21 Jan 91
Mooring 254	4.478	-48.308	350	2037		ADCP	09 Sep 89 - 21 Jan 91
Mooring 254	4.478	-48.308	400	2037		ADCP	09 Sep 89 - 21 Jan 91
Mooring 254	4.478	-48.308	800	2037		Aanderaa	09 Sep 89 - 21 Jan 91
Mooring 254	4.478	-48.308	1400	2037		VACM	09 Sep 89 - 21 Jan 91
Mooring 254	4.478	-48.308	1800	2037		VACM	09 Sep 89 - 27 Nov 90
Mooring 262	5.294	-46.811	160	3421		VACM	08 Sep 89 - 22 Jan 91
Mooring 262	5.294	-46.811	310	3421		Aanderaa	08 Sep 89 - 22 Jan 91
Mooring 262	5.294	-46.811	860	3421		Aanderaa	08 Sep 89 - 02 Jan 91
Mooring 262	5.294	-46.811	1460	3421		VACM	08 Sep 89 - 22 Jan 91
Mooring 262	5.294	-46.811	2060	3421		VACM	08 Sep 89 - 22 Jan 91
Mooring 262	5.294	-46.811	2860	3421		VACM	08 Sep 89 - 04 Feb 90
Mooring 262	5.294	-46.811	3360	3421		VACM	08 Sep 89 - 22 Jan 91
Mooring 274	3.877	-48.723	60	482		VACM	25 Sep 90 - 09 Aug 91
Mooring 274	3.877	-48.723	110	482		VACM	25 Sep 90 - 14 Sep 91
Mooring 274	3.877	-48.723	310	482		VACM	25 Sep 90 - 14 Sep 91



## WOCE component ACM6 (northwest Atlantic)

mooring name	lat	lon	instr (meters)	depth water (meters)	depth instr type	dates
1121	43.099	-49.033	381	1493	Aanderaa RCM5	01 Aug 93 - 11 Sep 93
1121	43.099	-49.033	785	1493	Aanderaa RCM5	01 Aug 93 - 21 Aug 93
1121	43.099	-49.033	1391	1493	Aanderaa RCM5	01 Aug 93 - 05 Sep 94
1122	43.067	-48.633	330	2449	Aanderaa RCM5	01 Aug 93 - 01 Jul 95
1122	43.067	-48.633	734	2449	Aanderaa RCM5	01 Aug 93 - 01 Jul 95
1122	43.067	-48.633	1440	2449	Aanderaa RCM5	01 Aug 93 - 01 Jul 95
1123	42.951	-48.183	346	3262	Aanderaa RCM5	11 Aug 93 - 03 May 95
1123	42.951	-48.183	751	3262	Aanderaa RCM5	02 Aug 93 - 03 May 95
1123	42.951	-48.183	1456	3262	Aanderaa RCM5	02 Aug 93 - 03 May 95
1123	42.951	-48.183	2461	3262	Aanderaa RCM5	02 Aug 93 - 02 Apr 95
1123	42.951	-48.183	3162	3262	Aanderaa RCM5	02 Aug 93 - 03 May 95
1124	42.717	-47.385	381	3894	Aanderaa RCM5	02 Aug 93 - 30 Jun 95
1124	42.717	-47.385	786	3894	Aanderaa RCM5	02 Aug 93 - 30 Jun 95
1124	42.717	-47.385	1492	3894	Aanderaa RCM5	02 Aug 93 - 30 Jun 95
1124	42.717	-47.385	2497	3894	Aanderaa RCM5	02 Aug 93 - 30 Jun 95
1124	42.717	-47.385	3494	3894	Aanderaa RCM5	02 Aug 93 - 02 Jul 95
1124	42.717	-47.385	3794	3894	Aanderaa RCM5	02 Aug 93 - 02 Jul 95
1125	42.566	-46.686	377	4392	Aanderaa RCM5	03 Aug 93 - 01 Mar 95
1125	42.566	-46.686	782	4392	Aanderaa RCM5	03 Aug 93 - 01 Mar 95
1125	42.566	-46.686	1488	4392	Aanderaa RCM5	03 Aug 93 - 01 Mar 95
1125	42.566	-46.686	2493	4392	Aanderaa RCM5	03 Aug 93 - 01 Mar 95
1125	42.566	-46.686	3490	4392	Aanderaa RCM5	03 Aug 93 - 01 Mar 95
1125	42.566	-46.686	4292	4392	Aanderaa RCM5	03 Aug 93 - 01 Mar 95
1126	42.353	-46.005	409	4701	Aanderaa RCM5	04 Aug 93 - 02 May 95
1126	42.353	-46.005	814	4701	Aanderaa RCM5	04 Aug 93 - 02 May 95
1126	42.353	-46.005	1519	4701	Aanderaa RCM5	04 Aug 93 - 02 May 95
1126	42.353	-46.005	2518	4701	Aanderaa RCM5	04 Aug 93 - 19 Aug 94
1126	42.353	-46.005	3509	4701	Aanderaa RCM5	04 Aug 93 - 02 May 95
1126	42.353	-46.005	4006	4701	Aanderaa RCM5	04 Aug 93 - 02 Sep 94
1126	42.353	-46.005	4601	4701	Aanderaa RCM5	04 Aug 93 - 02 May 95
1127	42.101	-45.317	374	4786	Aanderaa RCM5	04 Aug 93 - 27 Feb 95
1127	42.101	-45.317	779	4786	Aanderaa RCM5	04 Aug 93 - 28 Nov 94
1127	42.101	-45.317	2488	4786	Aanderaa RCM8	04 Aug 93 - 27 Feb 95
1127	42.101	-45.317	3486	4786	Aanderaa RCM8	04 Aug 93 - 27 Feb 95
1127	42.101	-45.317	3988	4786	Aanderaa RCM5	04 Aug 93 - 18 Nov 94
1127	42.101	-45.317	4686	4786	Aanderaa RCM5	04 Aug 93 - 27 Feb 95
1128	41.907	-44.575	416	4888	Aanderaa RCM5	05 Aug 93 - 01 May 95
1128	41.907	-44.575	821	4888	Aanderaa RCM5	05 Aug 93 - 01 May 95
1128	41.907	-44.575	1526	4888	Aanderaa RCM8	05 Aug 93 - 01 May 95
1128	41.907	-44.575	3528	4888	Aanderaa RCM8	05 Aug 93 - 01 May 95
1128	41.907	-44.575	4029	4888	Aanderaa RCM5	05 Aug 93 - 01 May 95
1128	41.907	-44.575	4788	4888	Aanderaa RCM5	05 Aug 93 - 01 May 95



**WOCE component ACM7 (northeast Brazil continental slope)  
September 1989 - October 1990**

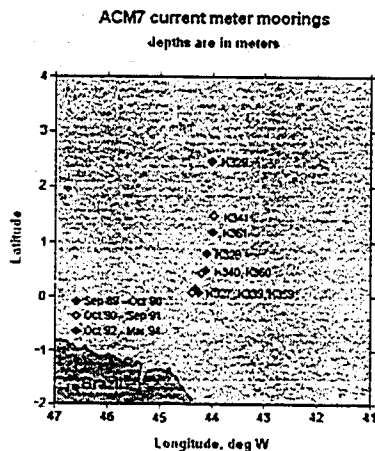
mooring name	lat	lon	instr (meters)	depth water (meters)	depth instr type	dates
K327	0.087	-44.390	50	545	ADCP	07 Sep 89 - 10 Oct 90
K327	0.087	-44.390	100	545	ADCP	07 Sep 89 - 10 Oct 90
K327	0.087	-44.390	150	545	ADCP	07 Sep 89 - 10 Oct 90
K327	0.087	-44.390	200	545	ADCP	07 Sep 89 - 10 Oct 90
K327	0.087	-44.390	250	545	ADCP	07 Sep 89 - 10 Oct 90
K327	0.087	-44.390	300	545	ADCP	07 Sep 89 - 10 Oct 90
K328	0.833	-44.070	72	3989	Aanderaa RCM	06 Sep 89 - 06 Apr 90
K328	0.833	-44.070	246	3989	Aanderaa RCM	06 Sep 89 - 19 Feb 90
K328	0.833	-44.070	824	3989	Aanderaa RCM	06 Sep 89 - 05 May 90
K328	0.833	-44.070	1990	3989	Aanderaa RCM	06 Sep 89 - 11 Oct 90
K328	0.833	-44.070	2588	3989	Aanderaa RCM	06 Sep 89 - 11 Oct 90
K328	0.833	-44.070	3695	3989	Aanderaa RCM	06 Sep 89 - 11 Oct 90
K329	2.483	-43.970	781	4191	Aanderaa RCM	06 Sep 89 - 05 Apr 90
K329	2.483	-43.970	1369	4191	Aanderaa RCM	06 Sep 89 - 13 Feb 90
K329	2.483	-43.970	3486	4191	Aanderaa RCM	06 Sep 89 - 08 Oct 90
K329	2.483	-43.970	3991	4191	Aanderaa RCM	06 Sep 89 - 02 Feb 90

**October 1990 - September 1991**

mooring name	lat	lon	instr (meters)	depth water (meters)	depth instr type	dates
K339	0.087	-44.390	50	545	ADCP	13 Oct 90 - 08 Sep 91
K339	0.087	-44.390	100	545	ADCP	13 Oct 90 - 08 Sep 91
K339	0.087	-44.390	150	545	ADCP	13 Oct 90 - 08 Sep 91
K339	0.087	-44.390	200	545	ADCP	13 Oct 90 - 08 Sep 91
K339	0.087	-44.390	250	545	ADCP	13 Oct 90 - 08 Sep 91
K339	0.087	-44.390	368	545	Aanderaa RCM	13 Oct 90 - 08 Sep 91
K340	0.420	-44.250	50	3340	ADCP	14 Oct 90 - 08 Sep 91
K340	0.420	-44.250	100	3340	ADCP	14 Oct 90 - 08 Sep 91
K340	0.420	-44.250	150	3340	ADCP	14 Oct 90 - 08 Sep 91
K340	0.420	-44.250	200	3340	ADCP	14 Oct 90 - 08 Sep 91
K340	0.420	-44.250	250	3340	ADCP	14 Oct 90 - 08 Sep 91
K340	0.420	-44.250	300	3340	ADCP	14 Oct 90 - 08 Sep 91
K340	0.420	-44.250	305	3340	Aanderaa RCM	14 Oct 90 - 08 Sep 91
K340	0.420	-44.250	847	3340	Aanderaa RCM	14 Oct 90 - 02 Sep 91
K340	0.420	-44.250	1440	3340	Aanderaa RCM	14 Oct 90 - 08 Sep 91
K340	0.420	-44.250	1745	3340	Aanderaa RCM	14 Oct 90 - 08 Sep 91
K340	0.420	-44.250	2042	3340	Aanderaa RCM	13 Oct 90 - 08 Sep 91
K340	0.420	-44.250	2637	3340	Aanderaa RCM	13 Oct 90 - 08 Sep 91
K340	0.420	-44.250	3235	3340	Aanderaa RCM	13 Oct 90 - 08 Sep 91
K341	1.550	-44.010	50	4108	ADCP	14 Oct 90 - 09 Sep 91
K341	1.550	-44.010	100	4108	ADCP	14 Oct 90 - 09 Sep 91
K341	1.550	-44.010	150	4108	ADCP	14 Oct 90 - 09 Sep 91
K341	1.550	-44.010	200	4108	ADCP	14 Oct 90 - 09 Sep 91
K341	1.550	-44.010	250	4108	ADCP	14 Oct 90 - 09 Sep 91
K341	1.550	-44.010	300	4108	ADCP	14 Oct 90 - 09 Sep 91
K341	1.550	-44.010	350	4108	ADCP	14 Oct 90 - 09 Sep 91
K341	1.550	-44.010	830	4108	Aanderaa RCM	14 Oct 90 - 09 Sep 91
K341	1.550	-44.010	2020	4108	Aanderaa RCM	14 Oct 90 - 08 Sep 91
K341	1.550	-44.010	2814	4108	Aanderaa RCM	14 Oct 90 - 09 Sep 91
K341	1.550	-44.010	3409	4108	Aanderaa RCM	14 Oct 90 - 09 Sep 91
K341	1.550	-44.010	3704	4108	Aanderaa RCM	14 Oct 90 - 13 Jul 91

### October 1992 - March 1994

mooring name	lat	lon	instr (meters)	depth water (meters)	depth	instr type	dates
k359	0.243	-44.310	50	2880		ADCP	28 Oct 92 - 09 Feb 93
k359	0.243	-44.310	100	2880		ADCP	28 Oct 92 - 09 Feb 93
k359	0.243	-44.310	151	2880		ADCP	28 Oct 92 - 09 Feb 93
k359	0.243	-44.310	200	2880		ADCP	28 Oct 92 - 09 Feb 93
K359	0.243	-44.310	450	2885		Aanderaa RCM	28 Oct 92 - 05 Dec 93
K359	0.243	-44.310	700	2885		Aanderaa RCM	28 Oct 92 - 21 Dec 93
K359	0.243	-44.310	947	2885		Aanderaa RCM	28 Oct 92 - 04 Mar 94
K359	0.243	-44.310	1500	2885		Aanderaa RCM	28 Oct 92 - 12 Nov 93
K359	0.243	-44.310	1786	2885		Aanderaa RCM	07 Nov 92 - 19 Sep 93
K359	0.243	-44.310	2100	2885		Aanderaa RCM	28 Oct 92 - 19 Dec 93
K359	0.243	-44.310	2503	2885		Aanderaa RCM	28 Oct 92 - 05 Mar 94
k360	0.617	-44.167	49	3660		ADCP	28 Oct 92 - 04 Mar 94
k360	0.617	-44.170	100	3660		ADCP	28 Oct 92 - 04 Mar 94
k360	0.617	-44.170	151	3660		ADCP	28 Oct 92 - 04 Mar 94
k360	0.617	-44.170	200	3660		ADCP	28 Oct 92 - 04 Mar 94
K360	0.617	-44.170	440	3660		Aanderaa RCM	28 Oct 92 - 04 Mar 94
K360	0.617	-44.170	690	3660		Aanderaa RCM	28 Oct 92 - 16 Jan 94
K360	0.617	-44.170	957	3660		Aanderaa RCM	28 Oct 92 - 20 Nov 93
K360	0.617	-44.170	1490	3660		Aanderaa RCM	28 Oct 92 - 10 Oct 93
K360	0.617	-44.170	1787	3660		Aanderaa RCM	28 Oct 92 - 24 Oct 93
K360	0.617	-44.170	2084	3660		Aanderaa RCM	28 Oct 92 - 03 Mar 94
K360	0.617	-44.170	2482	3660		Aanderaa RCM	05 Dec 92 - 23 Oct 93
K360	0.617	-44.170	2981	3660		Aanderaa RCM	28 Oct 92 - 04 Mar 94
k361	1.186	-44.040	50	4110		ADCP	29 Oct 92 - 04 Mar 94
k361	1.186	-44.040	101	4110		ADCP	29 Oct 92 - 04 Mar 94
k361	1.186	-44.040	151	4110		ADCP	29 Oct 92 - 04 Mar 94
k361	1.186	-44.040	199	4110		ADCP	29 Oct 92 - 04 Mar 94
K361	1.186	-44.040	430	4110		Aanderaa RCM	29 Oct 92 - 19 Feb 94
K361	1.186	-44.040	687	4110		Aanderaa RCM	29 Oct 92 - 03 Dec 93
K361	1.186	-44.040	1483	4110		Aanderaa RCM	29 Oct 92 - 08 Dec 93
K361	1.186	-44.040	1785	4110		Aanderaa RCM	29 Oct 92 - 23 Apr 93
K361	1.186	-44.040	2985	4110		Aanderaa RCM	29 Oct 92 - 03 Mar 94
K361	1.186	-44.040	3785	4110		Aanderaa RCM	29 Oct 92 - 03 Mar 94
K361	1.186	-44.040	4035	4110		Aanderaa RCM	29 Oct 92 - 03 Mar 94





All of the time series from this experiment have been filtered and have a time increment of 12 hours. The diurnal tides and all higher frequencies have been removed. In the case of an ADCP the term "instr depth" above refers to bin depth.

### WOCE component ACM8

ACM8 took place in the North Atlantic, with particular emphasis on measuring the southward flow of cold, dense bottom water southwestward across the Iceland-Faroe Ridge and the Denmark Strait, and the flow northward of shallower waters of tropical and subtropical origin. The experiment went forward in three phases.

#### Denmark Strait Overflow (a part of WOCE component ACM8) September 1986 - June 1987

mooring name	lat	lon	instr (meters)	depth water (meters)	depth instr type	dates
8606	62.895	-35.858	1980	2640	Aanderaa RCM5	09 Sep 86 - 26 Jun 87
8606	62.895	-35.858	2530	2640	Aanderaa RCM5	09 Sep 86 - 26 Jun 87
8607	63.430	-36.570	1536	2046	Aanderaa RCM5	09 Sep 86 - 26 Jun 87
8607	63.430	-36.570	1936	2046	Aanderaa RCM5	09 Sep 86 - 26 Jun 87

#### June 1987 - July 1988

mooring name	lat	lon	instr (meters)	depth water (meters)	depth instr type	dates
8701	63.707	-36.972	919	1220	Aanderaa RCM5	26 Jun 87 - 01 Jul 88
8701	63.707	-36.972	1120	1220	Aanderaa RCM5	26 Jun 87 - 01 Jul 88
8702	63.605	-37.032	1247	1648	Aanderaa RCM5	27 Jun 87 - 03 Oct 87
8702	63.605	-37.032	1548	1648	Aanderaa RCM5	27 Jun 87 - 01 Jul 88
8703	63.485	-36.290	1585	1986	Aanderaa RCM5	27 Jun 87 - 30 Jun 88
8703	63.485	-36.290	1886	1986	Aanderaa RCM5	27 Jun 87 - 30 Jun 88
8704	63.278	-35.893	1754	2355	Aanderaa RCM5	27 Jun 87 - 30 Jun 88
8704	63.278	-35.893	2255	2355	Aanderaa RCM5	28 Jun 87 - 30 Jun 88
8705	63.117	-35.555	1869	2572	Aanderaa RCM5	28 Jun 87 - 30 Jun 88
8705	63.117	-35.555	2472	2572	Aanderaa RCM5	28 Jun 87 - 30 Jun 88
8706	62.902	-35.107	1903	2706	Aanderaa RCM5	28 Jun 87 - 30 Jun 88
8706	62.902	-35.107	2606	2706	Aanderaa RCM5	28 Jun 87 - 30 Jun 88
8707	62.640	-34.507	2032	2835	Aanderaa RCM5	28 Jun 87 - 30 Jun 88
8707	62.640	-34.507	2735	2835	Aanderaa RCM5	28 Jun 87 - 30 Jun 88

#### July 1988 - June 1989

mooring name	lat	lon	instr (meters)	depth water (meters)	depth instr type	dates
8801	63.482	-36.298	1622	1984	Aanderaa RCM5	02 Aug 88 - 21 May 89
8801	63.482	-36.298	1924	1984	Aanderaa RCM5	03 Jul 88 - 29 Jun 89
8801	63.482	-36.298	1965	1984	Aanderaa RCM5	03 Jul 88 - 29 Jun 89
8802	63.620	-36.730	1298	1660	Aanderaa RCM5	03 Jul 88 - 29 Jun 89
8802	63.620	-36.730	1641	1660	Aanderaa RCM5	03 Jul 88 - 29 Jun 89
8803	63.695	-36.987	998	1260	Aanderaa RCM7	03 Jul 88 - 02 Mar 89
8803	63.695	-36.987	1241	1260	Aanderaa RCM7	03 Jul 88 - 29 Jun 89

8804	63.278	-35.870	1733	2345	Aanderaa RCM5	04 Jul 88 - 29 Jun 89
8804	63.278	-35.870	2285	2345	Aanderaa RCM5	04 Jul 88 - 26 Aug 88
8804	63.278	-35.870	2326	2345	Aanderaa RCM5	04 Jul 88 - 31 Jul 88
8805	63.118	-35.542	1895	2569	Aanderaa RCM5	04 Jul 88 - 09 Jun 89
8805	63.118	-35.542	2509	2569	Aanderaa RCM5	04 Jul 88 - 29 Jun 89
8806	62.907	-35.110	1871	2706	Aanderaa RCM5	04 Jul 88 - 28 Jun 89
8806	62.907	-35.110	2646	2706	Aanderaa RCM5	04 Jul 88 - 28 Jun 89
8806	62.907	-35.110	2687	2706	Aanderaa RCM5	04 Jul 88 - 20 Sep 88
8807	62.653	-34.515	2052	2827	Aanderaa RCM5	04 Jul 88 - 28 Jun 89
8807	62.653	-34.515	2767	2827	Aanderaa RCM5	04 Jul 88 - 28 Jun 89
8807	62.653	-34.515	2808	2827	Aanderaa RCM5	04 Jul 88 - 28 Jun 89
8808	62.237	-33.810	2042	2917	Aanderaa RCM5	05 Jul 88 - 05 Feb 89
8808	62.237	-33.810	2857	2917	Aanderaa RCM5	05 Jul 88 - 26 Mar 89
8808	62.237	-33.810	2898	2917	Aanderaa RCM5	05 Jul 88 - 26 Jun 89

### July 1989 - August 1990

mooring name	lat	lon	Instr (meters)	depth water (meters)	depth instr type	dates
8906	62.783	-34.802	2421	2756	Aanderaa RCM5	02 Jul 89 - 06 Mar 90
8906	62.783	-34.802	2736	2756	Aanderaa RCM5	02 Jul 89 - 12 Nov 89
8907	63.000	-35.335	2229	2634	Aanderaa RCM5	02 Jul 89 - 06 Mar 90
8907	63.000	-35.335	2571	2634	Aanderaa RCM5	02 Jul 89 - 06 Mar 90
8907	63.000	-35.335	2614	2634	Aanderaa RCM5	02 Jul 89 - 06 Mar 90
8908	63.202	-35.728	2026	2463	Aanderaa RCM5	02 Jul 89 - 06 Aug 90
8908	63.202	-35.728	2443	2463	Aanderaa RCM5	02 Jul 89 - 22 Oct 89
8909	63.383	-36.088	1788	2153	Aanderaa RCM5	03 Jul 89 - 07 Mar 90
8909	63.383	-36.088	2090	2153	Aanderaa RCM5	03 Jul 89 - 07 Mar 90
8909	63.383	-36.088	2133	2153	Aanderaa RCM5	03 Jul 89 - 07 Mar 90
8910	63.557	-36.505	1402	1767	Aanderaa RCM4S	03 Jul 89 - 08 Mar 90
8910	63.557	-36.505	1704	1767	Aanderaa RCM5	03 Jul 89 - 06 Sep 89
8910	63.557	-36.505	1747	1767	Aanderaa RCM5	04 Jul 89 - 31 Oct 89
8911	63.657	-36.858	1180	1445	Aanderaa RCM5	04 Jul 89 - 05 Sep 89
8911	63.657	-36.858	1382	1445	Aanderaa RCM5	05 Jul 89 - 07 Mar 90
8911	63.657	-36.858	1425	1445	Aanderaa RCM5	05 Jul 89 - 19 Aug 89

### March 1990 - July 1991

mooring name	lat	lon	instr (meters)	depth water (meters)	depth instr type	dates
9001	64.750	-30.550	1198	2200	Aanderaa RCM5	09 Mar 90 - 10 Jul 90
9001	64.750	-33.550	1679	2200	Aanderaa RCM5	09 Mar 90 - 10 Jul 90
9001	64.750	-30.550	2180	2200	Aanderaa RCM5	09 Mar 90 - 10 Jul 90
9002	64.913	-30.668	1155	2005	Aanderaa RCM5	09 Mar 90 - 10 Jul 90
9002	64.913	-30.668	1906	2005	Aanderaa RCM5	09 Mar 90 - 10 Jul 90
9002	64.913	-30.668	1987	2005	Aanderaa RCM5	09 Mar 90 - 10 Jul 90
9003	65.165	-30.783	880	1500	Aanderaa RCM5	09 Mar 90 - 10 Jul 90
9003	65.165	-30.783	1231	1500	Aanderaa RCM5	09 Mar 90 - 10 Jul 90
9003	65.165	-30.783	1482	1500	Aanderaa RCM5	09 Mar 90 - 10 Jul 90
9004	65.255	-30.848	750	1200	Aanderaa RCM5	09 Mar 90 - 10 Jul 90
9004	65.255	-30.848	1182	1200	Aanderaa RCM5	09 Mar 90 - 10 Jul 90
9005	65.298	-31.115	680	1080	Aanderaa RCM5	09 Mar 90 - 10 Jul 90
9005	65.298	-31.115	981	1080	Aanderaa RCM5	09 Mar 90 - 15 Apr 90
9005	65.298	-31.115	1062	1080	Aanderaa RCM5	09 Mar 90 - 10 Jul 90
9006	63.622	-32.927	1634	2738	Aanderaa RCM5	12 Jul 90 - 30 Jul 91
9006	63.617	-32.927	2136	2738	Aanderaa RCM5	12 Jul 90 - 30 Jul 91
9006	63.622	-32.927	2638	2738	Aanderaa RCM5	12 Jul 90 - 12 Jul 91
9006	63.622	-32.927	2720	2738	Aanderaa RCM5	12 Jul 90 - 06 Sep 90

9008	64.272	-33.630	1249	2001	Aanderaa RCM5	12 Jul 90 - 16 Jul 91
9008	64.272	-33.630	1631	2001	Aanderaa RCM5	12 Jul 90 - 20 Jul 91
9008	64.272	-33.630	1983	2001	Aanderaa RCM5	12 Jul 90 - 09 Jun 91
9009	64.430	-33.780	1528	1731	Aanderaa RCM5	12 Jul 90 - 30 Jul 91
9009	64.430	-33.780	1670	1731	Aanderaa RCM5	12 Jul 90 - 30 Jul 91
9009	64.430	-33.780	1712	1731	Aanderaa RCM5	12 Jul 90 - 21 Oct 90
9010	64.550	-33.927	992	1494	Aanderaa RCM4S	12 Jul 90 - 19 Jul 91
9010	64.550	-33.927	1394	1494	Aanderaa RCM4S	12 Jul 90 - 13 Jul 90
9010	64.550	-33.917	1476	1494	Aanderaa RCM5	12 Jul 90 - 30 Jul 91
9011	64.720	-34.105	940	1142	Aanderaa RCM4S	12 Jul 90 - 30 Jul 91
9011	64.720	-34.105	1124	1142	Aanderaa RCM5	12 Jul 90 - 30 Jul 91

### February 1995 - November 1995

mooring name	lat	lon	instr (meters)	depth water (meters)	depth	instr type	dates
9501	63.270	-35.868	2221	2323		Aanderaa RCM8	24 Feb 95 - 29 Nov 95
9501	63.270	-35.868	2262	2323		Aanderaa RCM8	24 Feb 95 - 29 Nov 95
9501	63.270	-35.868	2303	2323		Aanderaa RCM8	24 Feb 95 - 29 Nov 95
9503	63.482	-36.307	1850	1952		Aanderaa RCM8	25 Feb 95 - 29 Nov 95
9503	63.482	-36.307	1891	1952		Aanderaa RCM8	25 Feb 95 - 29 Nov 95
9503	63.482	-36.307	1932	1952		Aanderaa RCM8	25 Feb 95 - 29 Nov 95

### December 1996 - August 1997

mooring name	lat	lon	instr (meters)	depth water (meters)	depth	instr type	dates
9603	63.487	-36.278	1849	1949		Aanderaa RCM8	11 Dec 96 - 30 Jul 97
9603	63.487	-36.278	1849	1949		Aanderaa RCM8	30 Jul 97 - 18 Aug 97
9603	63.487	-36.278	1889	1949		Aanderaa RCM8	11 Dec 96 - 04 Apr 97
9603	63.487	-36.278	1929	1949		Aanderaa RCM8	11 Dec 96 - 25 Mar 97
9604	63.272	-35.870	2223	2323		Aanderaa RCM8	11 Dec 96 - 18 Aug 97
9604	63.272	-35.870	2263	2323		Aanderaa RCM8	11 Dec 96 - 25 Mar 97
9604	63.272	-35.870	2303	2323		Aanderaa RCM8	11 Dec 96 - 06 Apr 97

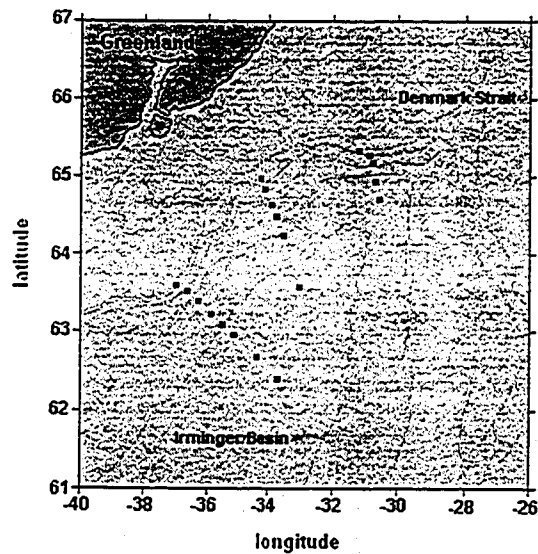
### August 1997 - August 1998

mooring name	lat	lon	instr (meters)	depth water (meters)	depth	instr type	dates
9702	63.553	-36.502	1683	1785		Aanderaa RCM8	19 Aug 97 - 20 Aug 98
9702	63.553	-36.502	1724	1785		Aanderaa RCM8	19 Aug 97 - 20 Aug 98
9702	63.553	-36.502	1765	1785		Aanderaa RCM8	19 Aug 97 - 20 Aug 98
9703	63.477	-36.298	1892	1994		Aanderaa RCM8	19 Aug 97 - 20 Aug 98
9703	63.477	-36.298	1933	1994		Aanderaa RCM8	19 Aug 97 - 13 Apr 98
9703	63.477	-36.298	1974	1994		Aanderaa RCM8	19 Aug 97 - 28 Jul 98
9704	63.365	-36.070	2085	2208		Aanderaa RCM8	19 Aug 97 - 21 Aug 98
9704	63.365	-36.070	2136	2208		Aanderaa RCM8	19 Aug 97 - 21 Aug 98
9704	63.365	-36.070	2188	2208		Aanderaa RCM8	19 Aug 97 - 21 Aug 98
9705	63.277	-35.858	2266	2368		Aanderaa RCM8	19 Aug 97 - 20 Aug 98
9705	63.277	-35.858	2307	2368		Aanderaa RCM8	19 Aug 97 - 06 Aug 98
9705	63.277	-35.858	2348	2368		Aanderaa RCM8	19 Aug 97 - 31 Jul 98
9706	63.117	-35.538	2467	2590		Aanderaa RCM8	19 Aug 97 - 20 Aug 98
9706	63.117	-35.538	2518	2590		Aanderaa RCM8	19 Aug 97 - 20 Aug 98
9706	63.117	-35.538	2570	2590		Aanderaa RCM8	19 Aug 97 - 20 Aug 98

## August 1998 - August 1999

mooring name	lat	lon	Instr (meters)	depth water (meters)	depth instr type	dates
98UK1	63.482	-36.302	1877	1980	Aanderaa RCM8	24 Aug 98 - 19 Aug 99
98UK1	63.482	-36.302	1918	1980	Aanderaa RCM8	24 Aug 98 - 19 Aug 99
98UK1	63.482	-36.302	1960	1980	Aanderaa RCM8	24 Aug 98 - 19 Aug 99
98UK2	63.282	-35.867	2254	2356	Aanderaa RCM8	24 Aug 98 - 19 Aug 99
98UK2	63.282	-35.867	2295	2356	Aanderaa RCM8	24 Aug 98 - 19 Aug 99
98UK2	63.282	-35.867	2336	2356	Aanderaa RCM8	24 Aug 98 - 19 Aug 99

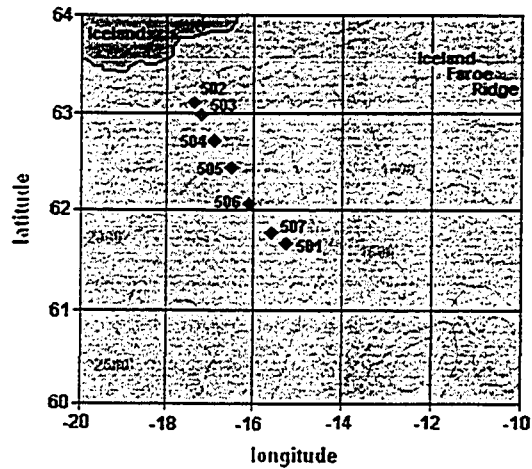
**Denmark Strait Overflow (ACM8)**  
mooring locations are shown in red



**Iceland-Faroe Overflow**  
(a part of WOCE component ACM8)

mooring name	lat	lon	instr (meters)	depth water (meters)	depth instr type	dates
501 (A)	61.738	-15.398	2281	2291	Aanderaa RCM5	15 Jul 90 - 22 Aug 91
502 (B)	63.143	-17.297	1018	1028	Aanderaa RCM5	14 Jul 90 - 14 Aug 91
503 (C)	62.998	-17.109	1291	1301	Aanderaa RCM5	15 Jul 90 - 20 Aug 91
504 (D)	62.718	-16.820	1135	1800	Aanderaa RCM5	15 Jul 90 - 22 Aug 91
504 (D)	62.718	-16.820	1465	1800	Aanderaa RCM5	15 Jul 90 - 17 Jan 91
504 (D)	62.718	-16.820	1790	1800	Aanderaa RCM5	15 Jul 90 - 27 Jul 90
505 (E)	62.440	-16.471	1403	2056	Aanderaa RCM5	15 Jul 90 - 12 Apr 91
505 (E)	62.440	-16.471	1722	2056	Aanderaa RCM5	15 Jul 90 - 22 Aug 91
505 (E)	62.440	-16.471	2046	2056	Aanderaa RCM5	15 Jul 90 - 22 Aug 91
506 (F)	62.063	-16.055	2225	2235	Aanderaa RCM5	15 Jul 90 - 24 Aug 91
507 (G)	61.832	-15.623	1975	2306	Aanderaa RCM5	15 Jul 90 - 12 Jun 91
507 (G)	61.832	-15.623	2296	2306	Aanderaa RCM5	15 Jul 90 - 17 Aug 91

### Iceland-Faroe Overflow



### German component of ACM8 September 1991 - September 1992

mooring name	lat	lon	instr (meters)	depth water (meters)	depth	instr type	dates
A1	59.140	-34.030	263	2855		Aanderaa RCM8	08 Sep 91 - 01 Jun 92
A1	59.140	-34.030	876	2855		Aanderaa RCM8	08 Sep 91 - 05 Sep 92
A1	59.140	-34.030	2088	2855		Aanderaa RCM8	08 Sep 91 - 05 Sep 92
A1	59.140	-34.030	2551	2855		Aanderaa RCM8	08 Sep 91 - 05 Sep 92
B1	59.000	-32.808	209	2110		Aanderaa RCM8	08 Sep 91 - 05 Sep 92
B1	59.000	-32.808	822	2110		Aanderaa RCM8	08 Sep 91 - 05 Sep 92
B1	59.000	-32.808	1534	2110		Aanderaa RCM8	08 Sep 91 - 05 Sep 92
B1	59.000	-32.808	1996	2110		Aanderaa RCM8	08 Sep 91 - 05 Sep 92
F1	52.340	-16.347	210	3510		Aanderaa RCM5	19 Sep 91 - 30 Aug 92
F1	52.340	-16.347	510	3510		Aanderaa RCM5	19 Sep 91 - 30 Aug 92
F1	52.340	-16.347	810	3510		Aanderaa RCM5	19 Sep 91 - 30 Aug 92
F1	52.340	-16.347	2010	3510		Aanderaa RCM5	19 Sep 91 - 29 Aug 92
F1	52.340	-16.347	3460	3510		Aanderaa RCM5	19 Sep 91 - 19 Feb 92

### August 1992 - October 1993

mooring name	lat	lon	instr (meters)	depth water (meters)	depth	instr type	dates
A2	59.135	-34.073	861	2630		Aanderaa RCM4	05 Sep 92 - 21 Oct 93
A2	59.135	-34.073	2063	2630		Aanderaa RCM5	05 Sep 92 - 21 Oct 93
A2	59.135	-34.073	2526	2630		Aanderaa RCM5	05 Sep 92 - 29 Jun 93
E2	54.288	-25.857	175	3030		Aanderaa RCM4	02 Sep 92 - 11 Sep 93
E2	54.288	-25.857	2825	3030		Aanderaa RCM8	02 Sep 92 - 14 Sep 93
F2	52.378	-16.362	181	3481		Aanderaa RCM4	30 Aug 92 - 05 Aug 93
F2	52.378	-16.362	481	3481		Aanderaa RCM5	30 Aug 92 - 10 Sep 93
F2	52.378	-16.362	781	3481		Aanderaa RCM5	30 Aug 92 - 05 Sep 93
F2	52.378	-16.362	1981	3481		Aanderaa RCM5	30 Aug 92 - 10 Sep 93
F2	52.378	-16.362	2981	3481		Aanderaa RCM8	30 Aug 92 - 04 Sep 93
F2	52.378	-16.362	3431	3481		Aanderaa RCM8	30 Aug 92 - 05 Aug 93

### September 1993 - May 1994

mooring name	lat	lon	instr (meters)	depth water (meters)	depth instr type	dates
E3	54.413	-25.862	439	3299	Aanderaa RCM5	15 Sep 93 - 27 May 94
E3	54.413	-25.862	1040	3299	Aanderaa RCM4	15 Sep 93 - 27 May 94

### May 1994 - June 1995

mooring name	lat	lon	instr (meters)	depth water (meters)	depth instr type	dates
A4	59.152	-34.000	269	2850	Aanderaa RCM7	31 May 94 - 10 Jun 95
A4	59.152	-34.000	882	2850	Aanderaa RCM7	31 May 94 - 10 Jun 95
A4	59.152	-34.000	2092	2850	Aanderaa RCM8	31 May 94 - 10 Jun 95
A4	59.152	-34.000	2551	2850	Aanderaa RCM8	31 May 94 - 02 Aug 94
E4	54.422	-25.902	439	3300	Aanderaa RCM5	27 May 94 - 06 Jun 95
E4	54.422	-25.902	1041	3300	Aanderaa RCM5	27 May 94 - 06 Jun 95
E4	54.422	-25.902	3095	3300	Aanderaa RCM5	27 May 94 - 02 Jun 95

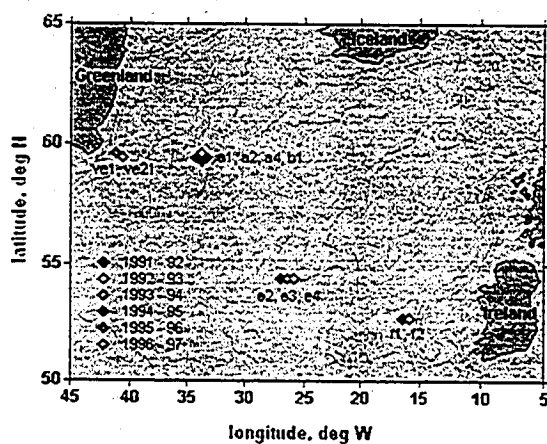
### October 1995 - July 1996

mooring name	lat	lon	instr (meters)	depth water (meters)	depth instr type	dates
VE1	59.585	-41.162	2192	2312	Aanderaa RCM8	03 Oct 95 - 23 Jul 96
VE1	59.585	-41.162	2292	2312	Aanderaa RCM8	03 Oct 95 - 23 Jul 96

### July 1996 - August 1997

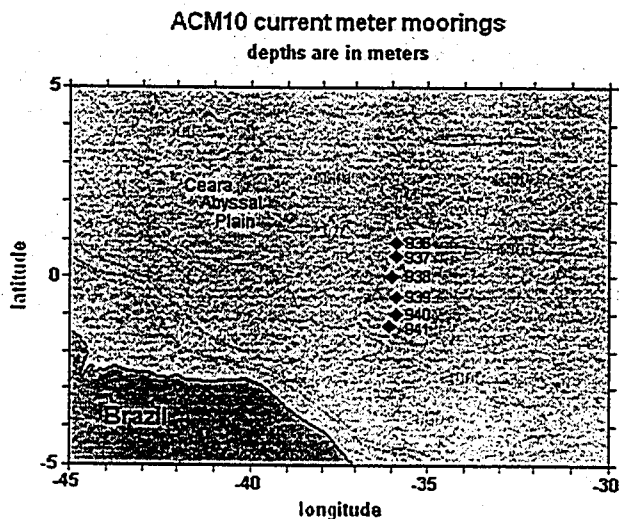
mooring name	lat	lon	instr (meters)	depth water (meters)	depth instr type	dates
VE21	59.418	-40.607	2567	2689	Aanderaa RCM8	23 Jul 96 - 24 Aug 97

ACMS current meter moorings (German component)  
depths are in meters



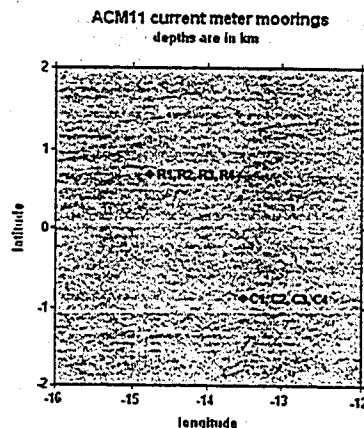
## WOCE component ACM10 Brazil Basin northwestern boundary

mooring name	lat	lon	instr (meters)	depth water (meters)	depth instr type	dates
WHOI 936	0.836	-35.900	3297	4486	VACM	29 Sep 92 - 01 Jun 94
WHOI 936	0.836	-35.900	3896	4486	VACM	29 Sep 92 - 01 Jun 94
WHOI 936	0.836	-35.900	4096	4486	VACM	29 Sep 92 - 01 Jun 94
WHOI 936	0.836	-35.900	4297	4486	VACM	29 Sep 92 - 01 Jun 94
WHOI 937	0.502	-35.903	3900	4540	VACM	29 Sep 92 - 01 Jun 94
WHOI 937	0.502	-35.903	4100	4540	VACM	29 Sep 92 - 01 Jun 94
WHOI 937	0.502	-35.903	4300	4540	VACM	29 Sep 92 - 01 Jun 94
WHOI 938	-0.005	-35.991	2993	4536	VACM	30 Sep 92 - 31 May 94
WHOI 938	-0.005	-35.991	3293	4536	VACM	30 Sep 92 - 31 May 94
WHOI 938	-0.005	-35.991	3593	4536	VACM	30 Sep 92 - 31 May 94
WHOI 938	-0.005	-35.991	3892	4536	VACM	30 Sep 92 - 31 May 94
WHOI 938	-0.005	-35.991	4093	4536	VACM	30 Sep 92 - 31 May 94
WHOI 938	-0.005	-35.991	4292	4536	VACM	30 Sep 92 - 31 May 94
WHOI 938	-0.005	-35.991	4485	4536	VACM	30 Sep 92 - 31 May 94
WHOI 939	-0.501	-35.901	3885	4485	VACM	01 Oct 92 - 31 May 94
WHOI 939	-0.501	-35.901	4085	4485	VACM	01 Oct 92 - 31 May 94
WHOI 939	-0.501	-35.901	4285	4485	VACM	01 Oct 92 - 31 May 94
WHOI 940	-0.980	-35.932	3907	4396	VACM	02 Oct 92 - 30 May 94
WHOI 940	-0.980	-35.932	4107	4396	VACM	02 Oct 92 - 30 May 94
WHOI 940	-0.980	-35.932	4307	4396	VACM	02 Oct 92 - 30 May 94
WHOI 941	-1.332	-36.082	3899	4449	VACM	02 Oct 92 - 03 Jun 94
WHOI 941	-1.332	-36.082	4099	4449	VACM	02 Oct 92 - 03 Jun 94



## WOCE component ACM11 Rochambe and Chain Fracture Zones

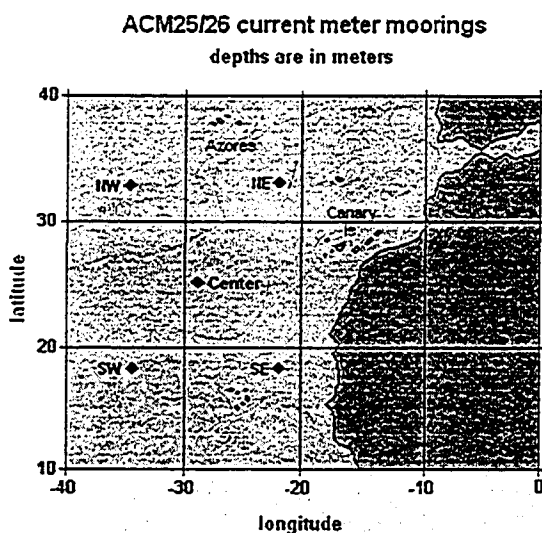
mooring name	lat	lon	instr (meters)	depth water (meters)	depth instr type	dates
R1	0.728	-14.767	1700	4235	Aanderaa RCM5	17 Nov 92 - 31 Oct 94
R1	0.728	-14.767	2000	4235	Aanderaa RCM8	17 Nov 92 - 31 Oct 94
R1	0.728	-14.767	2800	4235	Aanderaa RCM5	17 Nov 92 - 31 Oct 94
R1	0.728	-14.767	3750	4235	Aanderaa RCM8	17 Nov 92 - 31 Oct 94
R1	0.728	-14.767	3950	4235	Aanderaa RCM5	17 Nov 92 - 31 Oct 94
R1	0.728	-14.767	4100	4235	Aanderaa RCM8	17 Nov 92 - 31 Oct 94
R3	0.687	-14.765	3950	4375	Aanderaa RCM5	18 Nov 92 - 31 Oct 94
R3	0.687	-14.765	4100	4375	Aanderaa RCM8	18 Nov 92 - 31 Oct 94
R3	0.687	-14.765	4200	4375	Aanderaa RCM5	09 May 93 - 31 Oct 94
R3	0.687	-14.765	4315	4375	Aanderaa RCM8	18 Nov 92 - 31 Oct 94
R4	0.663	-14.763	1700	4325	Aanderaa RCM5	18 Nov 92 - 01 Nov 94
R4	0.663	-14.763	2000	4325	Aanderaa RCM8	18 Nov 92 - 01 Nov 94
R4	0.663	-14.763	3200	4325	Aanderaa RCM8	18 Nov 92 - 01 Nov 94
R4	0.663	-14.763	3750	4325	Aanderaa RCM5	18 Nov 92 - 01 Nov 94
R4	0.663	-14.763	3950	4325	Aanderaa RCM8	18 Nov 92 - 01 Nov 94
R4	0.663	-14.763	4100	4325	Aanderaa RCM5	18 Nov 92 - 01 Nov 94
R4	0.663	-14.763	4265	4325	Aanderaa RCM8	18 Nov 92 - 01 Nov 94
C1	-0.870	-13.538	1700	4225	Aanderaa RCM5	19 Nov 92 - 02 Nov 94
C1	-0.870	-13.538	2000	4225	Aanderaa RCM8	19 Nov 92 - 02 Nov 94
C1	-0.870	-13.538	2800	4225	Aanderaa RCM5	19 Nov 92 - 02 Nov 94
C1	-0.870	-13.538	3750	4225	Aanderaa RCM8	19 Nov 92 - 02 Nov 94
C1	-0.870	-13.538	3950	4225	Aanderaa RCM5	19 Nov 92 - 02 Nov 94
C1	-0.870	-13.538	4100	4225	Aanderaa RCM8	19 Nov 92 - 02 Nov 94
C1	-0.870	-13.538	4165	4225	Aanderaa RCM5	19 Nov 92 - 26 Jul 94
C2	-0.898	-13.520	3950	4625	Aanderaa RCM8	19 Nov 92 - 02 Nov 94
C2	-0.898	-13.520	4100	4625	Aanderaa RCM5	19 Nov 92 - 02 Nov 94
C2	-0.898	-13.520	4230	4625	Aanderaa RCM8	19 Nov 92 - 02 Nov 94
C2	-0.898	-13.520	4365	4625	Aanderaa RCM5	19 Nov 92 - 02 Nov 94
C2	-0.898	-13.520	4550	4625	Aanderaa RCM8	19 Nov 92 - 02 Nov 94
C3	-0.915	-13.508	3950	4425	Aanderaa RCM8	20 Nov 92 - 03 Nov 94
C3	-0.915	-13.508	4100	4425	Aanderaa RCM5	20 Nov 92 - 03 Nov 94
C3	-0.915	-13.508	4230	4425	Aanderaa RCM8	20 Nov 92 - 03 Nov 94
C3	-0.915	-13.508	4365	4425	Aanderaa RCM5	20 Nov 92 - 03 Nov 94
C4	-0.933	-13.500	1700	4160	Aanderaa RCM5	20 Nov 92 - 03 Nov 94
C4	-0.933	-13.500	2000	4160	Aanderaa RCM8	20 Nov 92 - 03 Nov 94
C4	-0.933	-13.500	3200	4160	Aanderaa RCM5	20 Nov 92 - 03 Nov 94
C4	-0.933	-13.500	3750	4160	Aanderaa RCM8	20 Nov 92 - 03 Nov 94
C4	-0.933	-13.500	3950	4160	Aanderaa RCM5	20 Nov 92 - 03 Nov 94
C4	-0.933	-13.500	4100	4160	Aanderaa RCM8	20 Nov 92 - 03 Nov 94





## WOCE component ACM25/26 (Subduction)

The Subduction experiment produced 232 current meter and temperature records from 5 moorings, each of which was occupied three times.



### ACM25 Center Mooring June 1991 - February 1992

mooring name	lat	lon	instr (meters)	depth water (meters)	depth instr type	dates
Center 1	25.532	-28.953	10	5670	VMCM	23 Jun 91 - 11 Feb 92
Center 1	25.532	-28.953	50	5670	VMCM	23 Jun 91 - 11 Feb 92
Center 1	25.532	-28.953	60	5670	Branker Temp Recorder	23 Jun 91 - 11 Feb 92
Center 1	25.532	-28.953	70	5670	VMCM	23 Jun 91 - 11 Feb 92
Center 1	25.532	-28.953	80	5670	Branker Temp Recorder	23 Jun 91 - 11 Feb 92
Center 1	25.532	-28.953	100	5670	Branker Temp Recorder	23 Jun 91 - 11 Feb 92
Center 1	25.532	-28.953	110	5670	VMCM	23 Jun 91 - 11 Feb 92
Center 1	25.532	-28.953	130	5670	Branker Temp Recorder	23 Jun 91 - 11 Feb 92
Center 1	25.532	-28.953	1500	5670	VMCM	23 Jun 91 - 11 Feb 92
Center 1	25.532	-28.953	3500	5670	VMCM	23 Jun 91 - 11 Feb 92

### February 1992 - October 1992

mooring name	lat	lon	instr (meters)	depth water (meters)	depth instr type	dates
Center 2	25.532	-28.953	1	5670	Branker Temp Recorder	12 Feb 92 - 14 Oct 92
Center 2	25.532	-28.953	10	5670	VMCM	12 Feb 92 - 14 Oct 92
Center 2	25.532	-28.953	30	5670	VMCM	12 Feb 92 - 14 Oct 92
Center 2	25.532	-28.953	50	5670	VMCM	12 Feb 92 - 01 Aug 92
Center 2	25.532	-28.953	60	5670	Branker Temp Recorder	12 Feb 92 - 14 Oct 92
Center 2	25.532	-28.953	70	5670	VMCM	12 Feb 92 - 13 Oct 92
Center 2	25.532	-28.953	80	5670	Branker Temp Recorder	12 Feb 92 - 14 Oct 92
Center 2	25.532	-28.953	90	5670	VMCM	12 Feb 92 - 14 Oct 92

Center 2	25.532	-28.953	100	5670	Branker Temp Recorder	12 Feb 92 - 14 Oct 92
Center 2	25.532	-28.953	110	5670	VMCM	12 Feb 92 - 14 Oct 92
Center 2	25.532	-28.953	130	5670	Branker Temp Recorder	12 Feb 92 - 14 Oct 92
Center 2	25.532	-28.953	150	5670	VMCM	12 Feb 92 - 14 Oct 92
Center 2	25.532	-28.953	200	5670	VMCM	12 Feb 92 - 14 Oct 92
Center 2	25.532	-28.953	300	5670	VMCM	12 Feb 92 - 14 Oct 92
Center 2	25.532	-28.953	310	5670	VMCM	12 Feb 92 - 14 Oct 92
Center 2	25.532	-28.953	400	5670	Branker Temp Recorder	12 Feb 92 - 14 Oct 92
Center 2	25.532	-28.953	580	5670	Branker Temp Recorder	12 Feb 92 - 14 Oct 92
Center 2	25.532	-28.953	1500	5670	VMCM	12 Feb 92 - 14 Oct 92
Center 2	25.532	-28.953	3500	5670	VMCM	12 Feb 92 - 14 Oct 92

### October 1992 - June 1993

mooring name	lat	lon	instr (meters)	depth water (meters)	depth instr type	dates
Center 3	25.532	-28.953	1	5670	Branker Temp Recorder	15 Oct 92 - 16 Jun 93
Center 3	25.532	-28.953	10	5670	VMCM	15 Oct 92 - 16 Jun 93
Center 3	25.532	-28.953	30	5670	VMCM	15 Oct 92 - 16 Jun 93
Center 3	25.532	-28.953	50	5670	VMCM	15 Oct 92 - 16 Jun 93
Center 3	25.532	-28.953	60	5670	Branker Temp Recorder	15 Oct 92 - 16 Jun 93
Center 3	25.532	-28.953	70	5670	VMCM	15 Oct 92 - 15 Jun 93
Center 3	25.532	-28.953	80	5670	Branker Temp Recorder	15 Oct 92 - 07 Jun 93
Center 3	25.532	-28.953	90	5670	VMCM	15 Oct 92 - 16 Jun 93
Center 3	25.532	-28.953	100	5670	Branker Temp Recorder	15 Oct 92 - 16 Jun 93
Center 3	25.532	-28.953	110	5670	VMCM	15 Oct 92 - 16 Jun 93
Center 3	25.532	-28.953	130	5670	Branker Temp Recorder	15 Oct 92 - 16 Jun 93
Center 3	25.532	-28.953	200	5670	VMCM	15 Oct 92 - 16 Jun 93
Center 3	25.532	-28.953	300	5670	VMCM	15 Oct 92 - 16 Jun 93
Center 3	25.532	-28.953	310	5670	VMCM	15 Oct 92 - 16 Jun 93
Center 3	25.532	-28.953	400	5670	Branker Temp Recorder	15 Oct 92 - 07 Jun 93
Center 3	25.532	-28.953	580	5670	Branker Temp Recorder	15 Oct 92 - 07 Jun 93
Center 3	25.532	-28.953	750	5670	VMCM	15 Oct 92 - 16 Jun 93
Center 3	25.532	-28.953	1500	5670	VMCM	15 Oct 92 - 16 Jun 93
Center 3	25.532	-28.953	3500	5670	VMCM	15 Oct 92 - 16 Jun 93

### ACM25 Northeast Mooring June 1991 - February 1992

mooring name	lat	lon	instr (meters)	depth water (meters)	depth instr type	dates
Northeast 1	33.001	-21.996	10	5274	VMCM	18 Jun 91 - 14 Feb 92
Northeast 1	33.001	-21.996	30	5274	VMCM	18 Jun 91 - 14 Feb 92
Northeast 1	33.001	-21.996	50	5274	VMCM	18 Jun 91 - 14 Feb 92
Northeast 1	33.001	-21.996	80	5274	Branker Temp Recorder	18 Jun 91 - 14 Feb 92
Northeast 1	33.001	-21.996	90	5274	VMCM	18 Jun 91 - 14 Feb 92
Northeast 1	33.001	-21.996	130	5274	Branker Temp Recorder	18 Jun 91 - 14 Feb 92
Northeast 1	33.001	-21.996	150	5274	VMCM	18 Jun 91 - 14 Feb 92
Northeast 1	33.001	-21.996	200	5274	VMCM	18 Jun 91 - 14 Feb 92

### February 1992 - October 1992

mooring name	lat	lon	instr (meters)	depth water (meters)	depth instr type	dates
Northeast 2	33.003	-22.004	1	5274	Branker Temp Recorder	20 Feb 92 - 01 Oct 92
Northeast 2	33.003	-22.004	10	5274	VMCM	20 Feb 92 - 01 Oct 92

Northeast 2	33.003	-22.004	30	5274	VMCM	20 Feb 92 - 01 Oct 92
Northeast 2	33.003	-22.004	50	5274	VMCM	20 Feb 92 - 01 Oct 92
Northeast 2	33.003	-22.004	60	5274	Brancker Temp Recorder	20 Feb 92 - 01 Oct 92
Northeast 2	33.003	-22.004	70	5274	VMCM	20 Feb 92 - 01 Oct 92
Northeast 2	33.003	-22.004	80	5274	Brancker Temp Recorder	20 Feb 92 - 01 Oct 92
Northeast 2	33.003	-22.004	90	5274	VMCM	20 Feb 92 - 01 Oct 92
Northeast 2	33.003	-22.004	100	5274	Brancker Temp Recorder	20 Feb 92 - 01 Oct 92
Northeast 2	33.003	-22.004	110	5274	VMCM	20 Feb 92 - 01 Oct 92
Northeast 2	33.003	-22.004	130	5274	Brancker Temp Recorder	20 Feb 92 - 01 Oct 92
Northeast 2	33.003	-22.004	150	5274	VMCM	20 Feb 92 - 01 Oct 92
Northeast 2	33.003	-22.004	200	5274	VMCM	20 Feb 92 - 01 Oct 92
Northeast 2	33.003	-22.004	300	5274	Brancker Temp Recorder	20 Feb 92 - 01 Oct 92
Northeast 2	33.003	-22.004	400	5274	Brancker Temp Recorder	20 Feb 92 - 04 May 92
Northeast 2	33.003	-22.004	580	5274	Brancker Temp Recorder	20 Feb 92 - 01 Oct 92

### October 1992 - June 1993

mooring name	lat	lon	instr (meters)	depth water (meters)	depth instr type	dates
Northeast 3	33.001	-21.996	1	5274	Brancker Temp Recorder	02 Oct 92 - 07 Jun 93
Northeast 3	33.001	-21.996	10	5274	VMCM	02 Oct 92 - 14 Jun 93
Northeast 3	33.001	-21.996	30	5274	VMCM	02 Oct 92 - 11 Apr 93
Northeast 3	33.001	-21.996	50	5274	VMCM	02 Oct 92 - 11 Apr 93
Northeast 3	33.001	-21.996	60	5274	Brancker Temp Recorder	02 Oct 92 - 07 Jun 93
Northeast 3	33.001	-21.996	70	5274	VMCM	02 Oct 92 - 14 Jun 93
Northeast 3	33.001	-21.996	80	5274	Brancker Temp Recorder	02 Oct 92 - 07 Jun 93
Northeast 3	33.001	-21.996	90	5274	VMCM	02 Oct 92 - 14 Jun 93
Northeast 3	33.001	-21.996	100	5274	Brancker Temp Recorder	02 Oct 92 - 07 Jun 93
Northeast 3	33.001	-21.996	110	5274	VMCM	02 Oct 92 - 14 Jun 93
Northeast 3	33.001	-21.996	130	5274	Brancker Temp Recorder	02 Oct 92 - 07 Jun 93
Northeast 3	33.001	-21.996	150	5274	VMCM	02 Oct 92 - 14 Jun 93
Northeast 3	33.001	-21.996	200	5274	VMCM	02 Oct 92 - 14 Jun 93
Northeast 3	33.001	-21.996	300	5274	Brancker Temp Recorder	02 Oct 92 - 07 Jun 93
Northeast 3	33.001	-21.996	400	5274	Brancker Temp Recorder	02 Oct 92 - 14 Jun 93
Northeast 3	33.001	-21.996	580	5274	Brancker Temp Recorder	02 Oct 92 - 14 Jun 93
Northeast 3	33.001	-21.996	750	5274	Brancker Temp Recorder	02 Oct 92 - 14 Jun 93
Northeast 3	33.001	-21.996	1500	5274	Brancker Temp Recorder	02 Oct 92 - 14 Jun 93

### ACM25 Northwest Mooring July 1991 - August 1991

mooring name	lat	lon	instr (meters)	depth water (meters)	depth instr type	dates
Northwest 1	32.910	-33.892	10	3608	Brancker Temp Recorder	03 Jul 91 - 02 Aug 91
Northwest 1	32.910	-33.892	30	3608	Brancker Temp Recorder	03 Jul 91 - 02 Aug 91
Northwest 1	32.910	-33.892	50	3608	Brancker Temp Recorder	03 Jul 91 - 22 Jul 91
Northwest 1	32.910	-33.892	70	3608	Brancker Temp Recorder	03 Jul 91 - 02 Aug 91
Northwest 1	32.910	-33.892	80	3608	Brancker Temp Recorder	03 Jul 91 - 02 Aug 91
Northwest 1	32.910	-33.892	90	3608	Brancker Temp Recorder	03 Jul 91 - 02 Aug 91
Northwest 1	32.910	-33.892	110	3608	Brancker Temp Recorder	03 Jul 91 - 02 Aug 91
Northwest 1	32.910	-33.892	150	3608	VMCM	03 Jul 91 - 02 Aug 91
Northwest 1	32.910	-33.892	200	3608	VMCM	03 Jul 91 - 02 Aug 91

## February 1992 - October 1992

mooring name	lat	lon	instr (meters)	depth water (meters)	depth instr type	dates
Northwest 2	32.907	-33.889	1	3608	Brancker Temp Recorder	24 Feb 92 - 23 Oct 92
Northwest 2	32.907	-33.889	10	3608	Brancker Temp Recorder	24 Feb 92 - 23 Oct 92
Northwest 2	32.907	-33.889	30	3608	Brancker Temp Recorder	24 Feb 92 - 23 Oct 92
Northwest 2	32.907	-33.889	50	3608	Brancker Temp Recorder	24 Feb 92 - 23 Oct 92
Northwest 2	32.907	-33.889	60	3608	Brancker Temp Recorder	24 Feb 92 - 23 Oct 92
Northwest 2	32.907	-33.889	70	3608	Brancker Temp Recorder	24 Feb 92 - 23 Oct 92
Northwest 2	32.907	-33.889	80	3608	Brancker Temp Recorder	24 Feb 92 - 23 Oct 92
Northwest 2	32.907	-33.889	90	3608	Brancker Temp Recorder	24 Feb 92 - 23 Oct 92
Northwest 2	32.907	-33.889	100	3608	Brancker Temp Recorder	24 Feb 92 - 23 Oct 92
Northwest 2	32.907	-33.889	110	3608	Brancker Temp Recorder	24 Feb 92 - 23 Oct 92
Northwest 2	32.907	-33.889	130	3608	Brancker Temp Recorder	24 Feb 92 - 23 Oct 92
Northwest 2	32.907	-33.889	150	3608	VMCM	24 Feb 92 - 17 Jun 92
Northwest 2	32.907	-33.889	300	3608	Brancker Temp Recorder	24 Feb 92 - 23 Oct 92
Northwest 2	32.907	-33.889	400	3608	Brancker Temp Recorder	24 Feb 92 - 23 Oct 92
Northwest 2	32.907	-33.889	580	3608	Brancker Temp Recorder	24 Feb 92 - 23 Oct 92
Northwest 2	32.907	-33.889	750	3608	Brancker Temp Recorder	24 Feb 92 - 23 Oct 92
Northwest 2	32.907	-33.889	1500	3608	Brancker Temp Recorder	24 Feb 92 - 23 Oct 92

## October 1992 - March 1993

mooring name	lat	lon	Instr (meters)	depth water (meters)	depth instr type	dates
Northwest 3	32.906	-33.893	1	3608	Brancker Temp Recorder	24 Oct 92 - 12 Mar 93
Northwest 3	32.906	-33.893	10	3608	Brancker Temp Recorder	24 Oct 92 - 12 Mar 93
Northwest 3	32.906	-33.893	30	3608	Brancker Temp Recorder	24 Oct 92 - 12 Mar 93
Northwest 3	32.906	-33.893	50	3608	Brancker Temp Recorder	24 Oct 92 - 12 Mar 93
Northwest 3	32.906	-33.893	60	3608	Brancker Temp Recorder	24 Oct 92 - 12 Mar 93
Northwest 3	32.906	-33.893	70	3608	Brancker Temp Recorder	24 Oct 92 - 12 Mar 93
Northwest 3	32.906	-33.893	80	3608	Brancker Temp Recorder	24 Oct 92 - 12 Mar 93
Northwest 3	32.906	-33.893	90	3608	Brancker Temp Recorder	24 Oct 92 - 12 Mar 93
Northwest 3	32.906	-33.893	100	3608	Brancker Temp Recorder	24 Oct 92 - 12 Mar 93
Northwest 3	32.906	-33.893	110	3608	Brancker Temp Recorder	24 Oct 92 - 12 Mar 93
Northwest 3	32.906	-33.893	130	3608	Brancker Temp Recorder	24 Oct 92 - 12 Mar 93
Northwest 3	32.906	-33.893	150	3608	VMCM	24 Oct 92 - 12 Mar 93
Northwest 3	32.906	-33.893	200	3608	VMCM	24 Oct 92 - 12 Mar 93
Northwest 3	32.906	-33.893	300	3608	Brancker Temp Recorder	24 Oct 92 - 12 Mar 93
Northwest 3	32.906	-33.893	400	3608	Brancker Temp Recorder	24 Oct 92 - 12 Mar 93
Northwest 3	32.906	-33.893	580	3608	Brancker Temp Recorder	24 Oct 92 - 12 Mar 93
Northwest 3	32.906	-33.893	750	3608	Brancker Temp Recorder	24 Oct 92 - 12 Mar 93
Northwest 3	32.906	-33.893	1500	3608	Brancker Temp Recorder	24 Oct 92 - 12 Mar 93

## ACM25 Southeast Mooring June 1991 - October 1991

mooring name	lat	lon	instr (meters)	depth water (meters)	depth instr type	dates
Southeast 1	18.002	-22.000	10	3297	VMCM	29 Jun 91 - 29 Sep 91
Southeast 1	18.002	-22.000	70	3297	Brancker Temp Recorder	29 Jun 91 - 09 Oct 91
Southeast 1	18.002	-22.000	80	3297	Brancker Temp Recorder	29 Jun 91 - 09 Oct 91
Southeast 1	18.002	-22.000	90	3297	Brancker Temp Recorder	29 Jun 91 - 09 Oct 91
Southeast 1	18.002	-22.000	100	3297	Brancker Temp Recorder	29 Jun 91 - 09 Oct 91
Southeast 1	18.002	-22.000	110	3297	Brancker Temp Recorder	01 Jul 91 - 30 Sep 91
Southeast 1	18.002	-22.000	130	3297	Brancker Temp Recorder	01 Jul 91 - 30 Sep 91
Southeast 1	18.002	-22.000	150	3297	Brancker Temp Recorder	01 Jul 91 - 30 Sep 91
Southeast 1	18.002	-22.000	200	3297	Brancker Temp Recorder	01 Jul 91 - 30 Sep 91
Southeast 1	18.002	-22.000	300	3297	Brancker Temp Recorder	01 Jul 91 - 30 Sep 91
Southeast 1	18.002	-22.000	400	3297	Brancker Temp Recorder	01 Jul 91 - 30 Sep 91
Southeast 1	18.002	-22.000	750	3297	Brancker Temp Recorder	01 Jul 91 - 30 Sep 91

## February 1992 - October 1992

mooring name	lat	lon	instr (meters)	depth water (meters)	depth instr type	dates
Southeast 2	17.995	-22.005	1	3297	Brancker Temp Recorder	09 Feb 92 - 06 Oct 92
Southeast 2	17.995	-22.005	10	3297	VMCM	09 Feb 92 - 06 Oct 92
Southeast 2	17.995	-22.005	30	3297	VMCM	09 Feb 92 - 06 Oct 92
Southeast 2	17.995	-22.005	50	3297	VMCM	09 Feb 92 - 03 Jun 92
Southeast 2	17.995	-22.005	60	3297	Brancker Temp Recorder	09 Feb 92 - 06 Oct 92
Southeast 2	17.995	-22.005	70	3297	Brancker Temp Recorder	09 Feb 92 - 06 Oct 92
Southeast 2	17.995	-22.005	100	3297	Brancker Temp Recorder	09 Feb 92 - 06 Oct 92
Southeast 2	17.995	-22.005	580	3297	Brancker Temp Recorder	09 Feb 92 - 06 Oct 92
Southeast 2	17.995	-22.005	1500	3297	Brancker Temp Recorder	09 Feb 92 - 06 Oct 92

## October 1992 - June 1993

mooring name	lat	lon	instr (meters)	depth water (meters)	depth instr type	dates
Southeast 3	17.995	-22.005	1	3297	Brancker Temp Recorder	07 Oct 92 - 07 Jun 93
Southeast 3	17.995	-22.005	10	3297	VMCM	07 Oct 92 - 19 Jun 93
Southeast 3	17.995	-22.005	30	3297	VMCM	07 Oct 92 - 19 Jun 93
Southeast 3	17.995	-22.005	50	3297	VMCM	07 Oct 92 - 19 Jun 93
Southeast 3	17.995	-22.005	60	3297	Brancker Temp Recorder	07 Oct 92 - 07 Jun 93
Southeast 3	17.995	-22.005	80	3297	Brancker Temp Recorder	07 Oct 92 - 19 Jun 93
Southeast 3	17.995	-22.005	90	3297	Brancker Temp Recorder	07 Oct 92 - 19 Jun 93
Southeast 3	17.995	-22.005	110	3297	Brancker Temp Recorder	07 Oct 92 - 19 Jun 93
Southeast 3	17.995	-22.005	130	3297	Brancker Temp Recorder	07 Oct 92 - 19 Jun 93
Southeast 3	17.995	-22.005	150	3297	Brancker Temp Recorder	07 Oct 92 - 19 Jun 93
Southeast 3	17.995	-22.005	200	3297	Brancker Temp Recorder	07 Oct 92 - 19 Jun 93
Southeast 3	17.995	-22.005	300	3297	Brancker Temp Recorder	07 Oct 92 - 19 Jun 93
Southeast 3	17.995	-22.005	400	3297	Brancker Temp Recorder	07 Oct 92 - 19 Jun 93
Southeast 3	17.995	-22.005	580	3297	Brancker Temp Recorder	07 Oct 92 - 07 Jun 93
Southeast 3	17.995	-22.005	750	3297	Brancker Temp Recorder	07 Oct 92 - 19 Jun 93
Southeast 3	17.995	-22.005	1500	3297	Brancker Temp Recorder	07 Oct 92 - 07 Jun 93

## ACM25 Southwest Mooring

June 1991 - November 1991

mooring name	lat	lon	instr (meters)	depth water (meters)	depth instr type	dates
Southwest 1	18.000	-33.993	10	5300	VMCM	25 Jun 91 - 02 Nov 91
Southwest 1	18.000	-33.993	30	5300	VMCM	25 Jun 91 - 02 Nov 91
Southwest 1	18.000	-33.993	50	5300	VMCM	25 Jun 91 - 02 Nov 91
Southwest 1	18.000	-33.993	60	5300	Brancker Temp Recorder	25 Jun 91 - 02 Nov 91
Southwest 1	18.000	-33.993	70	5300	VMCM	25 Jun 91 - 02 Nov 91
Southwest 1	18.000	-33.993	80	5300	Brancker Temp Recorder	25 Jun 91 - 02 Nov 91
Southwest 1	18.000	-33.993	90	5300	VMCM	25 Jun 91 - 02 Nov 91
Southwest 1	18.000	-33.993	100	5300	Brancker Temp Recorder	25 Jun 91 - 02 Nov 91
Southwest 1	18.000	-33.999	130	5300	Brancker Temp Recorder	25 Jun 91 - 02 Nov 91
Southwest 1	18.000	-33.993	150	5300	VMCM	25 Jun 91 - 02 Nov 91
Southwest 1	18.000	-33.993	200	5300	VMCM	25 Jun 91 - 02 Nov 91
Southwest 1	18.000	-33.999	300	5300	Brancker Temp Recorder	25 Jun 91 - 02 Nov 91
Southwest 1	18.000	-33.999	400	5300	Brancker Temp Recorder	25 Jun 91 - 02 Nov 91
Southwest 1	18.000	-33.993	580	5300	Brancker Temp Recorder	25 Jun 91 - 02 Nov 91

February 1992 - June 1992

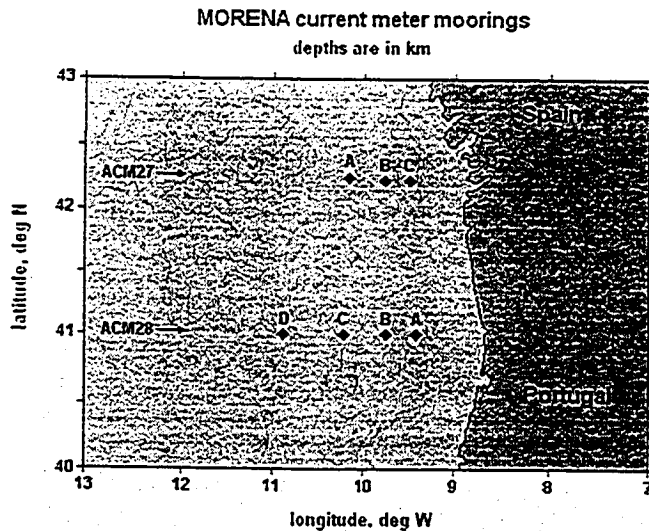
mooring name	lat	lon	instr (meters)	depth water (meters)	depth instr type	dates
Southwest 2	17.999	-34.011	1	5300	Brancker Temp Recorder	05 Feb 92 - 03 Jun 92
Southwest 2	17.999	-34.011	10	5300	VMCM	05 Feb 92 - 03 Jun 92
Southwest 2	17.999	-34.011	30	5300	VMCM	05 Feb 92 - 03 Jun 92
Southwest 2	17.999	-34.011	50	5300	VMCM	05 Feb 92 - 03 Jun 92
Southwest 2	17.999	-34.011	60	5300	Brancker Temp Recorder	05 Feb 92 - 03 Jun 92
Southwest 2	17.999	-34.011	70	5300	VMCM	05 Feb 92 - 03 Jun 92
Southwest 2	17.999	-34.011	80	5300	Brancker Temp Recorder	05 Feb 92 - 03 Jun 92
Southwest 2	17.999	-34.011	90	5300	VMCM	05 Feb 92 - 03 Jun 92
Southwest 2	17.999	-34.011	110	5300	VMCM	05 Feb 92 - 03 Jun 92
Southwest 2	17.999	-34.011	130	5300	Brancker Temp Recorder	05 Feb 92 - 03 Jun 92
Southwest 2	17.999	-34.011	150	5300	VMCM	05 Feb 92 - 03 Jun 92
Southwest 2	17.999	-34.011	200	5300	VMCM	05 Feb 92 - 03 Jun 92
Southwest 2	17.999	-34.011	300	5300	Brancker Temp Recorder	05 Feb 92 - 23 Feb 92
Southwest 2	17.999	-34.011	580	5300	Brancker Temp Recorder	05 Feb 92 - 23 Feb 92
Southwest 2	17.999	-34.011	1500	5300	Brancker Temp Recorder	05 Feb 92 - 23 Feb 92

October 1992 - May 1993

mooring name	lat	lon	instr (meters)	depth water (meters)	depth instr type	dates
Southwest 3	18.093	-33.900	1	5300	Brancker Temp Recorder	11 Oct 92 - 19 Feb 93
Southwest 3	18.093	-33.900	10	5300	VMCM	11 Oct 92 - 21 May 93
Southwest 3	18.093	-33.900	30	5300	VMCM	11 Oct 92 - 21 May 93
Southwest 3	18.093	-33.900	50	5300	VMCM	11 Oct 92 - 21 May 93
Southwest 3	18.093	-33.900	60	5300	Brancker Temp Recorder	11 Oct 92 - 21 May 93
Southwest 3	18.093	-33.900	70	5300	VMCM	11 Oct 92 - 21 May 93
Southwest 3	18.093	-33.900	90	5300	VMCM	11 Oct 92 - 21 May 93
Southwest 3	18.093	-33.900	100	5300	Brancker Temp Recorder	11 Oct 92 - 19 Feb 93
Southwest 3	18.093	-33.900	110	5300	VMCM	11 Oct 92 - 21 May 93
Southwest 3	18.093	-33.900	130	5300	Brancker Temp Recorder	11 Oct 92 - 21 May 93
Southwest 3	18.093	-33.900	150	5300	VMCM	11 Oct 92 - 21 May 93
Southwest 3	18.093	-33.900	200	5300	VMCM	11 Oct 92 - 21 May 93

Southwest 3	18.093	-33.900	300	5300	Brancker Temp Recorder	11 Oct 92 - 21 May 93
Southwest 3	18.093	-33.900	400	5300	Brancker Temp Recorder	11 Oct 92 - 19 Feb 93
Southwest 3	18.093	-33.900	750	5300	Brancker Temp Recorder	11 Oct 92 - 19 Feb 93
Southwest 3	18.093	-33.900	1500	5300	Brancker Temp Recorder	11 Oct 92 - 19 Feb 93

**WOCE component ACM27  
(part of the MORENA Project)**



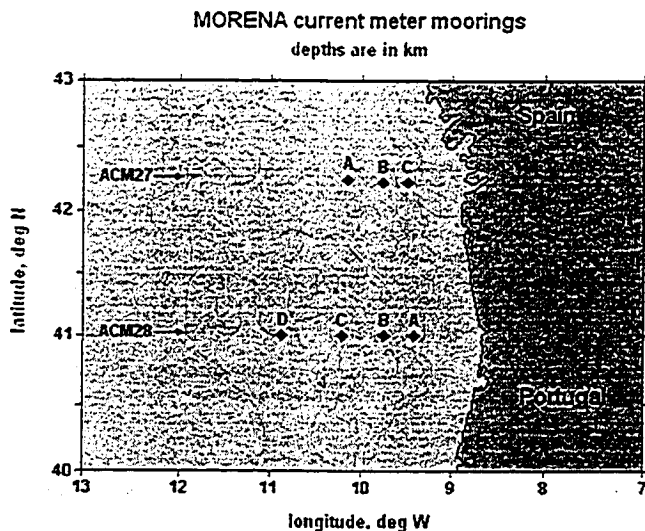
**May 1993 - May 1994**

mooring name	lat	lon	instr (meters)	depth water (meters)	depth	instr type	dates
Mooring A	42.267	-10.150	56	2700		Aanderaa RCM4S	29 May 93 - 04 May 94
Mooring A	42.267	-10.150	256	2700		Aanderaa RCM4S	29 May 93 - 04 May 94
Mooring A	42.267	-10.150	1156	2700		Aanderaa RCM4S	29 May 93 - 04 May 94
Mooring A	42.267	-10.150	2000	2700		Aanderaa RCM7	29 May 93 - 04 Mar 94

**May 1994 - November 1994**

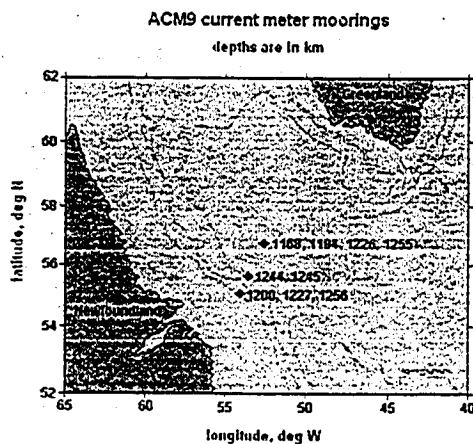
mooring name	lat	lon	instr (meters)	depth water (meters)	depth	instr type	dates
Mooring B	42.218	-9.802	337	2337		Aanderaa RCM4S	06 May 94 - 17 Nov 94
Mooring B	42.218	-9.802	837	2337		Aanderaa RCM4S	07 May 94 - 15 Nov 94
Mooring B	42.218	-9.802	2037	2337		Aanderaa RCM7	06 May 94 - 17 Nov 94
Mooring C	42.218	-9.509	338	1338		Aanderaa RCM4S	06 May 94 - 16 Nov 94
Mooring C	42.218	-9.509	838	1338		Aanderaa RCM4S	07 May 94 - 14 Nov 94
Mooring C	42.218	-9.509	1238	1338		Aanderaa RCM7	07 May 94 - 16 Nov 94

## WOCE component ACM28 (part of the MORENA Project)



mooring name	lat	lon	Instr (meters)	depth water (meters)	depth	instr type	dates
Mooring A	40.999	-9.475	294	1293		Aanderaa RCM7	31 May 93 - 23 Jun 93
Mooring A	40.999	-9.475	794	1293		Aanderaa RCM7	31 May 93 - 17 Jul 93
Mooring A	40.999	-9.475	1194	1293		Aanderaa RCM7	31 May 93 - 31 May 95
Mooring B	41.003	-9.748	843	2543		Aanderaa RCM7	30 May 93 - 01 Jun 95
Mooring B	41.003	-9.748	1243	2543		Aanderaa RCM7	30 May 93 - 01 Jun 95
Mooring B	41.003	-9.748	2243	2543		Aanderaa RCM8	30 May 93 - 01 Jun 95
Mooring C	41.016	-10.254	885	4085		Aanderaa RCM8	22 Nov 93 - 19 Sep 94
Mooring C	41.016	-10.254	1285	4085		Aanderaa RCM7	22 Nov 93 - 19 Sep 94
Mooring C	41.016	-10.254	3085	4085		Aanderaa RCM8	22 Nov 93 - 19 Sep 94
Mooring D	41.036	-10.908	153	3853		Aanderaa RCM4S	22 Nov 93 - 19 Sep 94
Mooring D	41.036	-10.908	653	3853		Aanderaa RCM7	22 Nov 93 - 19 Sep 94
Mooring D	41.036	-10.908	2853	3853		Aanderaa RCM8	22 Nov 93 - 19 Sep 94

## WOCE component ACM29 (Labrador Sea)





## May 1994 - June 1995

mooring name	lat	lon	instr (meters)	depth water (meters)	depth instr type	dates
1168	56.753	-52.455	110	3510	Aanderaa RCM8	29 May 94 - 13 Jun 95
1168	56.753	-52.455	760	3510	Aanderaa RCM8	29 May 94 - 13 Jun 95
1168	56.753	-52.455	1260	3510	Aanderaa RCM8	29 May 94 - 13 Jun 95
1168	56.753	-52.455	1760	3510	Aanderaa RCM8	29 May 94 - 13 Jun 95
1168	56.753	-52.455	2510	3510	Aanderaa RCM8	29 May 94 - 13 Jun 95
1168	56.753	-52.455	3476	3510	Aanderaa RCM8	29 May 94 - 13 Jun 95

## June 1995 - May 1996

mooring name	lat	lon	instr (meters)	depth water (meters)	depth instr type	dates
1194	56.752	-52.456	102	3502	Aanderaa RCM8	13 Jun 95 - 21 May 96
1194	56.752	-52.456	2502	3502	Aanderaa RCM8	13 Jun 95 - 21 May 96
1194	56.752	-52.456	3468	3502	Aanderaa RCM8	13 Jun 95 - 21 May 96
1200	55.122	-54.096	1000	1067	Aanderaa RCM8	12 Jun 95 - 19 May 96

## May 1996 - June 1998

mooring name	lat	lon	instr (meters)	depth water (meters)	depth instr type	dates
1227	55.120	-54.085	980	1000	Aanderaa RCM5	19 May 96 - 27 May 97
1226	56.744	-52.444	763	3513	Aanderaa RCM5	24 Oct 96 - 24 May 97
1226	56.744	-52.444	1263	3513	Aanderaa RCM5	24 Oct 96 - 24 May 97
1226	56.744	-52.444	2513	3513	Aanderaa RCM5	24 Oct 96 - 24 May 97
1226	56.744	-52.444	3479	3513	Aanderaa RCM5	24 Oct 96 - 24 May 97
1244	55.479	-53.655	201	2801	Aanderaa RCM5	21 Oct 96 - 27 Jun 98
1244	55.479	-53.655	1001	2801	Aanderaa RCM5	21 Oct 96 - 27 Jun 98
1244	55.479	-53.655	1501	2801	Aanderaa RCM5	21 Oct 96 - 27 Jun 98
1244	55.479	-53.655	2751	2801	Aanderaa RCM5	21 Oct 96 - 27 Jun 98
1255	56.725	-52.482	1750	3518	Aanderaa RCM8	25 May 97 - 04 Jun 98
1255	56.725	-52.482	2500	3518	Aanderaa RCM8	26 May 97 - 30 Jun 98
1256	55.122	-54.087	980	1061	Aanderaa RCM8	27 May 97 - 27 Jun 98

## Pre-WOCE Atlantic Ocean data

The following are the datasets that were available for the pre-WOCE period. These are roughly ordered by time, with the earliest experiments at the top of the list.

Rise Array (northwest Atlantic), 1974  
 POLYMODE (northwest Atlantic), 1974 - 1977  
 Moorings from the Bedford Institute, 1976 - 1980  
 Local Dynamics Experiment (northwest Atlantic), 1978 - 1979  
 Gulf Stream Extension, 1979 - 1980  
 LOTUS (northwest Atlantic), 1980 - 1984  
 Low Level Waste Ocean Dumping Project East, 1980 - 1984  
 CONSLEX (north Atlantic), 1982 - 1983  
 NEADS (north Atlantic), 1982 - 1983  
 Abyssal Circulation (northeast Atlantic), 1983 - 1984  
 Nares Abyssal Plain moorings, 1983 - 1986

## Rise Array

All of these files have a one-hour time increment. They were recorded originally with a time increment of 15 minutes but were low-pass filtered and subsampled at OSU.

mooring name	lat	lon	instr (meters)	depth water (meters)	depth instr type	dates
WHOI 524	39.125	-69.998	197	2893	VACM	11 Apr 74 - 05 Dec 74
WHOI 524	39.125	-69.998	202	2893	VACM	11 Apr 74 - 05 Dec 74
WHOI 524	39.125	-69.998	496	2893	VACM	11 Apr 74 - 05 Dec 74
WHOI 524	39.125	-69.998	1005	2893	DT-VACM	11 Apr 74 - 05 Dec 74
WHOI 524	39.125	-69.998	2013	2893	VACM	11 Apr 74 - 05 Dec 74
WHOI 524	39.125	-69.998	2512	2893	VACM	11 Apr 74 - 05 Dec 74
WHOI 525	39.118	-70.543	195	2801	VACM	12 Apr 74 - 05 Dec 74
WHOI 525	39.118	-70.543	997	2801	VACM	12 Apr 74 - 05 Dec 74
WHOI 525	39.118	-70.543	2005	2801	VACM	12 Apr 74 - 05 Dec 74
WHOI 526	38.783	-70.008	2006	3267	VACM	12 Apr 74 - 05 Dec 74
WHOI 526	38.783	-70.008	2810	3267	VACM	13 Apr 74 - 05 Dec 74
WHOI 527	39.163	-68.997	1977	3248	VACM	13 Apr 74 - 06 Dec 74
WHOI 527	39.163	-68.997	2781	3248	VACM	16 Apr 74 - 06 Dec 74
WHOI 528	38.587	-69.168	2329	3708	DT-VACM	13 Apr 74 - 06 Dec 74
WHOI 529	38.357	-69.993	2483	3683	VACM	13 Apr 74 - 06 Dec 74
WHOI 529	38.357	-69.993	3283	3683	VACM	14 Apr 74 - 06 Dec 74
WHOI 530	38.008	-70.010	2818	3802	VACM	14 Apr 74 - 13 Dec 74
WHOI 531	38.003	-69.308	3724	3933	VACM	15 Apr 74 - 12 Dec 74
WHOI 532	37.497	-69.332	3213	4398	DT-VACM	15 Apr 74 - 13 Dec 74
WHOI 533	37.505	-70.007	3182	4228	VACM	15 Apr 74 - 13 Dec 74
WHOI 533	37.505	-70.007	3981	4228	DT-VACM	16 Apr 74 - 13 Dec 74
WHOI 534	37.007	-69.997	3337	4349	VACM	16 Apr 74 - 15 Dec 74
WHOI 534	37.007	-69.997	4138	4349	VACM	16 Apr 74 - 15 Dec 74
WHOI 535	36.988	-69.328	3453	4483	VACM	16 Apr 74 - 13 Dec 74
WHOI 536	36.502	-69.332	3466	4502	VACM	17 Apr 74 - 14 Dec 74
WHOI 536	36.502	-69.332	4267	4502	VACM	16 Apr 74 - 14 Dec 74
WHOI 537	36.497	-70.000	4262	4484	VACM	17 Apr 74 - 15 Dec 74

## POLYMODE

All of these files have a one-hour time increment. Those from VACMs were recorded originally with a time increment of 15 minutes, but were low-pass filtered and subsampled prior to being included in the dataset.

mooring name	lat	lon	Instr (meters)	depth water (meters)	depth instr type	dates
WHOI 547	28.210	-54.943	496	5609	VACM	04 Aug 74 - 12 May 75
WHOI 547	28.210	-54.943	996	5609	VACM	05 Aug 74 - 12 May 75
WHOI 547	28.210	-54.943	4000	5609	VACM	04 Aug 74 - 30 Mar 75
WHOI 548	31.025	-60.072	2001	5550	VACM	06 Aug 74 - 09 May 75
WHOI 548	31.025	-60.072	4001	5550	VACM	06 Aug 74 - 08 Mar 75
WHOI 565	35.600	-55.083	4046	5162	VACM	10 May 75 - 17 Dec 75
WHOI 566	34.891	-55.028	604	5515	VACM	10 May 75 - 16 Dec 75
WHOI 566	34.891	-55.028	1005	5515	VACM	10 May 75 - 16 Dec 75
WHOI 566	34.891	-55.028	1505	5515	Geodyne 850	09 May 75 - 17 Dec 75
WHOI 566	34.891	-55.028	4006	5515	VACM	10 May 75 - 16 Dec 75
WHOI 567	31.598	-55.083	628	5296	VACM	15 May 75 - 14 Dec 75
WHOI 567	31.598	-55.083	1028	5296	VACM	15 May 75 - 14 Dec 75
WHOI 567	31.598	-55.083	4030	5296	VACM	15 May 75 - 14 Dec 75

WHOI 568	35.930	-59.028	4001	5205	VACM	16 May 75 - 09 Aug 75
WHOI 568	35.930	-59.028	599	5205	VACM	16 May 75 - 19 Dec 75
WHOI 568	35.930	-59.028	1000	5205	VACM	16 May 75 - 19 Dec 75
WHOI 568	35.930	-59.028	1500	5205	Geodyne 850	16 May 75 - 19 Dec 75
WHOI 580	31.587	-54.933	1494	5587	Geodyne 850	16 Dec 75 - 18 Oct 76
WHOI 580	31.587	-54.933	3995	5587	VACM	17 Dec 75 - 17 Oct 76
WHOI 581	34.927	-55.078	587	5502	VACM	19 Dec 75 - 15 Oct 76
WHOI 581	34.927	-55.078	990	5502	VACM	19 Dec 75 - 15 Oct 76
WHOI 581	34.927	-55.078	1494	5502	Geodyne 850	18 Dec 75 - 29 Feb 76
WHOI 581	34.927	-55.078	3995	5502	VACM	19 Dec 75 - 15 Oct 76
WHOI 582	35.600	-55.083	588	5107	VACM	20 Dec 75 - 14 Oct 76
WHOI 582	35.600	-55.083	3996	5107	VACM	20 Dec 75 - 14 Oct 76
WHOI 583	35.875	-55.042	605	5043	VACM	20 Dec 75 - 03 Mar 76
WHOI 583	35.875	-55.042	1008	5043	VACM	18 Apr 76 - 13 Oct 76
WHOI 583	35.875	-55.042	1492	5043	Geodyne 850	19 Dec 75 - 14 Oct 76
WHOI 583	35.875	-55.042	3993	5043	VACM	20 Dec 75 - 13 Oct 76
WHOI 584	35.948	-59.025	996	5202	VACM	21 Dec 75 - 01 Oct 76
WHOI 584	35.948	-59.025	1499	5202	Geodyne 850	20 Dec 75 - 02 Oct 76
WHOI 584	35.948	-59.025	4000	5202	VACM	21 Dec 75 - 01 Oct 76
WHOI 598	35.922	-59.038	1000	5206	VACM	04 Oct 76 - 26 May 77
WHOI 598	35.922	-59.038	1500	5206	Geodyne 850	03 Oct 76 - 27 May 77
WHOI 598	35.922	-59.038	4000	5206	VACM	04 Oct 76 - 26 May 77
WHOI 599	35.957	-55.463	3997	5457	VACM	05 Oct 76 - 27 May 77
WHOI 600	35.922	-54.740	599	5318	VACM	06 Oct 76 - 28 May 77
WHOI 600	35.922	-54.740	999	5318	VACM	06 Oct 76 - 28 May 77
WHOI 600	35.922	-54.740	1498	5318	Geodyne 850	05 Oct 76 - 29 May 77
WHOI 600	35.922	-54.740	3999	5318	VACM	06 Oct 76 - 28 May 77
WHOI 601	35.958	-53.782	603	5467	VACM	07 Oct 76 - 28 May 77
WHOI 601	35.958	-53.782	1003	5467	VACM	07 Oct 76 - 28 May 77
WHOI 601	35.958	-53.782	1503	5467	Geodyne 850	26 Oct 76 - 29 May 77
WHOI 601	35.958	-53.782	4003	5467	VACM	07 Oct 76 - 28 May 77
WHOI 602	41.490	-54.967	3993	4772	VACM	09 Oct 76 - 07 Jul 77
WHOI 603	40.452	-55.050	3996	5173	VACM	11 Oct 76 - 06 Jul 77
WHOI 604	39.487	-55.013	4002	5266	VACM	12 Oct 76 - 05 Jul 77
WHOI 605	38.480	-54.935	4003	5340	VACM	13 Oct 76 - 04 Jul 77
WHOI 605	38.480	-54.935	5240	5340	VACM	13 Oct 76 - 04 Jul 77
WHOI 606	37.488	-54.993	1014	5334	VACM	14 Oct 76 - 03 Jul 77
WHOI 606	37.488	-54.993	1513	5334	Geodyne 850	13 Oct 76 - 04 Jul 77
WHOI 606	37.488	-54.993	4013	5334	VACM	14 Oct 76 - 03 Jul 77
WHOI 607	36.500	-55.000	647	5445	VACM	15 Oct 76 - 15 Feb 77
WHOI 607	36.500	-55.000	4047	5445	VACM	15 Oct 76 - 02 Jul 77
WHOI 608	35.880	-55.077	605	5054	VACM	17 Oct 76 - 02 Jul 77
WHOI 608	35.880	-55.077	1005	5054	VACM	17 Oct 76 - 08 Apr 77
WHOI 612	31.587	-54.933	2503	5595	VACM	21 Oct 76 - 20 Jun 77
WHOI 612	31.587	-54.933	4003	5595	VACM	21 Oct 76 - 20 Jun 77

### Bedford Institute of Oceanography moorings

All of the time series in these files were low-pass filtered and decimated to one point per day.

#### November 1976 - May 1977

mooring name	lat	lon	instr (meters)	depth water (meters)	depth instr type	dates
129	40.468	-55.238	4000	5115	Aanderaa	05 Nov 76 - 11 May 77
130	40.477	-55.587	4000	5116	Aanderaa	05 Nov 76 - 10 May 77
131	40.463	-56.058	4000	5153	Aanderaa	07 Nov 76 - 10 May 77

## May 1978 - December 1978

mooring name	lat	lon	instr (meters)	depth water (meters)	depth instr type	dates
270	38.248	-50.121	4760	5420	Aanderaa	11 May 78 - 30 Nov 78
271	37.998	-49.640	4000	5420	Aanderaa	10 May 78 - 02 Dec 78
271	37.998	-49.640	4762	5420	Aanderaa	10 May 78 - 02 Dec 78
271	37.998	-49.640	4764	5420	Aanderaa	10 May 78 - 02 Dec 78

## December 1978 - September 1979

mooring name	lat	lon	instr (meters)	depth water (meters)	depth instr type	dates
312	37.762	-50.132	990	5420	Aanderaa	05 Dec 78 - 09 Sep 79
312	37.762	-50.132	1200	5420	Aanderaa	05 Dec 78 - 21 Feb 79
312	37.762	-50.132	1500	5420	Aanderaa	05 Dec 78 - 12 Sep 79
312	37.762	-50.132	3980	5420	Aanderaa	05 Dec 78 - 01 Jul 79
313	37.988	-49.632	1010	5420	Aanderaa	05 Dec 78 - 13 Sep 79
313	37.988	-49.632	1240	5420	Aanderaa	05 Dec 78 - 13 Sep 79
313	37.988	-49.632	1540	5420	Aanderaa	05 Dec 78 - 16 Aug 79
313	37.988	-49.632	4030	5420	Aanderaa	05 Dec 78 - 13 Sep 79
314	38.238	-50.142	5320	5420	Aanderaa	02 Dec 78 - 12 Sep 79

## September 1979 - April 1980

mooring name	lat	lon	instr (meters)	depth water (meters)	depth instr type	dates
346	39.610	-42.147	480	4995	Aanderaa	28 Sep 79 - 28 Apr 80
346	39.610	-42.147	790	4995	Aanderaa	28 Sep 79 - 28 Apr 80
346	39.610	-42.147	1490	4995	Aanderaa	28 Sep 79 - 28 Apr 80
346	39.610	-42.147	4000	4995	Aanderaa	28 Sep 79 - 28 Apr 80
347	38.457	-42.475	470	5080	Aanderaa	27 Sep 79 - 29 Apr 80
347	38.457	-42.475	1470	5080	Aanderaa	27 Sep 79 - 29 Apr 80
347	38.457	-42.475	4000	5080	Aanderaa	27 Sep 79 - 30 Apr 80

## Local Dynamics Experiment

All of these files have a one-hour time increment. They were recorded originally with a time increment of 15 minutes and were low-pass filtered and subsampled at OSU.

mooring name	lat	lon	instr (meters)	depth water (meters)	depth instr type	dates
WHOI 638	31.385	-69.482	636	5239	VACM	01 May 78 - 24 Dec 78
WHOI 639	31.163	-69.367	611	5211	VACM	01 May 78 - 24 Dec 78
WHOI 639	31.163	-69.367	830	5211	VACM	01 May 78 - 19 Jul 79
WHOI 640	31.023	-69.498	269	5355	VACM	01 May 78 - 21 Jul 79
WHOI 640	31.023	-69.498	394	5355	VACM	01 May 78 - 21 Jul 79
WHOI 640	31.023	-69.498	516	5355	VACM	01 May 78 - 21 Jul 79
WHOI 640	31.023	-69.498	616	5355	VACM	01 May 78 - 21 Jul 79
WHOI 640	31.023	-69.498	715	5355	VACM	01 May 78 - 17 Sep 78
WHOI 640	31.023	-69.498	839	5355	VACM	01 May 78 - 21 Jul 79
WHOI 640	31.023	-69.498	2008	5355	not available	01 May 78 - 17 May 79
WHOI 640	31.023	-69.498	3004	5355	not available	20 May 78 - 19 May 79
WHOI 640	31.023	-69.498	5250	5355	VACM	01 May 78 - 21 Jul 79
WHOI 640	31.023	-69.498	5332	5355	VACM	01 May 78 - 21 Jul 79

WHOI 641	31.168	-69.625	619	5254	VACM	02 May 78 - 13 May 79
WHOI 641	31.168	-69.625	839	5254	VACM	02 May 78 - 21 Jul 79
WHOI 642	30.975	-69.833	617	5299	VACM	02 May 78 - 21 Jul 79
WHOI 643	30.818	-69.615	611	5261	VACM	11 May 78 - 09 Nov 78
WHOI 643	30.818	-69.615	634	5261	VACM	11 May 78 - 09 Nov 78
WHOI 643	30.818	-69.615	858	5261	VACM	11 May 78 - 21 Jul 79
WHOI 644	30.592	-69.470	587	5216	VACM	11 May 78 - 23 Jul 79
WHOI 646	30.838	-69.367	567	5220	VACM	12 May 78 - 22 Jul 79
WHOI 647	31.000	-69.160	578	5200	VACM	12 May 78 - 22 Jul 79

### Gulf Stream Extension

All of these files were recorded originally with a time increment of 15 minutes. In the present archive they have been low-pass filtered and subsampled. A few of them have a time increment of one day; the rest have a time increment of one hour.

mooring name	lat	lon	instr (meters)	depth water (meters)	depth instr type	dates
WHOI 673	37.002	-42.007	640	4788	VACM	25 Oct 79 - 23 Nov 80
WHOI 673	37.002	-42.007	1530	4788	Geodyne Model 850	25 Oct 79 - 23 Nov 80
WHOI 673	37.002	-42.007	4026	4788	Geodyne Model 850	24 Oct 79 - 24 Nov 80
WHOI 674	39.768	-43.948	550	4695	VACM	27 Oct 79 - 21 Nov 80
WHOI 674	39.768	-43.948	4023	4695	Geodyne Model 850	26 Oct 79 - 22 Nov 80
WHOI 675	40.367	-45.332	570	4550	VACM	28 Oct 79 - 22 Nov 80
WHOI 675	40.367	-45.332	1530	4550	VACM	28 Oct 79 - 22 Nov 80
WHOI 676	39.050	-44.033	4658	4841	VACM	31 Oct 79 - 23 Nov 80
WHOI 676	39.050	-44.033	4697	4841	VACM	31 Oct 79 - 23 Nov 80
WHOI 676	39.050	-44.033	4747	4841	VACM	31 Oct 79 - 23 Nov 80
WHOI 676	39.050	-44.033	4779	4841	VACM	31 Oct 79 - 23 Nov 80
WHOI 676	39.050	-44.033	4829	4841	VACM	31 Oct 79 - 23 Nov 80
WHOI 677	38.973	-44.110	581	4960	VACM	01 Nov 79 - 23 Nov 80
WHOI 677	38.973	-44.110	1521	4960	VACM	01 Nov 79 - 15 Apr 80
WHOI 677	38.973	-44.110	4020	4960	VACM	31 Oct 79 - 23 Nov 80
WHOI 677	38.973	-44.110	4777	4960	VACM	01 Nov 79 - 23 Nov 80
WHOI 677	38.973	-44.110	4857	4960	VACM	01 Nov 79 - 23 Nov 80
WHOI 677	38.973	-44.110	4928	4960	VACM	01 Nov 79 - 23 Nov 80
WHOI 678	38.678	-45.623	1491	4944	Geodyne Model 850	01 Nov 79 - 21 Nov 80
WHOI 678	38.678	-45.623	3989	4944	Geodyne Model 850	01 Nov 79 - 21 Nov 80
WHOI 678	38.678	-45.623	4835	4944	VACM	02 Nov 79 - 21 Nov 80
WHOI 678	38.678	-45.623	4915	4944	VACM	02 Nov 79 - 21 Nov 80
WHOI 679	37.975	-46.633	506	5285	VACM	03 Nov 79 - 20 Nov 80
WHOI 679	37.975	-46.633	1504	5285	VACM	03 Nov 79 - 20 Nov 80
WHOI 680	38.875	-46.908	520	5335	VACM	03 Nov 79 - 19 Nov 80
WHOI 680	38.875	-46.908	1520	5335	VACM	03 Nov 79 - 19 Nov 80
WHOI 680	38.875	-46.908	4010	5335	Geodyne Model 850	03 Nov 79 - 19 Nov 80

### LOTUS (northwest Atlantic)

All of these files have been filtered and decimated to one point per day.

mooring name	lat	lon	instr (meters)	depth water (meters)	depth instr type	dates
WHOI 693	34.047	-70.005	110	5368	VACM	06 May 80 - 01 Dec 80
WHOI 765	34.015	-69.807	530	5366	VACM	10 May 82 - 13 Apr 83
WHOI 765	34.015	-69.807	1030	5366	VACM	10 May 82 - 13 Apr 83

WHOI 766	34.037	-70.043	30	5366	VMCM	12 May 82 - 11 Apr 83
WHOI 766	34.037	-70.043	130	5366	VACM	12 May 82 - 11 Apr 83
WHOI 766	34.037	-70.043	180	5366	VACM	12 May 82 - 11 Apr 83
WHOI 766	34.037	-70.043	230	5366	VACM	12 May 82 - 11 Apr 83
WHOI 766	34.037	-70.043	280	5366	VACM	12 May 82 - 11 Apr 83
WHOI 766	34.037	-70.043	330	5366	VACM	12 May 82 - 11 Apr 83
WHOI 766	34.037	-70.043	780	5366	VACM	12 May 82 - 11 Apr 83
WHOI 766	34.037	-70.043	1020	5366	VACM	12 May 82 - 11 Apr 83
WHOI 766	34.037	-70.043	1520	5366	VACM	12 May 82 - 11 Apr 83
WHOI 766	34.037	-70.043	4000	5366	VACM	12 May 82 - 11 Apr 83
WHOI 787	34.013	-70.060	15	5366	VACM	13 Apr 83 - 25 Sep 83
WHOI 787	34.013	-70.060	75	5366	VMCM	13 Apr 83 - 30 Oct 83
WHOI 787	34.013	-70.060	100	5366	VMCM	13 Apr 83 - 30 Oct 83
WHOI 787	34.013	-70.060	1000	5366	VMCM	13 Apr 83 - 30 Oct 83
WHOI 788	33.977	-70.007	100	5366	VACM	15 Apr 83 - 04 Dec 83
WHOI 788	33.977	-70.007	150	5366	VACM	15 Apr 83 - 01 May 84
WHOI 788	33.977	-70.007	200	5366	VACM	15 Apr 83 - 07 Oct 83
WHOI 788	33.977	-70.007	300	5366	VACM	15 Apr 83 - 01 May 84
WHOI 788	33.977	-70.007	350	5366	VACM	15 Apr 83 - 30 Apr 84
WHOI 788	33.977	-70.007	400	5366	VACM	15 Apr 83 - 01 May 84
WHOI 788	33.977	-70.007	450	5366	VACM	15 Apr 83 - 05 May 84
WHOI 788	33.977	-70.007	500	5366	VACM	15 Apr 83 - 01 May 84
WHOI 788	33.977	-70.007	600	5366	VACM	15 Apr 83 - 02 May 84
WHOI 788	33.977	-70.007	750	5366	VACM	15 Apr 83 - 30 Apr 84
WHOI 788	33.977	-70.007	1000	5366	VACM	15 Apr 83 - 29 Apr 84
WHOI 788	33.977	-70.007	1500	5366	VACM	15 Apr 83 - 30 Apr 84
WHOI 788	33.977	-70.007	2500	5366	VACM	15 Apr 83 - 04 May 84
WHOI 788	33.977	-70.007	4000	5366	VACM	15 Apr 83 - 29 Apr 84
WHOI 789	33.978	-69.758	500	5366	VACM	16 Apr 83 - 27 Apr 84
WHOI 789	33.978	-69.758	1000	5366	VACM	16 Apr 83 - 01 May 84
WHOI 790	33.778	-69.997	510	5366	VACM	17 Apr 83 - 28 Jan 84
WHOI 790	33.778	-69.997	1010	5366	VACM	17 Apr 83 - 01 May 84

**Current meter records from the LLWODP East Experiment  
(Low Level Waste Ocean Disposal Program)**

mooring name	lat	lon	instr (meters)	depth water (meters)	depth instr type	dates
CMME-1	32.643	-70.845	1060	5410	Aanderaa RCM5	16 Sep 80 - 02 Jul 81
CMME-1	32.643	-70.845	3240	5410	Aanderaa RCM5	16 Sep 80 - 02 Jul 81
CMME-1	32.643	-70.845	4060	5410	Aanderaa RCM5	16 Sep 80 - 02 Jul 81
CMME-1	32.643	-70.845	4910	5410	Aanderaa RCM5	16 Sep 80 - 02 Jul 81
CMME-1	32.643	-70.845	5360	5410	Aanderaa RCM5	16 Sep 80 - 02 Jul 81
CMME-2	32.767	-70.798	1320	5410	Aanderaa RCM5	03 Jul 81 - 01 Jun 82
CMME-2	32.767	-70.798	2890	5410	Aanderaa RCM5	03 Jul 81 - 01 Jun 82
CMME-2	32.767	-70.798	3950	5410	Aanderaa RCM5	03 Jul 81 - 01 Jun 82
CMME-2	32.767	-70.798	5340	5410	Aanderaa RCM5	03 Jul 81 - 01 Jun 82
CMME-4	32.725	-70.818	2880	5440	Aanderaa RCM5	02 Jun 82 - 28 Apr 83
CMME-4	32.725	-70.818	4100	5440	Aanderaa RCM5	02 Jun 82 - 28 Apr 83
CMME-4	32.725	-70.818	5400	5440	Aanderaa RCM5	02 Jun 82 - 28 Apr 83
CMME-5	32.342	-71.822	4050	5390	Aanderaa RCM5	30 May 82 - 29 Apr 83
CMME-5	32.342	-71.822	5350	5390	Aanderaa RCM5	30 May 82 - 29 Apr 83
CMME-6	36.277	-71.458	1180	4200	Aanderaa RCM5	28 May 82 - 03 May 83
CMME-6	36.277	-71.458	2730	4200	Aanderaa RCM5	28 May 82 - 03 May 83
CMME-6	36.277	-71.458	3350	4200	Aanderaa RCM5	28 May 82 - 03 May 83
CMME-6	36.277	-71.458	4160	4200	Aanderaa RCM5	28 May 82 - 03 May 83
Sandia BOM	36.362	-71.603	4195	4200	Aanderaa RCM5	28 May 82 - 03 May 83
CMME-9	34.928	-71.463	2810	4348	Aanderaa RCM5	27 Apr 83 - 25 Aug 84

CMME-9	34.928	-71.463	4300	4348	Aanderaa RCM5	27 Apr 83 - 25 Aug 84
CMME-11	34.468	-71.125	4750	4939	Aanderaa RCM5	27 Apr 83 - 22 Aug 84
CMME-11	34.468	-71.125	4820	4939	Aanderaa RCM5	27 Apr 83 - 18 Aug 84
CMME-11	34.468	-71.125	4835	4939	Aanderaa RCM5	27 Apr 83 - 10 Aug 84
CMME-12	33.703	-71.028	3770	5324	Aanderaa RCM5	28 Apr 83 - 01 Sep 84
CMME-12	33.703	-71.028	4830	5324	Aanderaa RCM5	28 Apr 83 - 28 Aug 84
CMME-12	33.703	-71.028	5250	5324	Aanderaa RCM5	28 Apr 83 - 03 Sep 84
CMME-13	32.772	-70.787	5400	5464	Aanderaa RCM5	30 Apr 83 - 28 Aug 84
CMME-13	32.772	-70.787	5430	5464	Aanderaa RCM5	30 Apr 83 - 24 Aug 84

## CONSLEX

(an experiment of the Institute of Oceanographic Sciences)

CONSLEX is an acronym but there is no record of its meaning.

mooring name	lat	lon	instr (meters)	depth water (meters)	depth instr type	dates
not available	60.212	-9.222	251	1463	Aanderaa	19 Mar 82 - 20 Mar 83
not available	60.212	-9.222	654	1463	Aanderaa	19 Mar 82 - 26 Mar 83
not available	60.212	-9.222	1055	1463	Aanderaa	19 Mar 82 - 20 Mar 83
not available	60.212	-9.222	1440	1463	Aanderaa	19 Mar 82 - 26 Mar 83
not available	57.293	-10.337	534	2201	Aanderaa	29 Apr 82 - 10 Nov 82
not available	57.293	-10.337	1035	2201	Aanderaa	28 Apr 82 - 25 Nov 82
not available	57.293	-10.337	1786	2201	Aanderaa	28 Apr 82 - 17 Nov 82
not available	52.985	-18.390	1771	3155	Aanderaa	30 Nov 82 - 03 Jul 83
not available	52.985	-18.390	3110	3155	Aanderaa	30 Nov 82 - 03 Jul 83
not available	53.425	-19.023	1263	2495	Aanderaa	30 Nov 82 - 04 Jul 83
not available	53.425	-19.023	2450	2495	Aanderaa	30 Nov 82 - 04 Jul 83
not available	54.087	-19.917	1290	1335	Aanderaa	03 Dec 82 - 04 Jul 83
not available	51.898	-17.623	3526	4440	Aanderaa	04 Dec 82 - 28 Dec 82
not available	51.898	-17.623	4395	4440	Aanderaa	04 Dec 82 - 05 Jul 83

## NEADS

(a British experiment in the North Atlantic)

mooring name	lat	lon	instr (meters)	depth water (meters)	depth instr type	dates
not available	52.455	-17.715	547	4135	Aanderaa RCM	29 Jun 82 - 03 Jul 83
not available	52.455	-17.715	1559	4135	Aanderaa RCM	29 Jun 82 - 03 Jul 83
not available	52.455	-17.715	2346	4135	Aanderaa RCM	29 Jun 82 - 03 Jul 83
not available	52.455	-17.715	3109	4135	Aanderaa RCM	29 Jun 82 - 03 Jul 83
not available	52.455	-17.715	3910	4135	Aanderaa RCM	29 Jun 82 - 03 Jul 83

## Abyssal Circulation (northwest Atlantic)

All of the time series from this experiment have been low-pass filtered and decimated to one point per day.

mooring name	lat	lon	instr (meters)	depth water (meters)	depth instr type	dates
WHOI 775	41.203	-63.023	500	4027	VACM	20 Mar 83 - 06 Aug 84
WHOI 775	41.203	-63.023	1390	4027	Geodyne/WHOI Model 850	20 Mar 83 - 06 Aug 84

WHOI 776	40.478	-62.060	520	4886	VACM	20 Mar 83 - 07 Aug 84
WHOI 776	40.478	-62.060	1520	4886	VACM	20 Mar 83 - 07 Aug 84
WHOI 776	40.478	-62.060	4010	4886	Geodyne/WHOI Model 850	20 Mar 83 - 07 Aug 84
WHOI 776	40.478	-62.060	4790	4886	VACM	20 Mar 83 - 07 Aug 84
WHOI 777	40.213	-61.592	4870	4970	VACM	21 Mar 83 - 07 Aug 84
WHOI 778	40.680	-61.502	4000	4760	Geodyne/WHOI Model 850	21 Mar 83 - 24 Aug 84
WHOI 779	40.940	-60.715	4010	4798	VACM	22 Mar 83 - 08 Aug 84
WHOI 780	39.478	-60.330	510	5140	VACM	22 Mar 83 - 09 Aug 84
WHOI 780	39.478	-60.330	1010	5140	Geodyne/WHOI Model 850	22 Mar 83 - 09 Aug 84
WHOI 780	39.478	-60.330	1500	5140	VACM	22 Mar 83 - 09 Aug 84
WHOI 780	39.478	-60.330	4000	5140	Geodyne/WHOI Model 850	22 Mar 83 - 09 Aug 84
WHOI 781	38.440	-59.257	4000	5165	VACM	23 Mar 83 - 05 Feb 84
WHOI 782	37.527	-58.288	1390	5165	Geodyne/WHOI Model 850	23 Mar 83 - 10 Aug 84
WHOI 782	37.527	-58.288	4010	5165	VACM	23 Mar 83 - 10 Aug 84
WHOI 783	35.647	-60.887	510	4721	VACM	24 Mar 83 - 11 Aug 84
WHOI 783	35.647	-60.887	4020	4721	VACM	24 Mar 83 - 11 Aug 84
WHOI 784	36.535	-63.072	510	5020	VACM	25 Mar 83 - 11 Aug 84
WHOI 784	36.535	-63.072	1410	5020	Geodyne/WHOI Model 850	25 Mar 83 - 11 Aug 84
WHOI 784	36.552	-63.072	4000	5020	VACM	25 Mar 83 - 11 Aug 84
WHOI 786	37.448	-64.998	500	4998	VACM	26 Mar 83 - 12 Aug 84
WHOI 786	37.448	-64.998	4000	4998	VACM	26 Mar 83 - 12 Aug 84

**Current meter records from the Nares Experiment  
(Subseabed Disposal Project, Nares Abyssal Plain)**

mooring name	lat	lon	instr (meters)	depth water (meters)	depth instr type	dates
Nares-1	23.200	-63.982	725	5847	Aanderaa RCM5	15 Aug 83 - 20 Sep 84
Nares-1	23.200	-63.982	2950	5847	Aanderaa RCM5	15 Aug 83 - 20 Sep 84
Nares-1	23.200	-63.982	4800	5847	Aanderaa RCM5	15 Aug 83 - 20 Sep 84
Nares-1	23.200	-63.982	5800	5847	Aanderaa RCM5	15 Aug 83 - 20 Sep 84
Nares-2	23.247	-64.030	775	5835	Aanderaa RCM5	21 Sep 84 - 21 Nov 85
Nares-2	23.247	-64.030	1465	5835	Aanderaa RCM5	21 Sep 84 - 21 Nov 85
Nares-2	23.247	-64.030	4800	5835	Aanderaa RCM5	21 Sep 84 - 21 Nov 85
Nares-2	23.247	-64.030	5800	5835	Aanderaa RCM5	21 Sep 84 - 13 Aug 85
Nares-3	23.252	-64.035	715	5846	Aanderaa RCM5	23 Nov 85 - 03 Nov 86
Nares-3	23.252	-64.035	1450	5846	Aanderaa RCM5	23 Nov 85 - 03 Nov 86
Nares-3	23.252	-64.035	2875	5846	Aanderaa RCM5	23 Nov 85 - 03 Nov 86
Nares-3	23.252	-64.035	5800	5846	Aanderaa RCM5	23 Nov 85 - 03 Nov 86



## **8.2. A Note about Rotor Type Current Meters**

There were three general types of current meters that were used in the collection of the WOCE data. They were all mechanical devices using rotors to obtain current speed. The following is a basic run-down on the main characteristics of these meters.

### **8.1.1 The RCM series of current meters**

Include the Geodyne and RCM4 current meters with sampling rates of  $3.75 \times 2^N$  min (i.e. 3.75, 7.5, 15, 30, 60 minutes) where  $N = (0, 1, 2, \dots)$  is an integer. Speed is obtained from the number of rotor revolutions for the entire sample interval, and is therefore an average value over the recording interval, while direction is the direction recorded at the end of the sample period and is therefore a single measurement (Emery and Thomson 1997).

### **8.2.2 The vector averaging current meter (VACM)**

Allows data to be acquired via “burst sampling” in which a rapid series of speed and direction measurements are averaged over a short interval of the sampling period. In vector-average mode, the instrument uses speed and direction to calculate the horizontal and vertical components of velocity. One of the main advantages of this setup is that the amount of recording spaced needed in sampling is greatly reduced (Emery and Thomson 1997).

### **8.2.3 Vector measuring current meter (VMCM)**

This current meter is able to accurately measure mean flow in conditions of unsteady oscillating flow, however the design is open which allows small strands of seaweed and other matter to enter into and clog the rotors (Emery and Thomson 1997).